

# INVESTIGATIONS ON THE PROPERTIES OF MAGNETISED PLASMA

Thesis Submitted for the Degree of  
Doctor of Philosophy (Science)  
of the  
University of North Bengal  
1981

SUDIPTA KUMAR SADHYA, M.Sc.

ST - VERP

STOCK TAKING-2011 |

Let  
530.44  
3 125

79056

SEP 1982

## A C K N O W L E D G E M E N T S.

At the very outset, I offer my deep sense of gratitude to Professor Samarendra Narayan Sen, Department of Physics, North Bengal University, for his keen interest, invaluable suggestions and timely guidance throughout the course of this investigation. The encouragement and inspiration received from him during the hours of my greatest stress and strain always served me as a beacon light and would ever be gratefully remembered.

I also owe my gratefulness to Professor K.G.Emeleus of Queen's University, Belfast for his useful comments and suggestions on Chapter VI.

I wish to record my thanks to many friends who helped me in carrying out the investigation. As an expression of my appreciation of their generous help, I list here their names: S. K. Bhadra, Engineer, C.Z.Instruments (India) Pvt. Ltd., S. Mukherjee, Lecturer, Malda College, R.K.Datta and S.K.Ghosh, Research Fellows, N.B.U. and finally and most importantly Dr. D. C. Jana, Lecturer, Siliguri College, Siliguri.

I acknowledge my indebtedness to the members of the Executive Council, N.B.U. - Sri B. K. Bajpaie, Registrar and Sri S.K.Ghosh, Deputy Registrar, N.B.U. for their kind help in accomplishing the project.

## II

I would also like to thank all staff of the Department of Physics and University Library, N.B.U., Fellow research workers, N.B.U., my colleagues of A.C. College, Jalpaiguri and Dr. A. Sen for their encouragement and S. Choudhury for typing the thesis.

Thanks are also due to the authorities of A.C. College, North Bengal University and University Grants Commission for kindly offering me a teacher fellowship.

(Sudipta Kumar Sadhya).

CONTENTS

<u>Chapter</u>	<u>Page No.</u>
CHAPTER I	1-71
1.1. General Introduction	1
1.2. Review of the previous work	3
1.2.1. Measurement of electron temperature and electron density in low density magnetised plasma by probe method.	3
1.2.2. Measurement of electron temperature in glow discharges in transverse magnetic field by spectroscopic method.	13
1.2.3. Low pressure diffuse mercury arc plasma in a longitudinal magnetic field.	29
1.2.4. Enhancement of spectral line inten- sities in longitudinal magnetic field.	37
1.2.5. Recombination.	40
1.3. Scope of the present work.	58
References.	64
CHAPTER II. Experimental set up.	72-92
2.1. Introduction	72
2.2. Discharge tubes.	73

2.3. Preparation of gases.	74
2.4. Measurements of pressure.	76
2.5. Magnets and power supplies.	79
2.6. Measurements of parameters of Plasma with and without magnetic field by probe method.	80
2.7. Diagnostics by spectroscopic method.	83
2.8. Measurements of variation of discharge current and voltage across a low pressure mercury arc in longitudinal magnetic field.	87
2.9. Measurements of persistence times of a mercury after-glow.	88
2.10. Possible sources of errors.	90
References.	92
CHAPTER III. Measurement of electron temperature and electron density in low density $\pi$ magnetised plasma by probe method.	
3.1. Introduction.	93
3.2. Experimental arrangement.	95
3.3. Results and Discussions.	97
3.3.1. Probe data analysis and methods of measurements of $T_e$ and $n_e$	97
3.3.2. Results	103
3.3.3. Discussions of the results.	106

3.4. Conclusions.	116
References	118
CHAPTER IV. Measurement of electron temperature in glow discharge in transverse magnetic field by spectroscopic method	119-144
4.1. Introduction.	<del>121</del> 119
4.2. Method of measurement.	121
4.2.1. Excitation rate co-efficient for hydrogen.	124
4.2.2. Excitation rate co-efficient for helium.	125
4.2.3. Measurements in magnetic field.	128
4.3. Experimental arrangement.	132
4.4. Results and calculations.	134
References.	144
CHAPTER V. Electron temperature dependence on the transverse magnetic field in a glow discharge in helium as obtained from spectroscopic measurements.	145-156
5.1. Introduction.	145
5.2. Method of measurement.	146
5.3. Experimental arrangement.	151
5.4. Results and Discussions.	152
References.	156

CHAPTER VI. Mercury arc plasma in an axial magnetic field.	157-192
6.1. Introduction.	157
6.2. Experimental measurements and results.	159
6.3. Discussion of results.	164
6.3.1. A model of mercury arc burning in air.	167
6.4. Conclusions.	189
References.	191
CHAPTER VII. Enhancement of spectral inten- sities of mercury triplet lines in longitudinal magnetic fields.	193-227
7.1. Introduction.	193
7.2. Experimental arrangement.	194
7.3. Results and Discussions.	195
7.3.1. Self absorption and enhancement factors in magnetic field.	198
7.3.2. Coupled variation of $n_e(\sigma)$ and $T_e$ with magnetic field.	209
7.3.3. Total intensity of triplet lines with and without magnetic field.	217
7.4. Conclusions.	224
References.	226

CHAPTER VIII. Persistence times in afterglows in mercury arc maintained by r.f. field in presence of magnetic field.	228-252
8.1. Introduction.	228
8.2. Experimental arrangement.	229
8.3. A description of the decay of visual intensity during the afterglow.	231
8.4. Results and Discussions.	233
8.4.1. Without magnetic field.	233
8.4.2. When an axial magnetic field is present.	248
References.	252
Summary and Conclusions.	253-258

.....

## CHAPTER I

### 1.1. GENERAL INTRODUCTION

Accurate measurement of plasma parameters such as electron density, collision frequency and electron temperature is essential for the proper understanding of the physical processes occurring in an ionised gas. Occasionally plasmas are subjected to magnetic field for confinement and other purposes. Hence the interaction processes between a magnetic field and plasma should be properly investigated. In this thesis measurements and calculations are described relating to positive column of electrical discharges confined in cylindrical discharge tubes when a magnetic field is present.

A number of diagnostic methods have been developed in recent years. In the present study the Langmuir probe method and spectroscopic method have been utilised to determine plasma properties. The diagnostics are complicated considerably in the presence of the magnetic field. In view of that some efforts have been made to incorporate the effect of magnetic field on the diagnostics.

In a magnetic field plasma parameters change. The changes in properties not only depend upon the value of the magnetic field, but also on the orientation of the field with the discharge tube axis. Experimentally, two types of orientations are suitable. One is when the

magnetic field is parallel to the axis of the discharge tube. This magnetic field is called a longitudinal or an axial magnetic field. Secondly, the magnetic field may be perpendicular to the axis of discharge and is known as a transverse magnetic field. Studies have been made for plasma properties when these two types of magnetic fields are <sup>or</sup>separately present.

A study of plasma properties in magnetic field not only reveals variations of the properties with magnetic field, but also enables us to verify the models that are applied to interpret the behaviour of plasmas. With these aims in mind we are carrying out investigations in our laboratory on the properties of magnetoplasma. The present work reports some results and their interpretation.

In the next subsection a review of relevant works has been presented. Thereafter, the scope of the present work has been explained. In Chapter II, details of the experimental set-ups have been described. In Chapter III through VIII, reports of investigations on properties of magnetoplasma have been described. Details of the references cited in the texts are given at the end of each chapter.

## 1.2. REVIEW OF THE PREVIOUS WORK

### 1.2.1. MEASUREMENT OF ELECTRON TEMPERATURE AND ELECTRON DENSITY IN LOW DENSITY MAGNETISED PLASMA BY PROBE METHOD.

The electric probe has long been used as a fundamental diagnostic tool for measuring local properties of plasma. The experimental arrangements generally are very simple. A small metallic electrode is placed in the plasma at the location of interest. External circuitry is provided to vary its electric potential. The current flowing to the probe is measured as a function of applied voltage. The current voltage diagram or the probe characteristic may provide important information about local properties of the plasma such as electron and ion number densities  $n_e$  and  $n_i$ , electron temperature  $T_e$ , the plasma potential  $V_s$  and electron distribution.

Probe theory is complicated because probes are boundaries to plasmas and near the boundaries the equations that govern the plasma behaviour change. A thin layer around the probe exists where electron and ion number densities differ, and the layer called ~~as~~ a sheath can sustain large electric fields. So the number of possibilities for a meaningful use of probes is subject to many restrictions, otherwise the results of probe measurements may be erroneously interpreted.

To every point in the plasma there is a corresponding potential  $V_s$ , with respect to a given reference point (for example a large electrode in contact with the plasma). This is known as space potential. If a probe (e.g. a small cylindrical conductor) is inserted at a point in plasma, due to unequal motions of electrons and ions, the probe quickly attains a potential negative with respect to  $V_s$ , this potential is known as floating potential  $V_f$  and a sheath is formed due to space charge effect. If the probe potential is raised to  $V_s$  by some external source, the probe is at the same voltage as the plasma and there is no sheath. Charged particles reach the probe with their thermal velocities and the electron current considerably exceeds the ion current. If the bias is now increased so that the probe is more positive than the plasma, the ions are increasingly repelled and the saturation electron current is drawn which is determined by effective area of the sheath. In the collisionless plasmas, the sheath thickness increases as the bias is made more positive and electron current never completely saturates.

If the probe is biased more negatively than  $V_s$  an increasing fraction of electrons is repelled and the probe current falls. The logarithmic slope of the characteristic in this region is equal to the local electron temperature. At  $V_f$ , the currents of electrons and ions

drawn to the probe are equal and the net current is zero. With increasing negative bias no electrons can reach the probe and ion saturation current is drawn. From electron and ion saturation currents, plasma local density can be determined.

Since Langmuir's (1924—1926) pioneer work, the theory of probes in the absence of magnetic fields has been extensively developed. In the absence of magnetic fields the response of a probe depends on a number of parameters. These parameters determine the various domain at which electric probe can operate. In the collisionless limit  $[\lambda \gg r_p, \lambda \gg \lambda_D]$  where  $\lambda$  is the mean free path of charged particles,  $r_p$  is the probe radius and  $\lambda_D$  is Debye shielding length given by  $\lambda_D = 4.9 (T_e / n_e)^{1/2}$  in cm.) the theory is practically complete and extensive computed results are available [Bernstein & Rabinowitz (1959) Lam (1965), Laframboise (1966)]. The continuum case ( $\lambda \ll \lambda_D \ll r_p$ ) has been treated by Su and Lam (1963) and Cohen (1963) and some attempts have been made to cover the intermediate regime [Wasserstrom, Su and Probstein (1965) Chou, Talbot & Willis (1966), Bienkowski and Change (1968)]. A systematic account of probe theories is given by Chung, ~~Ek~~ Tolbot and Touryan (1975).

It has been discussed by Chen et al (1968) that probe theory is particularly simple when  $\xi_p = r_p / \lambda_D$  which is called as "Debye ratio" is large ( $\gg 10$ ) and the sheath is thin so that the particle collection area is

essentially the geometric area of the probe; or when  $\xi_p$  is small ( $\ll 1$ ) and the sheath very thick so that probe current is governed by orbital motion theory of Langmuir. For a suitable choice of  $\xi_p$  in an experiment, it may be noted that  $\lambda_D$  is determined by the plasma source itself, whereas  $r_p$  is set only by the physical strength of the material of probe. Hence it might not be always possible to have the Debye ratio in the desired range. Fortunately for cylindrical probes, the computation of Laframboise (1966) shows that orbital motion theory is accurate for  $\xi_p < 5$  and this is easy to satisfy. For a spherical probe orbital motion approximation is useful for  $\xi_p \ll 1$  only.

Schott (1968) has enumerated conditions to be satisfied for an ideal probe operating in orbital motion approximation:

- The plasma to be homogeneous and quasi neutral in the absence of the probe.
- Electrons and ions to have Maxwellian velocity distributions with temperatures  $T_e$  and  $T_i$  respectively with  $T_e \gg T_i$ . The mean free paths of electrons and ions  $\lambda_e$  and  $\lambda_i$  to be large compared to all other relevant characteristic lengths. Each charged particle hitting the probe is to be absorbed and not to react with the probe material.

- The sheath has a well defined boundary. Outside this boundary the space potential is constant.
- The sheath thickness is small compared to the lateral dimensions of the probe so that edge effects can be neglected.

Particularly in low pressure plasmas the condition of Maxwellian velocity distribution is often violated. An essential progress in probe theory was achieved by the work of Druyvesteyn (1930), who showed that actual velocity distribution can be derived from the form of characteristic. Another disadvantage for cylindrical probes is that the potential falls off slowly with radius so that  $r_s$ , the "absorption radius" defining the effective collection area can be much larger than  $\lambda_D$ . At low densities the length  $l$  of the probe must be much greater than  $r_s$  (and hence greater than  $r_p$ ) in order to avoid end effects. The material for the probe should be resistant to sputtering, to heat and to chemical reaction. Furthermore, the work function of the material should be high in order to minimize secondary electron emission. For comparatively hot plasmas tungsten as probe material is a suitable choice. Nevertheless, the probe and its insulator support structure which is immersed in the plasma disturb the plasma and the measurements as well. Chung, Talbot and Touryan (1975) have reviewed the present state of knowledge about these disturbances.

Presence of magnetic field further complicates probe data interpretation. Experimentally it is known that the magnetic field substantially modifies the characteristics. The useful sharp knee at the space potential is blurred or disappears completely. For more positive probe voltages (i.e. for electron collection) the current decreases substantially from its value at zero field. In a magnetic field the particles are constrained to move at different rates along and across the field lines. The problem thus becomes an anisotropic one. The charged particles can travel only a distance of the order of their Larmor radii  $r_{L e, i}$  without making collision and when either  $r_{L e}$  or  $r_{L i}$  is of the order of  $r_p$  or less, collisions come into play even when the relevant mean free path  $\lambda$  is large compared to  $r_p$ . Thus the equations describing the problem in the neighbourhood of probe differ markedly from those valid far from the probe. The problem was tackled by several authors from different point of view and theories were interpreted in the light of experimental results. A systematic account has been provided by Chung, Talbot and Touryan (1975). The investigations of Chen et al (1968) who compared results obtained from probe measurements with those of other standard diagnostic techniques in magnetic field are of particular interest. After detailed experimental observations Chen et al recommended that if the requirements of spatial and temporal resolution permit, one should use a cylindrical probe with  $r_p \ll r_L \ll l$  and  $\xi_p$  small.

For such a Langmuir probe, orbital motion limited current approximation can be used. Recently Bakshet et al (1977) investigated the transition region on probe characteristic which is used to determine  $T_e$  and  $V_s$ . In strong magnetic fields, in which  $r_{Le}$  is much smaller than geometric dimension of probe, the magnetic field can affect the electron current drawn by the probe. So the standard methods for determining  $T_e$  and  $V_s$  may prove incorrect.

When the probe is large compared to mean free path, it collects so many electrons that the electrons in the surrounding space is absorbed more rapidly than they can be supplied by diffusion from the distant regions where they are produced. Therefore, electron collection by a positive probe is considerably reduced in presence of a magnetic field. The process of ion currents becomes relatively simple, because in most cases  $r_{Li} \gg r_{Le}$ . So it appears that electron density of magnetoplasma can be determined from ion saturation current to a Langmuir probe using usual probe theories without considering magnetic field effect. But Chang and Chen (1977), observed that for a low density ( $n_e \leq 10^{10} \text{ cm}^{-3}$ ) medium pressure plasma ( $p \geq 0.1 \text{ torr}$ ) in a weak magnetic field ( $B \leq 1 \text{ k gauss}$ ), an apparent increase of ion current comparable to the regular probe current caused by secondary electron emission from probe surface occurs. The influence of secondary electron emission becomes more complicated in a magnetic field. The plasma density obtained from electron saturation current by carefully applying the

probe theories in a magnetic field agrees closely with electron density determined from microwave measurements, but  $n_e$  obtained from ion saturation current using usual probe theories without magnetic field does not.

However, when magnetic field is small, effect of the field is significantly small to be neglected (Scott (1975)). It has been observed by Kagan and Perel (1969) that magnetic field has little effect on the probe characteristics for cylindrical probe ( $r_p \ll \lambda_e$ ) which is perpendicular to the magnetic field, so long  $r_p \ll r_{Le}$ .

At this point we shall discuss about the investigations carried out for determining the effect of magnetic field on the positive column of plasma with probe method. Cummings and Tonks (1941) investigated ~~on~~ the positive column of low pressure mercury vapour arc by probe method when a longitudinal magnetic field was present. They concluded that normal radial electron density ( $n_e$ ) distribution for a mercury plasma is not affected by the presence of longitudinal magnetic field. Subsequently Tonks (1941) obtained a theoretical interpretation. Later on Bickerton and von-Engel (1956) considered Cummings and Tonks' investigation inconclusive because of the difficulty of interpreting probe characteristics taken in presence of magnetic field. Cummings and Tonks observed a reduction of  $T_e$  with the increase of magnetic field. It may be noted here that value of magnetic field ( $B \leq 70$  Oe) is small enough to neglect magnetic field effect on probe characteristics.

Bickerton and von-Engel (1956) studied the positive column of a helium discharge in longitudinal magnetic field by tungsten cylindrical and molybdenum disc wall probes. They measured  $T_e$  from the gradient of semi-log plot of electron current and electron densities were measured by relative changes in ion saturation current in various magnetic field strength. The authors observed that above 1 torr the maximum magnetic field ( $B < 600$  gauss) has only a negligible effect on  $T_e$ . At the lowest pressure used (0.22 torr) the probe characteristics in a magnetic field indicates the presence of two groups of electrons, one having distinctly higher temperature than the other. Presence of two groups of electrons in a low pressure plasma was also confirmed by Uehara et al (1975) by probe measurements. Bickerton and von-Engel further observed that when a longitudinal field is applied  $T_e$  is reduced. For low pressure discharge with low current (glow discharges) a change in the radial electron distribution takes place with magnetic fields and  $n_e$  at ~~ax~~ axis rises with the increase of field. It was concluded that in some cases of very low pressure in zero magnetic field, the Langmuir theory of free ion fall describes best the properties of plasma whereas in a magnetic field of sufficient strength Schottky's theory of ambipolar diffusion applies.

Sen and Jana (1977) while investigating the current voltage characteristic of glow discharges in an axial magnetic field ( $B \leq 800$  G) in air ( $p = 0.5$  to 1 torr)

have observed that radial distribution of electrons can be represented by a Bessel function (Schottky's theory) in the presence of longitudinal magnetic field as well. Sen and Gupta (1969) from r.f. conductivity measurements in helium, neon and argon (  $p = 0.7$  torr ) in a longitudinal magnetic field (  $B \leq 550$  G ) have shown that Schottky's ambipolar diffusion theory is valid for these discharges in magnetic field and from the particle balance equation the authors found electron temperature to decrease with increasing field. Sen and Gupta also observed the Debye shielding distance decreases as the field increases.

Schott (1963) conducted probe measurement in a cylindrical diffusion chamber. An increase of electron temperature towards the wall at low values of magnetic field was observed. At high values of magnetic field, a radial decrease of  $T_e$  is found which is due to the transversal cooling down mechanism of electron gas by two particle collision.

While investigating on the enhancement of radiations from a helium plasma in longitudinal magnetic field Hegde and Ghosh (1979) made use of a Langmuir probe in the positive column. The authors observed that the electron temperature is reduced and axial electron density increases as the field (  $B \leq 700$  Oe ) increases. They did not discuss about the corrections of probe characteristics for the presence of the magnetic field.

For transverse magnetic field, Tonks (1939) has reported T.J. Killian's measurements on a low pressure (Outerwall temp. 38.6°C) mercury arc by probe method. Electron temperature and electron number density were determined from one wall to the other. An exponential variation of electron density with distance across the arc was observed. Apart from these probe measurements other measurements on the properties of plasma in the presence of transverse magnetic field have been made and investigations have been discussed in the next subsections.

1.2.2.       MEASUREMENTS OF ELECTRON TEMPERATURE IN GLOW  
DISCHARGES IN TRANSVERSE MAGNETIC FIELD  
BY SPECTROSCOPIC METHOD:

The ideal experimental method would be one in which the probing mechanism does not disturb unduly the processes to be investigated. Consequently a spectroscopic method is preferred to other diagnostic methods. Spectroscopy of laboratory plasmas covers a wide area of work, varying from atomic structure to plasma physics. All the areas have been identified and discussed by Burgess (1972). It is the presence and interactions between ions, neutrals, electrons and photons that lead to atomic processes which both affect the plasma and provide information on plasma state.

For glow discharges in which electron temperature (1-5 eV) and electron density ( $10^8$ - $10^9$  cm<sup>-3</sup>) are comparatively

small, electron temperatures can be deduced from relative intensities of spectral lines. To determine  $T_e$  from relative intensity method, spectral lines are selected for which relevant atomic processes is understood and the excited state continuity equation considering all of the collisional and radiative processes that populate and depopulate the state concerned is written down. The process of solving the excited state continuity equations, thus obtained, is very complex. Simplifications may be made by weighting the relative contribution of separate processes and establishing a certain type of equilibrium to prevail inside the discharge tube by considering dominating particle gain and loss terms.

Two types of equilibriums are of interest the local thermodynamic equilibrium model (LTE) and corona equilibrium model (CE).

When a plasma is in LTE, there exists a unique temperature which determines the velocity distribution function for species with the dominating reaction rate (usually the electrons). If such equilibrium exists, the analysis of the state of plasma is particularly simple since it is only such local plasma parameters as electron density, electron temperature and composition that determine the relevant populations. To obtain total LTE, the reverse of all fast processes must be maintained and exact balancing of total rates for complementary processes must be allowed to take place. Also, the relaxation times (reciprocal of the rates)

for the important processes must be shorter than characteristic times of significant variations in local plasma conditions. Since most plasma of interest are optically thin to internal radiation (except perhaps for the resonance lines), collisional processes are usually more important in establishing LTE than radiative processes. Consequently collisional de-excitation rates must exceed radiative decay rates for true LTE. In LTE, energy of every particular kind is distributed over all particles present in the gas according to Boltzmann distribution law and in case of ionization, this equilibrium relation leads to Saha equation.

The number density of electrons necessary to obtain complete LTE has been calculated by Griem (1964). This electron density is given by

$$n_e \geq 9 \times 10^{17} (E_2 / \chi_H)^3 (kT_e / \chi_H)^{1/2} \text{ cm}^{-3} \quad (1.1)$$

with  $E_2$  the energy of the first excited level and  $\chi_H$  the ionisation energy of hydrogen and  $k$  is the Boltzmann constant.  $E_2$ ,  $\chi_H$  and  $kT_e$  all expressed in eV. To calculate this criterion, Griem considered that for lowest excited state (resonance level) the collisional excitation rate is ten times the radiative rate from that level. Later on this criterion was corrected by Hey (1976) by considering finer values of Gaunt factor appearing in collisional excitation rate co-efficient and incorporating the effect of metastable-metastable collisions.

Wilson (1962) provided an equation for LTE to be valid as

$$n_e \geq 6 \times 10^{13} \chi_i^3 (kT_e)^{1/2} \text{ cm}^{-3} \quad (1.2)$$

$\chi_i$  is the ionisation energy of atom in eV. From these criteria, a single criterion for electron density necessary to maintain complete LTE in the discharge tube is (Elton, 1970)

$$n_e \geq C (kT_e)^{1/2} \chi_i^3 \text{ cm}^{-3} \quad (1.3)$$

where  $C$  is a constant equal approximately to  $1.4 \times 10^{13}$  assuming complete trapping of resonance lines and  $1.4 \times 10^{14}$  assuming no trapping whatsoever.

For stationary and spatially homogeneous plasmas, LTE can be expected to hold if collisional processes with electrons from assumed Maxwellian distribution dominate in the rate equations. Since cross-sections increase rapidly with principal quantum number, whereas radiative decay rates decrease, this is often the case only for states with principal quantum numbers exceeding a certain value for which radiative decay and collisional excitation rates are comparable. Under the above circumstances it is consistent to relate densities in states above the critical level with each other and to electron density in the same way as in a system in complete LTE. Richter (1968) has shown that the occupation number for states over this critical level are as in LTE with temperature  $T_e$  but the ground level is

overpopulated by a factor. So the states over the critical level is considered to be in partial LTE. The electron density required for a level with quantum number  $p$  to be in partial LTE with higher levels is after Griem (1964) approximately

$$n_e \geq 7 \times 10^{18} \frac{z^7}{p^{8.5}} (kT_e / \chi_H)^{1/2} \text{ cm}^{-3} \quad (1.4)$$

here ( $z$ ) is the charged state of atom. Strictly speaking this estimate applies only for hydrogen ions. For other atoms,  $p$  is identified as effective quantum number of the level defined as

$$p_{eff} = z \left( \frac{R}{T_\alpha - T_p} \right)^{1/2} \quad (1.5)$$

where  $R$  = Rydberg constant,  $T_\alpha$  is the ionisation limit,  $T_p$  is the term value of the level  $p$  and for neutral atoms  $z = 1$ . Drawin (1969) applied a semi-empirical formula of excitation rate co-efficient and made a correction to equation (1.4). Fujimoto (1973) treated LTE on the basis of a collisional radiative model for hydrogen ions and observed that LTE is identical with that enunciated by H.R.Griem.

When electron densities are too low for establishment of LTE, it is still possible to obtain equilibrium whereby the collisional excitation and ionisation is balanced by radiative decay and recombination respectively. This type of equilibrium generally prevails in solar corona, so it is known as

corona equilibrium (CE) model. In CE, the population of an excited level which can emit allowed spectral lines, is usually governed by collisional excitation from ground level and spontaneous radiative decay, but since decay is the faster process, the population is mainly in the ground level. CE can also be applied under restricted conditions to the line intensities of spectra from low density plasmas created in the laboratory. An approximate criterion for CE<sup>is</sup> to be valid for all excited levels is given by Wilson (1962) as,

$$n_e \leq 1.5 \times 10^{10} \chi_i^{-0.5} (kTe)^4 \text{ cm}^{-3} \quad (1.6)$$

here again  $\chi_i$  is the ionization potential of the atom in eV. Wilson also described a semi-corona (SC) domain when CE is valid except for levels close to ionisation limit. The criterion for SC domain in case of ions without metastable levels is

$$n_e \leq 10^{11} \chi_i^{1.5} (kTe)^2 \text{ cm}^{-3} \quad (1.7)$$

McWhirter (1965) proposed another condition for CE and Fujimoto (1973) interpreted CE in terms of a collisional radiative model.

When an actual plasma can not satisfy the criteria already stated, complexity arises and all of the collisional and radiative rate processes are to be considered for a particular level. This is particularly important for plasma in transition region (from SC to partial LTE). Fujimoto (1979)

has treated this transition region through quasi saturation phase (complete saturation phase means complete LTE) by ladder like excitation mechanism.

For spectroscopic diagnostics two assumptions are generally made and these assumptions make the problem easier to handle.

- (i) The plasma is optically thin. The optical thin-ness or thickness of radiation generally treated in terms of optical depth. In case of an optically thin plasma, the absorption of radiation is negligible. So the radiation of each individual atom leaves the plasma and contribute to observed intensity. It is generally believed that for CE all the light sources, and for LTE all light sources above  $10,000^{\circ}\text{K}$  are quite transparent even in the central parts of the line (perhaps with exception of resonance line) (Lochte-Holtgreven, 1968).
- (ii) Additional simplifications can be achieved if it is assumed that electron energy distribution is Maxwellian.

Here we shall discuss in some detail about the energy or velocity distribution functions of electrons. For probe diagnostics the nature of electron energy distribution function is experimentally determined, whereas for spectroscopic methods a knowledge of electron energy distribution function is necessary because the distribution function, generally designated by  $f$ , enters directly in the collision

integrals. Also, the presence of a magnetic field can effectively influence  $f$ .

In an active plasma, the collisional effects of free electrons rapidly establish an equilibrium velocity distribution which is Maxwellian in character. An electric field present in the discharge or elastic collisions of electrons with other atoms, can destroy this equilibrium distribution. The significance of this function is that  $f(\vec{r}, \vec{v}, t) d\vec{r} d\vec{v}$  denotes the number of electrons at position  $\vec{r}$  in  $d\vec{r}$ , with velocity  $\vec{v}$  in the range  $d\vec{v}$  at time  $t$ . The distribution function in terms satisfy an equation of continuity in position and velocity space i.e. Boltzmann transport equation. This equation equates the rate change of the number of electrons in  $d\vec{r} d\vec{v}$  to net flow of electrons into this volume element. The flow in position space results from the velocity of electrons, while in velocity space it results from their acceleration due both to collision with gas atoms and the applied electric field. To simplify the integro differential equation an assumption is made that the distribution function is almost spherically symmetric in velocity space, hence, can be adequately represented by first two terms of an expansion in spherical harmonics involving the direction of electron velocity. In this way the Boltzmann equation is solved and generally the distribution function of unknown form is obtained numerically.

Occasionally for plasma with high ionisation, the solved distribution function differs in a minor way from a Maxwellian one and von-Engel (1965) wrote "generally, the energy distribution of electrons in a gas moving in an electric field is approximately Maxwellian". If distribution function becomes a non-Maxwellian one the concept of electron temperature is important only in the sense of average energy. When the degree of ionisation is small the so-called non-Maxwellian interactions of electrons with other particles result in elastic and inelastic collisions. These collisions induce energy exchanges between charged, excited and neutral particles and conversions between potential and kinetic energies occur, consequently for these energy transfers,  $f$  is affected.

For inelastic collisions, it is the electrons in the tail of the distribution that participate in the energy exchange. For a low temperature plasma, a small percentage of high energetic electrons in the tail is lost due to inelastic collisions and the tail is depleted. The nature of the function is not appreciably altered for bulk electrons which can not excite or ionise. This argument led von-Engel (1965) to consider energy distribution function to be Maxwellian (particularly for helium gas).

Elton (1970) has described at least four criteria to be satisfied if the free electrons in plasma to have a Maxwellian velocity distribution. These are:

$$t_{ee} \ll t_{ff}, t_{eh}, t_{part}, t_{inel} \quad (1.8)$$

where  $t_{ee}$  is the energy relaxation time for colliding electrons. For a specific experiment, it must be much less than : (a)  $t_{ff}$  , the energy decay time for free free processes, (b)  $t_{eh}$  , the characteristic electron heating time, (c)  $t_{part}$  , the characteristic containment time for particles and lastly (d)  $t_{inel}$  , the relaxation time for electron impact including atomic processes such as excitation, ionisation etc. when the electron number density is comparatively high so that criteria (1.8) are fulfilled, the radiations from plasma also increase. Griem (1964) has expressed "most laboratory plasmas that emit enough light for spectroscopic observations are also sufficiently dense and long lived that the velocity distribution of electrons is very nearly Maxwellian at any instant of time and at any point in space".

Tonks and Allis (1937) investigated the effect of an external magnetic field on the electron velocity distribution function and Bernstein (1962) justified the use of a Maxwellian distribution for strong magnetic field in the approach via Boltzmann equation. It was experimentally observed by  $xp$  probe method that at least in longitudinal magnetic field electron energy distribution function is nearly Maxwellian (e.g. Bickerton and von-Engel (1956) for helium in 600 G field, Vorobjeva et al (1971) for pure mercury in 800 Oe field).

To report some measurements of properties of magnetoplasma by spectroscopic method: electron density in ring discharge (3.26 MHz) in argon ( $p = 2.50$  torr) in longitudinal magnetic field ( $B \leq 4.5$  kG) was measured by Ricketts (1970) by line intensity, and line to continuum intensity ratio method. The author selected lines of high lying levels assumed in LTE and observed marked decrease in  $T_e$  on the axis of discharge when axial magnetic field is applied. This temperature drop was explained in terms of possible heat transfer mechanism. An analysis of the profiles of certain HeI spectral lines emitted from a low pressure ( $p = 0.5$  torr) after glow plasma submitted to a magnetic field of  $10^5$  G has been provided by Drawin and Ramette (1979). The authors observed that a strong magnetic field leads to profound modification of the line profiles and complicates the diagnostics.

Now we shall discuss about the effect of a transverse magnetic field on the positive column of a low pressure discharge. As a cylindrical plasma column is subjected to a uniform transverse magnetic field it is pushed in the direction of Lorentz force. The electrons and ions are pushed in the same direction hence question of charge separation does not arise, only the gyrofrequencies of electrons and ions will be vectorially in opposite directions (clockwise and anticlockwise). So a deviation of density and potential distribution ~~is~~ from cylindrical symmetry occurs. As a consequence ~~there~~ there will be a potential difference between

points of the wall on a diameter perpendicular to magnetic field and this potential difference is known as Hall voltage. Qualitative descriptions of plasma column subjected to transverse magnetic field have been given by Francis (1956).

By utilising Tonks and Allis's (1937) expressions for electron drift in transverse magnetic field Beckman (1948) showed that the field deflects the column towards the wall with the result that the total loss of electrons and ions is increased. This causes an increase in electron temperature and axial electric field strength. Beckman (1948) observed that the axial electric field  $E$  is changed to  $E(\alpha + \beta^2/\alpha)^{1/2}$  in presence of a transverse magnetic field and electron density at a distance  $r$  from the axis and in field  $B$  is given by

$$n_B = n_0 \exp\left(-\frac{Cr \cos \phi}{2D_a}\right) J_0(2.405 \cdot r/R) \quad (1.9)$$

$n_0$  is the electron density at the axis,  $C$  is a constant depending on ion mobility,  $D_a$  is the ambipolar diffusion coefficient,  $J_0$  is the Bessel function of zero order and of first kind and  $\phi$  is the azimuthal co-ordinate. By measuring the voltage across a fixed distance by floating probe Beckman (1948) observed the electric field increases in a transverse magnetic field ( $B \leq 1000$  G) in gases like hydrogen, nitrogen, helium and neon.

Danders (1957) investigated on low pressure positive column in a homogeneous magnetic cross (transverse) field in Schottky manner and an equation of charge carrier density distribution was obtained. Current dependence on magnetic field was also examined experimentally.

Effect of a transverse magnetic field on low pressure glow discharges in different gases like, hydrogen, helium, neon etc. was also investigated by Sen et al (1971, 1972). The authors measured the discharge current and intensities of certain spectral lines in presence of field. Both the discharge current and spectral intensities were observed to increase first and after attaining a maximum at a certain magnetic field gradually decrease. In case of discharge current measurements, it was observed that the field ( $B_{max}$ ) at which the current becomes maximum is same for all gases and independent of pressure for the same initial discharge current, for spectral line intensity measurements,  $B_{max}$  differ for different wavelength of lines of a same gas. From Beckmann's (1948) analysis quantitative interpretations of the phenomena were produced. For smaller values of reduced magnetic field ( $B/p$ ) the authors modified Beckman's expression and have shown that the electric field and hence the electron temperature is changed by a transverse magnetic field as

$$E_B = E \left( 1 + C_1 \frac{B^2}{p^2} \right)^{1/2} \quad (1.10)$$

and

$$T_{eB} = T_e (1 + C_1 B^2/p^2)^{1/2} \quad (1.11)$$

where  $C_1$  is a constant for a particular gas given by

$$C_1 = \left\{ (e/m) (L/v_r) \right\}^2 \quad \text{where } e, m \text{ and } L$$

are charge mass and mean free path at a pressure of one torr of electrons and  $v_r$  is the electronic random velocity. The analysis was extended through the low pressure mercury arcs by Sen and Das (1973). Experimentally, the authors observed that for increasing transverse magnetic field ( $B \leq 300$  G) the arc current gradually decreases and voltage across the arc increases but the power consumed by the arc gradually increases and attaining a maximum value at a certain field decreases. Quantitative interpretation was given by considering enhanced charged particle loss and hence an increase in  $T_e$  and the decrease of axial electron number density. For low voltage cesium arc Bendarenko et al (1965) observed that as transverse magnetic field increases, the arc current decreases.

Recently Keneda (1977a, 1977b, 1978, 1979) in a series of papers studied the effect of transverse magnetic field ( $B \leq 300$  G) on neon glow discharges ( $p = 0.3 - 10$  torr). By measuring axial electric field strength by floating probes, Keneda observed that the axial field increases considerably with transverse magnetic field

at lower pressures and the author modified Beckman's expression by taking account of electron loss at wall.

Ecker and Kanne (1964) treated theoretically the case of cylindrical plasma column in a transverse magnetic field. The authors investigated on the problem mainly for two cases: (i) in collision free limit where Langmuir's theory of free fall applies and (ii) in collision dominated region where Schottky's ambipolar diffusion theory applies. In the collision dominated case, they found magnetic field does not change the temperature. The shift of maximum density distribution in the direction of Lorentz force was given a linear perturbation treatment (hence, small values of magnetic field was considered). While formulating the basic equations which may describe the collision dominated positive column in a transverse magnetic field, Ecker and Kanne wrote "the electron temperature is ~~also~~ calculated under the assumption that electron heat conduction is small in comparison to collision (elastic) losses. Then energy conservation law (for ~~ka~~ electrons) balances the energy gain in the electric field with energy loss due to collisions with neutral particles and axial electric field is constant due to Maxwellian's equation". But to have this balance equation realised for a real plasma a certain criterion (Ecker and Zöler, 1964) is to be fulfilled. This criterion is  $\lambda_e < 2R\gamma^{1/2}$  where  $\lambda_e$  is the mean free path of electrons,  $R$  the discharge tube radius and  $\gamma$  is the fractional energy

loss of electrons in an elastic collision. This condition is not satisfied in normal glow discharges and realised in practice only in cases of high current and comparatively high pressure arc discharges.

Blevin and Haydon (1958) have shown that a transverse magnetic field effectively increases the gas pressure from  $p$  to  $p_B$  so that

$$p_B = p \left( 1 + C_1 B^2 / p^2 \right)^{1/2} \quad (1.12)$$

$C_1$  has been already defined in equations (1.10) and (1.11). Assuming a Maxwellian velocity distribution of electrons and a constant average collision frequency, from the equivalent pressure concept, the variation of Townsend's first ionisation co-efficient in case of hydrogen is well understood in the high  $E/p$  region. But later on Haydon et al (1971) have argued that the velocity distribution for electrons in presence of transverse magnetic field may not be Maxwellian, so it is not appropriate to consider energy independent collision frequency when postulating equivalent pressure concept for electron behavior in hydrogen gas. From equivalent field concept of Allis (1956), Heylen and Bunting (1969) without assuming an 'a priori' constant collision frequency evolved an equivalent reduced electric field concept which reduces to more familiar equivalent pressure concept when electric field is kept constant. Using this concept and assuming Maxwellian velocity distribution for electrons,

the transverse and perpendicular mobilities and their ratio  $\tan \theta$  for electrons in hydrogen in transverse magnetic field (swarm expt.) are well explained. The average electron collision frequency was observed to vary with electron energy. This conception was further verified from experimental data obtained in case of other molecular gases like,  $\mu$  oxygen, air and nitrogen.

Some measurements have been reported in case of r.f. discharges and cathode region of hollow cathode discharges in magnetic field. Also there are reports for Hall voltage measurements in plasmas. Since the works are outside the scope of present investigation, we shall not discuss them.

### 1.2.3. LOW PRESSURE DIFFUSE MERCURY ARC PLASMA IN A LONGITUDINAL MAGNETIC FIELD:

Measurements on a low pressure mercury arc plasma in a longitudinal magnetic field was made by Tonks (1939) and by Cummings and Tonks (1941). Tonks (1939) observed that a longitudinal magnetic field leaves the point to point electron number density unchanged and does not alter the relative potential in cross section of the discharge tube. Thereafter, Cummings and Tonks (1941) found by probe method that electron temperature slightly decreases and axial electron density slight increases as the axial magnetic field ( $B \leq 70$  oe) increases. The authors stressed on the point that plasma may

react differently on the uniformity of the axial magnetic field. So the magnetic field must be a uniform one without radial ~~ax~~ component. From a detailed theory they concluded that 'normal' distribution for electrons and ions in the cross section is not altered in the presence of a longitudinal magnetic field. Tonks (1941) has calculated approximately the dispersal effect along a plasma column in longitudinal magnetic field. The solution for radial electron and ion distribution is the sum of a series of zero order Bessel functions. The first term, which is the normal distribution, is constant along the length of the column, while successive terms decrease with distance along the column at rates which are complicated functions of  $B$  and electron temperature.

In contrast Davies (1953) observed a small increase in electron temperature in a longitudinal magnetic field ( $B \leq 1580$  G) for a d.c. cesium plasma ( $p = 0.03$  to  $0.1$  torr) by measurements of intensity distribution in recombining spectrum. The observation of Davies can not be accounted for by existing theories, Bickerton and von-Engel (1956) have attributed this discrepancy between theory and experiment in the high current density ( $\approx 5A/cm^2$ ) used in a capillary tube by Davies. For very high current ( $i > 30$  A) arcs in argon ( $p < 1$  torr) in a longitudinal magnetic field ( $B = 2.3$  kG), Marhic and Kwan (1977) observed ~~ax~~ an axial variation of electron temperature and electron density.

vander-Sijde (1972) obtained variation of temperature and electron density profile for a hollow cathode argon arc in axial magnetic field ( $B \leq 1250$  G) from radiation profiles and electron temperature was found to decrease with the increase of the field. Wienecke (1963) obtained an increase of pressure in the hot region of a cylindrical symmetric arc in an axial magnetic field. Wienecke concluded that the forces exerted by magnetic field on charged particles modify diffusion current and since an energy transport is connected with the diffusion, it is also changed in magnetic field. Davies (1953) observed that a Maxwellian distribution of electron speed prevailed in longitudinal magnetic field. Maxwellian velocity distribution for electrons was also observed by Vorobjeva et al (1971) in mercury vapour arc in a longitudinal magnetic field ( $B \leq 800$  Oe) by probe method.

There is no clear cut definition of an arc. For a low pressure diffuse mercury arc Ecker and Zöler's (1964) criterion obtained from Ellenbaas-Heller heat balance equation, that energy gain of electrons in electric field is balanced by losses in elastic collisions, is not satisfied. On the contrary Ghosal, Nandi and Sen (1979) have shown that for such a discharge, the energy consumed by the discharge is lost mainly in ionizing collisions (also in excitation collisions) and the supplied energy is carried away by electrons and ions through ambipolar diffusion to

the wall of the discharge tube (also by radiation). But from definitions given by Pfender (1978) for an arc (e.g. (i) relative high current density, (ii) low cathode fall, (iii) high luminosity of the column), we call these diffuse discharges in mercury, a low pressure mercury arc. In these discharges, the volume ionisation is generally balanced by diffusion of charged particles. Ionisation in the volume is mainly by electron impacts of neutral and metastable atoms. Apart from diffusion, recombination of charged particles may play a role in the loss of charged particles. But in an active discharge, owing to the high value of electron temperature with respect to ion (or atom) temperature, recombination becomes comparatively less effective than diffusion. Two types of diffusion are known. One is the Langmuir free fall diffusion, effective in very low pressure region and the other is Schottky's ambipolar diffusion, operative in comparatively high pressure region. An ion fluid model described by Franklin (1976) covers these two domains through the transition region equally well. Electron temperature is calculated from a balance between particle loss and generation processes.

When a magnetic field is superimposed to a cylindrical plasma column, electron diffusion across and along the field becomes anisotropic and the radial diffusion is reduced. The plasma adjusts to this new situation by reducing its ionisation frequency which is determined by electron temperature. So a change in electron temperature is expected in a magnetic field. A reduction of electron temperature or axial  $E$

electric field in effect determines a reduced diffusion loss. The influence of longitudinal magnetic field on a cylindrical plasma column operating in Langmuir free fall domain has been treated by Self (1967). By ion fluid model which is equally responsive in high and low pressure regions, Franklin (1976) investigated on cylindrical plasmas subjected to axial magnetic field. Validity of ion fluid model was established by experimental evidences. According to Franklin the existence of longitudinal magnetic field can be regarded as an equivalent increase of pressure so far <sup>as</sup> radial motion is considered. Franklin (1976) further showed that due to decrease of radial diffusion of charged particles, ambipolar diffusion, if operative, will also be decreased in presence of a longitudinal magnetic field.

Some controversy arose regarding the ambipolarity assumption (in high pressure region) in the case of finite length cylinder with non-conducting walls placed in a longitudinal magnetic field. Disagreement between experimental data and ambipolar theory was observed (Geissler, 1970). Later on Chekmarev et al (1977) have analysed the diffusive decay of a weakly ionised gas in a finite length cylinder with non-conducting walls in presence of axial uniform magnetic field and have found that ambipolarity of diffusion is also preserved in presence of the field. The way a magnetic field influences the ambipolar diffusion is best described by Franck et al (1972). In the absence of

magnetic field the radial ambipolar field is positive, retarding plasma electrons and accelerating plasma ions. An increase of magnetic field causes a decrease in pure diffusion of electrons and ions. In classical theory pure diffusion of electrons and ions across magnetic field varies inversely with the square of the magnetic field in the absence of any instability,

$$D_{e\perp} = \frac{D_e}{1 + b_e^2 B^2}, \quad D_{i\perp} = \frac{D_i}{1 + b_i^2 B^2} \quad (1.13)$$

where  $b_e$  and  $b_i$  is electronic and ionic mobilities. Since at a given pressure electron mobility is larger than ion mobility by a factor  $10^2$  to  $10^3$ , electron diffusion is diminished to a larger extent than ion diffusion. So as magnetic field increases, at a particular magnetic field  $B_r$  the radial electric field vanishes when  $D_{e\perp} = D_{i\perp}$ . For magnetic field higher than  $B_r$ , the ambipolar electric field will be negative accelerating electrons to the ~~wall~~ wall and retarding the ions. To realise experimentally

$B_r$ , where reversal of ambipolar field occurs, is hardly possible. Generally  $B_r > B_{cr}$  where  $B_{cr}$  is the critical magnetic field where helical instabilities set in. Only for  $0 < B < B_{cr}$  classical ambipolar diffusion takes place, whereas for  $B > B_{cr}$  Kadomtsev instabilities set in.

In this context we shall discuss briefly about some of the anomalous behavior of column plasma in longitudinal magnetic field. Most of the anomalous behaviour have been studied in noble gases and <sup>in</sup> some molecular gases. For plasmas confined by a non-conducting discharge tubes, Hoh and Lehnert (1960) studied the effect of axial magnetic field in helium, hydrogen and krypton confined in long discharge tubes, so that diffusion to the ends can be neglected. The authors observed that upto a critical field  $B_{cr}$  the radial diffusion across the axial magnetic field decreases classically, but after  $B_{cr}$  the diffusion increases with B. Kadomtsev and Nedospasov (1960) interpreted the anomalous behaviour by discovering an instability in the form of helical wave which will be generated by longitudinal electric field at high values of magnetic field. This instability known as current convective instability enlarges the effective ambipolar diffusion with increasing magnetic field by  $E \times B$  drift which tends to drive the plasma electrons radially outward and to amplify diffusion. The value of  $B_{cr}$  is determined by the pressure. Later on Janzen et al (1970) observed in neon gas that the appearance of the instability depends upon the length of the discharge tube. For short discharge tubes ( $L \leq 15$  cm.) there is no instability. For comparatively long discharge tubes Deutsch and Pfau (1976) observed an anomalous increase of column gradient in axial magnetic field ( $B \ll B_{cr}$ ) in weak discharges

in noble gases. The anomalous behaviour was explained by accounting the radial change in energy distribution of electrons in relation to longitudinal magnetic field. Sato (1978) explained the same type of anomalous result as that of Deutsch and Pfau in terms of self excited ionisation waves (moving striations). Muira et al (1979) observed an abrupt decrease of axial electric field for a small interval of axial magnetic field in neon. After this fall the axial electric field rises again and decrease classically with the increase of field. The authors reported also the appearance of self excited ionisation waves along the abrupt fall of electric field.

Apart from these instabilities, another weak instability arises particularly in quiescent plasmas in axial magnetic field. This is known as drift dissipative instability (Timofeev, 1976). For current carrying discharges these instabilities are superposed by more strong current convective instabilities. Another type of anomalous diffusion known as Bohm diffusion which is proportional to reciprocal of magnetic field, is observed in highly ionised magnetoplasma confined in metal chambers. Behaviour of miscellaneous arc devices at normal pressure and exposed to magnetic field have been reviewed by Uhlenbusch (1976).

### 1.2.4. ENHANCEMENT OF SPECTRAL LINE INTENSITIES IN LONGITUDINAL MAGNETIC FIELD:

When a plasma column is subjected to a magnetic field there is a coupled change in the axial electron density and electron temperature. Since the spectral line intensities sometimes depend on these parameters, in a magnetic field there will be a change in spectral line intensities. In all types of magnetic fields (e.g. axial, transverse and rotational), enhancements of spectral line intensities have been observed.

Rokhlin (1939) studied the intensity distribution of spectral lines of mercury ( $p = 10^{-3}$  torr,  $\lambda = 1.5 - 4 \text{ \AA}$ ) and observed that for longitudinal magnetic field of limited extent having significant radial component, the intensities of mercury lines gradually increase and after attaining maxima gradually decrease. Takeyama and Takezaki (1968) observed emission enhancement of several He I and He II lines in a helium plasma ( $p = 0.4 - 4$  torr) in axial magnetic field ( $H \leq 6 \text{ k Oe}$ ). The enhancement factor observed was independent of pressure. Ricketts (1970) observed increase of intensities of argon spectral lines for an argon ring discharge in axial magnetic fields.

Forrest and Franklin (1966) advanced a theory regarding behaviour of low pressure positive column arc

discharges and calculated the radial light emission profile in axial magnetic field. The authors' theoretical model have been discussed in detail by Franklin (1976) and a contraction of radial column has been reported. Recently Hegde and Ghosh (1979) measured enhancements of He (I) and He (II) radiation from a helium glow discharge (  $p = 5 \times 10^{-3}$  torr ) in axial magnetic field (  $B \leq 700$  Oe ). The radiation was observed to increase and after passing through a maximum slightly to decrease with the increase of the field. Hegde and Ghosh developed a collisional radiative model (CRM) for helium for a quantitative interpretation of the phenomena and for justifying the CRM advanced by them. But in CRM generally collisional radiative ionisation is balanced by collisional radiative recombination of charged particles. Whereas in active discharges, collisional ionization is balanced by ambipolar diffusion to the tube wall and recombination in the volume is negligible. Subsequently Hegde and Ghosh (1979) found a very small collisional radiative recombination coefficient.

For ionic lines, Allen (1966) and Pinnington (1966) observed that the ionic lines are enhanced relatively by a factor of 150 times than the atomic lines in the magnetic field. However, these investigators studied the radiation enhancement phenomenon from the interest of observing Zeeman splitting. Allen (1966) recognised the problem that the so-called magnetic enhancement is not that the ionic

spectra is enormously brightened but that the arc spectrum is diminished (particularly for optically thick resonance lines). It should be noted here that the source used by these investigators are non-uniform ones, since radiation created at the central hot region is absorbed in the outer cooler region so that self reversal of the atomic (resonance) lines can occur.

The effects of transverse magnetic field on the radiation of a constricted discharge in helium, neon, nitrogen, hydrogen and mercury were observed by Kulkarni (1944). Sen, Das and Gupta (1972) observed that spectral intensity in glow discharges increases and after passing through a maximum decreases with the increase of transverse magnetic field. The authors gave quantitative explanation of the phenomenon considering coupled change of plasma parameters utilizing Beckman's (1948) analysis.

A group of investigators (Vukanovic' et al (1969), Pavlovic' et al (1979)) investigated the effect of homogeneous, inhomogeneous and rotating magnetic fields on the spectral intensities of free burning d.c. arcs. Their interest lies in finding a way for increasing line strength for finer spectrochemical analysis and from that point of view the authors recommended the application of an inhomogeneous and rotating magnetic field on the d.c. free burning arc because of large enhancement of spectral lines in those types of fields.

## 1.2.5. RECOMBINATION

For partially ionised gases, a particularly important reaction rate is that for electron ion recombination. In general two processes dominate in the loss side of charged particles' continuity equations - one is the ambipolar diffusion loss term and the other is a volume recombination loss term. By ambipolar diffusion, the charged particles created in the volume of the plasma by some mechanism diffuse away to the wall of the discharge vessel where they recombine and subsequently return to the plasma as neutral atoms in ground state. The charged particles may also recombine in the plasma volume through any of several possible mechanisms with oppositely charged particles and thereby create neutral particles in excited or ground states. In an afterglow plasma, when the electron temperature relaxes to a value corresponding to the ion temperature, loss due to ambipolar diffusion of charged particles, which is directly proportional to the ratio of electron temperature to ion temperature, reduces and thus in suitable conditions like a high gas pressure or a large discharge vessel, recombination reaction may dominate over that of ambipolar diffusion.

The macroscopic recombination coefficient  $\alpha$  is defined by the relation (in the absence of ionization processes

as in an afterglow)

$$\frac{dn_e}{dt} = -\alpha n_e n_i \quad (1.14)$$

where  $n_e$  and  $n_i$  denote the number density of electrons and ions with which the electrons are recombining respectively.

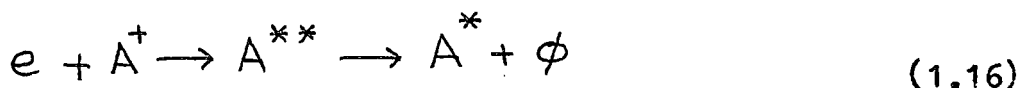
If an electron is to recombine with an atomic or molecular ion, recombination energy which is the sum of internal energy of the ion and kinetic energy of electron is released. The ability of the system to dispose of this excess energy determines the probability that recombination will occur. Considering the principles of conservation of linear and angular momenta, in the review articles, McDaniel (1964) and Massey and Gilbody (1974) have analysed electron-ion recombination in terms of separate reactions of the following types: radiative, dielectronic, three body collisional and dissociative recombinations.

If the energy released in recombination of an electron  $e$  and an ion  $A^+$  is carried off by a photon  $\phi$ , then it is a radiative recombination. This process may be represented by the reaction equation



Another way of handling the excess energy of recombination is to form a neutral atom in which two electrons are

simultaneously excited. The energy of the resulting doubly excited atom lies above the series limit and is energetically unstable, but can be stabilised by the emission of a photon in a transition to a lower bound level. This process of dielectronic recombination may be represented by the reaction

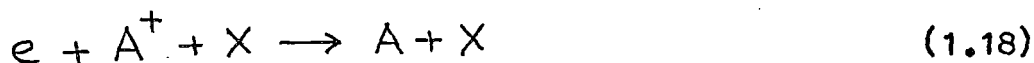


A star (\*) denotes an excited state.

If the recombination energy is carried off as increased kinetic energy by a third body involved in the collisions, then three body recombination occurs. Because electrons have such a small mass in comparison with other particles, the case in which the third body is an electron is distinguished, so that

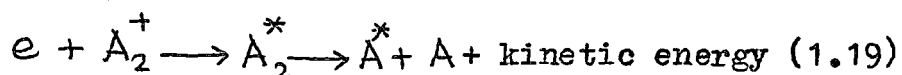


and the case where the third body is some heavy particle X



The above process involving a neutral third body becomes important at sufficiently high neutral gas pressure, even though the neutral particles are no more effective than a positive ion in removing energy from an electron. At ordinary pressures this recombination reaction should be very slow.

In the event that the electron recombines with a molecular ion  $A_2^+$ , a particularly effective process is to have the recombination energy go into dissociating the molecule and into increasing the kinetic energy of the resulting products. This process of dissociative recombination is represented by reaction equation



In the course of dissociative recombination, the electron colliding with the molecular ion is captured to the autoionization level. Since the interaction between the atoms in the autoionization state is repulsive, they move apart. If the autoionization state does not have time to decay while the atoms move apart to certain distance, the result is a stable state of the dissociated particles.

In a system if chiefly ionised species are the molecular ions, large effective recombination is observed, then there seems to be little doubt that dissociative recombination, first suggested by Bates and Massey (1947), can occur rapidly enough to account for the observed decay rate.

The first theoretical calculations for dissociative recombination were made by Bates (1950). He analysed the problem as a two state process. First the excited unstable molecule is formed, whose constituents then move

apart under the influence of their mutual repulsion thereby preventing autoionization. The expression for dissociative recombination coefficient  $\alpha$  was derived from the Franck Condon principles in terms of the autoionization life time and the time for effective separation to occur.

Thereafter, Warke (1966) derived the rate of dissociative electron capture by  $O_2^+$  ions in a semiclassical formalism in which heavy ions are treated classically and the electrons quantum mechanically. For  $H_2^+$  ions cross section of dissociative recombination was calculated by Bauer and Wu (1956) and by Wilkins (1966) in a Born approximation. A theoretical model for estimating the value of dissociative recombination coefficient has been described by Watson (1975).

But accurate computation for any specific ion would be extremely difficult to perform, in as much as  $\alpha$  an abinitio calculation requires detailed knowledge of the wave functions of all the molecular and atomic states of the reaction and their potential energy curves and autoionization probabilities as a function of inter-nuclear separation of atoms. Smirnov (1977) pointed out other difficulties of this complicated process. The number of autoionization states is large (sometimes infinite) and recombining molecular ion can be in excited vibrational states and this fact also influences the magnitude of  $\alpha$ .

Actual values of  $\alpha$  depend on the ionic species involved, but it is still possible to identify the order of magnitude of  $\alpha$  for each of the recombining processes described above. In Table (1.1) the characteristic values are shown. Values correspond to room temperature, <sup>and</sup> have been computed by Mitchner and Krugar (1973).

TABLE 1.1

Characteristic values of  $\alpha$  .

Process	$\alpha$ ( $\text{cm}^3 \text{sec}^{-1}$ ) T = 300°K.
1. Radiative	$10^{-12}$
2. Three body (electron) $n_e = 10^{13} \text{ cm}^{-3}$	$9 \times 10^{-7}$
3. Three body (heavy particle)	
helium ( 1 atoms. <sup>o</sup> pressure)	$7 \times 10^{-9}$
argon ( " " )	$7 \times 10^{-11}$
air ( " " )	$2 \times 10^{-7}$
hydrogen( " " )	$2 \times 10^{-7}$
4. Dielectronic	$10^{-12}$
5. Dissociative	$10^{-7}$

The description of recombination in terms of above mentioned independent reaction processes is traditional. In general however, these processes may be coupled. Bates, Kingston and McWhirter (1962) have demonstrated a coupling. The authors argued that loss mechanism in very tenuous plasma (astrophysical) is generally referred as radiative recombination and three body electron collisional recombination may be applied to the loss mechanism in very dense plasma. These two mechanisms are really the two limiting cases of a more general loss mechanism which was called collisional radiative recombination by Bates et al. This general loss mechanism is not simply the sum of the two limiting types for it results from the combination of interacting collisional and radiative processes of ionisation, recombination excitation and de-excitation which can occur in a decaying plasma. Then a statistical ~~xx~~ treatment is applied and quantitative result for  $\alpha_{CR}$  is obtained. Sometimes under suitable conditions the order of magnitude of  $\alpha_{CR}$  becomes equal to  $10^{-7} \text{ cm}^3/\text{sec}$ . Thus when in a decaying plasma molecular ions can not be identified to be present, the recombination is of collisional radiative type.  $\alpha_{CR}$  has been calculated for hydrogen, hydrogen ions, helium and for helium ions. For other elements, the computation becomes difficult to perform owing to large number of complicated excited states and for lack of knowledge for respective cross-section datas.

Most measurements of the electron ion recombination coefficient are made by measuring electron concentrations and other parameters in a plasma as a function of time after cutting off the exciting source. Under many conditions in these experiments, the electron temperature is the same as the gas temperature, but in some cases it is maintained higher through application of auxiliary heating of electrons, as through microwave pulse. The microwave method, first utilised by Biondi and Brown (1949) for measuring  $\alpha$  in helium appears to be most reliable in current use. The experimental arrangements have been described by Biondi (1951). The general principle of microwave technique is this: High purity gas is admitted at a desired pressure in a cylindrical quartz bottle located inside a cylindrical microwave cavity. A pulse discharge of variable time duration is then produced by microwave energy fed from a magnetron. The chief effect of the electrons produced in the discharge is to change the resonant frequency of the cavity. If the spatial distribution of the electrons in the bottle is known, absolute values of average electron density can be obtained from measured frequency shift during an afterglow.

For a recombining plasma if  $n_e = n_i$  and at  $t = 0$ ,  $n_e = n_e(0)$ , the solution of eqn.(1.14) is

$$\frac{1}{n_e(t)} = \frac{1}{n_e(0)} + \alpha t \quad (1.20)$$

so that the reciprocal of the number density is a linear function of time with slope  $\alpha$ . Thus  $\alpha$  can be determined from the loss rate of charge particles. When ambipolar diffusion is the main loss mechanism, decay rate of charged particles is an exponential one. Accurate values of  $\alpha$  is difficult to determine because other loss processes like diffusion (in some cases attachment) are present, because electrons may continue to be produced after primary discharge is turned off. Gray and Kerr (1962) have published a theoretical analysis of after glow decay in which they considered both diffusion and recombination loss processes. Considering these loss processes a non-linear differential equation is obtained,

$$\frac{\partial n_e(\vec{r}, t)}{\partial t} = -\alpha n_e^2(\vec{r}, t) + D_a \nabla^2 n_e(\vec{r}, t) \quad (1.21)$$

here  $D_a$  is the ambipolar diffusion coefficient. Gray and Kerr solved this equation numerically for widely different conditions, i.e. initial electron density distribution, cavity filling factor and ratio of recombination loss rate to diffusive loss rate  $\beta$  and for both spherical and infinite cylindrical geometries. Equation (1.21) has also been solved numerically by Oskam (1958) for infinite plane parallel geometry and by Frammhold, Biondi and Mehr (1968) for geometries having cylindrical symmetries.

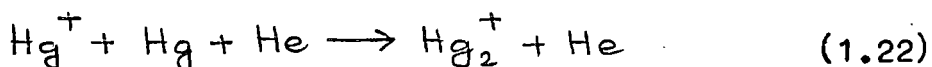
The results obtained experimentally are analysed numerically by the above mentioned method. In few cases, the criteria for obtaining accurate values of  $\alpha$  appeared to have been met. In many cases the criteria were definitely not fulfilled, whereas in others no decision could be made. However, for a fair measurement of  $\alpha$ , importance is given for the following conditions:

- i) Measurements be made under condition in which  $\beta$  is large,
- ii) attachment losses should be as small as possible,
- iii) in order to maintain as simple an analysis of afterglow as possible, it is necessary that electron energy distribution maintains a stationary value,
- iv) all the loss processes in general depend on  $T_e$ . In order to have simple conditions, it is necessary sometimes <sup>that</sup> the electrons are in thermal equilibrium with gas molecules,
- v) for the assumption  $n_e = n_i$  to be made, it is necessary that ions present should be of a single type.

Furthermore, measured values of  $\alpha$  are not very meaningful (in the sense of type of recombination) unless the identity of the recombining ions is definitely known. Positive identification is obtained by mass ~~px~~ spectrometric probing or by spectroscopic observation of the plasma while recombination is occurring.

As we are interested in afterglows in mercury vapour, we shall review the measurements made in mercury afterglows. Mohler (1937) was first to determine  $\alpha$  for mercury vapour. He used a probe to measure electron density after cut-off of an intense direct current discharge in mercury at 0.27 torr pressure.  $T_e$  in the afterglow was of the order of 2000°K and  $\alpha$  was found to be  $2.3 \times 10^{-10}$  cm<sup>3</sup>/sec. Mierdel (1943) however, has found that decay rate of electron density under very similar condition indicates an ambipolar diffusion type electron loss rather than recombination. Thereafter, Dandurand and Holt (1951) studied the electron removal processes in mercury afterglow by microwave technique and also by observing the visible and near ultraviolet light intensity and spectrum associated with the afterglow by a gated photomultiplier. They observed that the rate of electron density decay is determined at low pressure by ambipolar diffusion and at higher pressure by attachment. At the higher pressure region, some recombination is present and probably accounts for the line spectrum in afterglow (especially the bands at 3448 Å and 3480 Å). Value of  $\alpha$  was found to be  $5 \times 10^{-9}$  cm<sup>3</sup>/sec (corresponding  $T_e$  is around 2000°K) and the authors remarked that results was made complex by the presence of metastables in the plasma. Biondi (1953) investigated on the processes

involving ions and metastable atoms in mercury afterglows. He argued that studies of electron production and removal in gases of large molecular weights were complicated by the fact that the electrons might not attain thermal equilibrium with the gas during afterglow measurements. As a result only qualitative remarks could be made concerning the processes occurring in mercury. This difficulty has been overcome by adding helium in mercury to reduce the electron energy decay time and measurements could be made of the behaviour of thermal electrons in a mercury helium mixture. Helium acts as a recoil gas and keeps  $D_a$  small but leads to only a very small rate of complex or negative ion (by attachment) formation. In an afterglow in such a mixture, the ion population consists almost exclusively of ions of mercury and not of rare gas because its ionization potential is higher than that of mercury. Biondi applied the microwave techniques to determine the electron density decay rates. It was observed that atomic mercury ions are converted to molecular mercury ions by the reaction

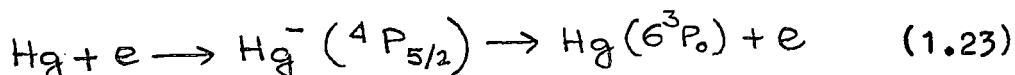


and the reaction occurs at a rate  $140 (P_{\text{Hg}} \cdot P_{\text{He}})$   $\text{sec}^{-1}$ . In comparatively high pressure region, these molecular ions recombine with electrons and the measured value of dissociative recombination coefficient of  $\text{Hg}_2^+$  ions

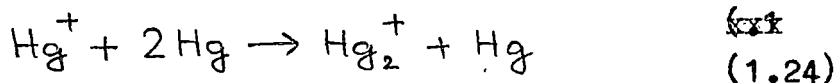
with electrons is  $5.5 \times 10^{-7} \text{ cm}^3/\text{sec.}$  at  $400^\circ\text{K.}$  The author disagreed with Dandurand and Holt on the possibility of attachment. On the other hand he found that at the pressure over 1 torr, the electron density decay curve shows increasing evidence of recombination.

Baibulatov (1966) while investigating on the de-ionisation of a mercury plasma noted that when the ionising field is switched off, the production of new ion pairs practically ceases and charged particle concentration then decreases, approaching a finite but small value. For a mercury plasma of pressure 0.01 to 0.1 torr, deionisation takes place mainly through the diffusion of ion electron gas to the walls of the discharge vessel as well as through reduction of electron temperature as a result of inelastic electron scattering.

Thereafter, Nishikawa, Fuji-e and Suita (1971) investigated on the atomic collision processes occurring in a flowing afterglow excited by D.C. discharge by triple probe and optical measurements. They found that the decrease in intensity of mercury atomic lines is rapid near the discharge source followed by a slow rate some what distant from the source. The rapid decrease in line intensities near the source may be due to the electron attachment process thereby producing temporary negative ions by the reaction



From decrease in density of metastable atoms some what distant from the source, the diffusion coefficient and the rate  $\alpha$  at which metastable atoms are converted to metastable molecules are graphically obtained. Slow intensity decrease somewhat distant from the source is related to dissociative recombination.  $\alpha$  was measured to be  $3.7 \times 10^{-7} \text{ cm}^3 \text{ sec.}^{-1}$  which is 1.5 times smaller than that of M.A.Biondi. This discrepancy was attributed to relatively high electron temperature (0.12 eV) in comparison with the electron temperature in the afterglow reported by M.A.Biondi. The molecular ions are formed by the reaction



The short duration afterglow of an r.f. (28.5 MHz) discharge in mercury has been examined by Aubrecht et al (1960) at different temperatures (60°C - 215°C). The authors concluded that enhancement of intensity of mercury atomic lines in the afterglow of r.f. discharge are produced by ionizing collisions between metastable mercury atoms. The decay is produced predominantly by volume ion electron recombination. The decay of the atomic lines in the afterglow is not affected by r.f. power supplied to the discharge. At higher temperature ( $>> 468^\circ\text{K}$ ), molecular bands appear and intensities of atomic lines decrease and decay more rapidly.

Another afterglow study in mercury vapour was done by McCoubrey (1954). This was a spectroscopic observation for persistence time of  $4850 \text{ \AA}$   $3350 \text{ \AA}$  bands during the afterglow. This experiment was not intended for a measurement of electron density decay rate, rather it was observed that  $6^3P_0$  atoms are converted to metastable diatomic  $Hg_2$  ( $^3O_u^-$ ) molecules by a three body collision involving two normal atoms and a value for diffusion coefficient of metastable atoms was obtained.

Generally dissociative recombination coefficient may depend on other parameters of a plasma afterglow. We shall discuss the interesting problem of temperature variation of  $\alpha$ . In the investigations made by Frammhold Biondi and Mehr (1968) in neon and by Ogram et al (1980) in krypton, the microwave techniques were utilised to determine  $T_e$  dependence of  $\alpha$ . In those experiments electrons do not relax to gas temperature during the afterglows, on the other-hand the temperature is controlled by steady microwave heating. As  $T_e$  is raised, ambipolar diffusion is also increased. However, it was observed that if every unstable molecule (in excited state) formed, dissociates before autoionization can take place then the initial capture step is rate limiting and a dependence of as  $T_e^{-0.5}$  is observed. If however, stabilisation of reaction by dissociation is rate limiting then a variation as  $T_e^{-3/2}$  is predicted.

In some experiments for determination of recombination coefficient superimposed axial magnetic fields were used. But in all the analyses it is tacitly assumed that  $\alpha$  does not depend on a magnetic field. Kuckes et al (1961) measured recombination in helium afterglow in a B-1 stellarator. In these experiments the degree of ionization was high from almost 100% to 2% as helium pressure was varied from 0.25 to 100 microns. It was observed in the experiment that (1) the loss rate is independent of the confining magnetic field between 2.9 to 3.5 kilogauss, (2) the intensity of light which is shown by spectral analysis to originate from the recombining helium atoms, is proportional to the electron loss rate, independent of pressure and magnetic field. The recombination was identified as three body one.

Knechtli and Wada (1961) measured recombination coefficient of a highly ionised (90% degree of ionisation) quiescent Cs plasma in steady state, without any current through the discharge and in a superimposed magnetic field of 1500 gauss. The experiments were not intended for investigating magnetic field dependence of  $\alpha$ , but for establishing the suitability of this type of currentless quiescent discharge in plasma behaviour study and to identify the nature of recombination of Cs plasma. However,  $\alpha$  measured in the experiments was substantially lower than the values reported in literature. The authors interpreted this in terms of low probability of formation of molecular ions leading to dissociative recombination, so that radiative or three body electronic recombination which have a

slower rate than dissociative recombination might be the possible loss mechanism.

Thereafter, D'Angelo and Rynn (1961) investigated in the same type of Q-machine cold plasma device on Cs and K. In this machine which is similar to that of Knechtli and Wada, Cs and K Plasma is produced by surface ionisation on a hot tungsten plate of Cs and K atoms from an atomic beam oven. No current was used and Langmuir probes were used for diagnostics. It was concluded by the authors that when no current is passed through the plasma, a  $1/B^2$  dependence of particle diffusion perpendicular to imposed magnetic field ( $B = 9$  kilo gauss) is observed. Although the experiment was not designed for an accurate determination of  $\alpha$ , it was assumed that  $\alpha$  which was identified as threebody collisional radiative was constant with magnetic field.

Recently Fowler (1978) in a paper entitled "A possible dependence of recombination on magnetic field" has suggested that beam maintenance experiments of D'Angelo and Rynn in Cs and K and of Simon (1959) in molecular nitrogen gas which were designed to ~~disapprove~~<sup>test</sup> Bohm diffusion may instead have revealed the existence of unsuspected magnetic field effect upon recombination.

Fowler argued that it is the low angular momentum overlap between plane waves and orbital wave functions which makes electronic recombination such an improbable

process, the rapid decrease that electron cyclotron radii undergo in a magnetic field might be expected to improve this situation drastically, especially for recombination into Rydberg states. The quantum number of the Bohr orbit which has the same angular momentum as a cyclotron orbit in a field of  $B$  tesla is  $120 B^{-1/3}$ . Therefore, the phenomenon is in fact unknown in ordinary discharge afterglow experiments, because they are conducted at moderate pressure ( $\sim 1$  torr) rarely permit states to exist much above  $n = 20$  (below which  $B$  must be greater than 200 tesla to observe an effect). But the beam experiments which were conducted between  $10^{-6}$  and  $10^{-3}$  torr would have permitted states as high as  $n = 200$ , and could easily have been influenced at 0.1 to 1.0 tesla fields employed. On the basis of D'Angelo and Rynn's data, Fowler suggested that behaviour of  $\alpha$  for Cs and K would be

$$\alpha = 5 \times 10^{-18} + (3 \times 10^{-34} p + 4.8 \times 10^{-17}) B \quad [\text{m}^3/\text{s}] \quad (1.25)$$

with  $p$  in  $\text{m}^{-3}$  and  $B$  in tesla. The three terms are radiative recombination, threebody magnetic induced recombination and radiative magnetic induced recombination. Fowler concluded that purpose of his paper is merely to point out the possibility of a new avenue of research, and to suggest the desirability of some direct experiments of recombination coefficient in a magnetic field.

### 1.3. SCOPE OF THE PRESENT WORK

It is well known that properties of a plasma change in presence of magnetic field and the change in the properties is reflected in the change of values of plasma parameter. Characteristics of magnetoplasma have been reviewed by Francis (1956), von-Engel (1965), Chen (1974) and by Franklin (1976). In a magnetic field constant in space and time a charged particle possessing a radial velocity component moves in a helical path. The motion can be visualised as a combination of circular motion around a point, known as guiding centre and a linear motion of the guiding centre. A positive charge gyrates counter clockwise when viewed in the direction of magnetic field while an electron gyrates clockwise. Franklin (1976) has discussed the criteria for effective magnetisation of electrons and ions. In comparatively low values of magnetic field, the electrons are only effectively magnetised.

A description of plasma properties would include a detailed knowledge of the populations of all bound electronic states, a knowledge of the translational energies of electrons and various atomic species, and a determination of free electron densities. For understanding the behaviour of plasma in magnetic field, measurements of above parameters when a magnetic field is present is desirable.

For cylindrical plasmas in usual discharge tubes the positive column represents the true plasma region. In this region quasineutrality of charged particles is maintained. But in a magnetic field due to magnetisation of charged particles loss processes as well as the gain processes also change. These changes are manifest in corresponding changes in electron temperature and axial electron density. In the present investigation the following properties of a magnetoplasma have been investigated.

- A. Electron temperature and electron density in low density magnetised plasma by probe method.

Following the quantitative analysis of Beckman, analytical expressions for the variation of electron temperature and electron density in a transverse magnetic field have been obtained by Sen and Gupta (1971). When the field is axial a detailed experimental analysis of these parameters has been provided by Bickerton and von-Engel (1956) and Aikawa (1976) has also studied the anisotropy of the electron distribution function by measuring the electron temperature in the direction of the magnetic field as well as in the perpendicular direction. As most of the effects of the magnetic field depend on the manner in which these parameters are affected by the field itself it is proposed to measure the electron temperature and electron density and their variation in both the transverse and axial magnetic fields.

It will also be of interest to see how the electron energy distribution is affected by the magnetic field. Furthermore this study is expected to show how the orientation of the magnetic field with the discharge tube axis can influence the plasma properties.

B. Investigation of plasma parameters by spectroscopic method.

Since by probe measurements we obtain the local properties of plasma, for average properties other types of diagnostics are desirable. Investigations have therefore been carried out on measurement of electron temperature variation of a glow discharge in transverse magnetic field for hydrogen and helium gases by spectroscopic methods. As little work has been reported to include the effect of magnetic field on spectroscopic diagnostic itself, we have discussed the feasibility of the technique in detail and have obtained the variation of electron temperature in a transverse magnetic field and compared the results with theoretical analysis.

C. Mercury arc plasma in an axial magnetic field.

Due to availability of mercury in pure form and for immense practical utility low pressure mercury discharges in different conditions have been exhaustively studied. Actually certain types of mercury discharges

(e.g. Hg - A discharges) are said to be best understood (Ingold, 1978). So a study of low pressure mercury arc discharge placed in an axial magnetic field has been undertaken to see the manner in which electron temperature and electron density are affected by the axial field. Properties of arc differ in some ways from those of glow discharges. In this study it is proposed to investigate the physical processes ~~at~~ actually occurring in an arc plasma. Hence in the present investigation air is the background gas which enables us to study how excitation ionization and deionization processes are influenced by the presence of air. For mercury arcs, associative ionization process is found to be a dominating ionization process. The effect of this process in positive column with and without magnetic field has been treated in detail and a relation ~~xxx~~ between axial electron density and electron temperature has been obtained and compared with experimental results.

D. Influence of magnetic field on the enhancement of intensities of triplet series of mercury.

The radiation enhancement of intensities of sharp series triplet lines of mercury with longitudinal magnetic field has been studied with the object of understanding the processes of population and depopulation in different atomic states under the action of magnetic field. The theory of

positive column was reviewed in the light of enhancement measurements. The influence of the field on metastable populations of mercury has been demonstrated.

E. Persistence times in afterglows in mercury arc maintained by r.f. field in presence and in absence of magnetic field.

The effect of an axial magnetic field on decay processes of a special type of mercury afterglow has been studied in this section. Since in mercury arc discharge, large number of molecular ions are found to be present, dissociative recombination of charged particles becomes a dominating loss process in the afterglows. So an investigation of particle loss processes in magnetic field may effectively determine the dependence of recombination on external magnetic fields. Apart from recombination other dominating loss mechanisms like diffusion and drift decrease in an axial magnetic field and recombination is considered to be independent of field. Recently Fowler (1978) has expressed his reservation on the constancy of recombination with magnetic field. So an investigation on loss processes in magnetic field is desirable for the proper knowledge of plasma loss mechanisms.

Under these headings it is proposed to study the interaction of the magnetic field with the plasma by measuring some of the plasma parameters and their variation  $\alpha$  in the magnetic field. It is expected that this study will throw light on the physical processes  $\alpha$  occurring in the a magnetoplasma.

## REFERENCES

1. Aikawa, H. (1976), J. Phys.Soc. Japan, 40, 1741.
2. Allen, L. (1966), Proc. Phys.Soc. 87, pt.2, 585.
3. Allis, W.P. (1956) in Hand-b. Phys. 21 (Ed.S. Flugge Springer-Verlag, Berlin).
4. Aubrecht, J.A., Whitcomb, B.M., Anderson, R.A. and Pickett, R.C. (1968), J.Opt.Soc. Am. 58, 196.
5. Baibulatov, F.Kh. (1966) Sov.Phys.Uspekhi, 9, 451.
6. Baksht, F.G., Dyuzhev, G.A., Tsirkel', B.I. Shkol'nik, S.M., Yur'ev, V.G., Antonov, S.V. Vainberg, L.I. and Kazanets, G.I. (1977). Sov. Phys. Tech. Phys. 22, 940, 944.
7. Bates, D.R. (1950), Phys. Rev. 78, 492.
8. Bates, D.R., Kingston, A.E. and McWhirter, R.W.P. (1962), Proc.Roy.Soc. A267 297 and *ibid* A270 155.
9. Bates, D.R. and Massey, H.S.W. (1947), Proc.Roy.Soc. A192, 1
10. Bauer, E. and Wu, T. (1956) Can.J.Phys.34, 1436.
11. Beckman, L. (1948) Proc.Phys.Soc. 61, 515.
12. Bendarenko, ~~И~~ I.I., Gus'kov, Yu.K. and Lebedev, M.A. (1965) Sov.Phys.Tech.Phys. 10, 635.
13. Bernstein, I.B. and Rabinowitz (1959) Phys.Fluids 2, 112.
14. Bernstein, M.J. (1962) Phys.Rev.127, 335, 342.

15. Bickerton, R.J. and von-Engel, A. (1956) Proc. Phys. Soc. 76, 468.
16. Bienkowski, G.K. and Chang, K.W. (1968) Phys. Fluids 11, 784.
17. Biondi, M. A. (1951) Rev. Sci. Instr. 22, 500.
18. Biondi, M. A. (1953) Phys. Rev. 90, 730.
19. Biondi, M.A. and Brown, S.C. (1949) Phys. Rev. 75 1700.
20. Blevin, H.A. and Haydon, S.C. (1958) Aust. J. Phys. 11, 18.
21. Burgess, D.D. (1972) Space Sci. Rev. 13, 493.
22. Chang, J. S. and Chen, S.L. (1977) J. Phys. D. 10 979.
23. Chekmarev, I.B., Simkina, T.Yu. and Yuferev, V.S. (1977) Plasma Phys. 19 15.
24. Chen, F.F. (1974), Introduction to plasma Physics (Plenum Press, N.Y.).
25. Chen, F.F. Etievant, C. and Mosher, D. (1968) Phys. Fluids, 11 811.
26. Chou, Y.S., Talbot, L. and Willis, D.R. (1966) Phys. Fluids, 9 2150.
27. Chung, P.M., Talbot, L. and Touryan, K.T. (1975) Electric probes in stationary and flowing plasmas: Theory and application (Springer-Verlag, Berlin).

28. Cohen, I.M. (1963) Phys. Fluids 6, 1492.
  29. Cummings, C.S. and Tonks, L. (1941) Phys.Rev.6  
59, 514.
  30. D'Angelo, N. and Rynn, N. (1961) Phys.Fluids 4, 1301.
  31. Danders, M. (1957) Z.Agrew. Phys. 9, 223.
  32. Dandurand, P. and Holt, R. (1951) Phys. Rev.82 868.
  33. Davies, L.W. (1953) Proc.Phys.Soc. B66, 33.
  34. Deutsch, H. and Pfau, S. (1976) Beitr. Plasma Phys.  
16 23.
  35. Drawin, H.W. (1969) Z.Phys. 228, 99.
  36. Drawin, H.W. and Ramette, J. (1979) Z.Naturf. 34a, 1051.
  37. Druyvesteyn, M.J. (1930) Z.Phys. 64 790.
  38. Ecker, G. and Kame, H. (1964) Phys.Fluids 7, 1834.
  39. Ecker, G. and Zoler, O. (1964), Phys.Fluids 7, 1996.
  40. Elton, R.C. (1970) in Methods of experimental Physics,  
Vol.9A (Eds:HR.Griem and R.H.Lovberg, Academic Press, N.Y).
  41. Forrest, J.R. and Franklin, R.N. (1966) Brit. J.Appl.  
Phys. 17, 1569.
  42. Fowler, R.G. (1978) Phys. Lett. 65A, 239.
  43. Frammhold, L. Biondi, M.A. and Mehr, F.J. (1968)  
Phys. Rev. 165, 44.
  44. Francis, G. (1956) in Handb. Phys. Vol.22 (Ed.S.Flugge,  
Springer-Verlag, Berlin).
  45. Franck, G. Held, R. and Pfeil, H.D. (1972) Z.Naturf  
27a 1439.
- 

46. Franklin, R.N. (1976) Plasma phenomena in gas discharges (Oxford University Press).
47. Fujimoto, T. (1973) J. Phys. Soc. Japan 34 216, 1429.
48. Fujimoto, T. (1979a) J. Phys. Soc. Japan, 47, 265, 273.
49. Geissler, K.H., (1970) Phys. Fluids 13 935.
50. Ghosal, S.K., Nandi, G.P. and Sen, S.N. (1979) Int. J. Electronics 47, 415.
51. Gray, E.P. and Kerr, D.E. (1962) Ann. Phys. (N.Y.) 17, 276.
52. Griem, H.R. (1964) Plasma Spectroscopy (McGraw Hill Book Co., N.Y.).
53. Haydon, S.C. McIntosh, A.I. and Simpson, A.A. (1971) J. Phys. D 4 1257.
54. Hegde, M.S. and Ghosh, P.K. (1979) Physica 97C, 275.
55. Hey, J.D. (1976) J.Q.S.R.T. 16, 69.
56. Heylen, A.E.D. and Bunting, K.A. (1969) Int. J. Electronics 27, 1.
57. Hoh, F.C. and Lehnert, B. (1960) Phys. Fluids 3, 600.
58. Ingold, J.H. (1978) in Gaseous electronics, Vol.1 (Eds: M.N. Hirsh and H.J. Oskam, Academic Press, N.Y).
59. Janzen, G., Mosher, F. and Rauchle, E. (1970) Z. Naturf. 25a, 992.
60. Kadomtsev, B.B. and Nedospasov, A.V. (1960) J. Nucl. Energy, Part C 1, 230.
61. Kagan, Yu, M. and Perel, V.I. (1969) Sov. Phys. Tech. Phys. 13, 1348.

62. Kaneda, T. (1977a) Jap. J. Appl. Phys. 16, 1887, 2293.
63. Kaneda, T. (1977b) Phys. Lett. 63A, 288.
64. Kaneda, T. (1978) J. Phys. D. 11, 279.
65. Kaneda, T. (1979) J. Phys. D. 12, 61.
66. Knechtli, R.C. and Wada, J.Y. (1961) Phys. Rev. Lett. 6, 215, also in Proc. Inst. Radio Engrs. 49 (1961) 1926, Phys. Rev. Lett. 10 (1963) 513.
67. Kuches, A.F., Motley, R.W., Hinnoy, E. and Hirschberg, J.G. (1961) Phys. Rev. Lett. 6, 337.
68. Kulkarni, S.B. (1944) Curr. Sci. 13, 254.
69. Laframboise, J.G. (1966) Univ. of Toronto, Institute of Aerospace Studies Report 100.
70. Lam, S.H. (1965) Phys. Fluids 8, 73, 1002.
71. Langmuir, I. (1924-1926) in Collected works of Irving Langmuir, Vols. 3, 4 & 5. (Ed. C.G. Suits, Pergamon Press, N.Y., 1961).
72. Lochte-Holtgreven, W. (1968) in Plasma diagnostics (North Holland Publishing Co., Amsterdam).
73. Marhic, M.E. and Kwan, L.I. (1977) J. Appl. Phys. 48, 3713.
74. Massey, H.S.W. and Gilbody, H.B. (1974) Electronic and Ionic impact phenomena, Vol. 4, (Oxford University Press).
75. McCoubrey, A.O. (1954) Phys. Rev. 93, 1249.
76. McDaniel, E.W. (1964) Collision phenomena in ionised gases (John Wiley, N.Y.)
77. McWhirter, R.W.P. (1965) in Plasma diagnostic, Techniques (Eds.: R.H. Huddleston & S.L. Leonard, Academic Press, N.Y.).

78. Mierdel, G. (1943) Z. Phys. 121, 574.
79. Mitchner, M. and Krugar, Jr., C.H. (1973).  
~~80x~~ Partially ionised gases (John Wiley, N.Y).
80. Mohler, F.L. (1937) J. Research Nat.Bur.Standards  
19, 559.
81. Muira, K., Imazu, S. and Takamatsu, T. (1979)  
 Japan. J.Appl.Phys. 18, 1203.
82. Nishikawa, M., Fuji-e, Y. and Suita, T. (1971)  
 J.Phys. Soc. Japan 31, 910.
83. Ogram, G.L., Chang, J. and Hobson, R.M. (1980)  
 Phys. Rev. 21A, 982.
84. Oskam, H.J., (1958) Philips Res. Rep. 13, 335.
85. Pavlovic, B.V., Mihailidi, T.A. and Georgijevic, I.  
 (1979) Teh.Fiz. (J.Engng. Phys.) 20, 41 and  
 references therein.
86. Pfender, P. (1978) in Gaseous electronics, Vol.I  
 (Eds.: M.N.Hirsh, H.J. Oskam, Academic Press, N.Y).
87. Pinnington, E.H. (1966) Proc. Phys. Soc. 87 pt.2, 586.
88. Richter, J. (1968) in Plasma diagnostics, (Ed.W.  
 Lochter Holtgreven, North Holland Publishing Co.,  
 Amsterdam).
89. Ricketts, B.W. (1970) J.Phys. D.3, 1678.
90. Rokhlin, G.N. (1939) Fiz.Zh. 1, 347.
91. Sato, M. (1978), J.Phys. D. 11, L101.
92. Schott, L. (1963) CR VI Conf.Int.Phen.d'Ionisation  
 dan les gaz. (Paris, S.E.R.M.A.) 2, 171.

93. Schott, L. (1968) in Plasma diagnostics (Ed. W. Lochte-Holtgreven, North Holland Publishing Co., Amsterdam).
94. Self, S.A. (1967) Phys. Fluids 10 1569.
95. Sen, S.N. and Das, R.P. (1973) Int.J. Electronics 34, 527.
96. Sen, S.N., Das, R.P. and Gupta, R.N. (1972) J. Phys. D. 5, 1260.
97. Sen, S.N. and Gupta, R.N. (1969), Ind. J. Pure & Appl. Phys. 7, 462.
98. Sen, S.N. and Gupta, R.N. (1971), J. Phys. D. 4, 510.
99. Sen, S.N. and Jana, D.C. (1977) J. Phys. Soc. Japan 43, 1729.
100. Simson, A. (1959) An introduction to thermonuclear research (Pergamon, N.Y.).
101. Smirnov, B.M. (1977) Introduction to Plasma Physics (Mir Publishers, Moscow).
102. Stott, P.E. (1975) in Courses on Plasma diagnostics and data acquiring system (Eds. A. Eubank and E. Sindoni, Editrice Compositori, Bologna).
103. Su, C.H., and Lam, S.H. (1963) Phys. Fluids, 6, 1479.
104. Takeyama, H. and Takezaki, Y. (1968) J. Q.S.R.T. 8, 1023, 1863.
105. Timofeev, B. (1976) Sov. Phys. Usp. 19, 149.

106. Tonks, L. (1939) Phys. Rev. 56, 360.
107. Tonks, L. (1941) Phys. Rev. 59, 522.
108. Tonks, L. and Allis, W.P. (1937) Phys. Rev. 52, 710.
109. Uehara, K., Hagiwara, S., Yatsu, K. and Kojima, S. (1975) Jap.J.Appl.Phys. 14, 1761.
110. Uhlenbusch, J. (1976) Physica 82C, 61.
111. Vander-Sijde, B. (1972), J.Q.S.R.T. 12, 1497, 1517.
112. von-Engel, A. (1965) Ionised gases, 2nd. Edn. (Oxford University Press).
113. Vorobjeva, N.A., Zaharova, V.M., and Kagan, Yu.M. (1971) 9th.Int.Conf.on Phen.Ionised Gases p.260.
114. Vukanovic, V., Georgijevic, V., Vukanovic, D. and Todorovic, M. (1969) Spectrochim Acta 24B 555.
115. Warke, C.S. (1966), Phys. Rev. 144, 120.
116. Wasserstrom, E., Su., C.H. and Probststein, R.F. (1965) Phys. Fluids 8, 56.
117. Watson, W.D. (1975) in Atomic and Molecular Physics and Interstellar matter (Les Houches Session 26. North Holland Publishing Co., Amsterdam).
118. Wienecke, R. (1963) Z.Naturf. 18a, 1151.
119. Wilkins, R.L. (1966) J.Chem.Phys. 44, 1884.
120. Wilson, R. (1962), J.Q.S.R.T. 2, 477.

## CHAPTER II

### EXPERIMENTAL SET UP.

#### 2.1. Introduction

In this work experimental investigations and theoretical interpretation on the properties of magnetoplasma have been carried out. We have measured the parameters of positive column of discharges in magnetic field by different methods. To study the effect of magnetic field, a low pressure plasma with a low input power is desirable. In a low pressure discharge, as the mean free times of the plasma particles become larger, plasma transport properties will be affected more by the magnetic field. In general the magnetic fields used in our experiments can effectively magnetise the electrons and ions may be considered to be uninfluenced by the field. Before any set of observations a steady state of the discharge was obtained, thereafter, magnetic field was introduced and the plasma properties were measured. Measurements were made on glow and arc discharges when either a longitudinal (axial) or a transverse magnetic field was present.

## 2.2. Discharge tubes

All the discharge tubes in which measurements were carried out were constructed of pyrex glass. For glow discharge measurements the tubes were fitted with brass (80% Cu, 20% Zn) and aluminium electrodes and for low pressure mercury arcs, the arcs were struck in between mercury pools. Two types of arc tubes were constructed - vertical and horizontal and the tubes were fitted to simple traps through standard joints as shown in Fig.2.1. In this way, the mercury vapour going out of the discharge tube could condense smoothly and could return to the tube. Otherwise, it was observed that mercury would condense in the joining rubber tubes and a mercury plug would be formed in the passage and thereby would disturb the vacuum system. The dimensional parameters of the discharge tubes and the electrodes used etc. for different measurements have been shown in Table 2.1.

The discharge tubes were thoroughly cleaned by chromic acid, pet-ether and distilled water and dried on the pump. Then the tubes were heat baked in an electric oven in the usual way. Finally the tubes were heated on the pump by passing currents for several days (and for several hours before each set of observations) to degas them. For removing the occluded gases from the electrodes, both the electrodes were used as cathodes alternately by reversing the currents

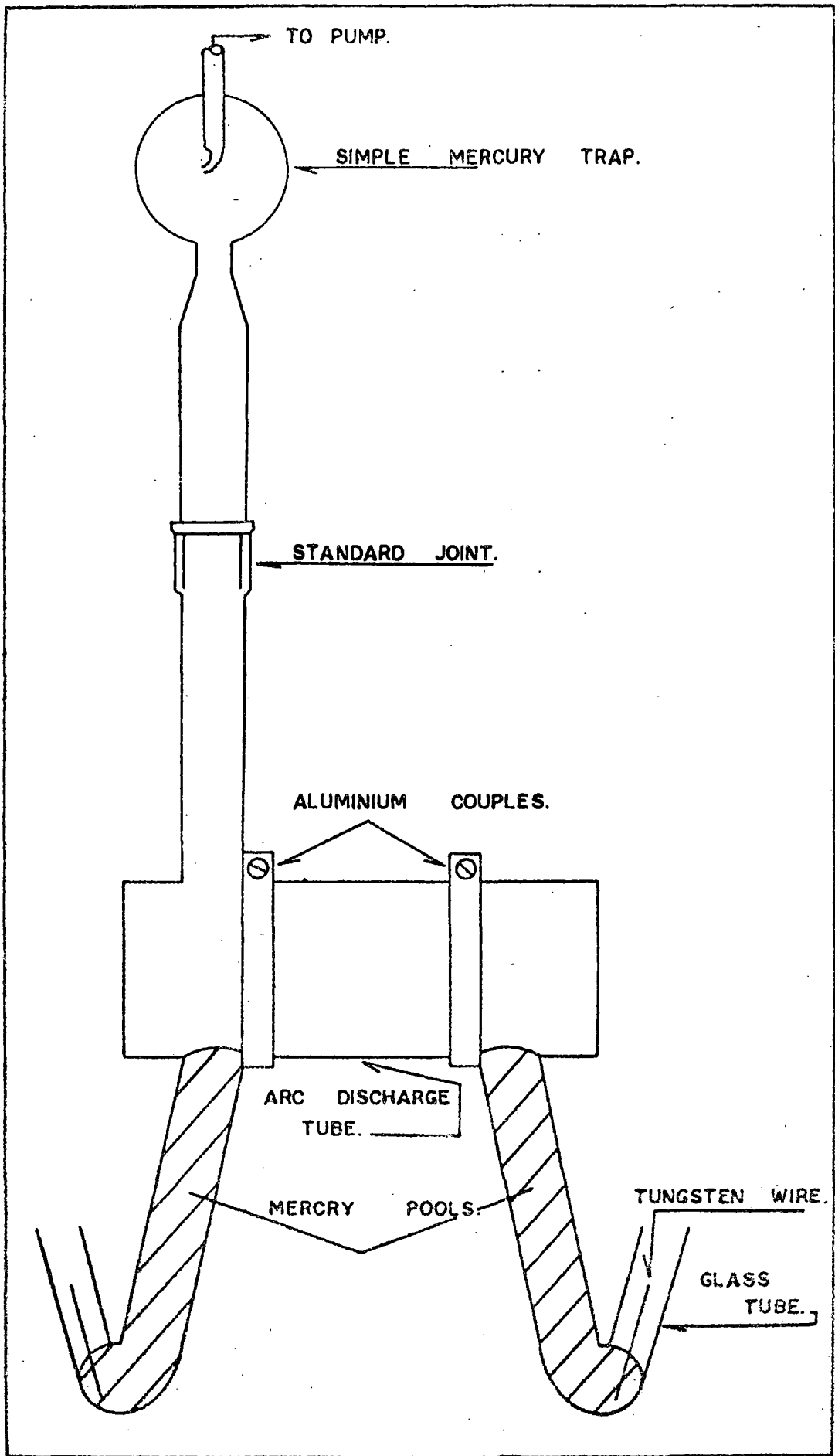


FIG. 2.1. A MERCURY ARC DISCHARGE TUBE.

through the discharge. The tubes were then flushed with the desired gas for two or three days and then the gas was introduced through a microleak of a needle valve to a desired pressure. The experimental set up of a typical experiment has been shown in fig. 2.2.

### 2.3. Preparation of gases

For measurements in dry air, the air was ~~pa~~ passed through two U-tubes containing phosphorus pentoxide powder and caustic potash pellets to remove traces of water vapour, then it was introduced to the discharge tube through a needle valve. Hydrogen and oxygen gases were prepared from electrolysis of a warm solution of pure barium hydroxide in between platinum electrodes in a U-tube. For hydrogen, the gas evolved from the cathode was passed through a hard glass tube containing copper spiral heated electrically. The gas was next passed through series of U-tubes containing phosphorous pentoxide powder and caustic potash pellets. The oxygen gas, evolved in the anode of the electrolysis tube was passed through a flask containing concentrated sulphuric acid. The nitrogen gas was supplied by Indian Oxygen Limited and was passed through concentrated sulphuric acid. After purification has been done in the stated manners the gases were stored in a round bottomed glass flask which is connected to the discharge tube. For measurements in the glow discharges in transverse

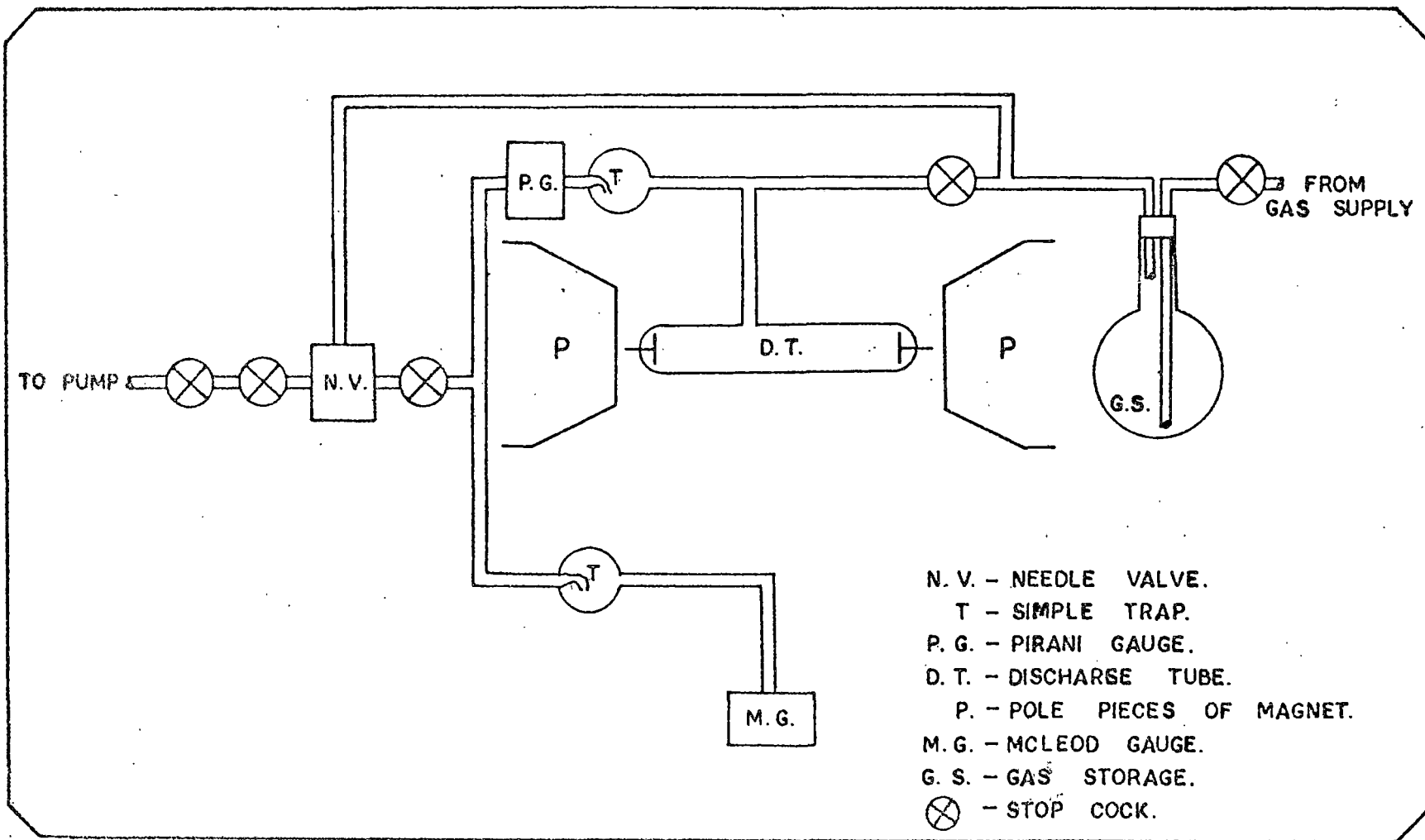


FIG. 2.2.

Fig. 2.2. An experimental set up in longitudinal magnetic field.

TABLE 2.1

Dimensional parameters and other characteristics of the discharge tubes.

Experiments with reference to chapter number.	Dimensions of discharge tubes			Electrodes used and seperation.	Remarks.
	Innder diameter (cm)	length (cm)	Thickness of the tube wall		
1. Probe measurements in trans- verse magnetic field (Chap.III)	4	22	$\approx 0.1$ cm.	brass 16.9 cm.	
2. Probe measurements in longi- tudinal magnetic field(Chap.III)	2.5	8.5	$\approx 0.1$ cm.	brass 5.5 cm.	
3. Measurement of electron tempe- rature of glow discharge in transverse magnetic field(Chap.IV &V)	1.5	19.5	$\approx 0.1$ cm	aluminium 17.5 cm.	at the central region, the tube is constricted with diameter appx. 0.5 cm.
4. Measurements of plasma parameters of low pressure mercury arc in longitudinal magnetic field (Chapter VI and VII)	1.5	8	0.14 cm.	mercury pools <del>arc</del> $\approx 7$ cm.	vertical dis- charge tubes.
5. Investigations on glow processes of low pressure mercury after- glow in axial magnetic field (Chapter VIII)	3.6	9	0.17 cm.	mercury pools $\approx 7$ cm.	horizontal tube fitted with two aluminium coup- lers for r.f. voltage supply.

magnetic field by spectroscopic method, the discharge tubes filled with hydrogen and helium gas at a pressure of one torr was supplied by a supplier. For the usual discharge tubes, after several days of run for outgasing and observation purposes, the glass wall would become coated by impurity materials due to sputtering of the cathode. In this way, these tubes could not be used for spectroscopic measurements, so built-in tubes with aluminium electrodes were preferable. The tubes were constricted in the central portion where magnetic field was applied. The constriction greatly enhanced the radiation output. In the spectrum, no lines of considerable intensity (in the visible region) of any impurity material was observed.

For mercury arcs, triple distilled mercury was used. In course of experiments, occasionally the mercury in the tubes was replaced by fresh supply and the discharge tubes were cleaned and degassed.

#### 2.4. Measurements of pressure

~~Rix~~ Pressure of the gas in the discharge tube was measured by a Mcleod gauge filled with triple distilled mercury. It has been shown in fig. 2.2 that pressure in the discharge tube could not be measured directly because the tube was placed in between the pole pieces of electromagnet,

but a parallel line was used. At the junction between these two vacuum lines the pressure is the same and if the conductance of the two lines are identical, the pressure in the discharge tube would be equal to that at the McLeod gauge. Dushman and Lafferty (1962) have discussed that effective pumping speed,  $S_{eff}$  is given

$$\frac{1}{S_{eff}} = \frac{1}{S} + \frac{1}{C} \quad (2.1)$$

where  $S$  is the speed of the pump (50 litres/min) and  $C$  is the total conductance of the line. For viscous flow, conductance of a line is given by

$$C = 2.84 \frac{a^4}{l} P_2 \quad \text{litre/sec} \quad (2.2)$$

where  $a$  and  $l$  are the radius and length of the tubes and  $P_2$  the upstream pressure. So the parallel lines as shown in fig. 2.2 were identical as far as possible. The lines were made of rubber and polythene pressure tubes. For the same reason, the needle valve was placed in between the junction of identical lines and the pump. A pirani gauge was used in the discharge tube line and through it the pressure of air could be compared. For built-in glow discharge tubes, the pressure was stated to be one torr.

The pressure of mercury vapour was determined from standard tables (Hodgman, 1956) after noting the inside wall temperature ( $T_w$ ) of the discharge tube which is equal to the outside wall temperature increased by the temperature drop over the tube wall resulting from the energy which is dissipated in the tube and carried away via the tube wall (Verweij, 1960). The outside wall temperature was measured by a mercury in glass thermometer when the arc was in a steady state. Generally the arcs were cooled by electric fans. So a steady state of an arc corresponded to a steady outer wall temperature. The temperature drop as calculated by Verweij can be estimated by assuming that the total energy dissipated  $W = E i$  per cm. of tube length ( $E$  is the intensity of electric field, measured by noting the voltage across the arc minus standard cathode fall of 10 volts as determined by Lamar and Crompton (1931), then divided by arc length and  $i$  is the arc current). This energy is carried away by thermal conduction through the surface area of 1 cm. of tube length, thus through  $2 \pi R$  cm<sup>2</sup> ( $R$  = internal radius of the discharge tube), since the amount of energy which escapes as radiation through the tube wall is relatively small, the ultraviolet resonance radiation being absorbed within a very small penetration depth in pyrex glass wall. The temperature drop  $\Delta T_w$  is given by

$$W = 2 \pi R K \frac{\Delta T_w}{d} \quad (2.3)$$

where  $d$  is the thickness of glass wall (0.14 cm) and  $K$  is the thermal conductivity of the glass ( $K_{\text{pyrex}} = 11 \times 10^{-3}$  joule/cm/sec/°C). For a typical operation of arc at a current of 2.5 amp.,  $\Delta T_w$  amounted to 7-8°C. A plot of saturated vapour pressure of mercury ( $P_{\text{Hg}}$ ) with  $T_w$  has been shown in fig. 2.3. Since number density of ground state mercury atoms  $n_g$  is directly related with  $P_{\text{Hg}}$  by the relation

$$n_g = 3.3 \times 10^{16} \frac{P_{\text{Hg}}}{T_w} \quad (2.4),$$

in fig. 2.3,  $n_g$  also has been plotted against  $T_w$ . In all of the arc measurements, dry air was admixed with mercury vapour. The pressure of dry air was measured by the McLeod gauge.

## 2.5. Magnets and power supplies

In the experiments electromagnets were used. Depending upon the diameters and lengths of the discharge tubes, the ~~size~~ diameter of the pole-pieces (10 cm. x 8 cm. square and 5 cm diameter) and length between them were adjusted. For a specific experiment, the pole-pieces were so chosen that the magnetic field was uniform and without any radial component at the location of discharge tube. For measurements in axial magnetic field, the total discharge tube was placed in between the pole-pieces as shown in

Was this checked?  
If so, how?

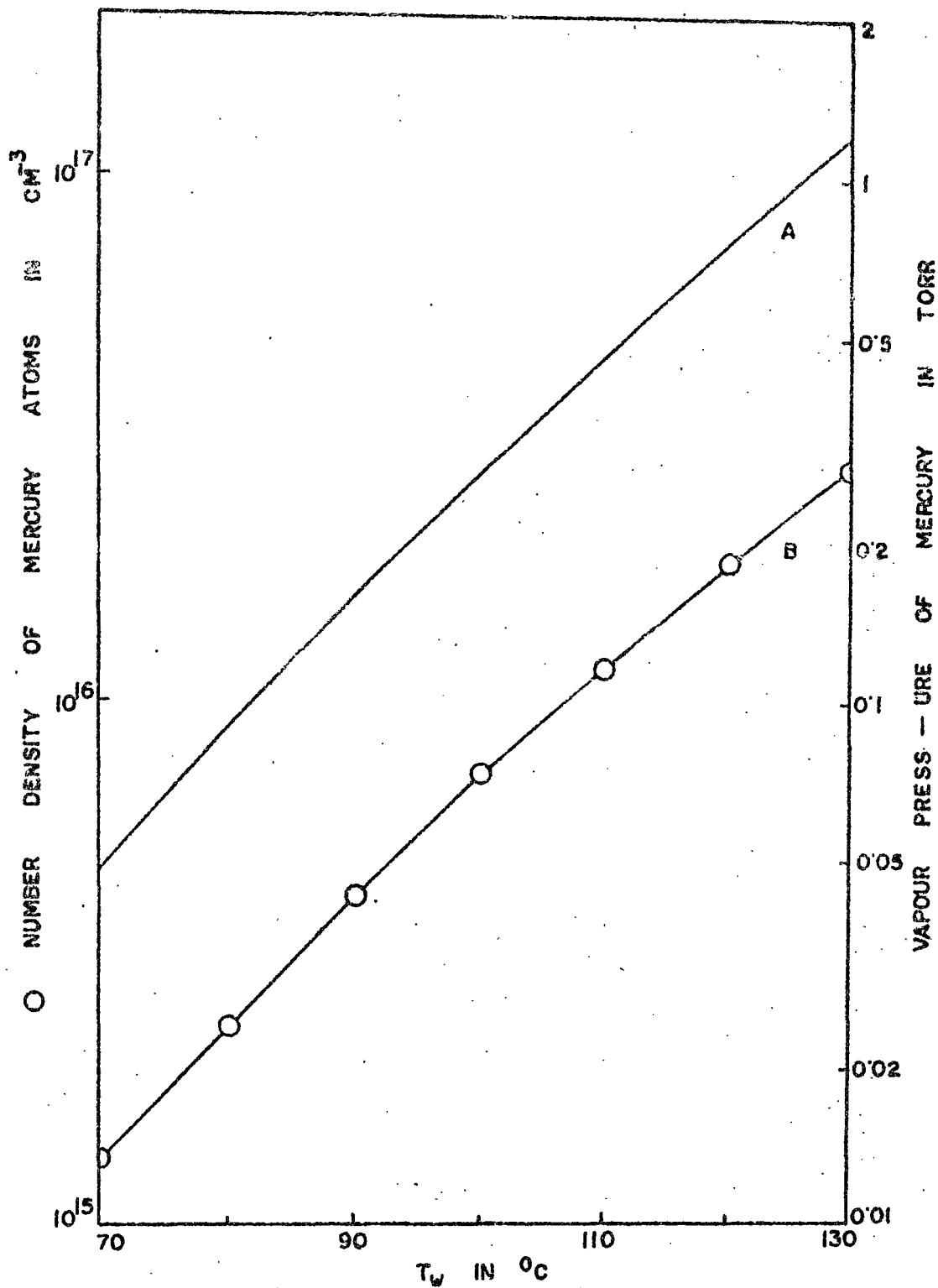


FIG. 2.3.

Fig. 2.3. Variation of vapour pressure and number density of mercury atoms with temperature of outer wall ( $T_w$ ) of the discharge tube.

fig. 2.4, when a transverse magnetic field was used only a portion of positive column of the discharge where measurements were carried out, was placed in between the pole-pieces (fig. 2.5 (b) ).

The magnetic fields were measured by a calibrated differential gauss meter. The electromagnets were powered by a stabilised d.c. supply. where?

The power supply for generating glow discharges, was a stabilised electronic d.c. supply ( 0 - 1200 g volts in steps of 105 volts). The circuit for construction of the power supply was taken from Radio Amateur's Handbook (1965). The supply was connected to discharge tubes via a high wattage balast resistor (fig. 2.4). For a.c. glow discharges, 50 Hz common supply was used through a step up transformer whose input was connected to an auto-transformer. The mercury arcs were struck by a d.c. generator (200 - 240V.) whose voltage output could be adjusted to a constant value by an variable external resistor. For glow discharges, the ~~discharge~~ discharge current was varied between 8 to 30 mA. and arc current was varied between 1.5 to 5 A.

## 2.6. Measurements of parameters of plasma with and without magnetic field by probe method

The parameters that were measured are electron temperature and axial electron density of the discharge. A cylindrical Langmuir probe of 0.019 cm. diameter was inserted

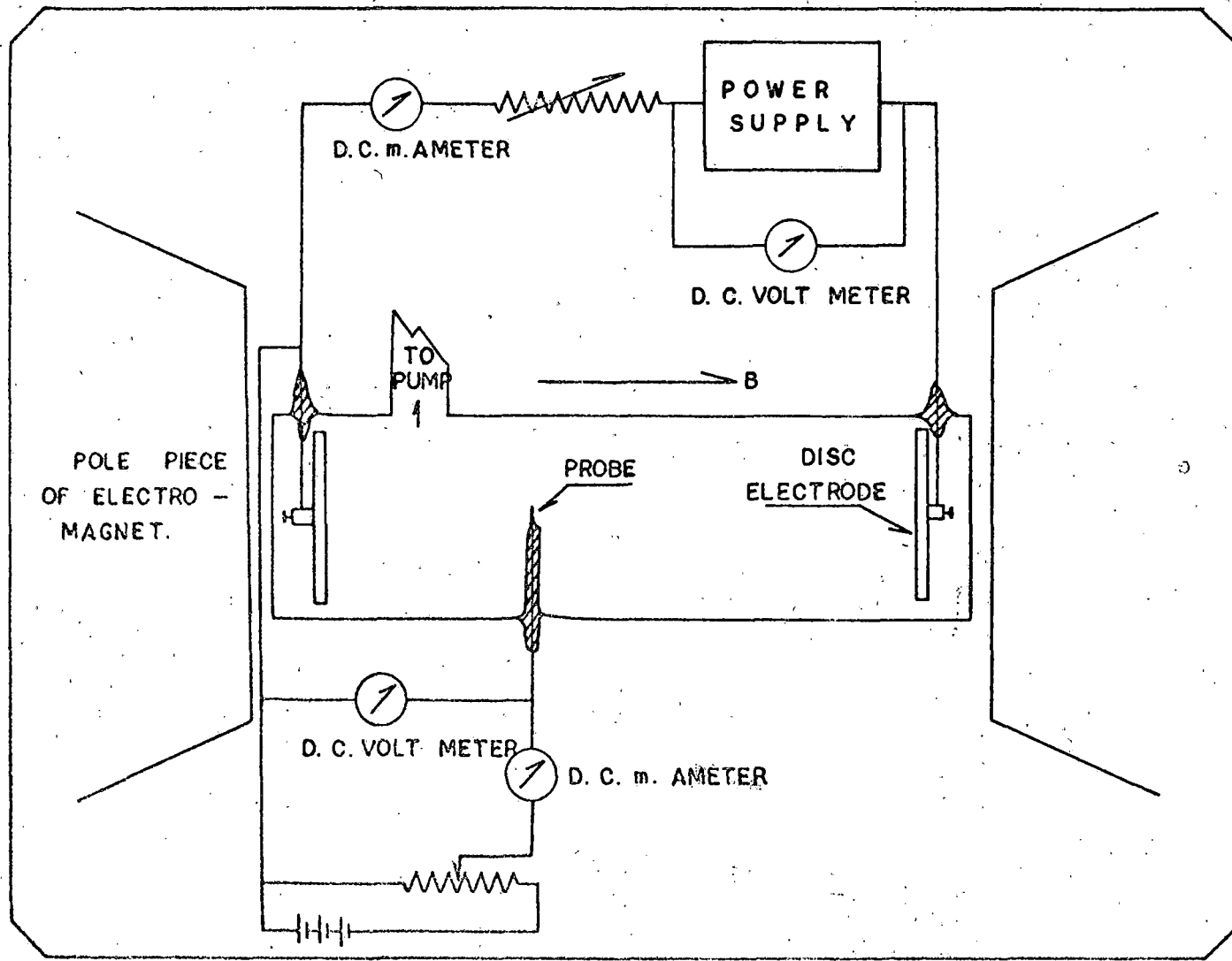


Fig. 2.4. Probe circuit and discharge tube circuit.

FIG. 2.4.

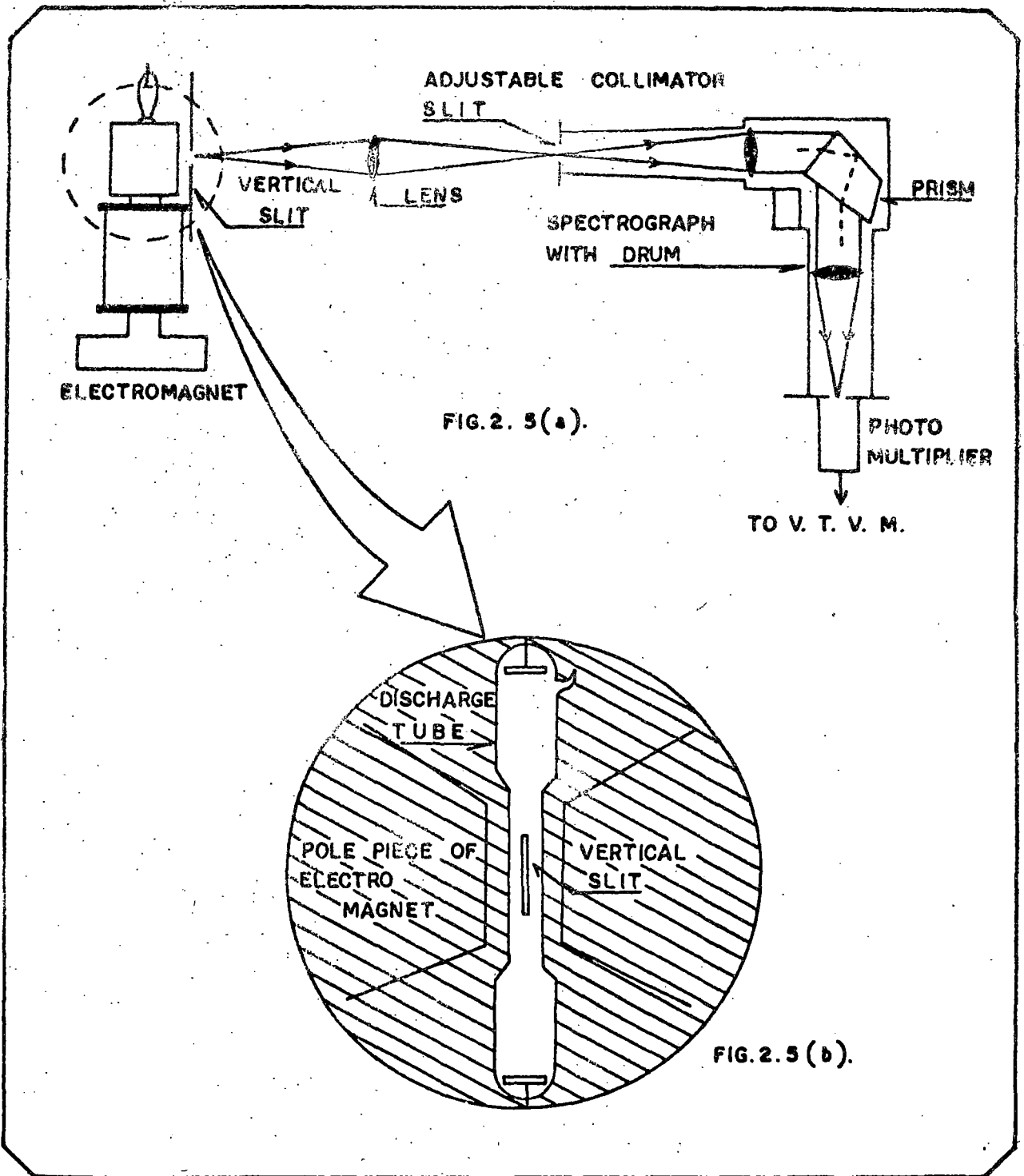


Fig. 2.5. Experimental set up for spectroscopic measurements.

in the discharge tube through a glass jacket. The material of probe was tungsten. The center of the probe was placed at the axis of the discharge tube and the probe was perpendicular to the axis and also to the magnetic fields when used. Generally the length of the probe ( $l$ ) should be much larger than radius ( $r_p$ ) of the probe. But an upper limit of the ratio  $l/r_p$  may be determined from the expression of electron saturation current to the probe

$$I_{e \text{ sat}} = -n_e e A_p \left( \frac{T_e}{2\pi m} \right)^{1/2} \quad (2.5)$$

where  $n_e$ ,  $T_e$ ,  $m$  and  $e$  are the number density, temperature, mass and charge of electrons and

$$A_p \text{ is the probe collection area, } A_p = 2\pi r_p l.$$

$I_{e \text{ sat}}$  is desired ~~ax~~ not too large so that probe would not become too hot (or incandescent) and damaged as a consequence of the energy delivered at the probe by the electron current. We utilised a 4.1 mm. long probe placed at a distance 2.5 cm. away from the anode for measurements in transverse magnetic field. For a tube of diameter 4 cm.  $l/r_p$  was nearly 43 and for measurements in longitudinal magnetic field the probe was 2.2 mm. long and placed 1.3 cm. away from the discharge, so that  $l/r_p \approx 23$  for a tube of diameter 2.5 cm.  $r_p$  was measured by a micrometer screw gauge and  $l$  by a travelling microscope. In this way the electron density that was determined ~~x~~ was not exactly the value at the axis but an average corres-

ponding to  $L$ . It will be shown in Chapter III that for the probes of these characteristic dimensions in practically all of the investigated discharges, the electron attraction characteristics may be interpreted according to orbital motion theory.

The probe measuring circuit has been shown in fig. 2.4. The probes were biased with a d.c. dry battery through a potentiometer. The most important probe current was recorded by a Philips PM 2403 electronic multimeter which has a minimum of full scale deflection for a current of  $1 \mu A$ . Another advantage of this particular meter is that an automatic polarity reversal technique is built-in. So external polarity reversal was not necessary for going from ion current to electron current and a polarity reversal indicator meter clearly indicates the exact point of reversal. The other point of the probe circuit was connected to anode and the probe voltage which is generally negative with respect to anode was varied in steps of 0.5 - 2 volts. The probe current, which was measured, was the total current through the probe. Electron current  $I_e$  was determined by subtracting ion current  $I_i$  from the total probe current

$$I_e = I_{tot} + |I_i| \quad (2.6)$$

The details of probe data analysis have been given in chapter III.

## 2.7. Diagnostics by spectroscopic method

Spectroscopic method was utilised to determine electron temperature in both types of magnetic fields. In the investigations, the experimental set up was the same. A schematic diagram of the experimental set up has been shown in fig. 2.5 (a). The radiations from the axial regions of vertical discharge tube placed in between the pole pieces of the magnet after passing through a vertical slit was focussed by a double convex lens on the vertical slit of the collimator of the spectrograph. In the spectrograph, there was a Pellin-Broca prism for 90 degree deflection of the spectrum. Such a mounting was appropriate as a monochromator with fixed slit. The exit slit was in a direction 90 degree with the plasma source. The wavelength is changed by rotating the prism with a mechanical arrangement fitted with an accurately calibrated drum. The wavelengths of the radiations were further checked from standard values given in International Critical Tables (1926). Generally, this type of apparatus has a low resolving power which would be advantageous in our investigations and this will be discussed in Chapter IV. The slit width which could be varied with a micrometer arrangement, was varied from 0.25 mm. to 1 mm. depending on the response of lines chosen to the photomultiplier. For a set of observation however,

the slit width was fixed. For measuring  $T_e$ , two criteria for suitable line choice may be mentioned:

(i) The energy of separation of the upper states of the two transitions chosen should be comparable to the value of  $T_e$ . But this was not possible always. <sup>For</sup> From two lines in the visible region which had sufficient response to the detector the energy of separation of upper states some times became smaller than the value of  $T_e$ . One of the remedy<sup>ies</sup> that is suggested is to use one of the ionic lines and one atomic line. But in magnetic field the <sup>intensities of</sup> atomic and ionic lines vary differently. The reason behind is that atomic lines are determined by  $T_e$  and  $n_e$  which is affected by magnetic field, whereas for ionic lines, the radiation would be affected by magnetic field through  $T_e$ ,  $n_e$  and  $n_i$ . Moreover no sufficiently strong ionic line was observable in the discharges investigated.

(ii) the lines should be such that in the near vicinity there would be no other line, so that  $\int_0^{\infty} I_{\nu} d\nu$  is the measure of total intensity of a radiation with frequency  $\nu$  and in our investigation slit-widths were comparatively wide enough ~~to~~ as to detect the total intensity of radiation.

The collimator was focussed by rack and pinion arrangements, the selected line was focussed on the cathode of the photomultiplier M10FS29V  $\lambda$  operated at 1425 V. The head-on type photomultiplier which has low mean radiation equivalence of dark current was placed in a darkened chamber behind the exit slit. The power source of photo

multiplier was made in two sections: the first was 1200 V. stabilised pack to supply the dynode voltage while the second was used to furnish some 225 V. between the final dynode and the anode (fig. 2.6). The last voltage source was also used to operate the vacuum tube voltmeter, which consisted of two 6J7 tubes operating with about 32V. on the plates and about 1.3 V negative grid bias. The grids were connected to the two ends of the resistor  $R_1$  ( $600 \text{ K}\Omega$ ), which was in series with the plate of the photomultiplier tube. When current flowed through this resistor, a voltage drop occurred and one of the 6J7 tubes drew less current producing an imbalance in the plate circuit. A 0-200  $\mu\text{A}$  meter between the plates measured this imbalance.

When the signal approximated 3V, the 6J7 reached cut-off, and beyond this point there was no increase in the meter deflection. With no light on photomultiplier tube and a rough balance obtained with  $R_4$ , the meter was set to zero with  $R_2$ . In this way the effect of photomultiplier dark current was eliminated completely. Then, with 3V or more applied to resistor  $R_1$ , the meter was set to full scale deflection by means of control  $R_3$ . The micro-meter at the out put recorded the intensity of the spectral line. The slit was adjusted so that meter deflection corresponding to the line with strongest response to the photomultiplier was well within the range of full scale deflection.

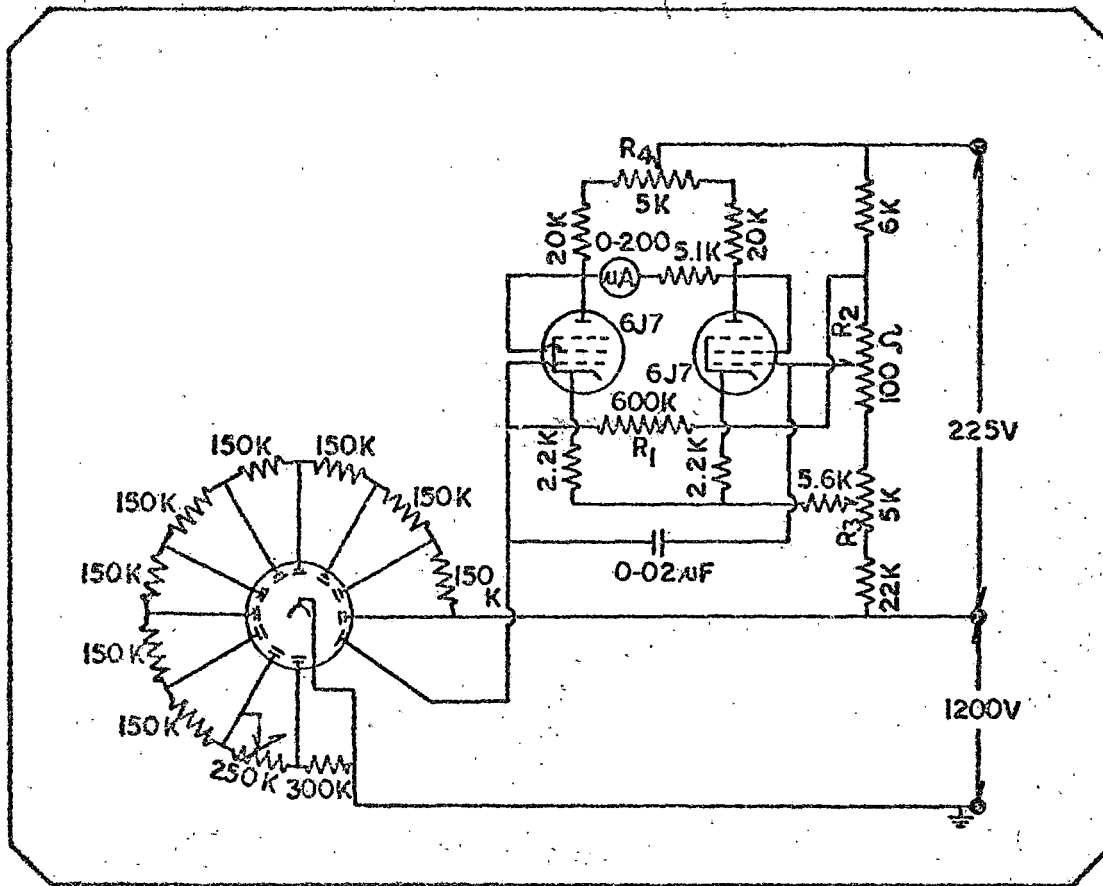


FIG. 2.6. PHOTOMULTIPLIER CIRCUIT.

The sensitivity of a photomultiplier depends on wavelength of incident radiation and on quantum efficiency of the cathode material (including the effect of photomultiplier's window material). Percentage Quantum efficiency of M10FS29V  $\lambda$ , taken from Carl Zeiss brochure No.40-637-2, has been reproduced in fig. 2.7. From this plot the cathode radiant sensitivity  $S$  in amperes per watt corresponding to a radiation of wavelength  $\lambda$  ( $\text{\AA}$ ) is calculated as

$$S = \frac{Q \lambda}{12395 \times 100} \quad (2.7)$$

here  $Q$  is the percentage quantum efficiency. From  $S$ , the relative spectral sensitivity for two lines was calculated and the microammeter reading for total intensities of lines was corrected for relative spectral response of the photomultiplier. Moreover emission coefficient corresponding to a radiation with frequency  $\nu$  which is directly proportional to observed total intensity can be separated into a continuous and discrete part

$$E_{\nu} = E_{\nu, c} + E_{\nu, L} \quad (2.8)$$

$E_{\nu, L}$ , contains the desired spontaneously emitted energy within the line,  $E_{\nu, c}$  was eliminated by balancing the V.T.V.M. to the null of meter reading with resistors in the circuit when the continuum radiations

Not clear  
What is  
E<sub>ν</sub>?

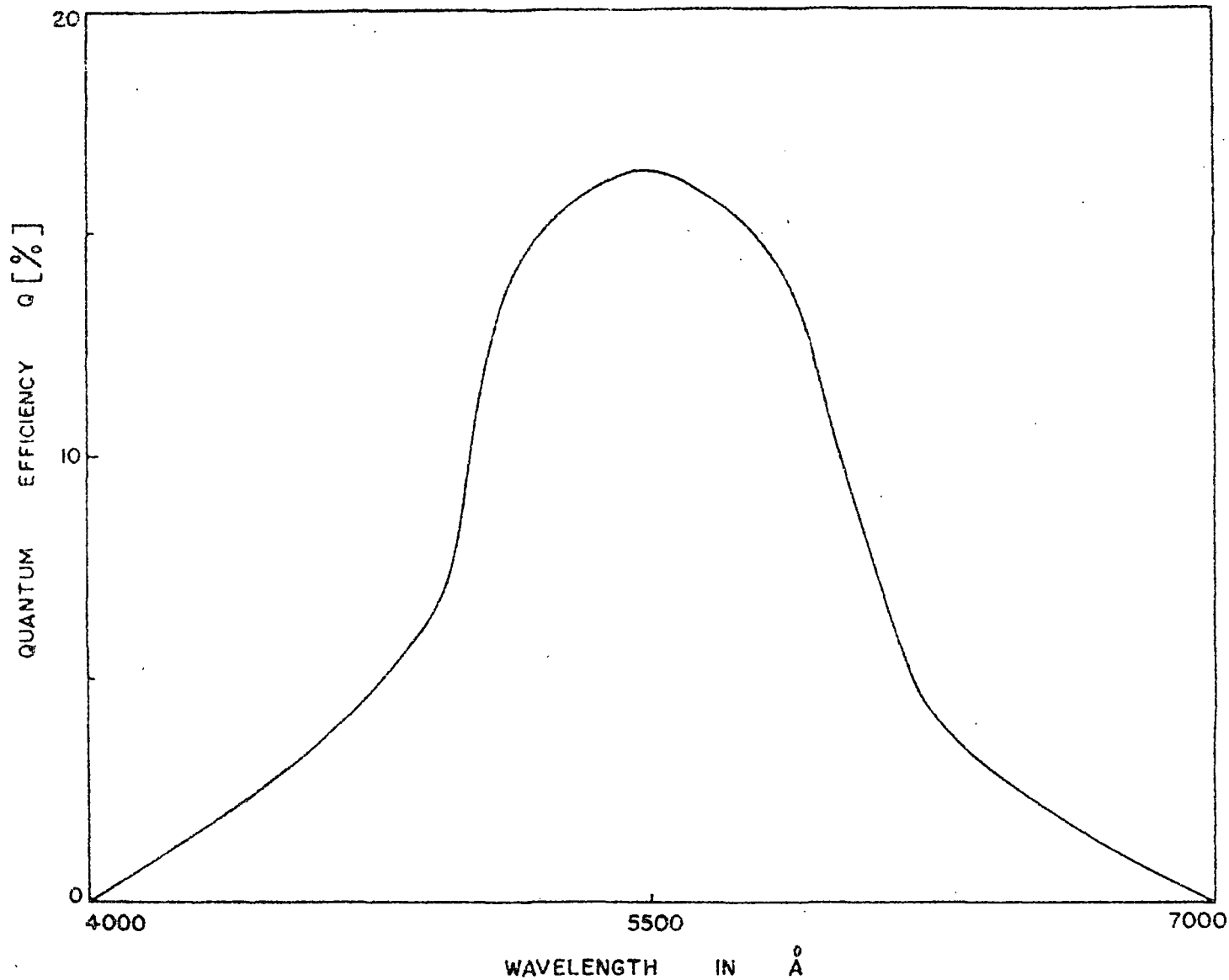


FIG. 2.7. QUANTUM EFFICIENCY IN % OF PHOTOMULTIPLIER  
 MIOFS29V $\lambda$  ( VEB CARL ZEISS JENA BROCHURE NO. 40-637-2. )

at the near vicinity of the line was focussed on the photo-multiplier tube cathode and the contribution for  $\epsilon_{v,c}$  was found to be negligible.

2.8. Measurements of variations of discharge current and voltage across a low pressure mercury arc in longitudinal magnetic field

The currents were recorded with 0-5A meter, connected in series with the discharge tube. A V.T.V.M. of internal resistance  $35 \text{ M}\Omega$  was utilised to measure the voltage across the arc.

It was observed during the experiments that with time the arc voltage slowly and gradually increased. Cobine (1958) explained the phenomenon as due to continuous evaporation of k cathode surface by heating. ~~From~~ For evaporation of cathode, the positive column increases. As electric field in the positive column tries to remain constant, the voltage drop across the arc increases continuously. A measurement of this continuous increase of voltage with time showed that, fortunately, in the range of discharge currents in our experiments, this was a slow process. The arcs were vertical and the cathode was the lower mercury pool. Our intention was that the evaporated cathode material may be compensated by the condensed

mercury that was returning to the lower pool by ~~gas~~ gravity. However, the measurements of variation of voltage and current with magnetic field were made rapidly enough so that the slower process as mentioned above may be neglected.

## 2.9. Measurements of persistence times of a mercury afterglow

Measurements of persistence times of a mercury afterglow (admixed with dry air) were carried out in a cylindrical discharge tube (details in fig. ~~2~~ 2.1, table 2.1). As we are interested to study the behaviour of a recombining plasma with and without a magnetic field, the effect due to diffusion transport was lessened by taking a discharge vessel with comparatively large diameter and dry air was admixed to increase the pressure.

Two aluminium couplers clamped in the middle of the discharge tube from outside were connected to a Hartley oscillator to supply the radio frequency voltage. The couplers were were separated by 2.35 cm. The level of r.f. power supplied by the oscillator was low enough so as ~~tax~~ not to cause a breakdown of the gas. A 6V6 ~~aa~~ vacuum tube was utilised as the oscillator. The r.m.s. voltage of the oscillator output was measured by a half wave rectifier made of 6H6 tube. The frequency was calibrated by a digital frequency meter. The measured r.m.s. voltages and frequencies corresponding to the dial readings of the condenser in the oscillator has been given in Table 2.2.

TABLE 2.2

r.m.s. voltage and frequency corresponding to condenser dial reading of the oscillator.

-----  
 Dial reading            r.m.s. voltage    ,    frequency  
                           , of r.f. oscilla-    ,  
                           tor (volts)            (MHz)  
 -----

1.	91.0	-
5	96.0	0.594
10	100.0	1.068
15	100.5	1.338
20	105.0	1.364
25	120.5	1.464
30	120.0	1.583
35	122.5	1.623

-----

During the experiments, the arc discharge was run for a few minutes, so that a steady condition was reached and  $T_w$  was noted. Then the primary arc discharge was switched off. Generally an afterglow persists for a ~~xxx~~ fraction of second. But due to the supply of r.f. power to the couplers, the glow persisted for longer time and then disappeared. When no r.f. power was supplied to the couplers, the afterglow did not persist and disappeared in

a fraction of second ~~as~~ usually. The persistence times of the glow with rf ~~power~~ power supplied were recorded by two stopwatches. The details of the measurement procedures have been discussed in chapter VIII. It will be discussed there that the decay processes (directly related to the persistence times) generally depends upon the temperature of the surrounding environment. So the persistence times were recorded in the same environment for a set and no forced cooling of the primary arc was made.

#### 2.10. Possible sources of errors

It was observed that for a discharge system to be leakproof, degassed and stable, several days of continuous running was needed. Our desire was that the plasma would exhibit the same physical behaviour day after day dependent only upon some externally controlled dial setting. Unfortunately, the very nature of the plasma is a non-linear one - not restricted to a single unique operating mode. From this point of view, a stabilised discharge free from striations and any other turbulence was desirable. Moreover, some times oscillations were visible in the plasma when a magnetic field was present. The oscillations were reflected in external measuring meters. These oscillations determined the upper limits of the magnetic fields used and below this limit the readings were acceptable. In probe method, the magnetic fields used were of

comparatively low values. In spectroscopic method, the readings of the output  $\mu\text{A}$  meter which measured the total intensities of a lines were observed to be stable after six to eight hours of warming up of the V.T.V.M. circuit. Nevertheless some sources of errors may be identified. There are: pressures were not measured at the discharge tube, but a parallel vacuum line was used. For built-in discharge tubes, the pressures were stated to be one torr which could not be verified. Pressure of mercury vapour was determined by noting  $T_w$  at a point of the discharge tube. Moreover, in calculation  $T_w$  was assumed equal to gas temperature  $T_g$  and  $T_g$  was considered to be uniform across the tube cross section. As it was not possible for us to determine  $T_g$  at the axis, the above assumption was made.

The purify of the gases was not checked. But it was assumed that the gases utilised were free from impurities. Spectroscopic investigation however, did not reveal the presence of any other gas as impurity.

What about  
Hg contamination  
from the  
method given

No correction was made either for possible contaminations of Langmuir probes or for changes of work function of comparatively hot probes. Moreover, the results obtained by a method could not be verified by another diagnostic method in the same condition of discharge.

Several other assumptions were also made in course of calculations and these will be discussed, subsequently.

## References:

1. Cobine, J.D. (1958), Gaseous conductors: theory and engineering applications (Dover Publication, New York).
2. Dushman, S. and Lafferty, J.M. (1962) Scientific Foundations of Vacuum Techniques, 2nd. Edn. (John Wiley, New York).
3. Hodgman, C.D. (1956), Hand Book of Chemistry and Physics, 38th. Edn. (Chemical Rubber Publishing Co., Ohio).
4. International Critical Tables of Numerical Data (1926), Vol.5 (McGraw Hill Book Co., NY).
5. Lamar, E.S. and Compton, K.T. (1931) Phys. Rev. 37 1069.
6. Radio Amateur's Hand Book (1965), 42nd. Edn. (American radio relay league, West Hartford).
7. Verweij, W. (1960), Philips Res. Rep. Suppl. No.2.

## CHAPTER III

MEASUREMENT OF ELECTRON TEMPERATURE AND ELECTRON DENSITY  
IN LOW DENSITY MAGNETISED PLASMA BY PROBE METHOD.

## 3.1. Introduction

The measurement of electron temperature and radial electron density in low density plasma in molecular gases magnetised by either a transverse or a longitudinal magnetic field have been carried out by Langmuir probe method. The probe method is one of the standard methods of measuring plasma parameters. The theory of Langmuir probe in zero magnetic field rests on two assumptions: (a) the dimension of probe and (b) the thickness of space-charge sheath surrounding the probe is small compared to the mean free path of the electrons and ions. The limitations as well as the validity of these assumptions have been discussed by a larger number of workers. Nevertheless, the values of the parameters obtained by this method compare very favourably with the values obtained by other standard methods.

As most of the effects of magnetic field on a plasma depend on the manner in which these parameters are affected by the field itself, an experimental study of the nature of variation of these parameters by probe method has been reported. This will enable us to put to a

direct experimental test the theoretical deductions regarding electron temperature and electron density variation in both longitudinal and transverse magnetic fields.

A magnetic field  $B$  applied to the plasma effectively reduces the free paths of the charged particles perpendicular to  $B$  to less than the radius of curvature  $\rho = mv/eB$ ,  $v$ ,  $m$  and  $e$  being the velocity, mass and charge of the particle and hence for a probe collecting across magnetic field assumption (a) becomes invalid in moderate magnetic field. For this purpose the magnetic field used in the present experiment has been kept below 100 G. The validity of assumption (b) depends upon the sheath thickness and thus on plasma density, type of gas and on  $B$ . In our experiment the plasma density has been kept relatively high ( $> 10^9/\text{cm}^3$ ) and the magnetic field below 100 G. Moreover in the experiment, molecular gases have been utilised and the electronic energy in the molecular gases is supposed to be much lower than in atomic gases because of the ability of the molecules to absorb energy from the electrons by vibrational and rotational excitation in collisions at low energies. Such excitation is not possible in monatomic gases. In this way the sheath thickness which is assumed to be of equal value to Debye length given by the expression (Krall and Trivelpiece, 1973),

$$\lambda_D = 4.9 (T_e / n_e)^{1/2} \text{ cm.} \quad (3.1)$$

where  $n_e$  and  $T_e$  are the number density ( $\text{cm}^{-3}$ ) and temperature ( $^{\circ}\text{K}$ ) of electrons, will be much less so that assumption (b) holds even when a magnetic field is present. Under these conditions, the electron temperature and electron density can be obtained as has been shown by Bohm et al (1949) and by Kagan and Perel (1969) as in the case without the field.

### 3.2. Experimental arrangement

The experiment in which electron temperature and electron density have been measured has been performed in two parts: (a) when the magnetic field is transverse, & (b) when the magnetic field is longitudinal, both with respect to the direction of the discharge current which is along the axis of discharge tube. Measurements have been made in d.c. glow discharges in air, hydrogen, nitrogen and oxygen. For molecular gases the excitation levels are widely spread out upto ionization potential and inelastic losses set up at low energies and these are so distributed so as to produce an approximate Maxwellian distribution.

For transverse field, the lines of force were exactly perpendicular to the axis of the discharge tube and the field was introduced in the positive column of plasma. For longitudinal magnetic field, the discharge tube was placed in between the pole pieces of electro-magnet, producing an uniform field without any radial

component at the location of discharge tube. The probes were of cylindrical tungsten wire of 0.019 cm. diameter. In case of transverse magnetic field it was 4.1 mm. long, hence the ratio  $l/r_p \approx 43$  ( $l$  is the length and  $r_p$  is the radius of the probe) and was placed at a distance 2.5 cm. away from the anode. In case of longitudinal magnetic field the probe was 2.2 mm. long,  $l/r_p \approx 23$  and was placed 1.3 cm. from the anode. The pressure of the gases in the experiment have been measured as described in chapter II and entered in Table 3.1.

Probe voltages were supplied by a dry battery and voltages were measured with respect to anode. Keeping the pressure constant, the magnetic field was introduced and the probe potential was changed from negative values with respect to plasma potential to positive values far into electron attraction region. Other details of the experimental arrangement have been given in chapter II.

TABLE 3.1

Pressure of discharge in different gases.

Gas	Pressure in torr in Transverse magnetic field.	Pressure in torr in Longitudinal magnetic field.
Air	0.4	0.6
Hydrogen	0.7	1.0
Oxygen	0.5	0.4
Nitrogen	0.5	0.6

The discharge currents were varied between 9 and 12 mA.

### 3.3. Results and Discussions

#### 3.3.1. Probe data analysis and methods of measurements ~~to~~ of $T_e$ and $n_e$

In figs. 3.1 through 3.5 probe currents and probe voltages with respect to anode have been plotted for different gases when either transverse or longitudinal magnetic field was present. Then the logarithm of probe current and probe voltage was plotted. The characteristics have three distinct parts: the region of positive ion saturation current, the region of partial electron current known as the electron temperature regime and the electron saturation current regime. It is observed that electron current  $I_e$  is never saturated. Increase in electron current with increasing positive potentials is expected due to growth of effective collecting area as the sheath expands. In principle the space potential (or the plasma potential) may be determined from the characteristic. When the two distinct parts in the electron attraction region of the characteristic have a sharp crossing known as knee of the characteristic, the voltage corresponding to knee or break off point is the space ~~pa~~ potential. In our experiment a sharp knee was not obtained, instead a round knee was observed. The possible reason may be either a deviation from Maxwellian distribution or drain diffusion. So, two tangents have been drawn to the

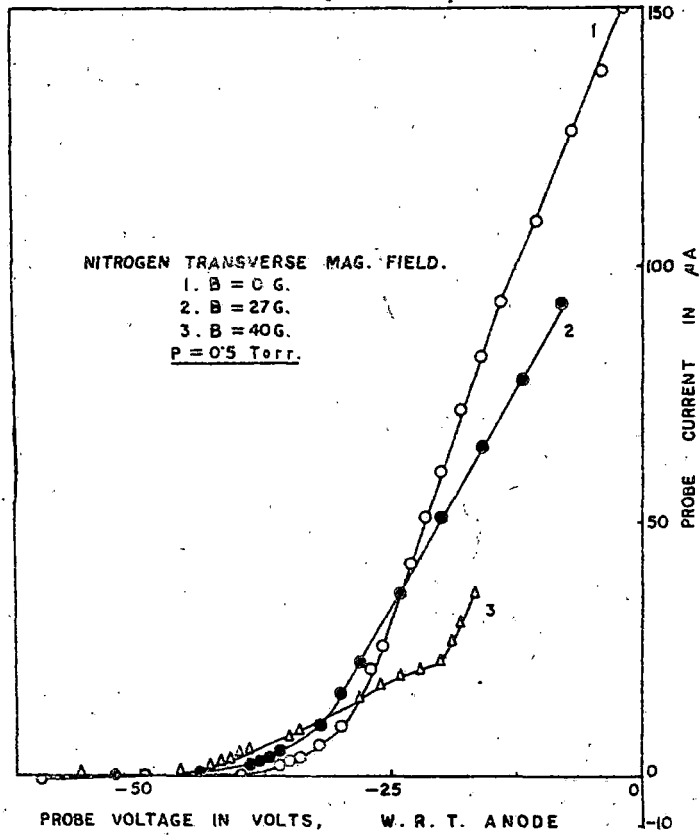


FIG. 3.1a.

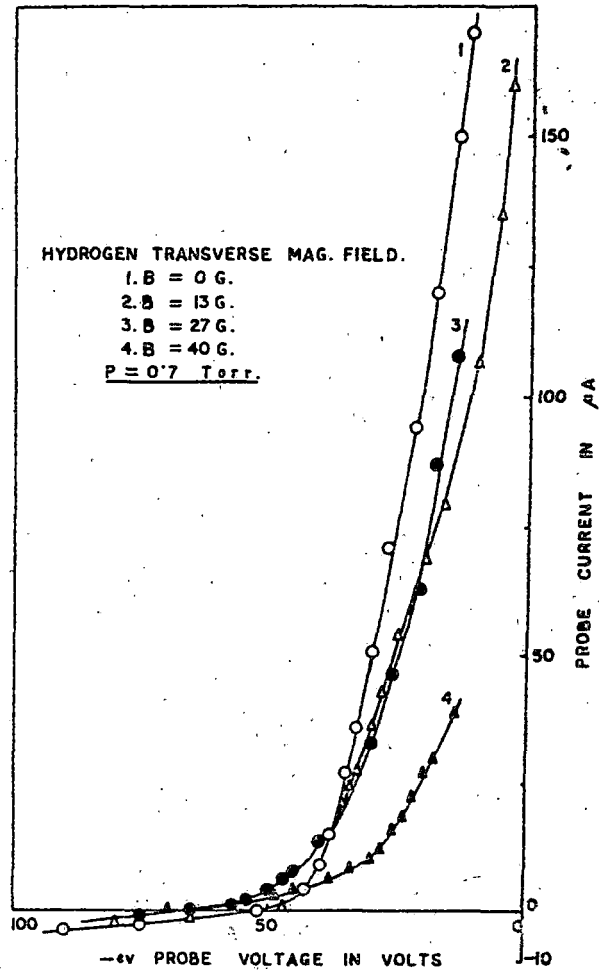


FIG. 3.1b

Fig. 3.1. Current-voltage characteristic of probe with and without transverse magnetic field for (a) nitrogen, (b) hydrogen.

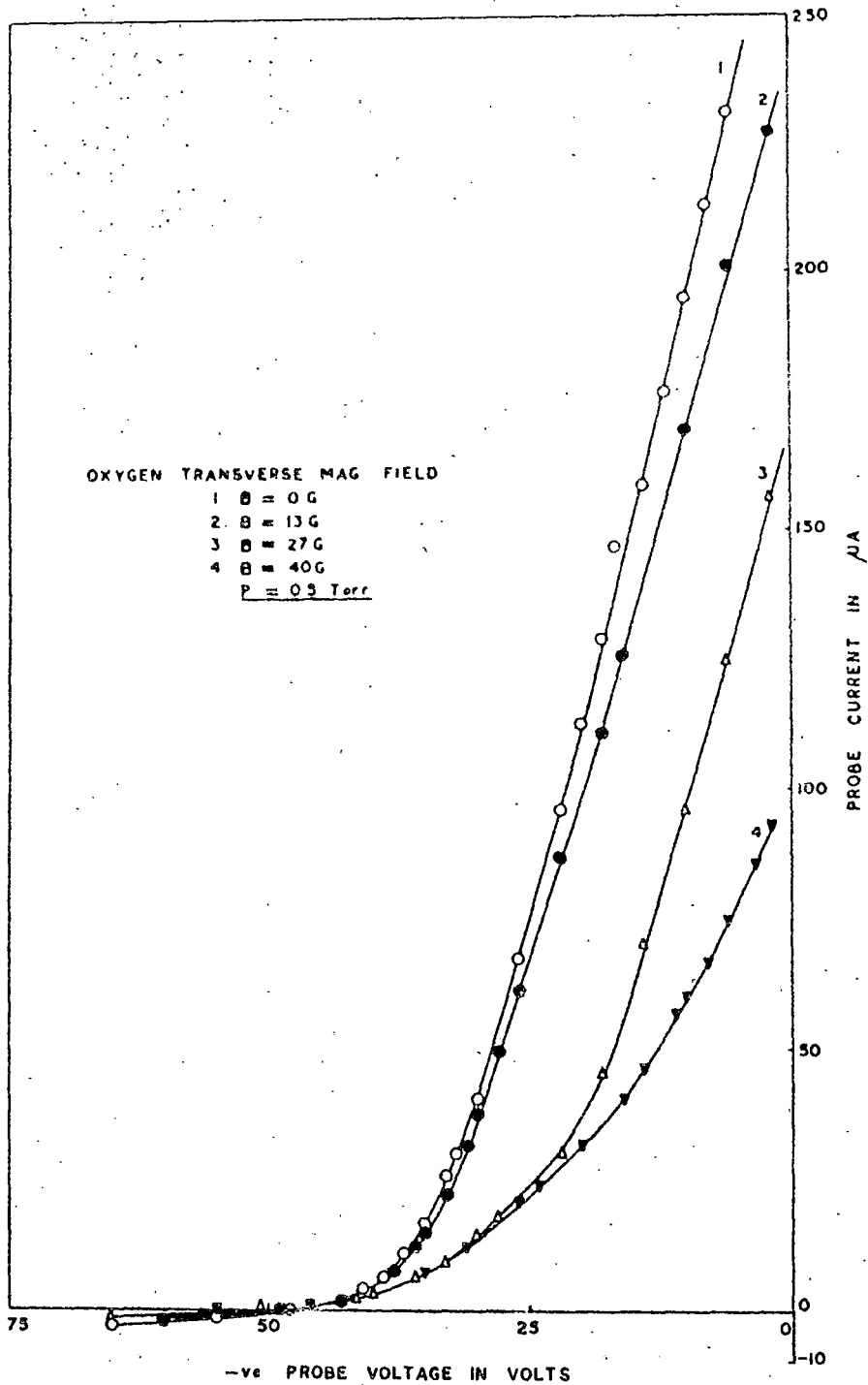


FIG. 3.2.

Fig. 3.2. Current-voltage characteristic of probe in oxygen in transverse magnetic field.

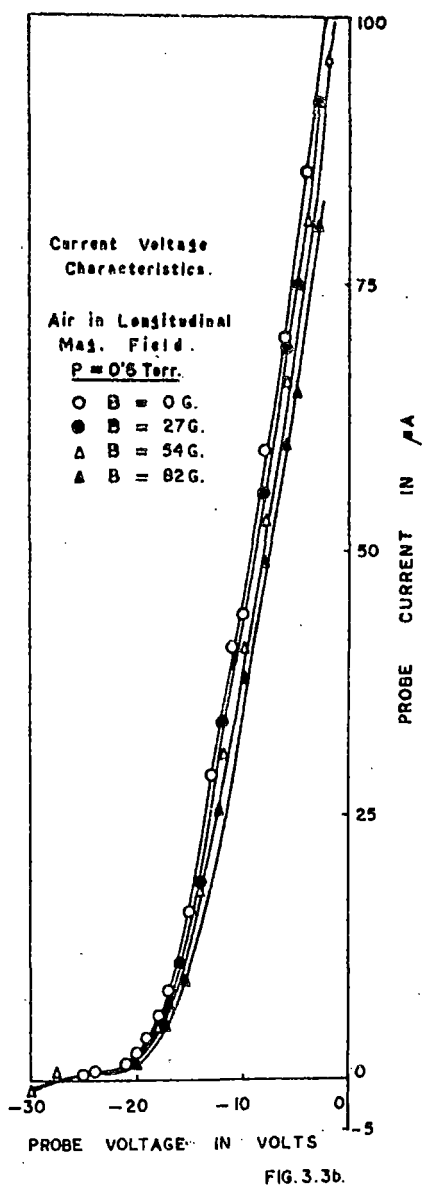
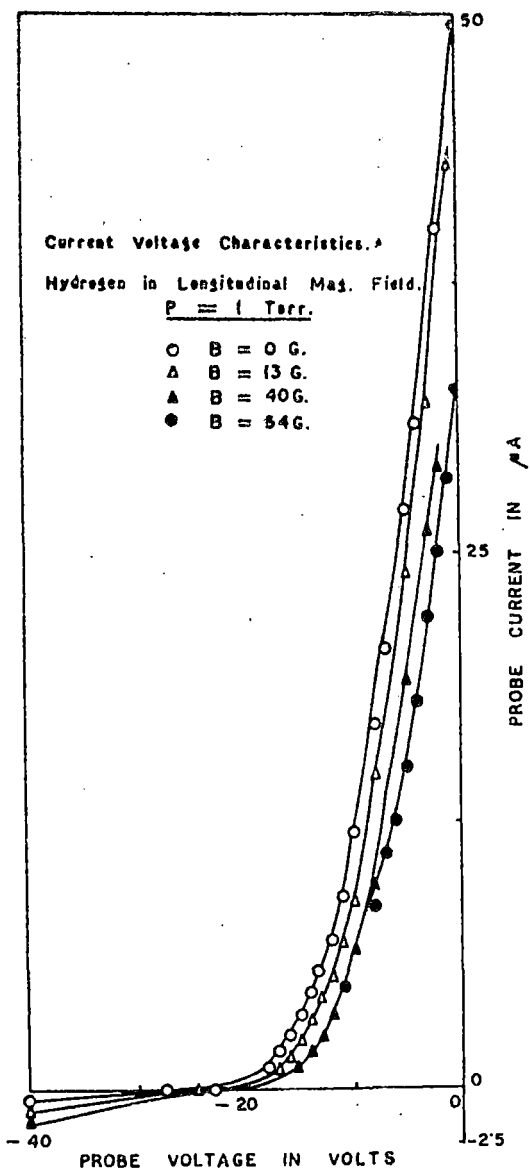


Fig. 3.3. Current-voltage characteristic of probe in longitudinal magnetic field in (a) hydrogen, (b) air.

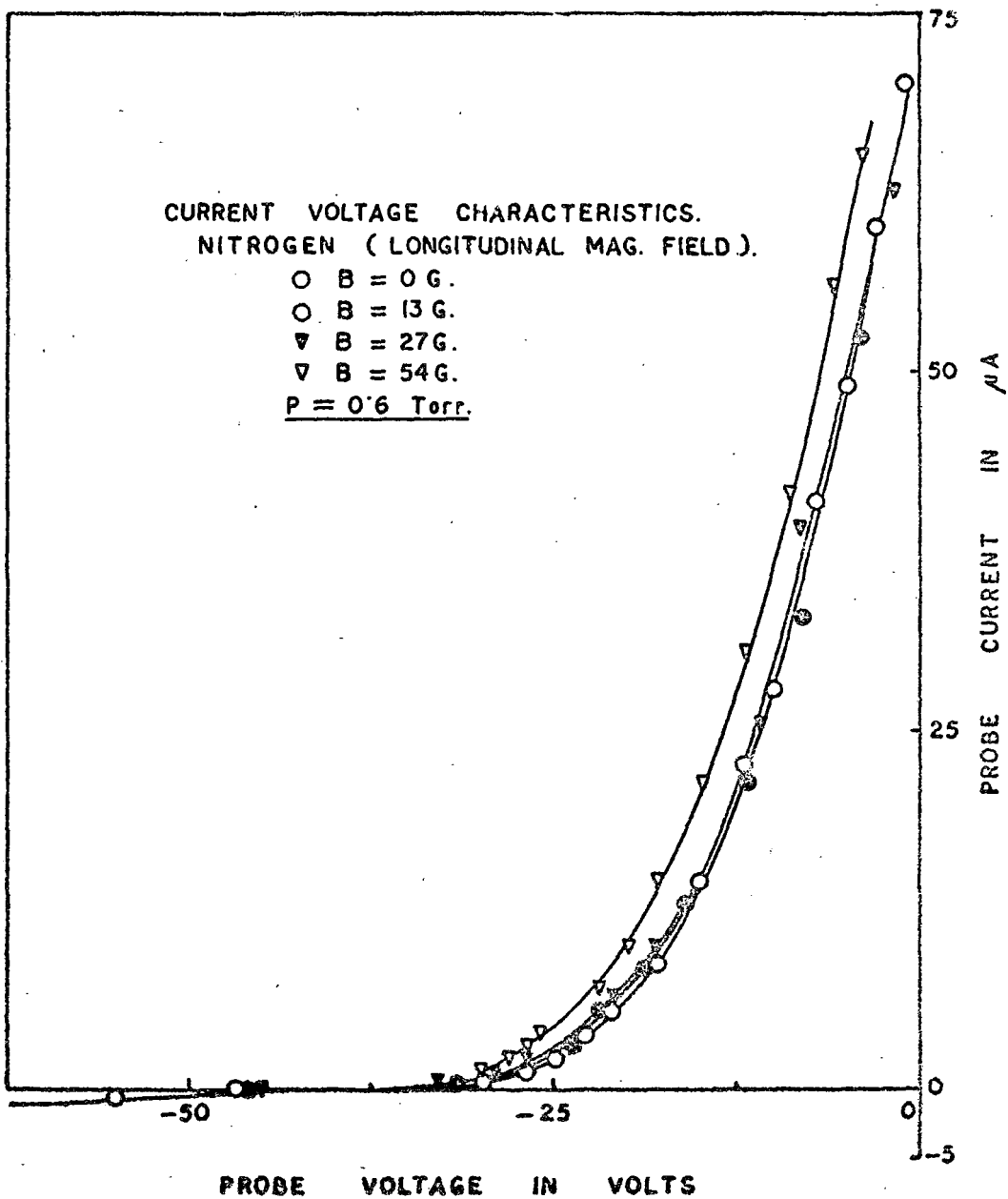


FIG. 3.4.

Fig. 3.4. Current-voltage characteristic of probe in nitrogen in longitudinal magnetic field.

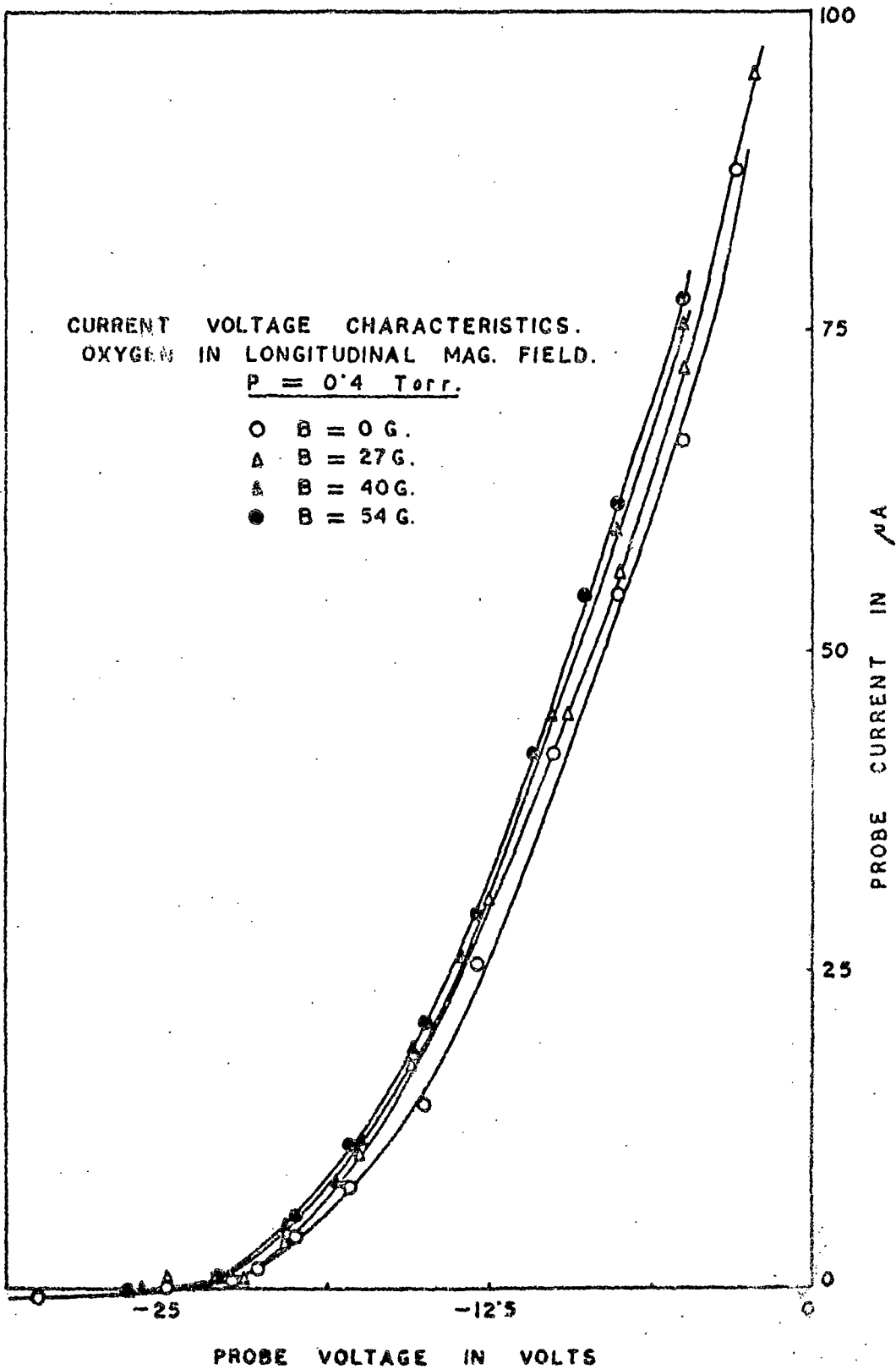


FIG. 3.5

Fig. 3.5. Current-voltage characteristic of probe in oxygen in longitudinal magnetic field.

electron temperature regime and electron saturation current regime on the semilogarithm plot of the characteristic and the crossing point of the two tangents represented the space potential. When space potentials have been determined, the saturated ion current at the space potential is determined by extrapolating the ion currents graphically from high negative probe potentials, linearly to the space potential. Such extrapolations have been shown in fig. 3.6 for air and oxygen in transverse magnetic field. The electron current  $I_e$  is determined by subtracting  $I_i$  from the probe current (eqn. 2.6).  $\log I_e$  has been finally plotted against probe potential ( $V_p$ ) and the characteristics have been obtained. The characteristics of gases with and without magnetic fields have been shown in figs. 3.7 to 3.14. In figs. 3.7 to 3.10, the gases were subjected to transverse magnetic field and for figs. 3.11 through 3.14, longitudinal magnetic fields were used.

For the analysis of the probe characteristics, the domain of the probe operation is to be determined. The four parameters, probe radius ( $r_p$ ), Debye length ( $\lambda_D$ ), mean free path of electrons and ions ( $\lambda_e$  and  $\lambda_i$ ) effectively determines the domain. In our experiment,

$r_p = 9.5 \times 10^{-3}$  cm.  $\lambda_D$  is determined from equation (3.1). For typical glow discharges,  $T_e$  varies from 1-5 eV and  $n_e$  from  $10^8$ - $10^{10}$   $\text{cm}^{-3}$ . In determining  $\lambda_D$ , we considered  $T_e = 5$  eV and  $n_e = 10^{10}$   $\text{cm}^{-3}$  as it will be seen later that experimental values obtained from probe characteristic in general are of these orders.

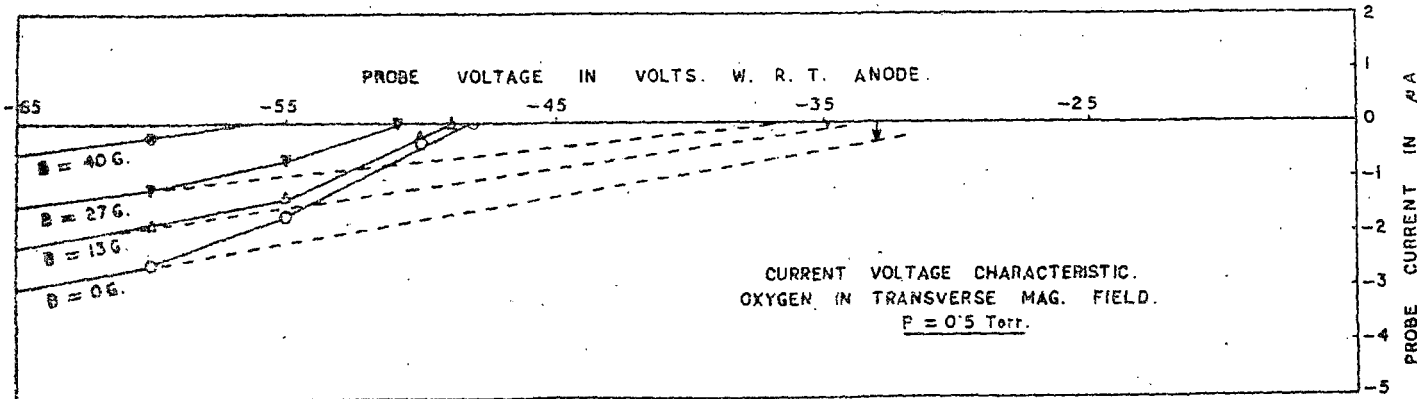
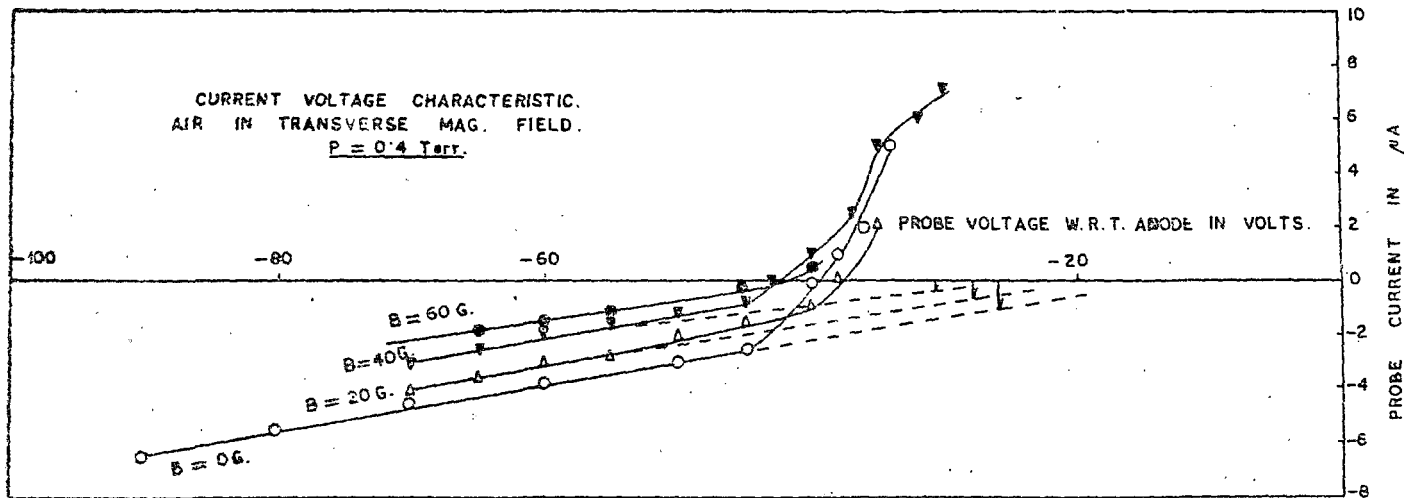


FIG. 3.6.

Fig. 3.6. Current-voltage characteristic of probe in air and oxygen and determination of saturation ion current at space potential by method of linear extrapolation.

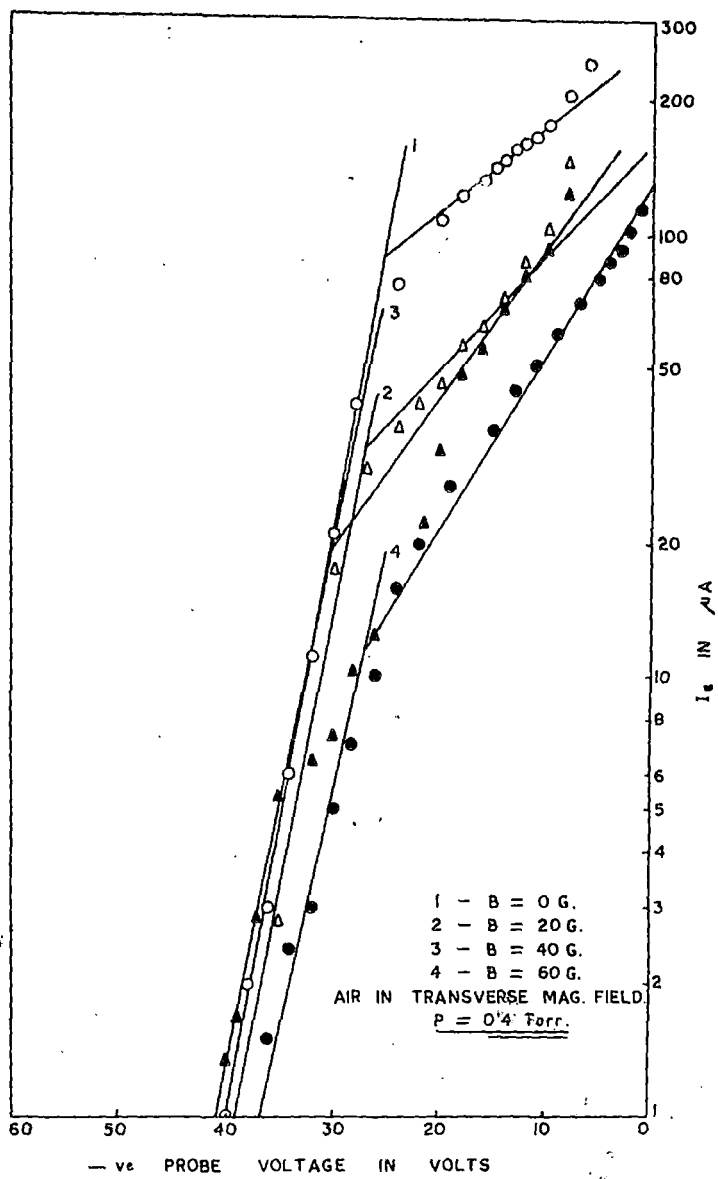


FIG. 3.7.

Fig. 3.7.  $\log I_e - V_p$  curves for air in transverse magnetic field.

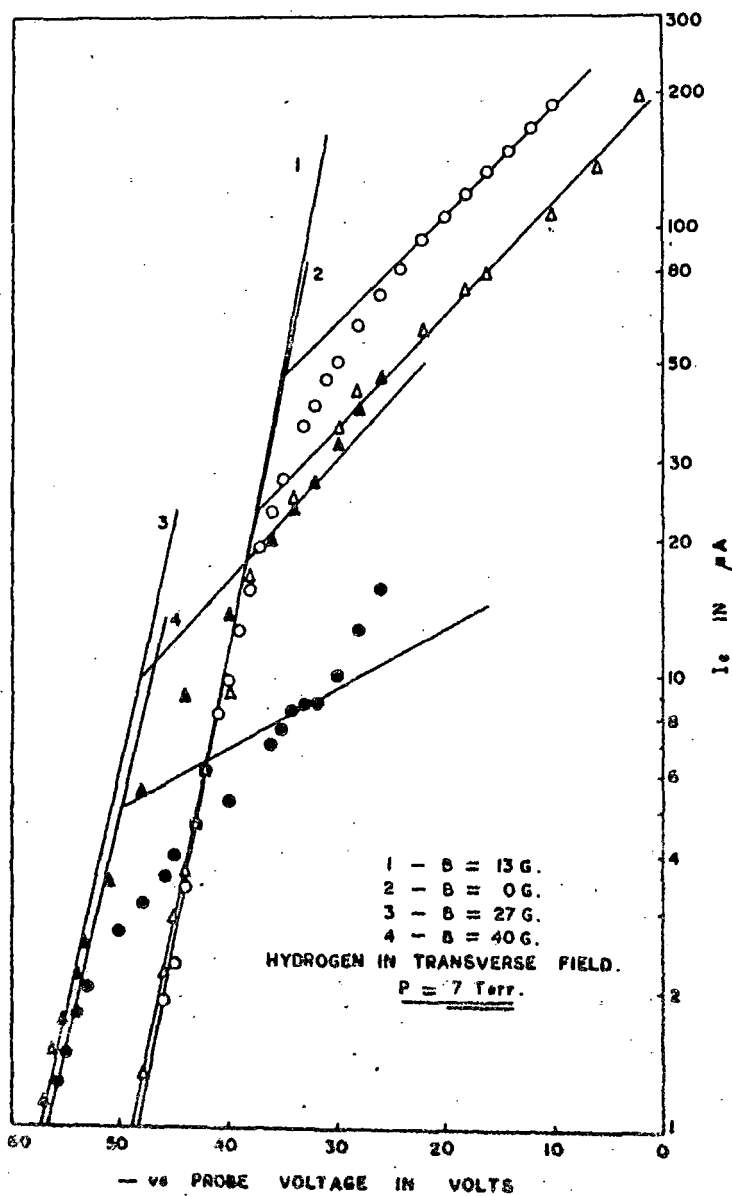


FIG. 3.8.

Fig. 3.8.  $\log I_e - V_p$  curves for hydrogen in transverse magnetic field.

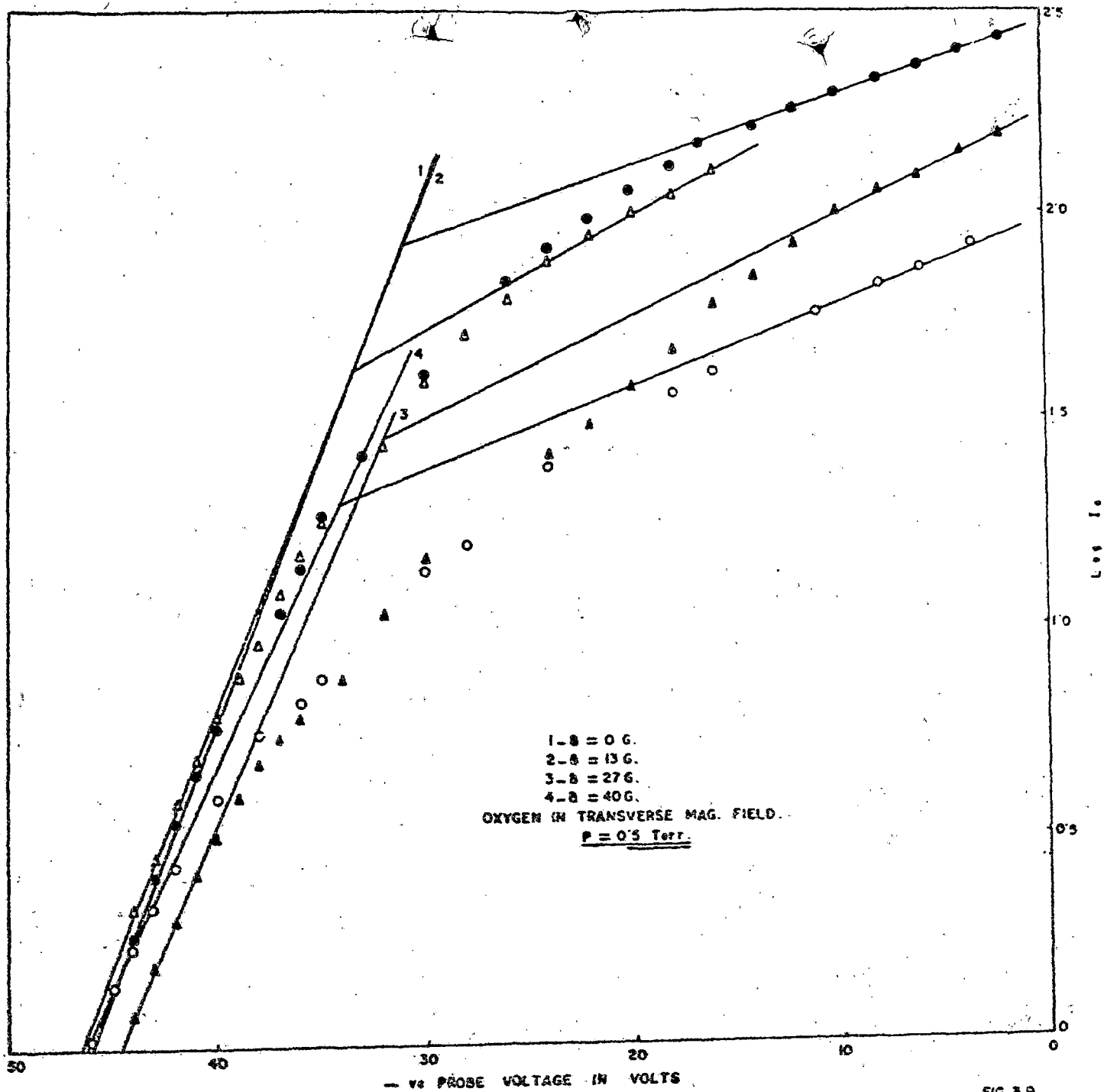


FIG. 3.9.

Fig. 3.9.  $\log I_e - V_p$  curves for oxygen in transverse magnetic field.

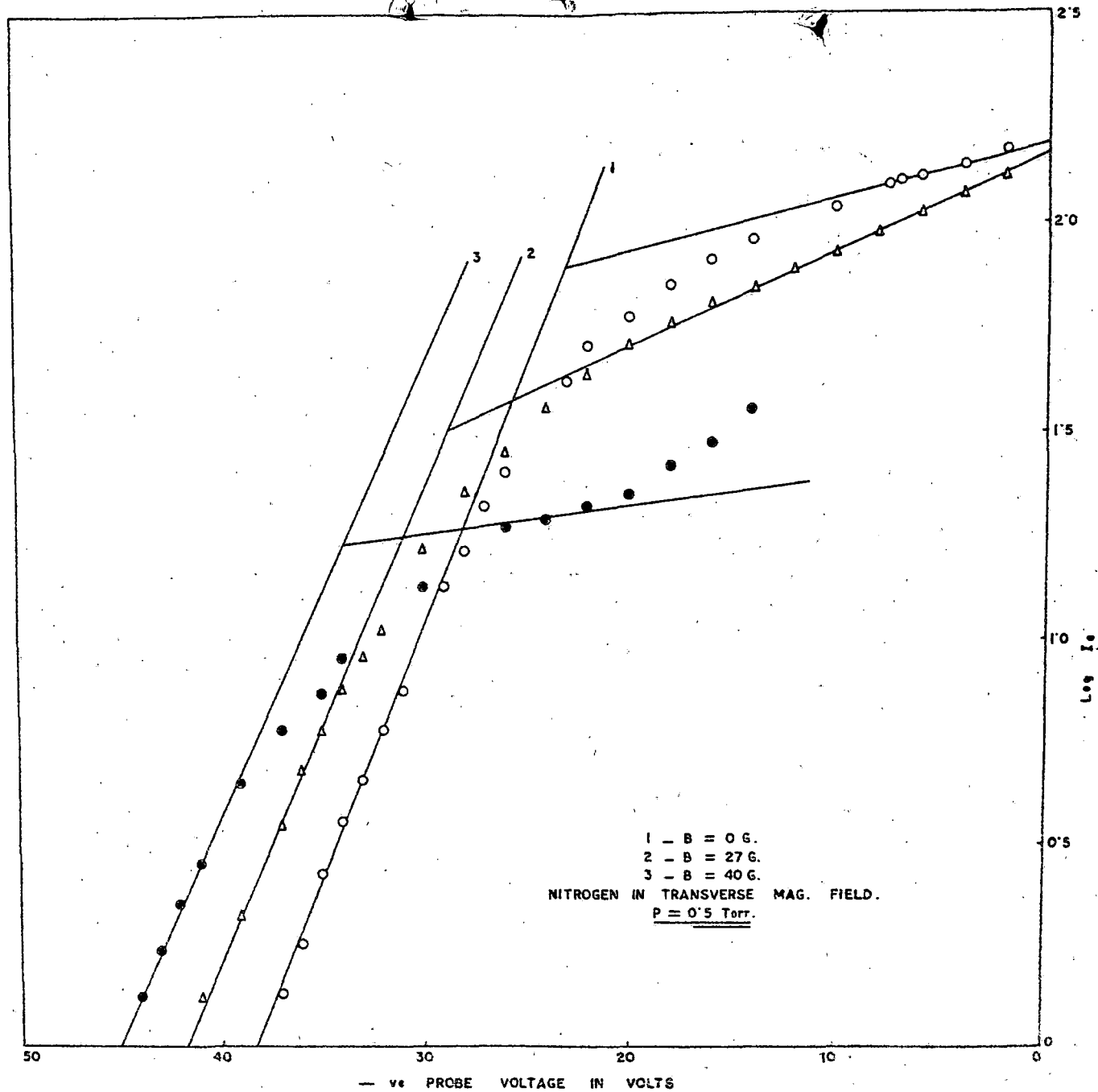


FIG. 3.10.

Fig. 3.10.  $\log I_e - V_p$  curves for nitrogen in transverse magnetic field.

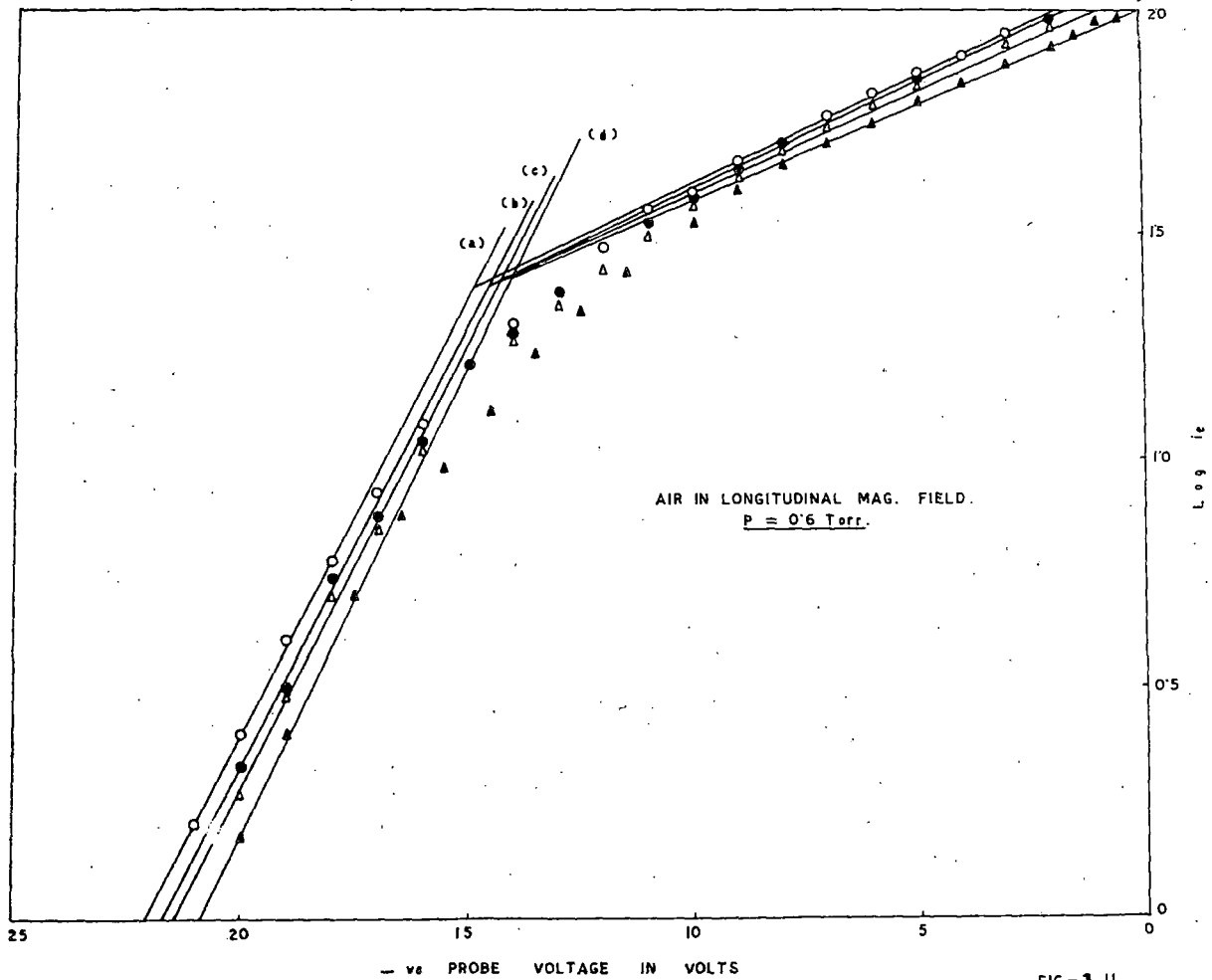


Fig. 3.11.  $\log I_e - V_P$  curves for air in longitudinal magnetic field (a)  $B = 0G$ , (b)  $B = 27G$ , (c)  $B = 54G$ , (d)  $B = 82G$ .

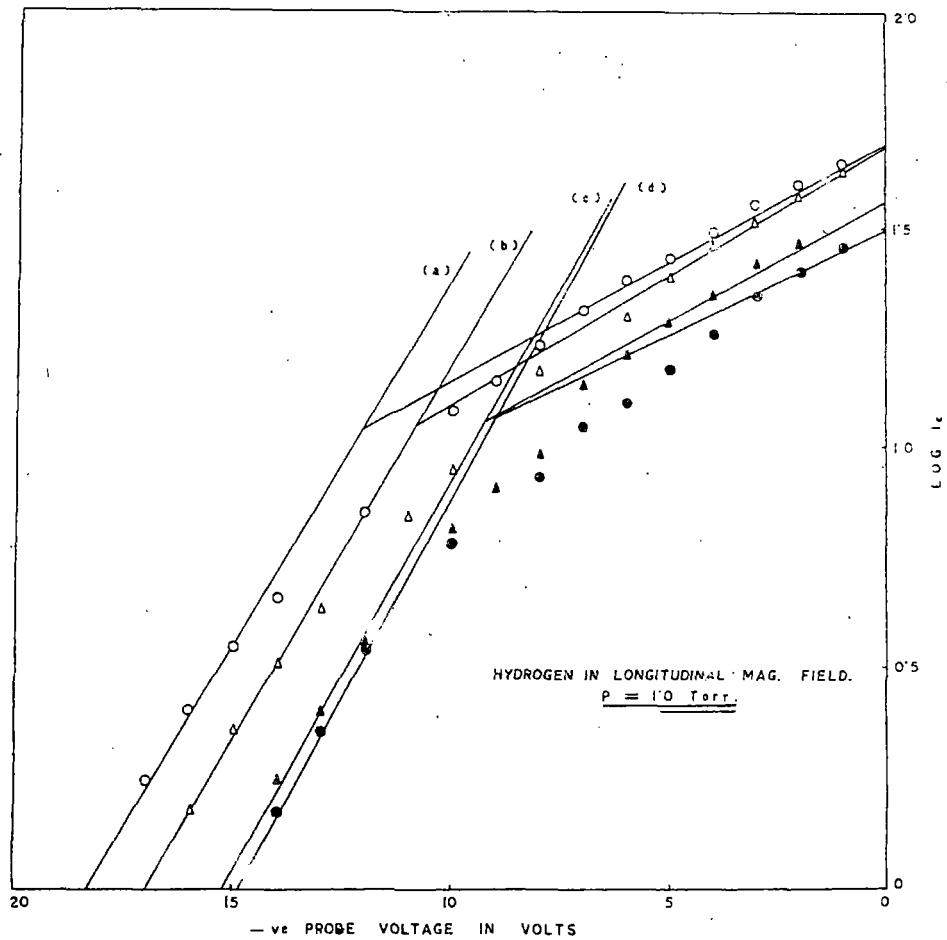


FIG-3.12.

Fig. 3.12.  $\log I_e - V_p$  curves for hydrogen in longitudinal magnetic field  
 (a)  $B = 0G$ , (b)  $B = 13G$ , (c)  $B = 40G$ , (d)  $B = 54G$ .

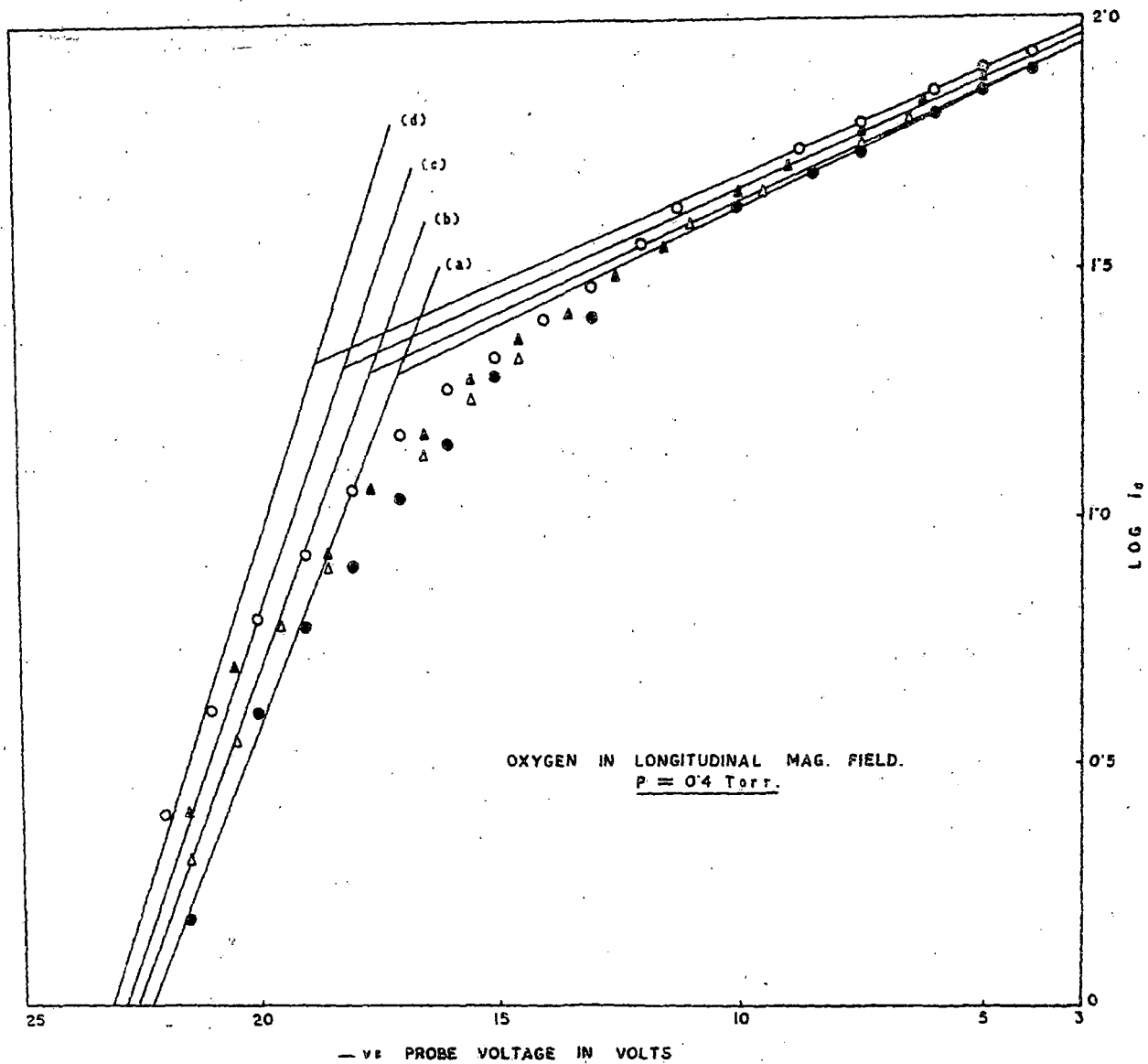


FIG-3.13.

Fig. 3.13.  $\log I_e - V_P$  curves for oxygen in longitudinal magnetic field (a)  $B = 0G$ ,  
(b)  $B = 13G$ , (c)  $B = 27G$ , (d)  $B = 54G$ .

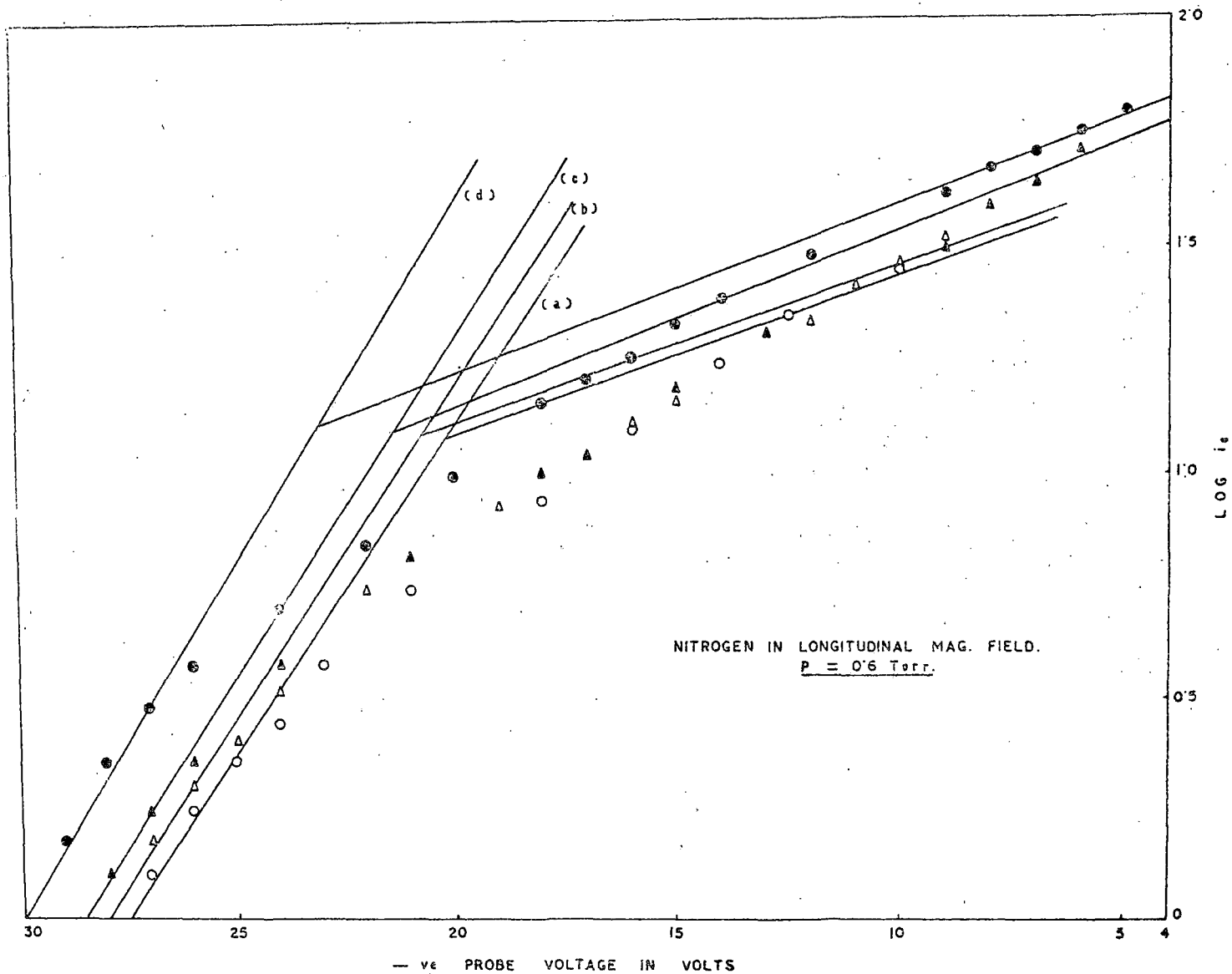


FIG-3.14.

Fig. 3.14.  $\log I_e - V_p$  curves for nitrogen in longitudinal magnetic field  
 (a)  $B = 0G$ , (b)  $B = 13G$ , (c)  $B = 27G$ , (d)  $B = 54G$ .

$\lambda_0$ , thus calculated was  $1.1 \times 10^{-2}$  cm. The mean free path of electrons  $\lambda_e$  may be estimated from values of collisions cross section ( $q_m$ ). But collision cross section is a function of electron energy. Huxley & Crompton (1974) have shown that  $q_m(\omega)$  may be replaced by an effective mean value  $q_m^*$  corresponding to a value of  $E/N$ . When the electron energy is greatly in excess of the mean energy of the gas molecules, and when inelastic collisions (like vibrational and rotational excitation) are important  $q_m^*$  becomes a function of  $E/N$  where  $E$  is the electric field intensity and  $N$  is the number density of molecules. For a Maxwellian distribution of electron energy,

$$q_m^* = 2.23 \times 10^{-10} \frac{E/N}{W(D/\mu)^{1/2}} \text{ cm}^2 \quad (3.2)$$

where  $E/N$  is expressed in townsend,  $W$ , the drift velocity at corresponding  $E/N$  is expressed in cm/sec. and  $(D/\mu)$ , the energy corresponding to  $E/N$  is in volts. For the values of  $E/N$  in our experiments, for different gases, the values of  $W$  and  $(D/\mu)$  are not available in literature for air, oxygen and nitrogen, so a model calculation for hydrogen gas for which datas are available (Huxley and Crompton, 1974) have been made. The cathode fall and anode fall for brass electrodes in hydrogen gas

(Francis, 1960) have been subtracted from total voltage drop across the discharge tube (1000 V). The potential thus obtained when divided by the length between the electrodes, gives  $E$ .  $E$  when divided by pressure of the hydrogen gas reduced to  $20^\circ\text{C}$  (temperature of gas in the discharge tube was nearly  $50^\circ\text{C}$ ), gives  $E/N$  corresponding to  $T = 293^\circ\text{K}$  and taking values of  $W$  and  $D/\mu$  corresponding to  $293^\circ\text{K}$ ,  $g_m^*$  is determined from equation (3.2).  $g_m^* N$  which is the inverse of  $\lambda_e$  is determined by finding  $N$  from pressure of the discharge reduced to  $0^\circ\text{C}$ , and  $\lambda_e$  thus calculated <sup>for</sup> from hydrogen at 0.7 torr pressure was  $6.3 \times 10^{-2}$  cm.  $\lambda_i$  has been determined from data given by von-Engel (1965), corrected by Sutherland constant. Actually the data given by von-Engel determines classical mean free path  $\lambda$  of hydrogen molecule in its own gas. But  $\lambda \leq \lambda_i \leq \sqrt{2}\lambda$ . The factor  $\sqrt{2}$  applied only when  $v_{ion} \gg v$  molecule. Considering  $\lambda = \lambda_i$ , for hydrogen  $\lambda_i$  has been calculated to be  $2.1 \times 10^{-2}$  cm. for pressure 0.7 torr. So it is found for hydrogen gas that  $\lambda_m \gg r_p$ ,  $\lambda_m \gg \lambda_D$  and  $\xi_p (= r_p/\lambda_D) < 5$ .  $\lambda_m$  is the smallest free path for collision between the charged and other particles of which plasma is composed. It is evident from Table 3.1 that for hydrogen, the pressures were comparatively larger than for other gases. So it is expected that for other gases  $\lambda_m$  would be greater so that above condition is fulfilled. In this condition the orbital motion

theory of Langmuir is valid.

The probe theory as developed by Langmuir gives electron current as

$$I_e = I_{re} \exp(-eV_p / kT_e) \quad (3.3)$$

where  $I_{re}$  is the random electron current, and  $k$  is the Boltzmann constant

$$I_{re} = \frac{1}{4} A_s n_e e \left( \frac{8kT_e}{m\pi} \right)^{1/2} \quad (3.4)$$

$A_s$  is the effective electron collection area of the probe and  $n_e$  is the unperturbed number density of electrons. From equation (3.3), electron temperature  $T_e$  corresponding to the assumed Maxwellian distribution is calculated by measuring the slope of the line in partial electron attraction region in a semilogarithmic plot of  $I_e$  versus  $V_p$ .  $I_{re}$  corresponds to the electron current to the probe at space potential which is determined from crossing point of the two tangents in the characteristics. The tangents were drawn in the following manner:

1. The tangent in the partial electron attraction region was drawn through more points of highly negative probe potential as it is in this region that the distribution is expected to be Maxwellian and equation (3.3) is valid for electron currents which are small compared to  $I_{re}$  (Schott, 1968).

2. The line in electron saturation current regime was drawn in such a manner that it passes through maximum number of points. The electron saturation current regime may be divided into two parts: one corresponding to a linear increase of  $I_e$  with  $V_p$  due to the growth of effective collecting area, as the sheath expands. When  $V_p$  is made more positive, a breakaway from this linear increase is observed. In this region the probe becomes very hot and the sheath expands so much that for a large potential drop across the sheath, the electrons can further ionise in their way to probe and a luminous region is created surrounding the probe. While drawing the tangent the points just below the breakaway point were utilised so that all points after breakaway limit are above the tangent.

Since the ratio  $l/r_p$  was very much greater than unity, the effective electron collection area  $A_s$  was considered to be equal to  $2\pi r_p l$ . Thus from equation (3.4) number density of electrons was determined.

The probes being always placed at right angles to the magnetic field, the same procedure for the measurement of electron temperature and electron density has been adopted in both the transverse and longitudinal magnetic field. In case of magnetic field following Uehara et al (1975), the effective probe area has been taken to be  $4r_p l$ .

### 3.3.2. Results

With the method of analysis of the probe data as reported in section 3.3.1, semilog plot of current voltage characteristics has been obtained for air, hydrogen, oxygen and nitrogen in transverse and longitudinal magnetic fields. It has been observed that the plots <sup>are</sup> straight lines with two different slopes for both with and without magnetic field.

From the slope of the straight lines electron temperature has been determined for all the gases and from the point of intersection of two tangents  $I_{re}$  has been determined from which electron density has been obtained. Table 3.2 shows the values of electron temperature and electron densities thus obtained, for transverse magnetic fields. The values of these parameters when a longitudinal magnetic field is present have been entered into Table 3.3.

TABLE 3.2

Values of  $T_e$  and  $n_e$  with and without transverse magnetic field.

Mag- netic field (G)	Air $p = 0.4$ torr		Hydrogen $p = 0.7$ torr		Oxygen $p = 0.5$ torr		Nitrogen $p = 0.5$ torr	
	$T_e$ eV	$n_e \times 10^{-9}$ $\text{cm}^{-3}$	$T_e$ eV	$n_e \times 10^{-9}$ $\text{cm}^{-3}$	$T_e$ eV	$n_e \times 10^{-9}$ $\text{cm}^{-3}$	$T_e$ eV	$n_e \times 10^{-9}$ $\text{cm}^{-3}$
0	7.63	4.87	7.83	2.53	7.90	4.52	8.03	4.19
13			8.16	1.92	8.17	3.50		
20	7.95	2.78						
27			9.12	0.78	8.74	2.17	8.64	2.57
40	8.23	1.59	9.53	0.39	9.34	1.52	9.34	1.35
60	8.89	0.91						

TABLE 3.3

Values of  $T_e$  and  $n_e$  with and without longitudinal magnetic field.

Mag- netic field, (G)	Air $p = 0.6$ torr		Hydrogen $p = 1.0$ torr		Oxygen $p = 0.4$ torr		Nitrogen $p = 0.6$ torr	
	$T_e$ eV	$n_e \times 10^{-9}$ $\text{cm}^{-3}$	$T_e$ eV	$n_e \times 10^{-9}$ $\text{cm}^{-3}$	$T_e$ eV	$n_e \times 10^{-9}$ $\text{cm}^{-3}$	$T_e$ eV	$n_e \times 10^{-9}$ $\text{cm}^{-3}$
0	5.26	4.74	6.03	2.05	4.13	4.85	6.79	2.13
13			5.94	2.09			6.70	2.18
27	5.15	4.82			3.86	4.91	6.59	2.25
40			5.68	2.16	3.65	5.02		
54	5.14	4.97	5.50	2.25	3.42	5.14	6.28	2.36
82	4.92	5.20						

It is evident from Table 3.2 and 3.3 that plasma parameters change with magnetic field. In case of transverse magnetic field the electron temperature increases where as radial electron density at some region near the axis decreases and in case of longitudinal magnetic field, the electron temperature decreases and the axial electron density increases.

### 3.3.3. Discussion of the results

In <sup>the</sup> case of longitudinal magnetic field, for cylindrical probe perpendicular to magnetic field, the electron temperature and electron density can be determined from the characteristic as in the case of zero field. Not much distortion in the probe characteristics was observed in the range of magnetic fields used. But distortion was present in the case of transverse magnetic field. In transverse field the knee becomes more and more round and the space potential undefined. In case of longitudinal magnetic field, from experimentally measured values of rf conductivity, Sen and Gupta (1969) have shown  $\lambda_D$  decreases with the increase of field. This is also in accordance with equation (3.1) as in the axial region  $T_e$  decreases and  $n_e$  increases. From the stand-point of probe measurements, a decrease in  $\lambda_D$  is welcome. For transverse field equation (3.1) predicts an increase of  $\lambda_D$  in the axial region. If  $\lambda_D$  increases, the

sheath and hence the effective probe collection area increases. When  $\lambda_D$  is comparable to  $\lambda_i$ , an increase of  $\lambda_D$  means collisions in the sheath. So when  $\lambda_D$  will be high, diffusion of particles have to be considered and the probe current would fall. So a rounded knee is expected in magnetic field for a probe perpendicular to the magnetic field and to discharge current mutually as the diffusion becomes anisotropic. Nevertheless we have utilised standard probe theory in this case in the anticipation that  $\lambda_D \neq \lambda_e$  and we are utilising the electron attraction region of the probe characteristic.

While investigating the effect of transverse magnetic field on glow discharges, Beckman (1948) observed that the longitudinal electric field increases with the increase of magnetic field and the radial electron distribution becomes asymmetric. From Beckman's analysis Sen, Das and Gupta (1972) obtained that  $k$  electron temperature when a magnetic field  $B$  is present is related to the zero field value by the relation

$$T_{eB} = T_e \left[ 1 + C_1 \frac{B^2}{p^2} \right]^{1/2} \quad (3.5)$$

where  $p$  is the pressure of the discharge and  $C_1$  is a constant for a particular gas given by

$$C_1 = \left( \frac{e}{m} \cdot \frac{\lambda_{e1}}{v_r} \right)^2 \quad (3.6)$$

$e, m, \lambda_{e1}$  and  $v_r$  are the charge, mass, mean free path at a pressure of 1 torr in  $0^\circ\text{C}$  and random velocity of the electrons respectively. Equation (3.5) is valid for conditions (i) in the domain where Schottky's ambipolar diffusion is valid (ii) the ionisation is mainly by electron impact ionisation collisions of the ground state molecules (iii) when  $B/p$  i.e. the value of reduced magnetic field is comparatively small. The experimental values of  $[(T_{eB}/T_e)^2 - 1]$  have been plotted against  $B^2/p^2$  for all the gas studied in fig. (3.15). It is observed that the curves are straight lines for the gases studied at low values of  $B/p$  in conformity with equation (3.5). The slopes of the curves are the value of  $C_1$  for the gases. Slopes are of different values, so that  $C_1$  is dependent on nature of the gas. From the slopes, the calculated values of  $C_1$  for different gases have been entered in second column of Table (3.4).

Sen and Gupta (1971) have shown that the ratio of the electron density at a distance  $r$  from the axis when the transverse magnetic field is present, to the value in the absence of the magnetic field is given by

$$n_{eB}/n_e = \exp(-aB) \quad (3.7)$$

where  $a = e E C_1^{1/2} r / 2 k T_e p$

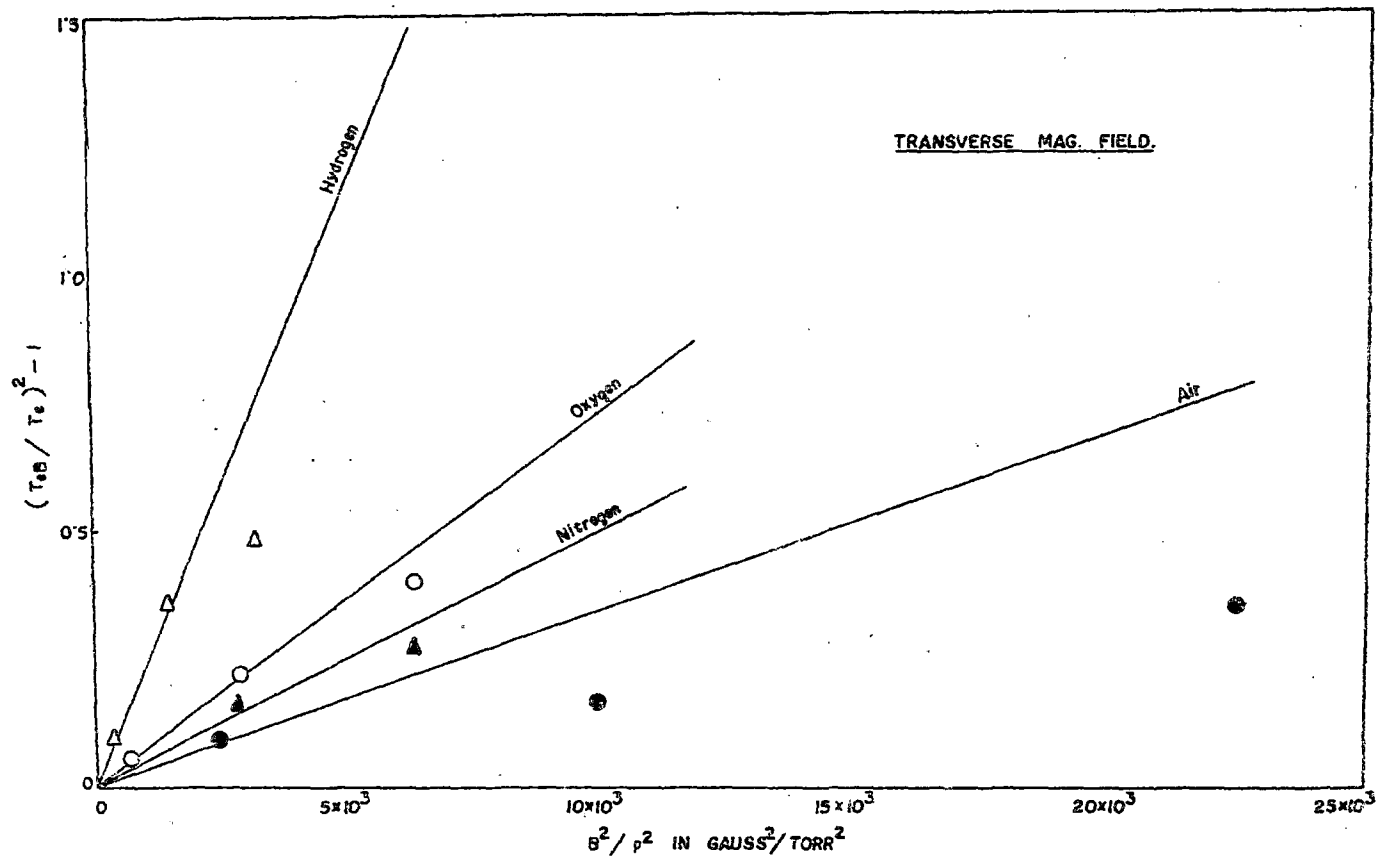


FIG. 3.15.

Fig. 3.15. Variation of  $((T_{eB}/T_e)^2 - 1)$  against  $B^2/p^2$  in transverse magnetic field.

From equation (3.7) it is evident that there will be a reduction of electron density and  $\log (n_e/n_{eB})$  will be proportional to  $B/p$ . From the experimentally obtained electron density,  $\log (n_e/n_{eB})$  has been plotted with  $B/p$  for different gases in fig. (3.16) and straight lines have been obtained. The experimental results after analysis thus indicate that Beckman's theoretical expressions as further modified by Sen et al (1971, 1972) with regard to electron temperature and radial distribution of electron density are valid for low values of  $B/p$ .

For longitudinal magnetic field Sen and Gupta (1969) obtained

$$T_{eB} = T_e + \frac{2T_e^2 \log \left[ \frac{1}{\sqrt{1 + C_1 B^2/p^2}} \right]}{T_e + 2eV_i/k} \quad (3.8)$$

$V_i$  is the ionisation potential of the molecule. Equation (3.8) is also valid when Schottky's ambipolar diffusion theory is valid and ion pairs are created by electron collisions with the ground state molecules. From equation (3.8), it may be shown

$$1 + C_1 \frac{B^2}{p^2} = \exp \left[ 2(T_e - T_{eB})\alpha \right] \quad (3.9)$$

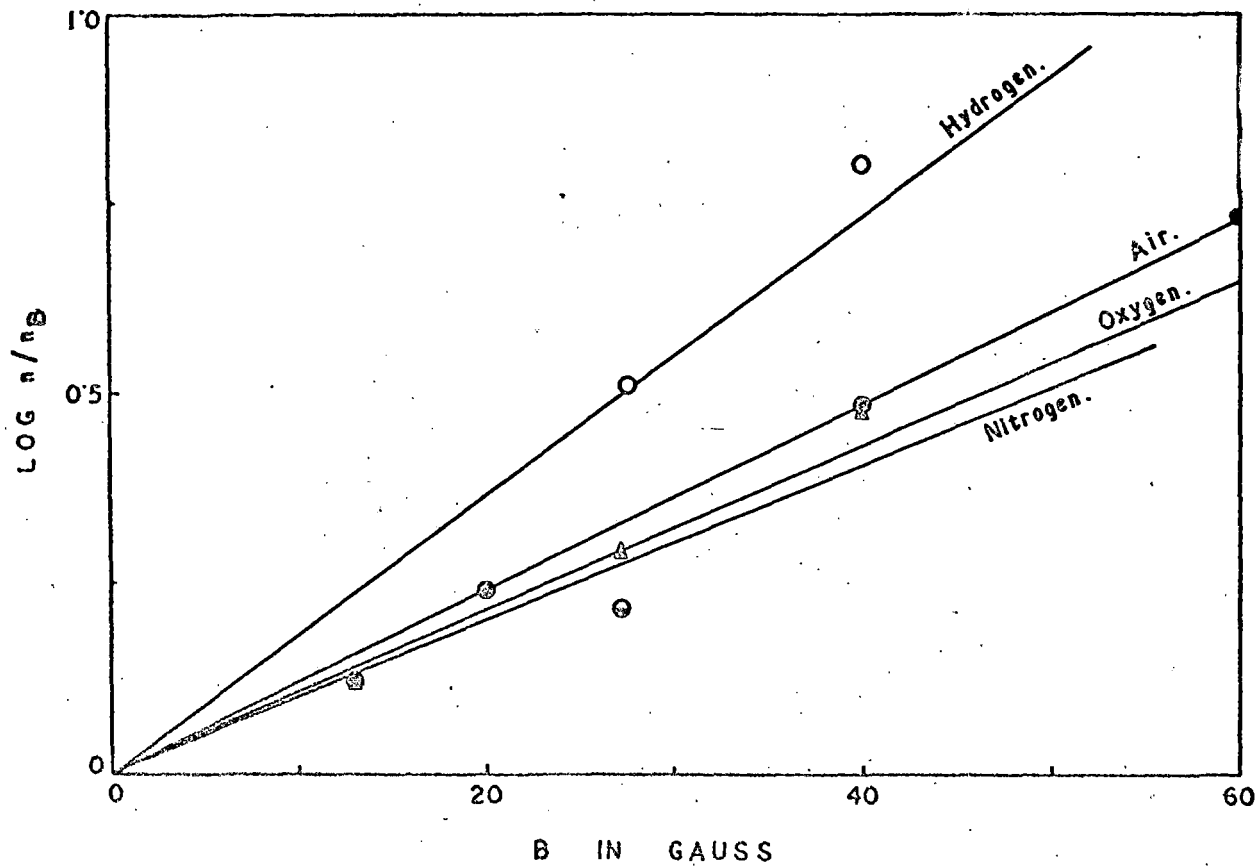


FIG.3.16.

Fig. 3.16. Variation of  $\log ( n/n_B )$  against transverse magnetic field.

where

$$\alpha = \left[ T_e + \frac{2eV_i}{k} \right] / 2T_e^2 \quad (3.10)$$

From equation (3.10)  $\alpha$  for different gases may be calculated if ionisation potentials are known. Ionisation potentials for hydrogen, oxygen and nitrogen molecules are 15.4, 12.5 and 15.8 eV respectively. Ionisation potential for air has been calculated from values of coefficients A and B defined by von-Engel (1965). These coefficients are defined as

$$A = \frac{1}{\lambda_{e1}} \quad , \quad B = \frac{V_i}{\lambda_{e1}} \quad (3.11)$$

where  $\lambda_{e1}$  is the value of  $\lambda_e$  at a pressure of 1 torr. From equation (3.11),

$$V_i = \frac{B}{A} \quad (3.12)$$

values of B and A for air have been given by von-Engel (1965) and from these value  $V_i$  is calculated to be 24.33 V. For longitudinal magnetic field, from the experimentally obtained electron temperatures,  $\exp. 2(T_e - T_{eB})\alpha$  has been plotted against  $B^2/p^2$  in fig. (3.17). The plots are straight lines with an intercept of unity as predicted by equation (3.9). From the slope of the lines  $C_1$  have been

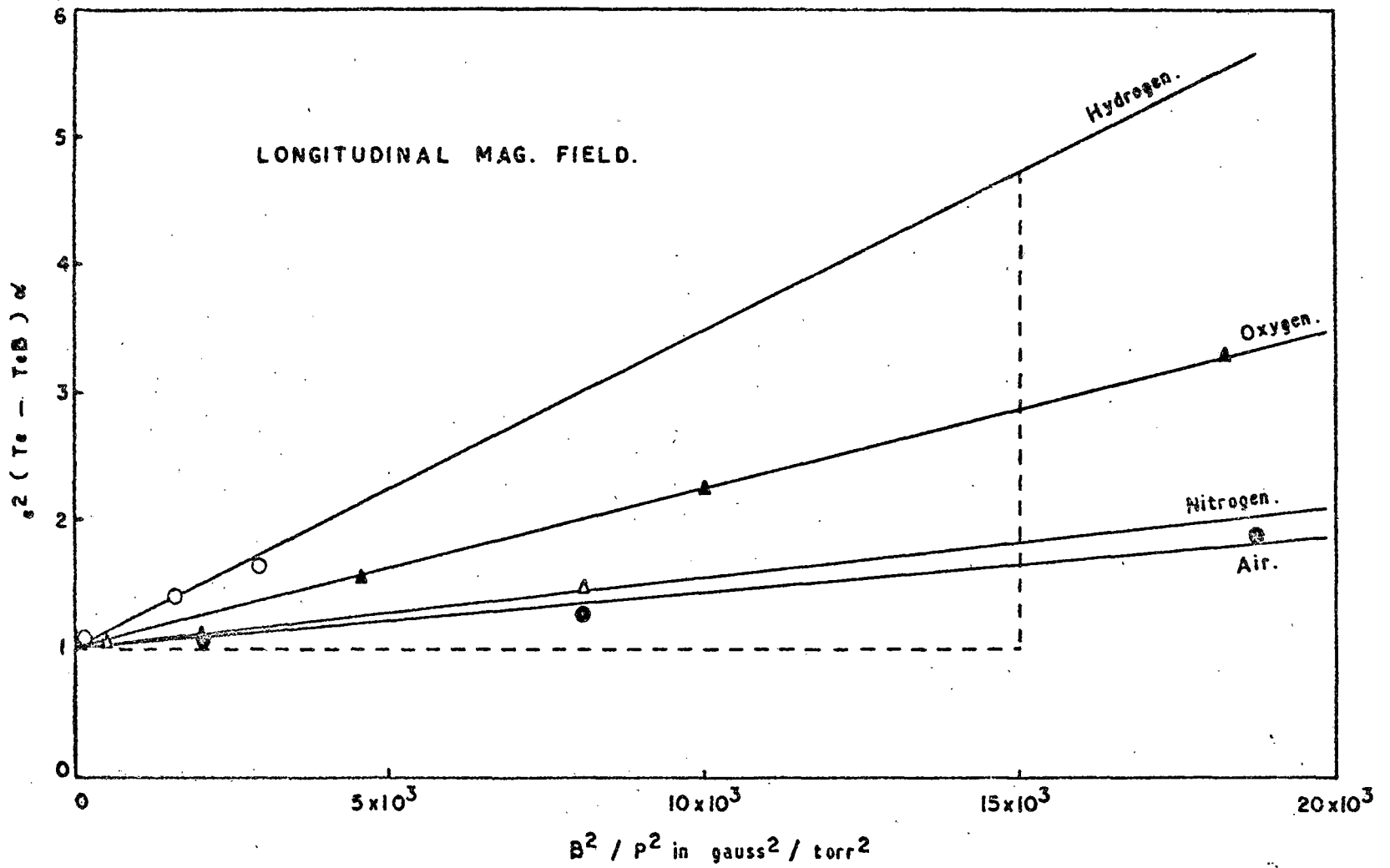


FIG. 3.17.

Fig. 3.17. Variation of  $e^2(T_e - T_{eB}) \alpha$  against  $B^2/p^2$  in longitudinal magnetic field.

calculated for all the gases and results thus obtained have been entered in the third column of Table 3.4.

TABLE 3.4

Values of  $C_1$  calculated for different ionised gases for transverse and longitudinal magnetic fields.

Gas	$C_1$ from transverse magnetic field measurement (torr <sup>2</sup> /gauss <sup>2</sup> )	$C_1$ from longitudinal magnetic field measurement (torr <sup>2</sup> /gauss <sup>2</sup> )
Air	$3.4 \times 10^{-5}$	$4.3 \times 10^{-5}$
Hydrogen	$2.31 \times 10^{-4}$	$2.48 \times 10^{-4}$
Oxygen	$7 \times 10^{-5}$	$12.5 \times 10^{-5}$
Nitrogen	$5 \times 10^{-5}$	$5.6 \times 10^{-5}$

It is evident that the values of  $C_1$  obtained quite independently from two sets of measurements agree very well in case of hydrogen and nitrogen. In case of air and specially in case of oxygen the agreement is not very close and this is definitely due to the fact that calculation of  $C_1$  in case of longitudinal magnetic field involves the knowledge of an

accurate value of  $V_i$ , the ionisation potential. In the case of air, there is uncertainty in the accepted value of  $V_i$  where as in case of oxygen, as has been shown by Thomson (1961) in their mass spectrographic measurements, there are present in an oxygen plasma  $O^-$ ,  $O_2^-$ ,  $O^+$  and  $O_2^+$  ions.  $O^-$  and  $O_2^+$  concentration are about equal in magnitude and formed over 90% of the ions present. So the value of  $V_i$  taken equal to that of oxygen molecular ions introduces an element of uncertainty in the value of  $C_1$ .

Sen and Jana (1977) have discussed that in case of molecular gases the radial distribution of electrons in a cylindrical discharge tube where Schottky's ambipolar diffusion theory is valid, is governed by the normal Bessel function. The authors have shown that the radial electron density increases when the plasma is confined by a uniform longitudinal magnetic field and deduced that

$$\frac{n_{eB}}{n_e} = \frac{J_0 \left[ \frac{r}{\Lambda} \left\{ \frac{\nu_{iB}}{\nu_i} \frac{T_e}{T_{eB}} \right\}^{1/2} \right]}{J_0 \left( \frac{r}{\Lambda} \right)} \quad (3.13)$$

where  $n_e$  is the electron density at a distance  $r$ .

$\nu_i$  and  $\Lambda$  are the ionisation frequency and diffusion length. The subscript B signifies a quantity when a magnetic field is present. The diffusion length  $\Lambda$  is

given by

$$\frac{1}{\Lambda^2} = \left(\frac{\pi}{L}\right)^2 + \left(\frac{2.405}{R}\right)^2 \quad (3.14)$$

$L$  and  $R$  being the distance between electrodes and radius of the discharge and  $1/\Lambda^2 = 4.067 \text{ cm}^{-2}$ . Further,

$$\frac{v_{iB}}{v_i} = \frac{\exp(-eV_i/kT_{eB}) [1 + eV_i/kT_{eB}]}{\exp(-eV_i/kT_e) [1 + eV_i/kT_e]} \quad (3.15)$$

Considering a value of  $r$ , from equation (3.13) the values of  $n_{eB}/n_e$  may be calculated. Taking  $r = 0.2 \text{ cm.}$ , the length of the probe, the calculated values of  $n_{eB}/n_e$  from eqn. (3.13) and the experimentally obtained values from probe data have been entered in Table 3.5.

TABLE 3.5.

Values of  $n_{eB}/n_e$  in longitudinal magnetic field.

Mag- ne- tic field, (G)	Air		Hydrogen		Oxygen		Nitrogen	
	Theo.	Expt.	Theo.	Expt.	Theo.	Expt.	Theo.	Expt.
13			1.0005	1.017			1.0002	1.025
27	1.001	1.016			1.004	1.047	1.0006	1.058
40			1.002	1.054	1.005	1.1		
54	1.003	1.047	1.0034	1.097	1.011	1.16	1.002	1.109
82	1.007	1.097						

The agreement between the theoretical and experimental results is not very satisfactory, but nevertheless the results do indicate that the axial electron density increases with a longitudinal magnetic field. One of the reasons for quantitative disagreement between theoretical and experimental values is the fact that whereas the theoretical expression expresses the electron density at a point distant  $r$  from the axis, in actual calculation we have taken an average value of  $r$  for the finite length of the probe because the whole area of probe is effective in collecting the electrons.

From experimentally obtained values of plasma parameter by probe method, it is thus evident that magnetic field influences a discharge column inconformity with observations of Beckman and Sen et al. In the analysis, the authors considered the plasma balance equation of the positive column. The magnetic field modifies the loss processes like ambipolar diffusion and mobility of charged particles and the plasma parameters change in magnetic field as the plasma adjusts to this new situation. The theoretical interpretations are in agreement with other models of positive column used. As far as for example we mention the ion fluid model discussed by Franklin (1976) when a longitudinal magnetic field is present. In this model a quantity  $\delta$ , which measures

particle collision frequency of momentum transfer relative to ionisation frequency, is of importance. Franklin discussed that when ionisation frequency  $\ll$  elastic collision frequency, the quantity  $\delta_i / \delta_e$  in a longitudinal magnetic field is changed by the relation

$$\left( \frac{\delta_i}{\delta_e} \right)_B = \frac{\delta_i}{\delta_e} \frac{1}{1 + c_1 \frac{B^2}{p^2}} \quad (3.16)$$

the subscripts  $i$  and  $e$  indicates ion and electron.  $c_1$  has been already defined and it is the square of mobility at a pressure of 1 torr at  $0^\circ\text{C}$ . When  $T_e$  is not large

$$\delta_i / \delta_e = \mu_e / \mu_i \quad (3.17)$$

$\mu$  is the mobility of a particle. In the range  $B/p < 0.5$  Tesla torr $^{-1}$ , only  $\mu_e$  is affected in a magnetic field so that,

$$\frac{\mu_e}{\mu_{eB}} = 1 + c_1 \frac{B^2}{p^2} \quad (3.18)$$

Equation (3.18) virtually speaks for an effective increase of pressure

$$\frac{p_B}{p} = \left( 1 + c_1 \frac{B^2}{p^2} \right)^{1/2} \quad (3.19)$$

Equation (3.19) was utilised by Sen and Gupta (1969) in the plasma balance equation of positive column to reduce equation (3.8).

### 3.4. Conclusions

The electron temperature and electron density in low temperature plasmas in air, hydrogen, oxygen and nitrogen magnetised by either a transverse or a longitudinal magnetic field have been measured by probe method. Experiments have been performed under the condition in which assumptions of probe theory are valid. The alignment of magnetic field with respect to the direction of the discharge current has a decisive effect on the values of the plasma parameters and thereby, we can bring out the difference in behaviour of a swarm of electrons and their associated properties in transverse and longitudinal magnetic fields. In case of transverse magnetic field, the electron temperature increases whereas radial electron density decreases upto a certain distance from the axis. Quantitative agreements for the variation of plasma parameters in transverse magnetic field have been obtained with existing theories for small values of  $k B/p$ . For longitudinal magnetic field, the electron temperature decreases whereas the radial electron density increases. This may be explained from an equivalent increase of pressure in longitudinal magnetic field as predicted by the theory.

For molecular gases, the excitation levels are widely spread out upto ionization potential and inelastic losses set up at low energies and these are so distributed so as to produce an approximate Maxwellian distribution for electron energy. The present investigation clearly indicates that ~~there~~ though the nature of electron energy distribution (in case of longitudinal magnetic field) remains Maxwellian in character in presence of or in absence of magnetic field, also it becomes a function of the magnetic field. For transverse magnetic field nothing specific about the electron energy distribution can be predicted owing to the distortion of the characteristics due to anisotropic diffusion. What has been measured in the present investigation is the average electron temperature and its variation with alignment of magnetic field.

## References:

1. Beckman, L. (1948) Proc. Phys.Soc. 61, 515.
2. Bohm, D., Burhop, E.H.S., Massey, H.S.W. and Williams, R.W. (1949) The characteristics of Electrical Discharges in Magnetic fields (McGraw Hill, New York).
3. Francis, G. (1960) Ionization phenomena in gases (Butterworths, London).
4. Franklin, R.N. (1976) Plasma phenomena in gas discharges (Oxford University Press).
5. Huxley, L.G.H. and Crompton, R.W. (1974) The diffusion and drift of Electrons in gases, p. 530 (John Wiley, NY).
6. Kagan, Y.M. and Perel, V.I. (1969) Sov.Phys. Tech. Phys. 13 1348.
7. Krall, N.A. and Trivelpiece, A.W. (1973) Principles of Plasma Physics (McGraw Hill, New York).
8. Schott, L. (1963) in Plasma diagnostics, (Ed.W. Lochte-Holtgreven, North Holland Publishing Co., Amsterdam).
9. Sen, S.N., Das, R.P. and Gupta, R.N. (1972) J.Phys. D. 5 1260.
10. Sen, S.N. and Gupta, R.N. (1969) Indian J.Pure Appl.Phys. 7, 462.
11. Sen, S.N. and Gupta, R.N. (1971), J.Phys.D.4, 510.
12. Sen, S.N. and Jana, D.C. (1977), J.Phys.Soc.Jap.43 1729.
13. Thomson, J.B. (1961) Proc.Roy.Soc. A262 503.
14. Uehara, K., Yatsu, K., Hagiwara, S. and Kojima, S. (1975) Japan J.Appl.Phys.14 1761.
15. von-Engel, A. (1965) Ionised Gases (2nd.Edn) p.31 & 181 (Oxford University Press).

## MEASUREMENT OF ELECTRON TEMPERATURE AND ELECTRON DENSITY IN LOW DENSITY MAGNETISED PLASMA BY PROBE METHOD

S. K. SADHYA, D. C. JANA and S. N. SEN

*Department of Physics, North Bengal University, Darjeeling*

*(Received 27 July 1978; after revision 5 October 1978)*

The measurement of electron temperature and electron density in low temperature plasmas in air, hydrogen, oxygen and nitrogen magnetised by either a transverse or a longitudinal magnetic field have been carried out by the probe method. The limitations of the probe theory and the precise method in measuring electron temperature and electron density both in the absence and in presence of the magnetic field have been discussed and the experiments have been performed under the conditions in which the assumptions of the probe theory are strictly valid. The general conclusion arrived at is that in case of transverse field, the electron temperature increases whereas the radial electron density decreases and in case of longitudinal field, the electron temperature decreases and the radial electron density increases. The results are also quantitative in agreement with the theoretical deductions of Beckman (1948) and Sen and Gupta (1971) in case of transverse magnetic field and that of Sen and Gupta (1969) and Sen and Jana (1977) in case of longitudinal magnetic field. Further, it is noted that in case of molecular gases the electron energy distribution is Maxwellian in presence of or in the absence of magnetic field but in the former case it becomes a function of  $(H/P)$  where  $H$  is the magnetic field and  $P$  is the pressure.

### INTRODUCTION

THE Langmuir probe method is one of the standard methods of measuring the plasma parameters such as electron density and electron temperature in a gaseous discharge. The theory of the probe in zero magnetic field rests on two assumptions: (a) The dimensions of the probe; and (b) the thickness of the space-charge sheath surrounding the probe is small compared with the mean free path of the electrons and ions. In connection with the probe theory, a parameter  $\xi_p = r_p/\lambda_d$  has been introduced by Chen, Etievant and Mosher (1968) where  $r_p$  is the radius of the probe and  $\lambda_d$  the Debye Shielding length for the repelled species. For cylindrical probe, the computations of Laframboise (1966) show that the orbital motion theory of Langmuir is accurate for  $\xi_p > 5$ . In our experimental set up, this condition is satisfied.

The limitations as well as the validity of these assumptions have been discussed by a large number of workers. Nevertheless, the values of the parameters obtained by this method compare very favourably with the values obtained by other standard methods. In our present programme of work in determining the momentum transfer cross section in a transverse magnetic field and the voltage current relation in a longitudinal magnetic field (Sen & Jana, 1977) or in studying the diffusion of electrons in a magnetic field, it has been assumed in explaining the observed experimental results that both the electron temperature and electron density distribution are affected by the magnetic field and the nature of the variation is different according

to the alignment of magnetic field with respect to the direction of the discharge current.

It has been deduced by Sen and Gupta (1971) that the electron temperature  $T_{eH}$  in presence of the magnetic field is given by

$$T_{eH} = T_e \left[ 1 + C_1 \frac{H^2}{P^2} \right]^{1/2}, \quad \dots (1)$$

when  $(H/P)$  is small and  $C_1 = \left( \frac{e}{m} \cdot \frac{L}{v_r} \right)^2$ , where  $L$  is the mean free path of the electron in the gas at a pressure of 1 torr and  $v_r$ , the random velocity of the electron. The validity and limitation of the deduction has been discussed in a number of papers (Sen & Gupta, 1971; Sen *et al.*, 1972; Sen & Das, 1973). Further, it has been shown by Beckman (1948) and Sen and Gupta (1971) that in a transverse magnetic field the radial electron density at a distance  $r$  from the axis is given by

$$n_H = n \exp \left[ \frac{-eHr}{4\sqrt{2mk}} \sqrt{\frac{R}{T_e}} \right], \quad \dots (2)$$

where  $R$  is the fraction of energy lost by an electron due to either elastic or inelastic collision. No direct experimental evidence of the validity of these deductions has been provided so far.

The situation is completely different when the direction of the magnetic field is along the direction of the discharge current. This problem has not been quantitatively studied so far but a detailed experimental analysis of the positive column in a longitudinal magnetic field has been provided by Bickerton and Von Engel (1956). Regarding the variation of radial electron density, Bickerton and Von Engel (1956) have obtained conclusive evidence that the radial electron density increases in a longitudinal magnetic field. Sen and Jana (1977) have shown that in case of molecular gases as well, the radial electron density increases when the plasma is confined by a longitudinal magnetic field, and deduced that

$$\frac{n_H}{n_0} = \frac{J_0 \left[ \frac{r}{\Lambda} \left\{ \frac{v_{iH}}{v_i} \frac{T_e}{T_{eH}} \right\}^{1/2} \right]}{J_0(r/\Lambda)} \quad \dots (3)$$

where  $v_i$  is the ionization frequency and  $\Lambda$  is the diffusion length. It is thus evident that the alignment of the magnetic field with respect to the direction of discharge current has a distinct effect on the plasma parameters specially the electron temperature and electron density distribution.

Aikawa (1976) has studied the anisotropy of the electron distribution function of a magnetised plasma by measuring the electron temperature ( $T_{e\parallel}$ ) in the direction of the magnetic field as well as in the perpendicular direction ( $T_{e\perp}$ ). He has observed that in strong magnetic field ( $H = 350$  G), electron temperature increases linearly with the magnetic field but for low values of the magnetic field the experimental results deviate from the linear curve. Kaneda (1977) has measured the electron temperature of a positive column with a transverse magnetic field and observed an increase of electron temperature with the increase of the magnetic field and the effect is more pronounced at lower gas pressure.

As most of the effects of magnetic field on a plasma depend on the manner in which these parameters are affected by the field itself, it is proposed in the present investigation to make an experimental study of the nature of the variation of these parameters by the probe method. This will enable us to put to a direct experimental test the theoretical deductions regarding electron temperature and electron density variation in both the longitudinal and transverse magnetic fields.

A magnetic field  $H$  applied to the plasma effectively reduces the free paths of the charged particles perpendicular to  $H$  to less than the radius of curvature  $\rho = \frac{mv}{eH}$ ,  $v$  being the velocity and  $m$ , the mass of the particle and hence for a probe collecting across the magnetic field assumption (a) becomes invalid in moderate magnetic field. For this purpose the magnetic field used in the present experiment has been kept below 100 gauss. The validity of assumption (b) depends upon the sheath thickness and thus on the plasma density, the type of the gas and on the magnetic field. In our experiment the plasma density has been kept relatively low ( $10^9/\text{c.c.}$ ) and the magnetic field is below 100 gauss. Under these conditions, the electron temperature and electron density can be obtained as has been shown by Bohm *et al.* (1949) as in the case without the field.

#### MEASUREMENT OF $T_e$ AND $n$ IN ABSENCE OF MAGNETIC FIELD

The probe theory as developed by Langmuir gives the electron current as

$$I_e = I_{r0} \exp(-eV_p/KT_e), \quad \dots (4)$$

where  $I_{r0}$  the random electron current and in the range  $\xi_p \gg 1$  the sheath is thin and Langmuir obtained for positive potential the saturation electron current

$$I_{r0} = \frac{1}{4} A_e n e \left( \frac{8KT_e}{m\pi} \right)^{1/2}, \quad \dots (5)$$

where  $A_e$  is the effective electron collection area of the probe,  $n$  is the unperturbed electron density. By eqn. (4) the electron temperature  $T_e$  corresponding to the assumed Maxwellian distribution is calculated by measuring the slope of the Boltzmann line in a semilogarithmic plot of  $I_e$  versus  $V_p$ . It is observed that  $I_e$  is never saturated. Increase in current with increasing positive potentials is expected due to growth of effective collecting area as the sheath expands.

A plot of  $\log I_e$  against  $V_p$  (shown in the figs.) indicates that instead of a sharp knee a round knee is obtained. As such the true space potential is not well defined. This is due to the disturbance of the plasma when the probe is drawing large electron current near the space potential. The convention of the linear-extrapolation of the curves at space potential was adopted to determine the space potential. The linear extrapolation was made in such a way that the "Boltzmann line" was drawn through more points of highly negative probe potential as it is in this region that the distribution is expected to be more Maxwellian (Schott, 1968). The other line is drawn in such a manner that it passes through the maximum number of points and lies below the points for which there is a departure from the semi log plot points. At first the total probe current was plotted against the probe voltage and an approximate value of space potential was obtained by the above procedure. Then  $I_e$  was

determined by subtracting  $I_i$  from the probe current. To get the value of  $I_i$  a linear extrapolation of  $I$  from highly negative probe potential to  $V_p = 0$  has been adopted as suggested by Schott (1968);  $\log I_s$  was finally plotted against  $V_p$  and electron temperature is obtained from the slope of the curve. The current corresponding to the space potential has been taken to be the electron saturation current from which the electron density can be obtained from eqn.(5).

#### MEASUREMENT IN MAGNETIC FIELD

The same procedure for the measurement of electron temperature and electron density has been adopted in both the transverse and longitudinal magnetic fields the probe being always placed at right angles to the magnetic field. In case of magnetic field following Uehara *et al.* (1975) the effective probe area  $A_e$  has been taken to be  $4al$ , where  $a$  is the radius and  $l$  the length of the probe.

It is worthwhile to mention that almost all previous determination of electron density has been made from ion saturation current but recently it has been mentioned by Chang and Chen (1977) that measurements made from ion saturation current are liable to be in error due to secondary emission from the probe surface and are not consistent with the values obtained by microwave method. They have shown that calculation of electron density from electron saturation current are in agreement with microwave measurements within 50 per cent. Hence in the present investigation electron density calculations have been made from electron saturation current.

#### EXPERIMENTAL ARRANGEMENT

The experiment in which electron temperature and electron density have been measured has been performed in two parts : (a) when the magnetic field is transverse; and (b) when the magnetic field is longitudinal; both with respect to the direction of the discharge current. Measurements have been made in d.c. glow discharges in air, hydrogen, nitrogen and oxygen on the assumption that electron energy distribution functions in these gases are expected to follow a Maxwellian distribution.

Pure and dry air was passed through phosphorus pentoxide and calcium hydroxide to remove traces of water vapour. Hydrogen and oxygen were prepared by the electrolysis of a strong solution of barium hydroxide. Hydrogen was passed through heated copper turnings, phosphorus pentoxide and calcium hydroxide and oxygen through concentrated sulphuric acid before being introduced into the discharge tube. Nitrogen gas was supplied by Indian Oxygen Company and the gas was passed through heated copper turnings and concentrated sulphuric acid.

Magnetic field was generated by an electromagnet energised by a stabilised power supply and the field was uniform between the pole pieces. For transverse field, the lines of force were exactly perpendicular to the axis of the discharge tube made of a pyrex glass tube 22 cm long and 4 cm in diameter. The field was introduced in the positive column of the plasma. For longitudinal measurements the discharge tube of length 8.5 cm. and 2.5 cm in diameter was placed between the pole pieces of the electromagnet which have the diameter of 3.5 cm which ensures that the magnetic field is uniform throughout the length of the tube because it is essential that the magnetic field should be free from radial components. The probes were of cylindrical

tungsten wire of 0.5 mm diameter. In case of transverse field, it was 4 mm long and placed at a distance of 2.5 cm from the anode where the magnetic field was applied. In case of longitudinal field it was 2 mm long and was placed 1.3 cm from the anode. Both the probes were inserted into the discharge tube by a glass jacket. The pressure was varied between 0.4 to 1 torr for different gases and was kept constant for a particular set of experiments by a needle valve and was measured by a McLeod gauge. The stationary discharge was made by a stabilized d.c. power supply and the discharge current was between 9 to 12 mA.

Probe voltages were supplied by a continuously varying dry battery and voltages were measured with respect to anode. The magnetic field was measured by a calibrated fluxmeter. Keeping the pressure constant for fixed discharge current the probe potential was varied from a high negative value to positive values and the corresponding probe current was noted in the microammeter. The procedure is repeated for different values of the transverse and longitudinal magnetic fields whose value has been allowed not to exceed 100 gauss in conformity with the limitations that should be observed for the validity of the probe theory in magnetic field.

### RESULTS AND DISCUSSION

In conformity with the method of analysis of the probe data as reported earlier in the paper, semilog plot of current voltage characteristics has been obtained for air, hydrogen, oxygen and nitrogen in case of transverse field and the representative curve for hydrogen is shown in Fig. 1. It is observed that the plot is a straight line with two different slopes for both with and without magnetic field which shows that probe theory can be applied to find the electron density and electron temperature in presence of magnetic field as well, provided the magnetic field and the main discharge current are kept at a low value. From the slope of the straight line drawn through the highly negative probe voltages the electron temperature has been determined for all the four gases, with and without magnetic field, and the results are entered in Table I.

To verify whether the theoretical expression previously deduced by Sen and Gupta (1971) that  $T_{eH} = T_e \left[ 1 + c_1 \frac{H^2}{P^2} \right]^{1/2}$  is valid the values of  $\left[ \frac{T_{eH}^2}{T_e^2} - 1 \right]$

TABLE I

*Values of electron temperature in electron volt with and without magnetic field*

Magnetic field in gauss	Air	Hydrogen	Oxygen	Nitrogen
	P = 0.4 torr	P = 0.7 torr	P = .5 torr	P = 0.5 torr
0	7.63	7.829	7.898	8.025
13		8.163	8.165	
20	7.95			
27		9.116	8.737	8.643
40	8.228	9.527	9.34	9.34
60	8.886			

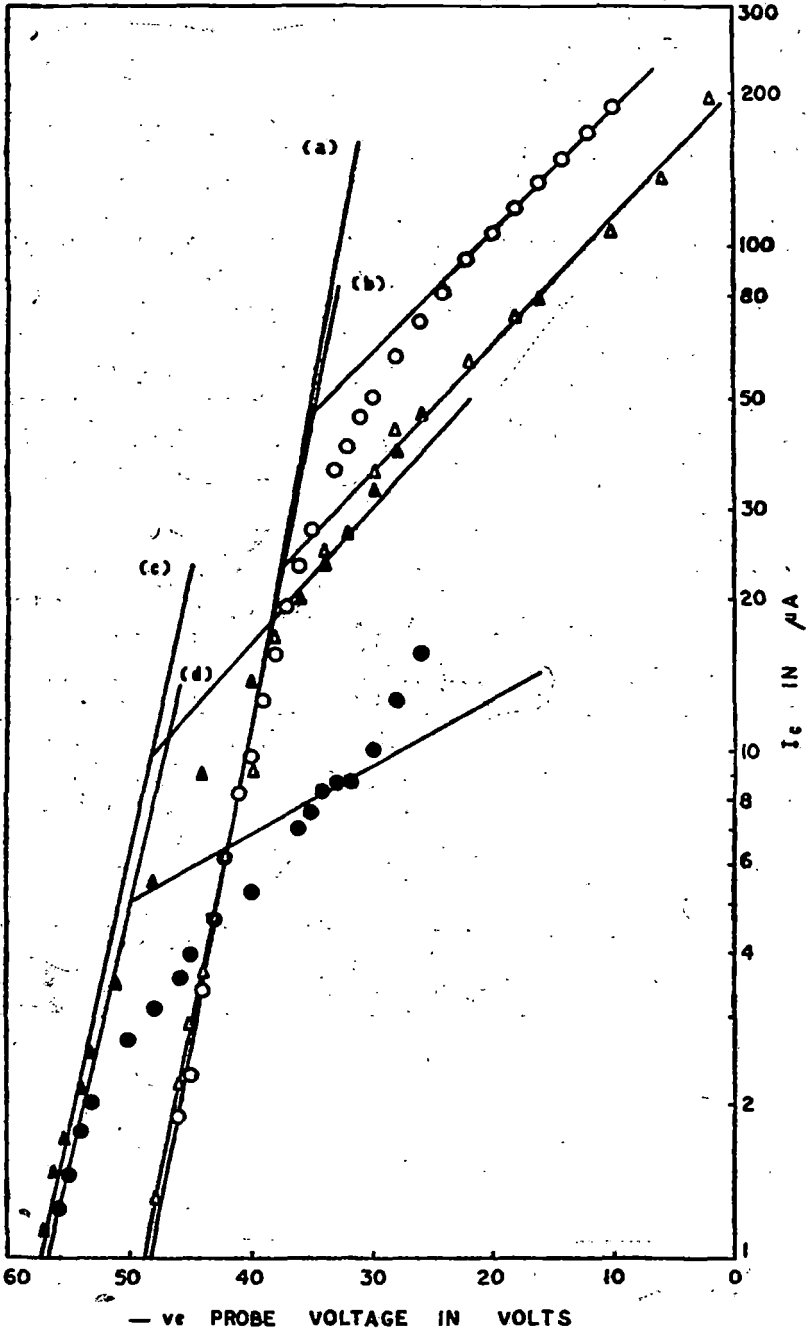


FIG. 1.  $\log I_e - V_p$  curves for hydrogen in transverse magnetic field.  
 (a)  $B = 0G$  (b)  $B = 13G$  (c)  $27G$  (d)  $B = 40G$ .

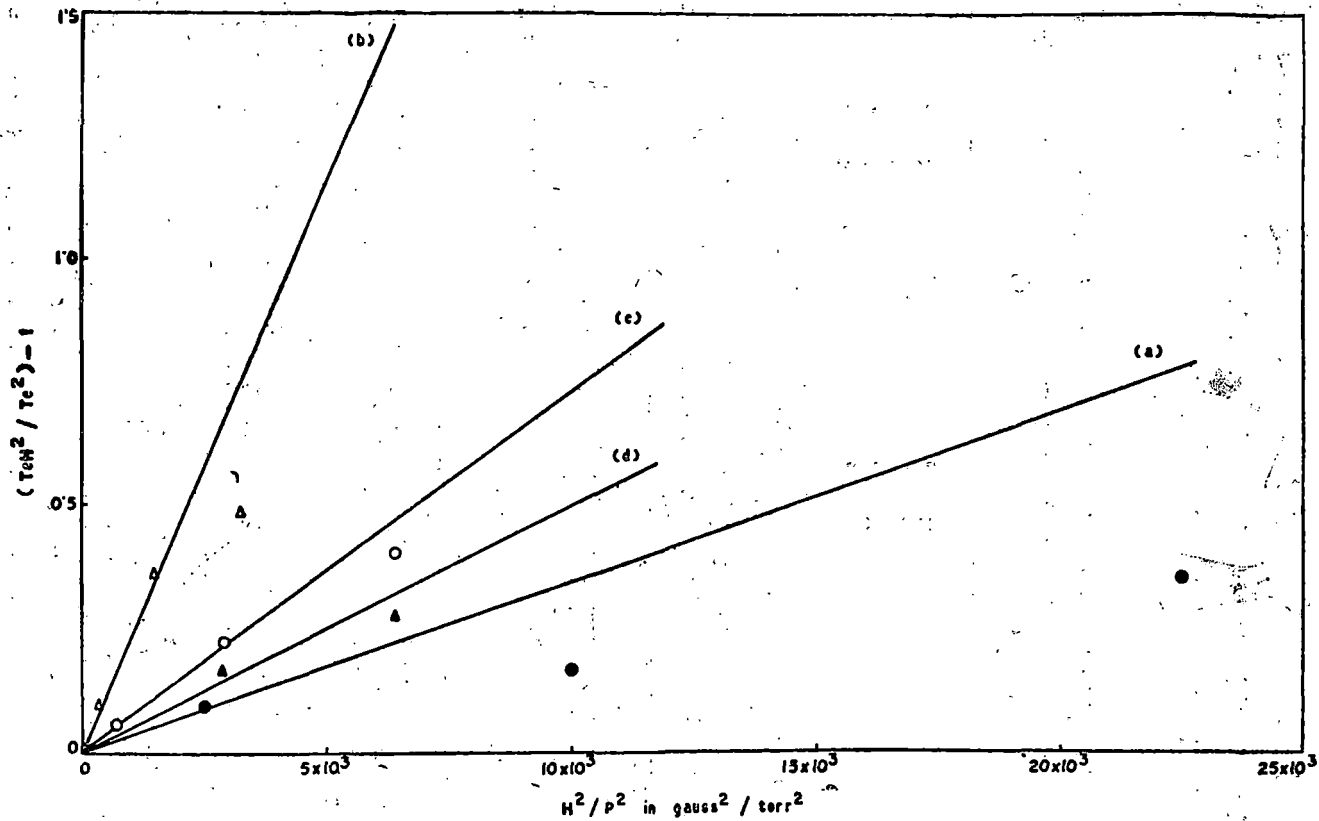


FIG. 2. Variation of  $\left[ \frac{T_e H^2}{T_e^2} - 1 \right]$  against  $H^2 / P^2$

(a) Air (b) Hydrogen (c) Oxygen (d) Nitrogen in Transverse magnetic fields.

have been plotted against  $H^2/P^2$  for all the gases studied and are represented in Fig. 2.

It is observed that curves are all straight lines for the gases studied in conformity with eqn. (1) but with different slopes from which the values of  $C_1 = \left( \frac{e}{m} \cdot \frac{L}{v_r} \right)^2$  have been calculated and entered for different gases in the second column of Table II.

TABLE II

*Values of  $C_1$  as calculated for different ionised gases for transverse and longitudinal magnetic fields*

Gas	$C_1$ from transverse magnetic field measurement	$C_1$ from longitudinal field measurement.
Air	$3.4 \times 10^{-5}$	$4.3 \times 10^{-5}$
Hydrogen	$2.31 \times 10^{-4}$	$2.48 \times 10^{-4}$
Oxygen	$7 \times 10^{-5}$	$12.5 \times 10^{-5}$
Nitrogen	$5 \times 10^{-5}$	$5.6 \times 10^{-5}$

The value of  $C_1$  as obtained here for different gases are of the same order as obtained previously by microwave and diffusion methods.

Besides electron temperature, the electron density with and without magnetic field has been determined experimentally. From the theoretical deduction (eqn. 2)

it is evident that if  $\log \frac{n}{n_H}$  is plotted against  $H$  the curve should be a straight line as is actually observed from the curve (Fig. 3) for different gases. The experimental results after analysis thus indicate that Beckman's theoretical expressions as further modified by Sen and Gupta with regard to electron temperature and radial distribution of electron density are valid specially for low values of  $(H/P)$ .

#### LONGITUDINAL MAGNETIC FIELD

The variation of the semi log plot of electron current and probe voltage in case of all the four gases has been obtained and a representative curve has been shown in Fig. 4. As in the case of transverse magnetic field the curves are straight lines with two different slopes and the electron temperature and electron density have been determined as before for all the gases. The values of electron temperature have been entered in Table III. It was previously deduced by Sen and Gupta (1969) in case of longitudinal magnetic field that

$$T_{eH} = T_e + \frac{2T_e^2 \log \left[ \frac{1}{[1 + c_1 H^2/P^2]^{1/2}} \right]}{\left[ T_e + \frac{2eV_i}{k} \right]} \quad \dots (6)$$

and from these results the values of  $C_1$  have been calculated by plotting  $e^{(T_e - T_{eH})/\alpha}$  against  $H^2/P^2$  (Fig. 5)

$$\text{where } \alpha = \frac{T_e + \frac{2eV_i}{K}}{2T_e^2}.$$

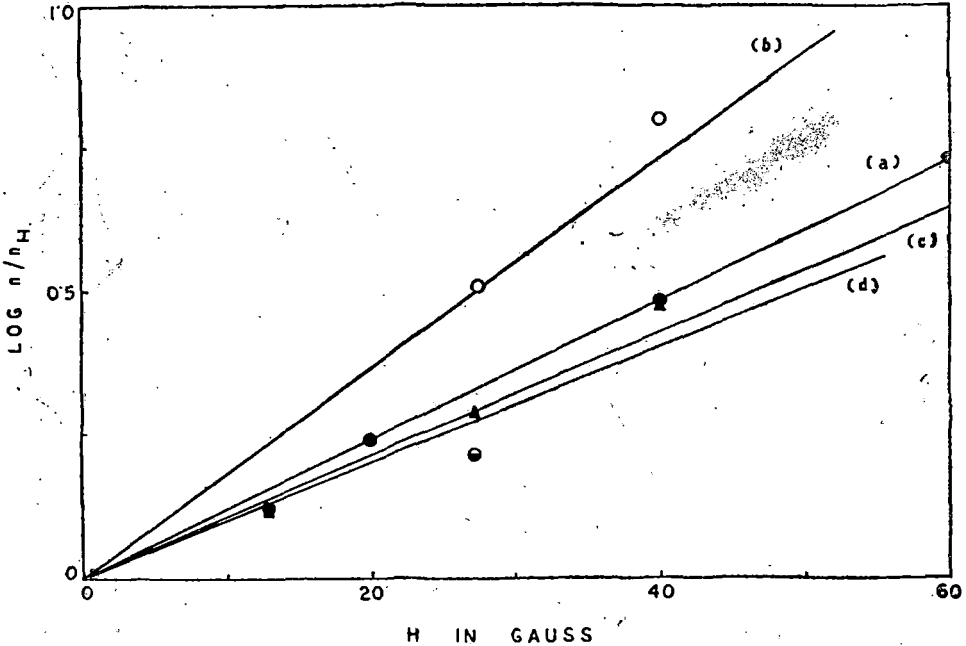


FIG. 3. Variation of  $\log (n/nH)$  against  $H$  for (a) Air (b) Hydrogen (c) Oxygen (d) Nitrogen in Transverse Magnetic field.

From the slope of the curves, the values of  $C_1$  have been calculated for all the gases and results thus obtained have been entered in the last column of Table II, for comparison. It is thus evident that the values of  $C_1$  obtained quite independently from the two sets of measurements agree very well in case of hydrogen and nitrogen. In case of air and specially in case of oxygen the agreement is not very close and this is definitely due to the fact that calculation for  $C_1$  in case of longitudinal magnetic field involves the knowledge of an accurate value of  $V_i$  the ionization potential. In the case of air, there is uncertainty in the accepted value of  $V_i$  whereas in case of oxygen as has been shown by Thomson (1961) in their mass spectrographic measurements there are present in an oxygen discharge not only  $O_2^+$  but also  $O^+$  which form 90 per cent of the ions and are present in equal amount and the value of  $V_i$  taken equal to that of oxygen introduces an element of uncertainty in the value of  $C_1$ .

To calculate theoretically the variation of  $n_e$  with the magnetic field and compare it with the experimental results, we have utilized the theoretical expression for  $n_H$  eqn. (3) as deduced by Sen and Jana (1977). The theoretical and experimental results are shown in Table IV.  $\Lambda$  the diffusion length is given by

$$\frac{1}{\Lambda^2} = \left(\frac{\pi}{h}\right)^2 + \left(\frac{2.405}{R}\right)^2, \quad h \text{ is the distance between the electrodes and}$$

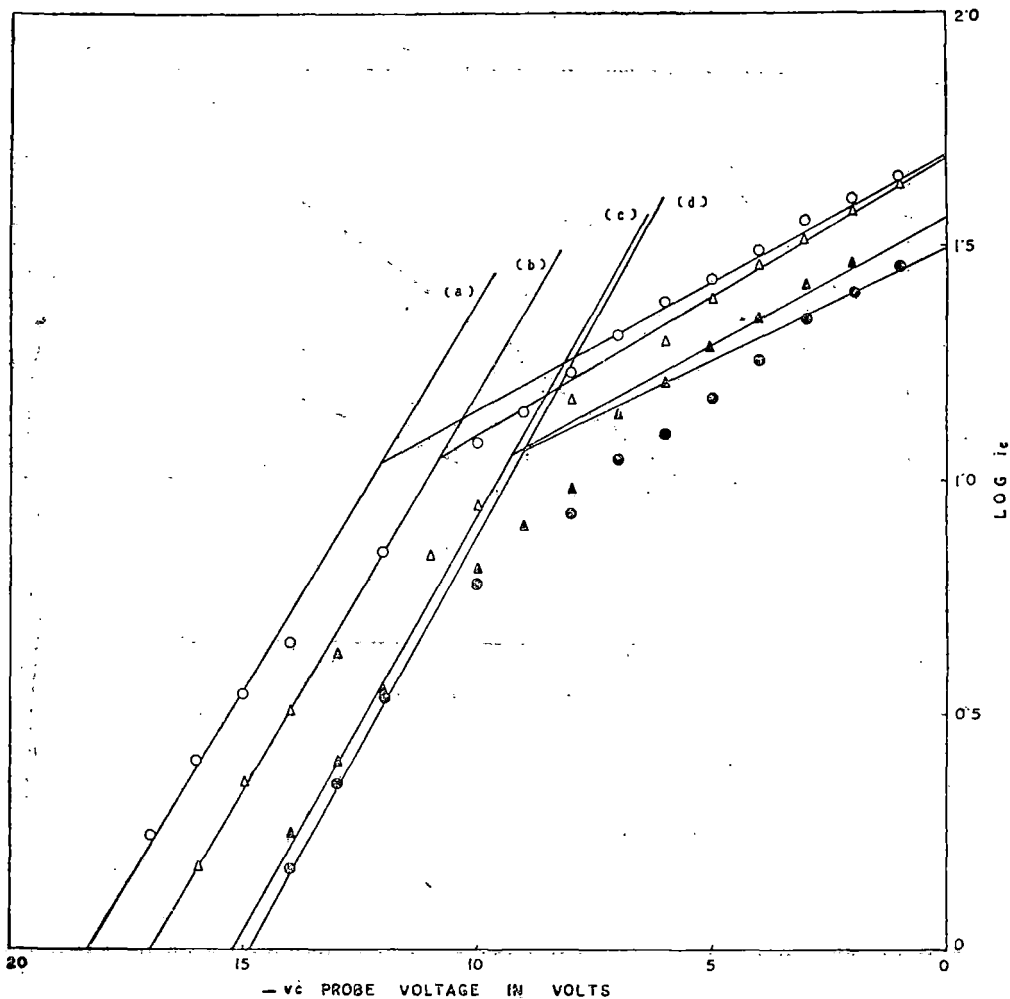


FIG. 4.  $\text{Log } I_e - V_p$  curves for Hydrogen in Longitudinal Magnetic field.  
 (a)  $B = 0\text{G}$  (b)  $B = 13\text{G}$  (c)  $B = 40\text{G}$  (d)  $B = 54\text{G}$

TABLE III

*Values of electron temperature in electron volt in longitudinal magnetic field*

Magnetic field	Air $P = 0.6$ torr	Hydrogen $P = 1$ torr	Oxygen $P = 0.4$ torr	Nitrogen $P = 0.6$ torr
0	5.263	6.026	4.126	6.787
13		5.937		6.696
27	5.165		3.863	6.589
40		5.684	3.652	
54	5.141	5.501	3.423	6.277
82	4.917			

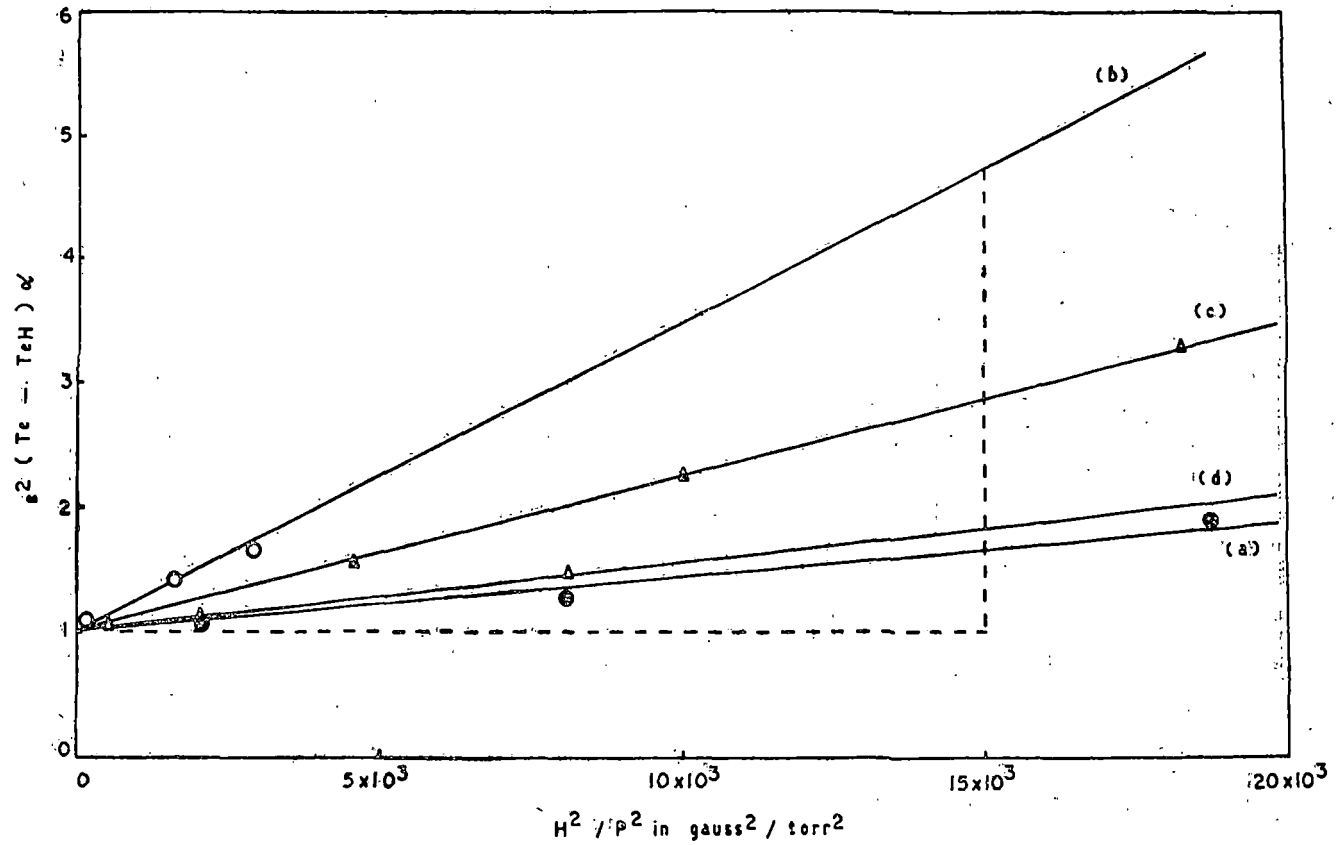


FIG. 5. Variation of  $e^2 (T_e - T_{eH}) \alpha$  against  $H^2/P^2$  for  
 (a) Air (b) Hydrogen (c) Oxygen (d) Nitrogen in Longitudinal Magnetic Fields.

TABLE IV

*Value of  $n_H/n$  in longitudinal magnetic field.*

Magnetic field in gauss	Air		Hydrogen		Oxygen		Nitrogen	
	Theor.	Experiment.	Theor.	Experiment.	Theor.	Experiment.	Theor.	Experiment.
13			1.0005	1.017			1.0002	1.025
27	1.001	1.016			1.004	1.047	1.0006	1.058
40			1.002	1.054	1.005	1.1		
54	1.003	1.047	1.0034	1.097	1.011	1.16	1.002	1.109
82	1.007	1.097						

R is the radius of the discharge tube and  $\frac{1}{\Lambda^2} = 4.0671 \text{ cm}^{-2}$  and  $r$  has been taken to be 0.2 cm. the average distance of the probe from the axis.

Further

$$\frac{v_i H}{v_i} = \left[ \frac{\exp\left(-\frac{ev_i}{KT_{eH}}\right)}{\exp\left(-\frac{ev_i}{KT_e}\right)} \right] \left[ \frac{1 + \frac{ev_i}{KT_{eH}}}{1 + \frac{ev_i}{KT_e}} \right]$$

Thus all the terms in the right hand side of eqn. (3) can be evaluated and values of  $n_H/n$  can be calculated.

The agreement between the theoretical and experimental results is not very satisfactory but nevertheless the results do indicate that the axial electron density increases with the magnetic field. The quantitative disagreement arises due to the fact that whereas the theoretical expression expresses the electron density at a point distant  $r$  from the axis, in actual calculation we have taken an average value of  $r$  for the finite length of the probe because the whole area of the probe is effective in collecting the electrons. We can thus conclude that the alignment of the magnetic field with respect to the direction of the discharge current has a decisive effect on the values of the plasma parameters, and thereby we can bring out the difference in the behaviour of a swarm of electrons and their associated properties in transverse and longitudinal magnetic fields. In case of a transverse magnetic field as postulated by Beckman (1948) and further deduced by Sen and Gupta (1971) the electron temperature increases whereas radial electron density decreases up to a certain distance from the axis and our direct measurements of these two parameters by the probe method show not only qualitative but also quantitative agreement for small values of  $(H/P)$ . In case of longitudinal magnetic field the electron temperature decreases whereas the radial electron density increases and the direct measurements of these two parameters in longitudinal magnetic field indicates quantitative agreement with theoretical predictions.

The problem investigated here is to be clearly distinguished from some experimental studies performed recently (Aikawa, 1976) in which anisotropy of electron temperature and electron distribution function in a magnetised plasma has been

studied, What has been measured in the present investigation is the average electron temperature and its variation with the alignment of the magnetic field with respect to the direction of the discharge current. Throughout our investigation, it has been assumed that the electron energy distribution is Maxwellian in character and is hence temperature-dependent though in general the distribution is non Maxwellian. However, in case of molecular gases the excitation levels are widely spread out up to ionization potential and inelastic losses set up at low energies and these are so distributed so as to produce an approximately Maxwellian distribution. The present investigation thus clearly indicates that though the nature of electron energy distribution remains Maxwellian in character in presence of magnetic field also it becomes a function of the magnetic field and is dependent upon the alignment of the magnetic field with respect to the discharge current.

## REFERENCES

- Aikawa, H. (1976). The measurement of the anisotropy of electron distribution function of a magnetised plasma. *J. phys. Soc. Japan*, **40**, 1741.
- Beckman, L. (1948). The influence of a transverse magnetic field on a cylindrical plasma. *Proc. phys. Soc. London*, **61**, 515.
- Bickerton, R. J., and Von Engel, A. (1956). The positive column in a longitudinal magnetic field. *Proc. phys. Soc.*, **B69**, 468.
- Bohm, D., Burhop, E. H. S., Massey, H. S. W., and Williams, R. W. (1949). *The Characteristics of Electrical Discharges in Magnetic field*. McGraw Hill Bk. Co. Inc., New York.
- Chang, J. S., and Chen, S. L. (1977). Electrostatic probe measurements of low-density medium-pressure magneto plasma. *J. Phys. D. appl. Phys.*, **10**, 979.
- Chen, F. F., Etievant, C., and Mosher, D. (1968). Measurement of low plasma densities in a magnetic field. *Phys. Fluid*, **11**, 811.
- Kaneda, T. (1977). The electron temperature of a positive column with a transverse magnetic field. *Japan, J. appl. Phys.*, **16**, 1887.
- Laframboise, J. (1966). *UTIAS Report No. 100*, Institute of Aerospace Studies, University of Toronto.
- Schott, L. (1968). *Electrical Probes in plasma Diagnostics*, North Holland Publishing Co., Amsterdam.
- Sen, S. N., and Gupta, R. N. (1969). Plasma parameters from r. f. conductivity measurements. *Indian J. pure appl. Phys.*, **7**, 462.
- (1971). Variation of discharge current in a transverse magnetic field in a glow discharge. *J. Phys. D. appl. Phys.*, **4**, 510.
- Sen, S. N., Das, R. P., and Gupta, R. N. (1972). Spectral line intensity in a glow discharge in a transverse magnetic field. *J. Phys. D. appl. Phys.*, **5**, 1260.
- Sen, S. N., and Das, R. P. (1973). Voltage current characteristics and power relation in arc plasma in a transverse magnetic field. *Int. J. Electron.*, **34**, 527.
- Sen, S. N., and Jana, D. C. (1977). Current voltage characteristics of glow discharge in longitudinal magnetic field. *J. phys. Soc. Japan*, **43**, 1729.
- Thompson, J. B. (1961). Electron energy distribution in plasma, IV. Oxygen & Nitrogen, *Proc. R. Soc.*, **A262**, 503.
- Uehara, K., Yatsu, K., Hagiwara, S., and Kojima, S. (1975). Ion saturation current of a plasma having two electron temperatures. *Japan J. appl. Phys.*, **14**, 1761.

## CHAPTER IV

### MEASUREMENT OF ELECTRON TEMPERATURE IN GLOW DISCHARGE IN TRANSVERSE MAGNETIC FIELD BY SPECTROSCOPIC METHOD.

#### 4.1. Introduction

It is now well established that plasma parameters undergo a significant change when the plasma column is acted upon by a magnetic field. Whereas in an axial field at low gas pressure the electron temperature is reduced and the axial electron density increased, in a transverse field the electron temperature is raised and the electron density lowered when the positive column is pressed against the wall of the vessel (Beckman, 1948, Sen et al 1971, 1972, Kaneda, 1979). The nature of change is dependent upon the alignment of magnetic field with respect to the discharge current. In chapter III, we have measured parameters of magnetoplasma by Langmuir probe method in air, hydrogen, oxygen and nitrogen in both transverse and longitudinal magnetic fields. In a transverse magnetic field the radial electron density decreases and electron temperature increases in accordance with theory of Beckman (1948) and Sen et al (1972) specially for small values of  $B/p$  ( $B$  = magnetic field,  $p$  = gas pressure). Kaneda (1979) has reported that in a plasma a transverse magnetic field causes the wall losses and electron temperature to increase. Sen et al (1972) observed that the

intensity of spectral lines increases with transverse magnetic field and after attaining a maximum value gradually decreases with the field. The field for maximum intensity depends upon the nature of the gas and wavelength of radiation. Assuming that the radial electron density decreases and electron temperature increases in a transverse magnetic field, the results have been quantitatively explained. To verify whether the assumption that  $T_{eB}$  rises with  $B$  is valid,  $T_{eB} = f(B)$  is measured by spectroscopic method.

In chapter III, it has been observed that in transverse magnetic field, the probe characteristics became distorted owing to collision in the sheath. In this chapter measurement of electron temperature in glow discharge in hydrogen and helium plasma in transverse magnetic field by spectroscopic method has been described. Spectroscopic method has one advantage over the probe method that it does not disturb the plasma unduly. Electron temperature can be deduced from relative intensities of spectral lines. Electron temperature enters into the emission line intensities through excitation rate coefficients which are also dependent on electron number density. Both  $T_e$  and  $n_e$  are affected by a transverse magnetic field. When ratio of spectral intensities of two lines of some element is considered, dependence on  $n_e$  cancels out and the ratio depends explicitly on  $T_e$ . So dependence of  $T_e$  on transverse magnetic field could be determined by this method.

#### 4.2. Method of measurement

It is well known that  $T_e$  cannot be determined from measured spectral intensities without some assumptions regarding the type of equilibrium that prevails inside the discharge tube. At the very beginning the question arises whether the LTE or SC (semi-corona) model is appropriate. To obtain LTE, the ~~xx~~ reverse of all fast processes must be maintained and exact balancing of total rates for complementary processes must be allowed to take place. Since the discharge tube plasma considered here is optically thin to internal radiation (except perhaps for the resonance lines) collisional processes are usually more important in establishing LTE than radiative processes. Consequently collisional decay rates must exceed radiative decay rates. Thus, at a sufficiently high electron density, collisional LTE can be achieved. When electron densities are too low for the establishment of LTE it is still possible to obtain equilibrium whereby collisional excitation and ionisation is balanced by radiative decay and recombination respectively for all levels except the high lying ones. This model is known as semi-corona model. Some necessary, but not sufficient criteria for the establishment of LTE or SC inside a discharge tube have been discussed in chapter I. Utilising the criteria of Griem (1964), Hey (1978) and Wilson (1962) the value of electron number density  $n_e$  has been calculated and entered in Table 4.1 for hydrogen and helium gas.

TABLE 4.1

Limiting values of  $n_e$  for different types of equilibria.

Criteria	For LTE			For par-	For SC	Esti- mated
	Griem (1964)	Hey (1976)	Wilson (1962)	tial LTE Griem (1964)	Wilson (1962)	
Glow discharge	$n_e \gg 10^{17}$	$n_e \gg 10^{18}$	$n_e \gg 2 \times 10^{17}$	$n_e \gg 1.7 \times 10^{14}$	$n_e \leq 6 \times 10^{12}$	$10^{10}$ to $10^{11}$
Hydrogen						
P = 1 torr $T_e = 1$ eV.						
Helium	$n_e \gg 2 \times 10^{18}$	$n_e \gg 10^{19}$	$n_e \gg 2 \times 10^{18}$		$n_e \leq 3 \times 10^{14}$	$10^{10}$ to $10^{11}$
P = 1 torr $T_e = 5$ eV.						

It is evident from the table that the estimated electron density of glow discharge is well within the range of applicability of SC model,  $n_e$  has been estimated a bit higher than typical value in glow discharge for the constriction of the discharge tube in the central region from where the radiations are escaping.

In SC model, for a weakly ionised plasma,

$$n_1 n_e X_{1j}(T_e) = n_j^* \sum_{m < j} A_{jm} \quad (4.1)$$

$X_{1j}(T_e)$  is the collisional excitation rate coefficient from ground state (designated by subscript 1) to  $j^{\text{th}}$  state.  $n_j^*$  is number density of excited neutral atoms in the  $j^{\text{th}}$  level and  $n_1$  is the number density of ground state atoms.

Considering the plasma to be steady, homogeneous and optically thin the intensity of a transition  $j \rightarrow i$

$$I_{ji} = \frac{h \ell \nu_{ji}}{4\pi} n_1 n_e X_{1j} \frac{A_{ji}}{\sum_{m < j} A_{jm}} \quad (4.2)$$

$h$  is the Planck's constant,  $\ell$  is the length of the emitting plasma column along the line of sight.  $\nu_{ji}$  and  $A_{ji}$  are the frequency and transition probability of the transition respectively.  $\sum_{m < j} A_{jm}$  is the reciprocal of life time  $\tau_j$  of the  $j^{\text{th}}$  state.

Considering two transitions ( $j \rightarrow i$ ) and ( $\lambda \rightarrow i$ ) and taking the ratio of the spectral intensities,

$$\frac{I_{ji}}{I_{\lambda i}} = \frac{\lambda_{\lambda i}}{\lambda_{ji}} \frac{X_{1j}}{X_{1\lambda}} \frac{A_{ji}}{A_{\lambda i}} \frac{\sum A_{\lambda m}}{\sum A_{jm}} \quad (4.3)$$

since

$$X_{1j} = \int_{v_0}^{\infty} Q_{1j}(v) v f(v) dv \quad (4.4)$$

where  $Q_{1j}(v)$  is the collisional excitation cross section of electrons from the ground level and  $v_0$  is the threshold value for the transition. Estimation for  $X_{1j}$  can be made if we have the knowledge of  $Q_{1j}$  and  $f(v)$  which is the electronic velocity distribution function. After integration in (4.4)  $X_{1j}$  becomes a function of electron temperature and  $T_e$  may be determined from equation (4.3).

#### 4.2.1. Excitation rate coefficient for hydrogen

For hydrogen we have considered M.J. Seaton's cross section for collisional excitation by electron. For a Maxwellian electron energy distribution, Allen (1963) has calculated

$$X_{1j} = 17.0 \times 10^{-4} \frac{f_{1j}}{\sqrt{T_e} E_j} 10^{-5040 E_j / T_e} P\left(\frac{E}{k T_e}\right) \quad (4.5)$$

where  $E_j$  is the excitation energy in eV of the  $j$ th level and  $f_{1j}$  is the absorption oscillator strength which is characteristic to an optically allowed transition ( $1 \rightarrow j$ , 1 is the ground state).  $P(E/k T_e)$  is the Gaunt factor which is

slowly varying function of frequency and  $T_e$ . Allen has calculated that when  $E/kT_e > 10$

$$P\left(\frac{E}{kT_e}\right) = 0.066 / \left(\frac{E}{kT_e}\right)^{1/2} \quad (4.6)$$

utilising equations (4.5) and (4.6) in (4.3)

$$\begin{aligned} I_{ji} / I_{li} &= \\ &= \frac{\lambda_{li}}{\lambda_{ji}} \frac{f_{1j}}{f_{1l}} \left(\frac{E_l}{E_j}\right)^{3/2} \frac{A_{ji}}{A_{li}} \frac{\sum A_{lm}}{\sum A_{jm}} 10^{5040(E_l - E_j)/T_e} \end{aligned} \quad (4.7)$$

or,

$$T_e = \frac{5040(E_l - E_j)}{\log \left[ \frac{I_{ji}}{I_{li}} \frac{\lambda_{ji}}{\lambda_{li}} \frac{f_{1l}}{f_{1j}} \left(\frac{E_j}{E_l}\right)^{3/2} \frac{A_{li}}{A_{ji}} \frac{\sum A_{jm}}{\sum A_{lm}} \right]} \quad (4.8)$$

#### 4.2.2. Excitation rate coefficient for helium

The transitions chosen for the helium are 4471.5 Å and 5876 Å with upper levels,  $1s4d^3D$  and  $1s3d^3D$ . Both the radiations are triplet lines. The excitation to these ~~upper~~ levels by electron impacts of the ground state helium atoms are known as optically forbidden transitions since the upper levels have no optically allowed spontaneous emission to the ground level. Values of the cross section of the forbidden transitions are virtually unknown. Green (1966) has

suggested one semi-empirical formula for cross section of helium.

$$Q_{1j}(E) = \frac{4R^2 \pi a_0^2 f_{1j}}{E_0^2} [1 - (E_0/E)]^{1/2} (E_0/E)^3 \quad (4.9)$$

where  $E$  and  $E_0$  are the energy of electrons and threshold energy of the transition ( $1 \rightarrow j$ ).  $R = 13.6$  eV is the Rydberg energy and  $a_0$  is the Bohr radius. For  $f_{1j}$  Green suggests using the oscillator strength of a 'companion' allowed transition. Benson and Kulander (1972) have shown that equation (4.9) when averaged over a Maxwellian velocity distribution for electrons, can be represented as

$$X_{1j} = \beta_{1j} T_e^{\gamma_{1j}} \exp\left(-\alpha_{1j} \frac{E_j}{kT_e}\right) \quad (4.10)$$

where  $\beta$ ,  $\gamma$  and  $\alpha$  are constants. Choosing  $f_{1 \rightarrow 4^3D} = 0.01$  and  $f_{1 \rightarrow 3^3D} = 0.1$ , Benson and Kulander calculated values for the constant, for 5875.6 Å line ( $1 \rightarrow j$ ):

$$\beta_{1j} = 1.17 \times 10^{-7}, \quad \gamma_{1j} = -0.368 \text{ and}$$

$$\alpha_{1j} = 1.01$$

for 4471.6 Å line ( $1 \rightarrow l$ ):  $\beta_{1l} = 1.06 \times 10^{-8}$ ,

$$\gamma_{1l} = -0.362 \quad \text{and} \quad \alpha_{1l} = 1.01$$

A calculation for excitation rate coefficients considering  $T_e = 25,000^\circ\text{K}$  shows

$$X_{1j} = 5.6765 \times 10^{-14} \quad \text{and} \quad X_{1l} = 4.0065 \times 10^{-15}$$

~~in c.g.s.~~

in C.G.S. unit, so that  $X_{1j} / X_{1\ell} \approx 14$ . Subtracting the contributions from  $\exp. (-\alpha_{ij} E_{ij} / kT_e)$  the ratio  $X_{1j} / X_{1\ell} \approx 10.5$ . Since after subtracting contribution from  $\exp. (-\alpha_{ij} E_{ij} / kT_e)$ , the remaining contribution comes mainly from the  $\beta_{ij}$  in equation (4.10), we can write

$$\frac{\beta_{1j}}{\beta_{1\ell}} = \frac{X_{1j} \text{ subtracted}}{X_{1\ell} \text{ subtracted}} = 10.5$$

whereas the calculated values are  $\beta_{1j} / \beta_{1\ell} = 11.7 / 1.06 = 11$ , so that the  $X_{1j}$  in equation (4.10) is sensitive to  $\beta_{1j}$ . But the factor  $f_{1j}$  enters into  $\beta_{1j}$  and an arbitrary choice for a 'companion' allowed transition for  $f_{1j}$ , influences  $\beta_{1j}$  and hence  $X_{1j}$ . The experimentally measured values by St. John, Miller and Lin (1964) are

$$X_{1j} = 1.13 \times 10^{-15} \text{ and } X_{1\ell} = 4.4 \times 10^{-16}$$

so that  $X_{1j} / X_{1\ell} = 2.95$ , which differs from calculated values of Benson and Kulander with arbitrary choice of  $f_{1j, 1\ell}$ . From experimentally obtained values, the ratio  $\beta_{1j} / \beta_{1\ell}$  is obtained as

$$\beta_{1j} / \beta_{1\ell} \approx X_{1j} / X_{1\ell} = 2.95$$

The difference in experimental and calculated values may be traced back to the arbitrary choice in  $f$  values.

For two lines  $j \rightarrow i$  and  $\ell \rightarrow i$

$$\frac{I_{ji}}{I_{li}} = \frac{\lambda_{li}}{\lambda_{ji}} \frac{\beta_{1j}}{\beta_{1l}} \frac{A_{ji}}{A_{li}} \frac{\sum A_{lm}}{\sum A_{jm}} \exp \left[ \frac{\alpha}{kT_e} (E_l - E_j) \right] \quad (4.11)$$

and

$$kT_e = \alpha (E_l - E_j) / \ln \left[ \frac{I_{ji}}{I_{li}} \frac{\lambda_{li}}{\lambda_{ji}} \frac{\beta_{1l}}{\beta_{1j}} \frac{A_{li}}{A_{ji}} \frac{\sum A_{jm}}{\sum A_{lm}} \right] \quad (4.12)$$

since  $\alpha_{1j} = \alpha_{1l} = \alpha$  and  $\gamma_{1j} = \gamma_{1l}$ . For  $\beta_{1j} / \beta_{1l}$  in equation (4.12) we have utilised the value 2.95 obtained experimentally by St. John et al (1964).

#### 4.2.3. Measurements in magnetic field

When the magnetic field  $B$  is applied

$$(I_{ji})_B = \frac{h\nu_{ji}}{4\pi} n_{1B} n_{eB} X_{1j}(T_{eB}) \left[ \frac{A_{ji}}{\sum_{m < j} A_{jm}} \right]_B \quad (4.13)$$

Hence

$$\frac{(I_{ji})_B}{I_{ji}} = \frac{n_{1B}}{n_1} \frac{n_{eB}}{n_e} \frac{X_{1j}(T_{eB})}{X_{1j}(T_e)} \frac{\left[ \frac{A_{ji}}{\sum A_{jm}} \right]_B}{\left[ \frac{A_{ji}}{\sum A_{jm}} \right]} \quad (4.14)$$

## A. Hydrogen.

Putting values of  $X_{ij}$  from eqn. (4.5) and

$$P(E/kT_{eB})/P(E/kT_e) = (T_{eB}/T_e)^{1/2} \quad (4.14)$$

in eqn. (4.14) we get

$$\frac{(I_{ji})_B}{I_{ji}} = \frac{n_{eB}}{n_e} \frac{n_{jB}}{n_j} \frac{[A_{ji}/\sum A_{jm}]_B}{A_{ji}/\sum A_{jm}} 10^{-5040 E_j} \left( \frac{1}{T_{eB}} - \frac{1}{T_e} \right) \quad (4.16)$$

Now

$$\left[ \frac{A_{ji}}{\sum A_{jm}} \right]_B / \frac{A_{ji}}{\sum A_{jm}} = \frac{(g_i)_B}{g_i} \frac{\tau_{jB}}{\tau_j} \frac{g_j}{(g_j)_B} \quad (4.17)$$

where  $g$  is the statistical weight of the level. Considering two lines

$$\frac{(I_{li})_B / (I_{ji})_B}{I_{li} / I_{ji}} = \frac{g_l (g_j)_B}{(g_l)_B g_j} \frac{\tau_{lB} \tau_j}{\tau_l \tau_{jB}} 10^{5040 (E_l - E_j)} \left( \frac{1}{T_e} - \frac{1}{T_{eB}} \right) \quad (4.18)$$

As the degeneracy is with respect to magnetic quantum number, in a magnetic field there will be splitting of the levels (Zeeman effect). As such, in a magnetic field they must be regarded as actually simple that is no longer degenerate. These different states are ascribed the same a priori probability or the same statistical weight. That is, it is

assumed that they will appear equally often under the same conditions. Hence if the lines belong to one and the same series and if our spectroscope is unable to resolve the Zeeman splitting we can assume,

$$\left. \begin{aligned} \frac{g_l}{g_{lB}} \cdot \frac{g_{jB}}{g_j} &= 1 \\ \tau_l = \tau_{lB} \text{ and } \tau_j &= \tau_{jB} \end{aligned} \right\} \quad (4.19)$$

Then from eqns. (4.18) and (4.19)

$$\frac{1}{T_e} - \frac{1}{T_{eB}} = \log \left[ \frac{(I_{li})_B}{I_{li}} / \frac{(I_{ji})_B}{I_{ji}} \right] / 5040 (E_l - E_j) \quad (4.20)$$

## B. Helium

Proceeding in the same manner and considering equation (4.12) it can be shown that

$$\frac{1}{kT_e} - \frac{1}{kT_{eB}} = \frac{\ln \left[ \frac{(I_{li})_B}{I_{li}} / \frac{(I_{ji})_B}{I_{ji}} \right]}{\alpha (E_l - E_j)} \quad (4.21)$$

So from equations (4.8), (4.12), (4.20) and (4.21) electron temperatures with and without magnetic field may be determined for hydrogen and helium plasma in SC model. In the above calculations it has been assumed that plasma be optically thin, homogeneous and has a Maxwellian distribution for electronic energy. The validity for optical thinness and

Maxwellian distribution has been already discussed in Chapter I. For homogeneity of plasma column along the line of sight, equation (4.3) suggests that plasma need not be homogeneous along the diameter of discharge column which is also the line of sight, for  $\int_{-R}^R I_r dr$  will be equal for the two transitions. Moreover, when a transverse magnetic field is present, electrons and ions are deflected towards the wall of the discharge tube in the direction of Lorentzian force. Thus the cylindrical symmetry of the plasma column is destroyed. But the column will be deflected in the direction of line of sight due to Lorentz force either towards the collimator or away from the collimator depending upon the direction of discharge current. In our experiment the deflection was towards the collimator. The inhomogeneity developed in the plasma column along the line of sight by a transverse magnetic field would be equal for both the lines, so that measurements are not affected by the inhomogeneity developed. While determining  $T_e$  either from eqn. (4.8) or (4.12) the relative spectral response of the photomultiplier is to be considered. But to determine  $T_{es}$  from eqns. (4.19) and (4.21), the relative spectral response does not affect the measurements since it is in no way a function of a distant magnetic field and the ratio of the line intensities has been considered.

### 4.3. Experimental arrangement

The discharge tubes which acted as the source of radiation were fitted with aluminium electrodes. Pure hydrogen and helium gases under a pressure of 1 torr have been introduced into the discharge tube and the discharge was excited by a stabilised d.c. power supply (1000 volts, 20 mA). An accurately calibrated constant deviation spectrograph was used to measure the wave length of the incident radiation. The slit of the spectrometer was illuminated by condensing the light from the source on to the slit. The spectral line to be studied was focussed on the cathode of the photomultiplier tube (M 10FS 29V $\lambda$ ). The sensitivity of a photomultiplier tube is not the same for all wavelengths as sensitivity depends on the wavelength of the incident radiation and on the quantum efficiency of the cathode material.

So the radiation intensity which is determined experimentally was corrected for relative spectral response of the photomultiplier. Details of the method have been given in Chapter II. The intensity was measured by a microammeter in the detector circuit and this intensity was the total intensity  $\int_0^{\infty} I_{\nu} d\nu$ . The transverse magnetic field was varied between zero to 1000 G and the experimental set up has been shown in fig. 2.5. For hydrogen, the spectral lines chosen are 4861.33 Å ( $n = 4 \rightarrow n = 2$ ) and 6562.73 Å ( $n = 3$  to  $n = 2$ ). For helium, the 4471.5 Å ( $4^3D \rightarrow 2^3P_1$ )

and  $5875.6 \text{ \AA}$  ( $3^3D_{123} \rightarrow 2^3P_1$ ) emission lines were chosen. The spectral lines chosen have been shown in fig. 4.1. For two emission lines  $I_{\lambda_1}$  and  $I_{\lambda_2}$  with wavelengths  $\lambda_1$  and  $\lambda_2$  and energies of the upper levels of the transitions  $E_1$  and  $E_2$ ,

$$\frac{d(I_{\lambda_1}/I_{\lambda_2})}{I_{\lambda_1}/I_{\lambda_2}} = \left[ \frac{E_2 - E_1}{kT_e} \right] \frac{d(kT_e)}{kT_e} \quad (4.22)$$

where  $kT_e$  is the electron temperature in eV. If  $(E_2 - E_1) / kT_e \geq 1$ , then an  $\alpha\%$  change in  $T_e$  results in  $\geq \alpha\%$  change in  $I_{\lambda_1} / I_{\lambda_2}$ . But if  $(E_2 - E_1) / kT_e < 1$ , then an  $\alpha\%$  change in  $T_e$  gives less than  $\alpha\%$  change in  $I_{\lambda_1} / I_{\lambda_2}$ . So it is desirable to have  $(E_2 - E_1) / kT_e \geq 1$  in a measurement. But in our experiment, for visible atomic transitions with sufficient response to the photomultiplier, the above criterion is not fulfilled. In that case it is preferable to use one ionic lines. But in a magnetic field the way an ionic line is affected is different to that of an atomic line. Generally the ionic lines are enhanced more in a magnetic field. For this reason and as no strong ionic line was observable in the experiment, we have chosen the transitions that have been mentioned.

Other details of the experimental set up have been described in Chapter II.

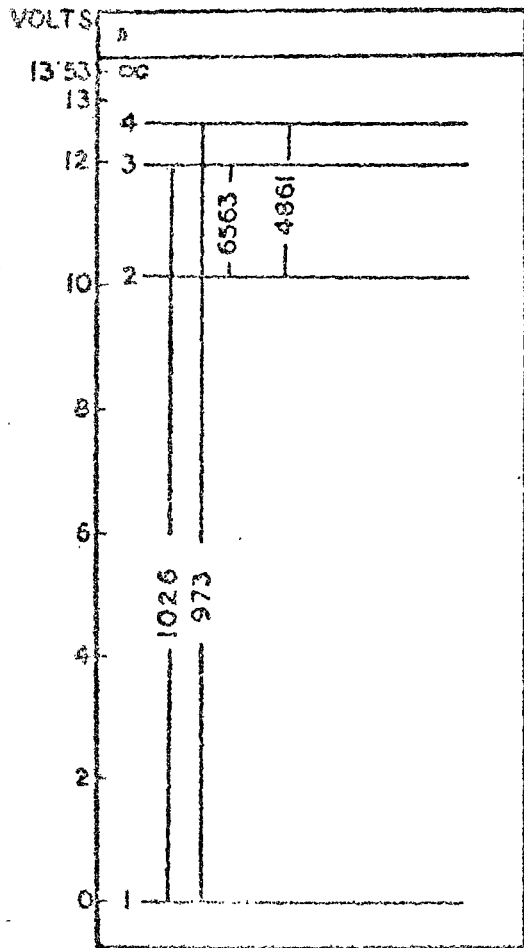


FIG. 4.1a ENERGY LEVELS OF THE LINES CHOSEN FOR HYDROGEN.

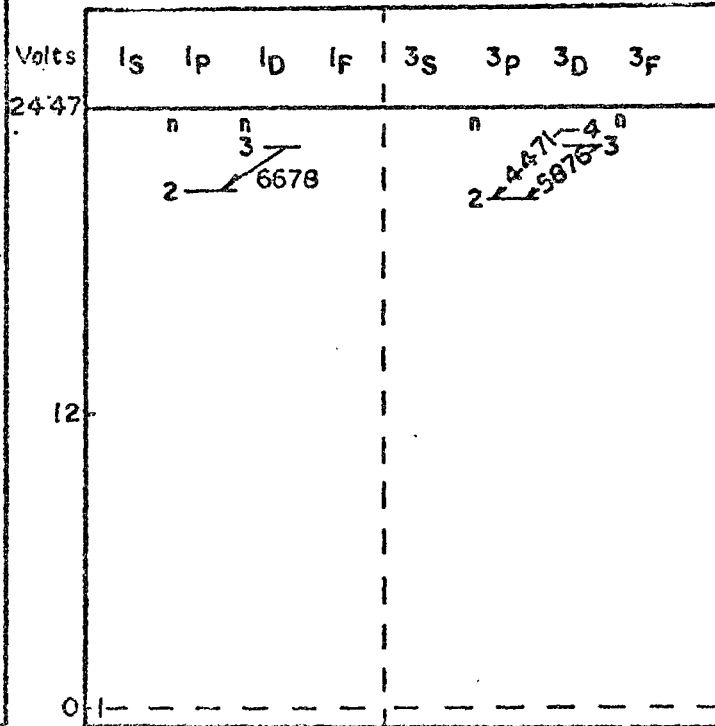


FIG. 4.1b ENERGY LEVELS OF THE LINES CHOSEN FOR HELIUM.

## 4.4. Results and Calculations

## A. Hydrogen

For hydrogen the values of the parameters appearing in eqn. (4.8) has been given in Table 4.2.

TABLE 4.2

Values of parameters for hydrogen.

$\lambda_{\alpha}$ (Å)	Transition	$f_{1\alpha}$	$A_{\alpha i} \times 10^{-6}$ Sec <sup>-1</sup>	$1/\tau_{\alpha}$ Sec <sup>-1</sup> $\times 10^{-6}$	$E_{\alpha}$ V
4861.3	$n = 4$ to $n = 2$	0.0372	32.866	127.12	12.75
6562.7	$n = 3$ to $n = 2$	0.1034	93.413	260.61	12.00

$A_{\alpha i}$  and  $\tau_{\alpha}$  values have been taken from Griem (1964) and Corney (1977).  $f$  values have been calculating using formula of Bethe and Salpeter (1957), for  $n \rightarrow m$  transition,

$$f_{mn} = \frac{2^5}{3^{3/2} \pi} \left( \frac{1}{n^2 - m^2} \right) \frac{1}{n^5} \frac{1}{m^3} \quad (4.23)$$

Since our spectrograph cannot resolve the fine structure of the levels, equation (4.23) was used to determine  $f$  values.

For hydrogen,

$I_{6563} / I_{4861} = 1.2$  and  $T_e$  was calculated to be  $1.017 \times 10^4$  °K.

Calculated values of electron temperature with and without a magnetic field have been entered in Table 4.3.

TABLE 4.3.

(Electron temperature calculated for hydrogen in SC model)

Magnetic field (G)	$B^2/p^2 \times 10^{-4}$ (G <sup>2</sup> /torr <sup>2</sup> )	$\ln \left[ \frac{(I_{li})_B}{(I_{li})_0} / \frac{(I_{lj})_B}{(I_{lj})_0} \right]$	$T_e \times 10^{-4}$ °K	$\left( \frac{T_{eB}}{T_e} \right)^2 - 1$
0	0	0	1.017	0
250	6.25	0.005	1.034	0.0276
360	13	0.00847	1.046	0.05
440	19.4	0.01424	1.06	0.08
475	22.6	0.01623	1.067	0.094
525	27.6	0.01933	1.076	0.113
600	36	0.026195	1.098	0.158
700	49	0.03261	1.118	0.202
840	70.6	0.0361	1.130	0.228
950	90.3	0.03735	1.134	0.238

Though for plasma, we are considering, LTE cannot hold, we have nevertheless calculated the electron temperature and its variation in the magnetic field when the plasma is in LTE for comparison purpose. In LTE

$$\frac{I_{ji}}{I_{ei}} = \frac{\lambda_{ei}}{\lambda_{ji}} \frac{A_{ji}}{A_{ei}} \frac{g_j}{g_e} \exp[(E_e - E_j)/kT_e] \quad (4.24)$$

Further

$$\left. \begin{aligned} A_{ji} &= 6.67 \times 10^{-1} \frac{g_i}{g_j} \frac{f_{ij}}{\lambda_{ji}^2} \\ A_{ei} &= 6.67 \times 10^{-1} \frac{g_i}{g_e} \frac{f_{ie}}{\lambda_{ei}^2} \end{aligned} \right\} \quad (4.25)$$

and

Hence

$$kT_e = \frac{E_e - E_j}{\ln\left(\frac{I_{ji}}{I_{ei}} \frac{\lambda_{ji}^3}{\lambda_{ei}^3} \frac{f_{ie}}{f_{ij}}\right)} \quad (4.26)$$

and

$$\frac{1}{T_e} - \frac{1}{T_{eB}} = \frac{k}{E_e - E_j} \ln \left[ \frac{(I_{ei})_B}{I_{ei}} / \frac{(I_{ji})_B}{I_{ji}} \right] \quad (4.27)$$

Calculated values of electron temperature with and without magnetic field has been entered in Table 4.4.

TABLE 4.4

$T_e$  of hydrogen with and without magnetic field in LTE.

Magnetic field B (Gauss)	$T_e \times 10^{-4}$ ( $^{\circ}\text{K}$ )	$(T_{eB}/T_e)^2 - 1$
0	1.4614	0
250	1.4945	0.0458
360	1.5181	0.079
440	1.5569	0.1351
475	1.5743	0.1606
525	1.5977	0.1953
600	1.6562	0.2789
700	1.7065	0.3637
840	1.7292	0.4000
950	1.7504	0.4341

B. Helium.

For helium the values of parameters determining

$T_e$  have been given in Table 4.5.

TABLE 4.5

$\lambda_{\alpha}$ ( $\text{\AA}$ )	$\frac{A_{\alpha i}}{\sum A_{\alpha m}}$	$\beta_{1j}/\beta_{1e}$	$\alpha_{1\alpha}$	$f_{1\alpha}$	$E_{\alpha}$ (V)
4471.5	1	2.95	1.01	0.12	23.7355
5875.6	1		1.01	0.62	23.0731

For the levels considered  $A_{\alpha i} / \sum A_{\alpha m} = 1$  because there is no other optically allowed transition which is sufficiently strong, from the levels. The choice for  $\beta_{1j} / \beta_{1e}$  has been already discussed in section 4.2.2.  $\alpha_{1\alpha}$  values have been taken from Benson and Kulander (1972), those of  $f_{i\alpha}$  for the transitions from Griem (1964). Energy values of levels have been taken from Moore (1971). Calculated values of electron temperature and its variation with transverse magnetic field have been shown in Table 4.6.

TABLE 4.6.

Electron temperature calculation for helium.

Magnetic field (G)	0	290	430	580
$I_{5876} (j \rightarrow i)$ (arbitrary unit) $\mu A$ reading.	160.0	162.0	163.5	166.0
$I_{4471} (l \rightarrow i)$ (arbitrary unit) $\mu A$ reading.	16.0	16.5	17.0	17.5
$\ln \left[ \frac{(I_{li})_B}{I_{li}} / \frac{(I_{ji})_B}{I_{ji}} \right]$	0.0184	0.0393	0.0528	0.069
$kT_e$ (eV) (SC model)	5.69	6.74	8.54	9.67
$kT_e$ (eV) (LTE model)	5.1	5.95	7.32	8.61

For calculating  $T_e$  without magnetic field the ratio  $I_{ji} / I_{ei} = 10$  as evident from Table 4.6 was corrected for photomultiplier response factor (Fig. 2.7) and after correction  $I_{ji} / I_{ei}$  was found to be 2.

#### 4.5. Discussions and Conclusions

To verify whether equation

$$T_{eB} = T_e \left[ 1 + C_1 \frac{B^2}{p^2} \right]^{1/2} \quad (4.28)$$

as deduced by Sen et al (1972) is valid for the plasma we are considering, we have plotted  $[(T_{eB}/T_e)^2 - 1]$  with  $B^2/p^2$  in Figs. (4.2) and (4.3) for hydrogen and helium. For hydrogen,  $C_1$  was calculated as

$$C_1 \text{ (Sc model)} = 0.426 \times 10^{-6}$$

$$C_1 \text{ (LTE model)} = 0.74 \times 10^{-6}$$

For helium,  $C_1$  value is  $6.25 \times 10^{-6}$  and more or less same for both the models.  $C_1$  is actually the square of the mobility of electrons in a gas of pressure one torr at  $0^\circ\text{C}$  and explicitly depends on  $\lambda_{e1}$ , the mean free path of electrons in a gas of one torr pressure.  $\lambda_{e1}$  is a function of electron energy, thus  $\lambda_{e1}$  depends on  $E/N$ . The experimentally obtained ratio of  $C_1$  for helium and hydrogen corresponding to  $E/N$  values of the discharges is 14.7. A compa-

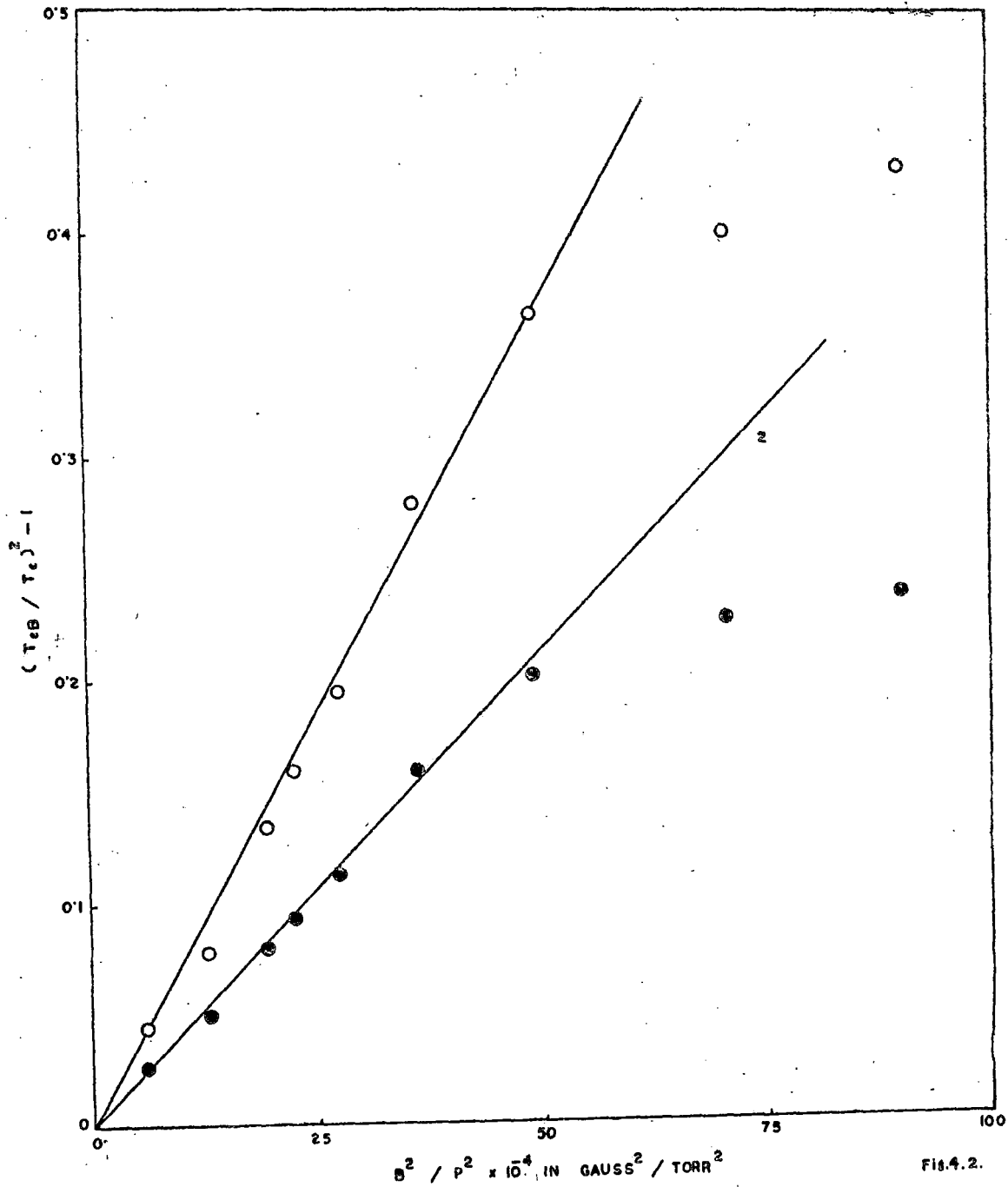


Fig. 4.2. Variation of  $(T_{eB}/T_e)^2 - 1$  with  $B^2/p^2$  for hydrogen in transverse magnetic field in SC (black circles) and LTE (white circles) models.

Fig. 4.3. Variation of  $(T_{eB}/T_e)^2 - 1$  with  $B^2/p^2$  for helium in transverse magnetic field in SC (white circles) and LTE (black circles) models.

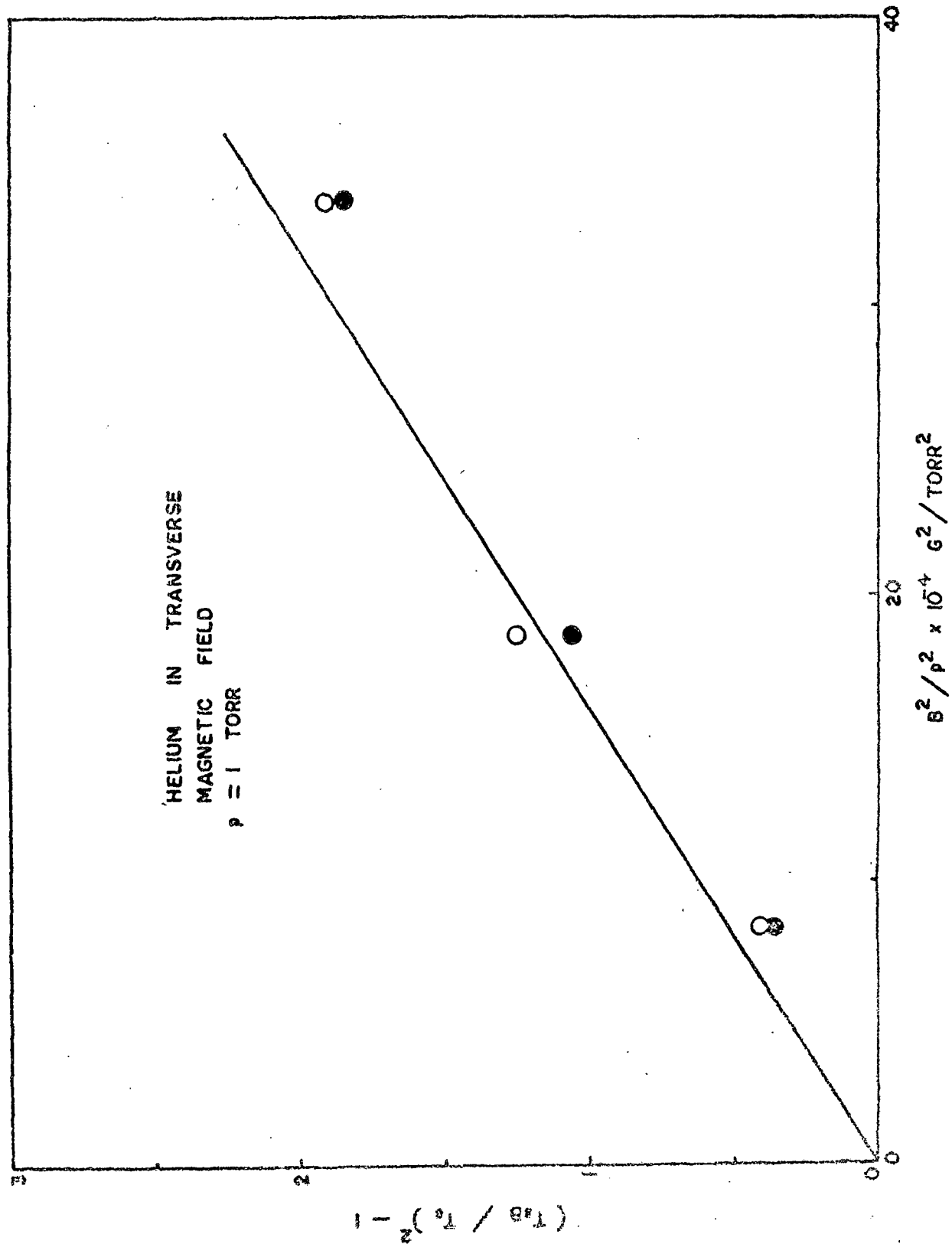


FIG. 4.3.

rison of this ratio with values obtained by other method is of interest. von-Engel (1965) has given the collision cross section  $Q_e$  ( $\text{cm}^{-1}$ ) of electrons at a pressure of 1 torr at  $0^\circ\text{C}$  for electron energies  $3 \times 10^{-2}$  eV. (molecular energies). Different values (5 and 23) for  $Q_e$  in helium have been given. The ratio  $Q_e$  (helium) /  $Q_e$  (hydrogen) calculated from A.H.von-Engel's table corresponding to  $3 \times 10^{-2}$  eV. energy, lies between 1.25 to 5.75 and the square of  $\frac{Q_e \text{ (helium)}}{Q_e \text{ (hydrogen)}}$  is between 1.56 and 33. But for a true comparison, E/N values of discharges should be ~~made~~<sup>same</sup>.

For hydrogen,  $C_1$  values found by probe method in chapter III and by spectroscopic method differ. The reason is the different values of E/N for the discharges. If we consider that the temperatures determined by different methods for different discharges (with E/N differing) are correct ~~than~~<sup>e/</sup> the temperatures would represent  $D/\mu$  where D and  $\mu$  are the coefficient of diffusion and mobility of electrons. Corresponding to these values of  $D/\mu$ , if we find out the corresponding E/N for hydrogen, from the graph given by Huxley and Crompton (1974), the ratio of E/N for probe experiment to E/N for spectroscopic experiment become 15 - 20 and the ratio of  $C_1$  value found by probe method and by spectroscopic method (S6 model) is 625 whose square root is 25.

For hydrogen  $C_1$  values obtained by SC and LTE models differ much but corresponding values for helium agrees very well. Actually LTE model is not a valid assumption under the conditions of discharges in our experiment, but we have calculated  $C_1$  values by LTE method for comparison. Actually  $T_e$  values may differ depending upon the models chosen, but in determining  $C_1$ , the ratio of electron temperatures e.g.  $(T_{eB}/T_e)^2 - 1$  is calculated which should not vary from model to model. So a comparison of  $C_1$  value for hydrogen and helium in different models have been made. From the comparison it is evident that calculation in SC model for helium is more certain than that of hydrogen. For helium, we have used experimentally obtained cross section values by St.John et al (1964) for determining excitation rate coefficients. The measurements of St.John et al was carried out in a low pressure chamber so that effects of imprisonment radiation and collisional excitation transfer can be neglected and this type of experimental values is needed for a true SC model. In the actual plasma in our experiment, SC equilibrium assumption was justified. The influence of triplet metastable state  $2^3S$ , on the population of higher triplet states have been neglected as no excitation from these metastable levels to the levels concerned has been taken into account. Phelps (1955) has shown that for helium below 10 torr pressure,  $2^3S_1$  level is quenched by

diffusion to the walls. A constriction in the central region of the discharge tube where experiment was carried out enhances the diffusion loss. Moreover, for helium, since the radiation  $3^3D_{123} \rightarrow 2^3P_2$  is very weak, we consider,  $A_{ji}\tau_j = A_{ei}\tau_e = 1$  i.e. the lines considered are the only transitions from the respective levels. Whereas for hydrogen values of  $A_{ji}\tau_j / A_{ei}\tau_e$  have been taken from Corney (1977) and the values were calculated theoretically from quantum mechanical basis which may have limited certainty.

It is thus evident that spectroscopic method can be adopted for measuring the electron temperature of a plasma in magnetic field as well. But a suitable choice of cross section data corresponding to the true model is to be found out.

The experimental result presented here show that equation (4.27) is valid for  $B/p$  as low as  $\leq 700 \text{ G. torr}^{-1}$ . The problem investigated here should be clearly distinguished from experimental studies by Aikawa (1976) in which anisotropy of the electron temperature and electron energy distribution function in a magnetised plasma has been studied. Here the average electron temperature and its variation in a magnetic field transverse to the direction of discharge current was measured assuming that the electron energy

distribution is Maxwellian and hence temperature dependent. It is evident that the majority of the electrons involved in the excitation and ionisation processes are those few with sufficiently high energy which occupy the tail of the distribution curve. Though the applied magnetic field will modify the energy distribution of these electrons only the distribution function of the majority of electrons remains unaltered and hence nearly Maxwellian and can be characterised by an electron temperature. The above measurement supports the theoretical deduction of Beckman (1948) and Sen et al (1972).

## References:

1. Aikawa, H. (1976), J. Phys.Soc. Japan 40 1741.
2. Allen, C.W. (1963), Astrophysical Quantities, 2nd. Edn. p. 42 (Athlone Press, London).
3. Beckman, L. (1948) Proc. Phys. Soc. 61 515.
4. Benson, R.S. and Kulander, J.L. (1972) Solar Phys. 27 305.
5. Bethe, H.A. and Salpeter, E.E. (1957) in Hand-b. Phys. 35 88 (Ed. S.Flugge, Springer-Verlag, Berlin).
6. Corney, A. (1977) Atomic and Laser Spectroscopy p.113 (Oxford University Press).
7. Green, A.E.S. (1966) AIAA/J 4 769.
8. Griem, H.R. (1964) Plasma Spectroscopy (McGraw Hill, NY).
9. Hey, J.D. (1976), J.Q.S.R.T. 16, 69.
10. Huxley, L.G.H. and Crompton, R.W. (1974).  
The diffusion and drift of electrons in gases,  
p. 621 (John Wiley, New York).
11. Kaneda, T. (1979) J.Phys. D.12, 61.
12. Moore, C.E. (1971) Atomic energy levels Vol.1,  
(N.B.S.Circular 467, Washington).
13. Phelps, A.V. (1955) Phys. Rev. 99 1307.
14. Sen, S.N., Das, R.P. and Gupta, R.N. (1972)  
J. Phys. D. 5 1260.
15. Sen, S.N. & Gupta, R.N. (1971) J.Phys.D.4 510.
16. St.John, R.M. Miller, F.L. and Lin, C.C.(1964)  
Phys. Rev. 134A 888.
17. von-Engel, A. (1965) Ionised gases, 2nd.Edn., p. 34  
(Oxford University Press).
18. Wilson, R.W. (1972), J.Q.S.R.T. 2, 477.

## Measurement of electron temperature in glow discharge in transverse magnetic field by spectroscopic method

S K Sadhya and S N Sen

Department of Physics, North Bengal University, Darjeeling, India

Received 23 May 1979, in final form 19 November 1979

**Abstract.** The electron temperature in the positive column of a glow discharge in hydrogen and helium as a function of the transverse magnetic field in the range of 0 to 1000 G has been obtained by measuring the intensities of two spectral lines having the same lower level. Since the electron number density in the column is of the order of  $10^{10} \text{ cm}^{-3}$  the semicorona model suitably modified has been used to calculate the plasma electron temperature in a magnetic field. For lower values of the field the variation of the electron temperature with the field can be represented by an expression deduced by Sen and Gupta following Beckman's theory. The electron energy distribution in a transverse field can thus be assumed to be nearly Maxwellian.

### 1. Introduction

It is now well established that plasma parameters undergo a significant change when the plasma column is acted upon by a magnetic field. Whereas in an axial field at low gas pressure the electron temperature is reduced and the electron density increased, in a transverse field the electron temperature is raised and the electron density lowered when the positive column is pressed against the wall of the vessel. (Beckman 1948, Sadhya *et al* 1979, Kaneda 1978.) The nature of the change is dependent upon the alignment of the magnetic field with respect to the direction of the discharge current. Sadhya *et al* (1979) have measured the axial electron density and electron temperature with Langmuir probes in air, hydrogen, oxygen and nitrogen in both the transverse and longitudinal magnetic fields. In a transverse magnetic field the radial electron density decreases and electron temperature increases in accordance with the theory of Beckman (1948) specially for small values of  $B/P$ ; ( $B$  = magnetic field,  $P$  = gas pressure). To verify experimentally whether the nature of variation is the same when a glow discharge column is in a transverse magnetic field the electron temperature and its variation has been measured in this paper using a spectroscopic method as reported by Davies (1953). He observed that in a longitudinal magnetic field the electron temperature in a radio frequency discharge is raised. Ricketts (1970) has measured the electron temperature and density of argon ring discharge at 2 to 50 Torr in a longitudinal magnetic field. The temperature distribution showed a large decrease at the centre indicating a rapid cooling of the electrons which diffuse across the magnetic field. Kaneda (1978) has reported that in a plasma a transverse magnetic field causes the wall losses and electron temperature to increase.

No spectroscopic measurement of the electron temperature of a plasma in a transverse magnetic field has been reported. Yet Sen and Gupta (1971) from the theoretical analysis of Beckman (1948) showed that in a transverse magnetic field  $B$ , the electron temperature  $T_{eB}$  should increase; for small  $B/P$

$$T_{eB} = T_e [1 + C_1 (B^2/P^2)]^{1/2} \quad (1)$$

where  $C_1 = (eL/mv_r)^2$ ,  $L$  is the mean free path of the electrons in the gas at 1 Torr and  $v_r$  is their random velocity.  $C_1$  is the square of the electron mobility at 1 Torr. Sen *et al* (1972) observed that the intensity of the spectral lines increases with transverse magnetic field and after attaining a maximum value gradually decreases with the field. The field for maximum intensity depends upon the nature of the gas and the wavelength of radiation. Assuming that the radial electron density decreases and the electron temperature increases in a transverse magnetic field the results have been quantitatively explained. To verify whether the assumption that  $T_{eB}$  rises with  $B$  is valid,  $T_{eB} = f(B)$  is measured by a spectroscopic method.

## 2. Method of measurement

The standard method of spectroscopically measuring  $T_e$  in a plasma is to measure the half-width of a spectral line. To study the effect of magnetic field  $B$  on  $T_e$ , a low pressure plasma with a low input power is necessary in order to make Doppler broadening negligible. Hence the method of calculating  $T_e$  by measuring the relative intensity of spectral lines has been adopted here.

It is well known that  $T_e$  cannot be determined from measured spectral line intensities without assuming the type of equilibrium in the discharge plasma. The question arises whether LTE or SC (semicorona) model is appropriate. When electron densities are too low for the establishment of LTE it is still possible to obtain equilibrium whereby collisional excitation and ionisation is balanced by radiative decay and recombination respectively which is known as the semicorona model. For a weakly ionised plasma,

$$n_1 n_e X_{1j}(T_e) = n_j^* \sum_{m < j} A_{jm}. \quad (2)$$

$X_{1j}(T_e)$  is the collisional excitation rate coefficient from the ground state to  $j$ th state, and  $n_j^*$  is the number density of excited neutral atoms in the  $j$ th level. Considering the plasma to be steady, homogeneous and optically thin

$$I_{ji} = \frac{h\nu_{ji}}{4\pi} n_1 n_e X_{1j} \frac{A_{ji}}{\sum_{m < j} A_{jm}}. \quad (3)$$

Assuming the electron energy distribution function to be Maxwellian, Allen (1963) has calculated that

$$X_{1j} = 17 \times 10^{-4} (f_{1j} / \sqrt{T_e E_j}) P(E/kT_e) 10^{-5040 E_j / T_e}. \quad (4)$$

$E_j$  is the excitation energy in electron volts and  $P(E/kT_e)$  is the average gaunt factor which is a slowly varying function of frequency and  $T_e$ ; when  $E/kT_e > 10$

$$P(E/kT_e) = 0.066 / (E/kT_e)^{1/2}. \quad (5)$$

Considering another transition  $l \rightarrow i$  and taking the ratio of the spectral intensities we obtain from (3), (4) and (5)

$$\frac{I_{ji}}{I_{li}} = \frac{\lambda_{li} f_{1j}}{\lambda_{ji} f_{1l}} \left( \frac{E_l}{E_j} \right)^{3/2} \frac{A_{ji}}{A_{li}} \frac{\sum_{m < l} A_{lm}}{\sum_{m < j} A_{jm}} 10^{5040(E_l - E_j)/T_e} \quad (6)$$

or

$$T_e = 5040(E_l - E_j) \left/ \lg \left[ \frac{I_{ji} \lambda_{ji} f_{1l}}{I_{li} \lambda_{li} f_{1j}} \left( \frac{E_j}{E_l} \right)^{3/2} \frac{A_{li}}{A_{ji}} \frac{\sum_{m < j} A_{jm}}{\sum_{m < l} A_{lm}} \right] \right. \quad (7)$$

This expression can be used for the measurement of electron temperature if the plasma is optically thin and excitations are by electron impact from the ground state and Wilson (1962) and de Vries and Mewe (1966) have shown that the approximate condition that has to be satisfied is

$$n_e \leq 10^{11} E_i^{3/2} (kT_e)^2 \text{ cm}^{-3}$$

where  $E_i$  and  $T_e$  are both in electron volts.

The electron density necessary for the semicorona model to hold is calculated from the above equation. For our present experiment the semicorona model is applicable.

### 2.1. Measurements in magnetic field

No measurement of electron temperature by the spectroscopic method in the transverse magnetic field has been reported so far. Sen *et al* (1972) observed that the intensity of a spectral line increases with the application of a transverse magnetic field. This effect has been utilised here to determine  $T_e$  by measuring the intensity of a line in the absence and in the presence of the field.

In the semicorona model we have shown that equation (3) holds. When the magnetic field is applied, from equations (3), (4) and (5) we obtain for the ratio of line intensities at  $B$  and at  $B=0$ .

$$\frac{(I_{ji})_B}{I_{ji}} = \frac{n_e B n_{1B}}{n_e n_1} \frac{(A_{ji} / \sum A_{jm})_B}{(A_{ji} / \sum A_{jm})} 10^{-5040[(1/T_{eB}) - (1/T_e)]} \quad (8)$$

Now

$$\left[ \frac{A_{ji}}{\sum A_{jm}} \right]_B \left/ \frac{A_{ji}}{\sum A_{jm}} \right. = \frac{(g_i)_B \tau_{jB}}{g_i \tau_j} \quad (9)$$

where  $\tau_j$  is the mean life in the  $j$ th level. Considering another line having the intensity  $I_{li}$  (transition  $l \rightarrow i$ ) and from equations (8) and (9)

$$\frac{(I_{ji})_B I_{li}}{(I_{li})_B I_{ji}} = \frac{(g_i)_B}{(g_i)} \frac{g_j}{(g_j)_B} \frac{\tau_l}{\tau_j} \frac{\tau_{jB}}{\tau_j} 10^{5040[(1/T_e) - (1/T_{eB})](E_l - E_j)} \quad (10)$$

As the degeneracy is with respect to magnetic quantum number in a magnetic field there will be splitting of the levels and these states are ascribed the same *a priori* 'probability' or the same statistical weight. Hence if the lines belong to one and the same series and if our spectrograph does not resolve the Zeeman splitting, we can assume

$$\frac{(g_i)_B}{g_i} \frac{g_j}{(g_j)_B} = 1$$

and also by the same assumption  $\tau_l = \tau_{lB}$  and  $\tau_j = \tau_{jB}$  then

$$\frac{(I_{jl})_B}{I_{jl}} \frac{I_{ul}}{(I_{ul})_B} = 10^{5040(E_l - E_j) \left[ \frac{1}{T_e} - \frac{1}{T_{eB}} \right]}$$

or

$$\frac{1}{T_e} - \frac{1}{T_{eB}} = \lg \left( \frac{(I_{jl})_B}{I_{jl}} \frac{I_{ul}}{(I_{ul})_B} \right) / 5040(E_l - E_j). \quad (11)$$

### 3. Experimental arrangement

The discharge tubes of 2.5 cm inner diameter and 15 cm length were fitted with aluminium electrodes and filled with pure hydrogen and helium at a pressure of 1 Torr. The discharge was excited by a stabilised DC power supply (1000 V, 10 mA). A constant deviation spectrograph was used. The slit was illuminated by condensing the light from the tubes on to the slit. The spectral line to be studied was focused on the cathode of the photomultiplier tube (M 10FS 29V $\lambda$ ). Since the sensitivity of a photomultiplier tube depends on the wavelength and on the quantum efficiency of the cathode material, proper correction has been made to standardise the intensity ratios of the spectral lines after Griem (1964). The detector circuit of Sen *et al* (1972) has been used here. The transverse magnetic field is provided by an electromagnet. It is varied from 0 to 1000 G and calibrated by a flux meter.

### 4. Results and discussion

The electron temperature of both a hydrogen and a helium plasma have been measured in the absence and in the presence of a magnetic field. For hydrogen the spectral lines chosen were

$$\lambda_{ul} = 4861.33 \text{ \AA} \quad E_l = 12.75 \text{ V}$$

$$\lambda_{jl} = 6562.73 \text{ \AA} \quad E_j = 12.00 \text{ V}$$

$$\frac{I_{jl}}{I_{ul}} = 1.25.$$

$f$  values are tabled in Griem (1964). Since our spectrograph cannot resolve the fine structure of the levels, the value of oscillator strength was found using the formula of Bethe and Salpeter (1957)

$$f_{mn} = \frac{2^5}{3^{3/2}\pi} \left( \frac{1}{n^2 - m^2} \right) \frac{1}{n^5} \frac{1}{m^3}$$

for  $n \rightarrow m$  transition. The values of  $A_{ji}$  and  $A_{jm}$  have been tabulated by Corney (1977) and Griem (1964). From equation (7)  $T_e$  in hydrogen was calculated  $T_e = 10\,200$  K.

For helium the spectral lines chosen were

$$\lambda_{ul} = 4471.5 \text{ \AA} \quad \lambda_{jl} = 5875.6 \text{ \AA}$$

$$E_l = 23.7355 \text{ V} \quad E_j = 23.0731 \text{ V}$$

For helium, excitations via metastable atoms have been neglected because the electron density is so low that the metastable levels are primarily quenched by diffusion to the

walls and by two- and three-body collisions. Phelps (1955) has shown that helium  $2^3S_1$  level is quenched in this way. Since the transition  $3^3D_{123} \rightarrow 2^3P_2$  is very weak  $A_{ji}\tau_{ij}/\tau_j A_{im}$  may be taken to be unity. The electron temperature for  $B=0$  in He is  $T_e=26\ 730$  K.

$T_e$  for  $H_2$  and He in the presence of a magnetic field has been obtained from equation (11).

Sen *et al* (1972) showed that assuming equation (1) the increase in intensity and the occurrence of a maximum in the intensity curve for a particular value of the magnetic field can be explained. The experimental verification of the theoretical deduction can be made from the experimental results obtained here.

Figures 1 and 2 show the variation of  $(T_{eB}/T_e)^2 - 1$  with  $B^2/P^2$ . The curves for  $H_2$  and He and low  $B/P$  are found to be straight lines but rise less steeply for higher

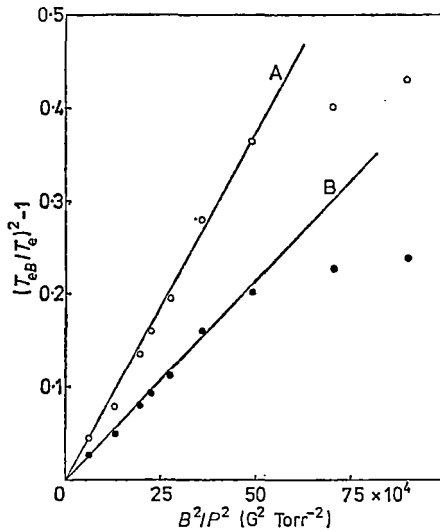


Figure 1. Variation of  $(T_{eB}/T_e)^2 - 1$  with  $B^2/P^2$  for hydrogen. A, from LTE model; B, from sc model.

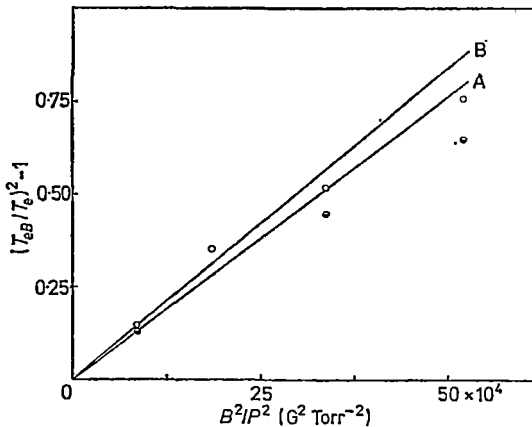


Figure 2. Variation of  $(T_{eB}/T_e)^2 - 1$  with  $B^2/P^2$  for helium. A, from LTE model; B, from sc model.

values of  $(B/P)$ . From the slope of the curve the value of  $C_1 = 0.426 \times 10^{-6}$  for  $H_2$  and  $C_1 = 1.68 \times 10^{-6}$  for He. These values agree quite well with the results obtained from radio frequency conductivity and microwave methods (Sen and Gupta 1970). By measuring the electron temperature by the probe method in a plasma in a transverse magnetic field it has been noted (Sadhya *et al* 1979) that  $T_e$  increases with  $B$  as given by expression (1).

The problem investigated here should be clearly distinguished from experimental studies by Aikawa (1976) in which the anisotropy of the electron temperature and electron distribution function in a transversely magnetised plasma has been studied. Here the average electron temperature and its variation in a magnetic field transverse to the direction of discharge current was measured assuming that the electron energy distribution is Maxwellian and hence temperature dependent. It is evident that the majority of the electrons involved in the excitation and ionisation processes are those few with sufficiently high energy which occupy the tail of the distribution curve. Though the applied magnetic field will modify the energy distribution of these electrons only, the distribution function of the majority of electrons remains unaltered and hence nearly Maxwellian and can be characterised by an electron temperature. The above measurements support the theoretical deductions of Beckman (1948).

It is thus evident that the spectroscopic method can be adopted for measuring the electron temperature of a plasma in magnetic field as well. The semicorona model is only valid for the determination of electron temperature in the positive column of a glow discharge if the electron density does not exceed  $10^{10} \text{ cm}^{-3}$ . It is also valid when the plasma is in a transverse magnetic field. Though in this case local thermodynamic equilibrium cannot hold we have nevertheless calculated the electron temperature and its variation in the magnetic field from

$$kT_e = (E_l - E_j) \left/ \ln \left( \frac{I_{ji} \lambda_{ji}^3 f_{il}}{I_{lu} \lambda_{lu}^3 f_{lj}} \right) \right. \quad (12)$$

and

$$\frac{1}{T_e} - \frac{1}{T_{eB}} = \frac{k}{(E_l - E_j)} \ln \left( \frac{(I_{lu})_B}{I_{lu}} \frac{I_{ji}}{(I_{jl})_B} \right).$$

The results have been plotted in figures 1 and 2 for comparison. It is seen that in a hydrogen plasma there is considerable difference between the results obtained from the two models, whereas in helium the results are almost identical. This is due to the fact that in helium the term  $A_{lu} \sum A_{jm} / A_{jl} \sum A_{lm}$  in equation (7) becomes unity and equation (7) becomes nearly identical with equation (12) whereas in hydrogen this ratio differs considerably from unity.

Sen *et al* (1972) assumed that equation (1) is valid over a wide range of  $B/P$  values and that the value of the magnetic field for which the intensity becomes a maximum can be obtained. However this proved to be not practicable because of numerous uncertain factors in the expression for  $B_{\text{max}}$ . The experimental results presented here show that equation (1) is valid for  $B/P$  as low as  $\leq 700 \text{ G Torr}^{-1}$ . Although the abscissae in figures 1 and 2 are in similar units of variable  $B/P$  the experimental variable for  $H_2$  and He was  $B$  since  $P$  and the tube diameter were kept constant (1 Torr, 2.5 cm).

## References

- Aikawa H 1976 *J. Phys. Soc. Japan* **40** 1741  
 Allen CW 1963 *Astrophysical Quantities* 2nd edn (London: Athlone Press)

- Beckman L 1948 *Proc. Phys. Soc.* **61** 515  
Bethe H A and Salpeter E E 1957 *Handb. d. Phys.* Ed S Flugge **35** 88 (Berlin: Springer-Verlag)  
Corney A 1977 *Atomic and Laser Spectroscopy* (Oxford: Clarendon Press)  
Davies L W 1953 *Proc. Phys. Soc.* **66B** 33  
de Vries R F and Mewe R 1966 *Phys. Fluids* **9** 414  
Griem H R 1964 *Plasma Spectroscopy* (New York: McGraw Hill)  
Kaneda T 1978 *Japan. J. Appl. Phys.* **17** 973  
Phelps A V 1955 *Phys. Rev.* **99** 1307  
Ricketts B W 1970 *J. Phys. D: Appl. Phys.* **3** 1678  
Sadhya S K, Jana D C and Sen S N 1979 *Proc. Ind. Nat. Sci. Acad. A* **45** 309  
Sen S N, Das R P and Gupta R N 1972 *J. Phys. D: Appl. Phys.* **5** 1260  
Sen S N and Gupta R N 1971 *J. Phys. D: Appl. Phys.* **4** 510  
— 1970 *Proc. Ind. Sci. Cong.* **57** 49  
Wilson R 1962 *J. Quant. Spectrosc. Radiat. Transfer* **2** 477

## CHAPTER V

### ELECTRON TEMPERATURE DEPENDENCE ON THE TRANSVERSE MAGNETIC FIELD IN A GLOW DISCHARGE IN HELIUM AS OBTAINED FROM SPECTROSCOPIC MEASUREMENTS.

#### 5.1. Introduction

In the previous chapter we have reported measurements of variation of electron temperature with transverse magnetic field of d.c. glow discharges in hydrogen and helium. It was observed there that for relatively small values of reduced magnetic field  $B/p$ , electron temperature in a magnetic field  $B$  is given by

$$T_{eB} = T_e \left[ 1 + C_1 \frac{B^2}{p^2} \right]^{1/2} \quad (5.1)$$

In this chapter we have reported measurement of variation of electron temperature with transverse magnetic field of a.c. (50 Hz) glow discharge in helium gas. In principle, a 50 Hz a.c. discharge is treated in the same manner as that of a d.c. glow discharge, but from the point of diagnostic, an a.c. glow discharge has the advantage that the radial symmetry of this type of discharge will be less affected in a transverse magnetic

field so that two cases e.g. the column deflected towards the collimator or away from the collimator do not arise. The lines selected for determining electron temperature with and without magnetic field by spectral intensity ratio method are the triplet line  $4471.5 \text{ \AA}$  ( $1s4d^3D \rightarrow 1s2p^3P^o$ ) and the singlet line  $6678 \text{ \AA}$  ( $1s3d^1D \rightarrow 1s2p^1P^o$ ). The selected lines have been shown in energy level diagram fig. 4.1.

## 5.2. Method of measurement

It has been observed that the dependence of electron energy on the cross section for excitation by electron impact differs for the singlet and triplet lines of neutral helium, so the singlet/triplet intensity ratio is a function of electron temperature in a tenuous helium plasma. It was first proposed by Cunningham (1955, USAEC Report Wash 289) to use this ratio to determine electron temperature of helium plasma. Since then, the method has been utilised in a large number of works. For two metastable levels  $2^3S$  and  $2^1S$  of helium, generally the population density of  $2^1S$  level is less than that of  $2^3S$  level as  $2^1S$  levels are quickly converted to  $2^3S$  levels by three body collisions. So it is stated that populations of triplet levels of helium in a well contained plasma are influenced by electron impact

excitation of the metastable  $2^3S$  level to other triplet levels. Mewe (1966) has deduced a criterion

$$n_e \ll (10^{12} - 10^{13}) d^{-1} \text{ cm}^{-3} \quad (5.2)$$

which is to be satisfied for well contained helium plasma of dimension  $d$  cm., so that the population of triplet levels are not influenced by  $2^3S$  metastable level population. For a constricted discharge  $d$  (= radius of the tube = 0.25 cm.) is small and hence R. Mewe's criterion is well satisfied along with the other criteria as in Table 4.1. When equation (5.2) is satisfied, the metastable atoms diffuse out to the wall of the discharge tube and the triplet level populations are determined from balance between excitation by electron impact of the ground state atoms and spontaneous radiative decay as in SC equilibrium condition.

One of the difficulty that is encountered while determining electron impact excitation rate coefficient  $\chi_{1j}$ , appropriate for as SC model, is that for low energy electrons, the theoretical treatment of electron impact excitation cross sections becomes questionable. In this low energy region, the Born approximation and the convenient sum rules associated with it break down and these have been the primary basis for most theoretical

calculations involving impact cross sections. So, what is needed is a systematic method that is capable of representing experimentally known cross sections, or which might permit us to use optical data or other information to infer unmeasured cross sections. The various systematic approaches from a classical or a quantum mechanical basis use rather varied mathematical formalisms. Nevertheless, each approach has been subjected to some phenomenological adjustment, and hence all of them embody experimental information to varying degrees. The approaches have been compared in several reviews (e.g. Green (1966)).

Since the radiations chosen for our experiment have no allowed transition toward the ground level ( $1S^21S$ ) the transitions ( $1S^21S \rightarrow 1S4d^3D$ ) and ( $1S^21S \rightarrow 1S3d^1D$ ), which enter into the particle balance equation in SC model, are known as optically forbidden transitions. Variens (1969) has discussed the limitations of binary or classical impact theories for optically forbidden transitions. One of the methods, as suggested by A.E.S. Green, is to select the absorption oscillator strength of a companion allowed transition and then treat the transition as an optically allowed transition, may lead to erroneous result for an arbitrary choice of oscillator strength. Such methods needed comparison with experimental

data and the necessary correction. Allen (1963) has described a semiempirical cross section for optically forbidden transition ( $1 \rightarrow j$ )

as

$$Q_{1j} = \pi a_0^2 \Omega(E) / g_1 E \quad (5.3)$$

where  $a_0$  is the Bohr radius,  $g_1$  is the statistical weight of ground level and  $\Omega(E)$  is the dimensionless collision strength which varies from zero at the threshold to a constant value of order unity at one Rydberg for atoms and remaining constant above this energy. For a Maxwellian electron energy distribution the excitation rate coefficient is given by

$$X_{1j} = \left( \frac{g}{m\pi} \right)^{1/2} (kT_e)^{-3/2} \int_{E_j}^{\infty} Q_{1j}(E) E \exp\left(-\frac{E}{kT_e}\right) dE \quad (5.4)$$

where  $m$ ,  $kT_e$  are the mass and energy in eV of electrons and  $E_j$  is the threshold energy for the transition ( $1 \rightarrow j$ ). For low energy electron collision, Benson and Kulander (1972) suggested that  $\Omega(E)$  may be considered constant with electron energies (within a Maxwellian distribution) if the electron energy exceeds one Rydberg and the constant value is equal to  $E_H/E_0$ , where  $E_H = 13.6$  eV and  $E_0 = E_j$  is the transition energy of the level in eV. So

So from equation (5.3) and (5.4)

$$X_{1j} = \frac{4 E_H \pi a_0^2}{g_1 E_j} \left[ \frac{k T_e}{2 \pi m} \right]^{1/2} \left[ \exp\left(-\frac{E_j}{k T_e}\right) \right] \left[ 1 - \exp\left(-\frac{E_H}{k T_e}\right) \right] \quad (5.5)$$

Excitation rate coefficient calculated from equation (5.5) compares well with experimental results. From the calculations of Benson and Kulander it appears that for  $T_e = 25,000^\circ\text{K}$  the ratio  $X_{1j} / X_{1l}$  for the two lines  $6678 \text{ \AA}$  and  $4471.5 \text{ \AA}$ , calculated from equation (5.5) is 1.31 whereas the experimentally determined value for  $X_{1j} / X_{1l}$  is 2.73 (St. John et al, 1964). But M.J. Seatons' cross-section with arbitrarily chosen absorption oscillator strengths gives

$X_{1j} / X_{1l}$  as 13.5. So  $X_{1j} / X_{1l}$  calculated from equation (5.5) agrees well with experimental data and it is the ratio  $X_{1j} / X_{1l}$  which enters into relative line intensity ratio.

For optically thin plasma, for two radiations ( $j \rightarrow i, l \rightarrow k$ ), the ratio of the intensities is

$$\frac{I_{ji}}{I_{lk}} = \frac{\lambda_{lk}}{\lambda_{ji}} \frac{X_{1j}}{X_{1l}} \frac{A_{ji}}{A_{lk}} \frac{\sum A_{lm}}{\sum A_{jm}} \quad (5.6)$$

For equation (5.6) and (5.5) we get

$$k T_e = (E_l - E_j) / \ln \left( \frac{I_{ji}}{I_{lk}} \frac{E_j}{E_l} \frac{\lambda_{ji}}{\lambda_{lk}} \right) \quad (5.7)$$

For radiations chosen

$$A_{ji} / \sum A_{jm} = A_{lk} / \sum A_{lm} = 1 \quad (5.8)$$

When a magnetic field is present

$$\frac{1}{kT_e} - \frac{1}{kT_{eB}} = \ln \left[ \frac{(I_{lk})_B}{I_{lk}} \frac{I_{ji}}{(I_{ji})_B} \right] / (E_i - E_j) \quad (5.9)$$

So from equation (5.7) and (5.9) electron temperatures without and with transverse magnetic field may be determined. The intensities of line need correction for ~~dx~~ differential response of the photomultiplier in determining temperature from equation (5.7), but when equation (5.9) is used to determine  $kT_{eB}$ , the correction is not needed.

### 5.3. Experimental arrangement

Experiments were performed on a helium glow discharge at a pressure of one torr. The discharge tube was connected to 50 Hz mains supply through the secondary of a step up transformer. Power to the step up transformer was fed to its primary coil through an auto-transformer. The discharge tube was held vertically and parallel to the collimator slit and was placed in between the pole-pieces of the electromagnet. The magnetic field was

varied between 0 - 1200 G.  $T_e$  and  $T_{eB}$  were determined from the ratio of the intensities of spectral lines 4471.5 Å and 6678 Å. An accurately calibrated spectrograph was used to measure the wavelength of the spectral lines. Each line was focussed on the cathode of the photomultiplier tube M10FS29V $_{\lambda}$  and the intensities were obtained by measuring the output of photomultiplier tube (details in chapter II). The intensities were corrected for the spectral response of the photomultiplier tube (5% and 9% respectively). The recorded output of the difference amplifier was found to be linearly proportional to known spectral intensities (International critical Table, 1929, Vol. 5), McGraw Hill Book Co.). It is to be noted that  $T_e$  and  $T_{eB}$  depend upon spectral intensities. To reduce possible error in the recording system, the width of the entrance slit was so adjusted to obtain a large deflection in the output microammeter of the difference amplifier, thereby increasing the sensitivity in the measurement of line intensity ratio.

#### 5.4. Results and discussions

The energy of the upper levels of the radiations chose are after Moore (1971).

$$\begin{aligned}
 4471.5 \text{ \AA} \quad (l \rightarrow k), \quad E_l &= 23.736 \text{ eV.} \\
 6678.2 \text{ \AA} \quad (j \rightarrow i), \quad E_j &= 23.073 \text{ eV.}
 \end{aligned}$$

value of  $kT_e$  obtained is 1.78 eV. Variation of electron temperature with transverse magnetic field has been shown in Table 5.1.

TABLE 5.1.

(Variation of electron temperature of a.c. helium glow discharge with transverse magnetic field).

Magnetic field (G)	$\frac{(I_{4771.5})_B}{I_{4771.5}} = x$	$\frac{(I_{6678})_B}{I_{6678}} = y$	$\frac{\ln(x/y)}{E_i - E_j}$	$kT_e$ (eV)
0	1	1	0	1.78
240	1.06383	1.05532	$1.2113 \times 10^{-2}$	1.82
390	1.12765	1.10212	$3.454 \times 10^{-2}$	1.90
550	1.18085	1.12765	$6.953 \times 10^{-2}$	2.03
650	1.21702	1.14893	$8.6835 \times 10^{-2}$	2.11
750	1.2468	1.17021	$9.562 \times 10^{-2}$	2.15
1000	1.38297	1.27659	$1.2072 \times 10^{-1}$	2.27

Values of  $[(T_{eB}/T_e)^2 - 1]$  versus  $B^2/p^2$  have been entered into Table 5.2.

TABLE 5.2

Values of  $[(T_{eB}/T_e)^2 - 1]$  Vs  $B^2/p^2$ .

$B^2/p^2$ $\times 10^{-5}$	0	0.576	1.521	3.025	4.225	5.625	10
$G^2/\text{torr}^2$							
$(\frac{T_{eB}}{T_e})^2 - 1$	0	0.0454	0.1394	0.3006	0.4052	0.4589	0.6263

In fig. (5.1),  $[(T_{eB}/T_e)^2 - 1]$  has been plotted against  $B^2/p^2$  and from the fig. it is observed that equation (5.1) as deduced by Sen et al (1972) is valid for electron temperatures for values of reduced magnetic field  $B/p \leq 670$  G/torr. For  $B/p > 670$  G/torr the deduction is not valid which is due to the fact that in deducing equation (5.1) from L. D Beckman's equation it was assumed that the reduced magnetic field  $B/p$  is small

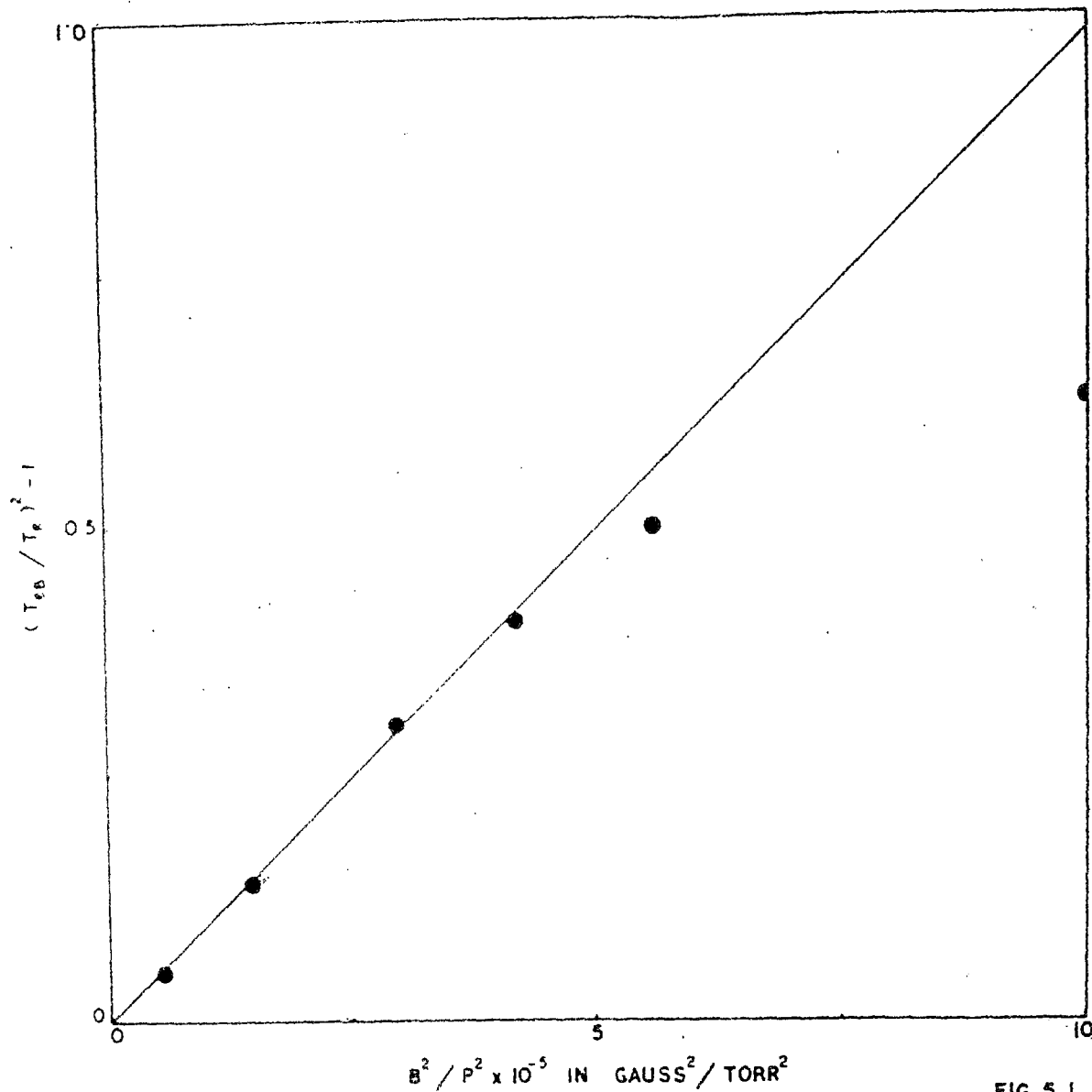


FIG. 5.1.

Fig. 5.1. Variation of  $(T_{eB}/T_e)^2 - 1$  with  $B^2/P^2$  for helium in transverse magnetic field (SC model).

Value of  $C_1$  calculated from the slope is  $0.99 \times 10^{-6}$ .  $C_1$  is the value of square of the electron mobility at a pressure of 1 torr at  $0^\circ\text{C}$ . So electron mobility at 1 torr pressure may be calculated as  $10^{-3}$  torr/G or  $10$  torr/kg (amp. sec.<sup>2</sup>)<sup>-1</sup>. (The conversion is  $10^4$  gauss = 1 kg/amp. sec.<sup>2</sup>). For a comparison of this value of mobility with other literature values, the value of  $E/N$  or  $E/p$  is needed. Value of  $E/N$  could not be determined experimentally. But from the value of electron temperature i.e.  $D/\mu$ , value of  $E/N$  is found from the table of Huxley and Crompton (1974) as  $E/N > 3 \text{ Td}$ . ( $E/N$  (TD) =  $3.03 E/p$ ). Considering  $E/p$   $10 \text{ V cm}^{-1} \text{ torr}^{-1}$  or  $E/p = 10^3 \text{ V m}^{-1} \text{ torr}^{-1}$ , value of drift velocity of electrons in helium at a pressure of 1 torr is calculated from the value of mobility from  $C_1$ , as  $10^4 \text{ m. sec.}^{-1}$ . This value compares well with a value given by Franklin (1976)  $6 \times 10^4 \text{ m. sec.}^{-1}$ .

## References

1. Allen, C.W. (1963) *Astrophysical Quantities*, 2nd. Edn. p. 43 (Athlone Press, London).
2. Benson, R.S. and Kulander, J.L. (1972) *Solar Phys.* 27, 305.
3. Franklin, R.N. (1976) *Plasma Phenomena in gas discharges* p.2 (Oxford University Press).
4. Green, A.E.S. (1966), *AIAA J* 4, 769.
5. Huxley, L.G.H. and Crompton, R.W. (1974) *The diffusion and drift of electrons in gases*, p. 603 (John Wiley, New York).
6. Mewe, R. (1966), *Brit. J. Appl. Phys.* 17 1239.
7. Moore, C.E. (1971) *Atomic Energy levels Vol.1* (N.B.S. Circular 467, Washington.)
8. Sen, S.N., Das, R.P. and Gupta, R.N., (1972) *J. Phys. D.* 5, 1260.
9. St. John, R.M., Miller, F.L. and Lin, C.C. (1964), *Phys. Rev.* 134A, 888.
10. Vriens, L. (1969) in *Case studies in atomic collisions Physics Vol.1* (Eds. E.W. McDaniel and M.R.C. McDowell, North Holland Publishing Co., Amsterdam).

REPRINTED FROM:

# PHYSICS LETTERS

Volume 79A, No. 2,3, 29 September 1980

**ELECTRON TEMPERATURE DEPENDENCE ON THE TRANSVERSE MAGNETIC FIELD  
IN A GLOW DISCHARGE AS OBTAINED FROM SPECTROSCOPIC MEASUREMENTS**

S.K. SADHYA and S.N. SEN

*Department of Physics, North Bengal University, Darjeeling, India*

pp. 162-164



NORTH-HOLLAND PUBLISHING COMPANY -- AMSTERDAM

## ELECTRON TEMPERATURE DEPENDENCE ON THE TRANSVERSE MAGNETIC FIELD IN A GLOW DISCHARGE AS OBTAINED FROM SPECTROSCOPIC MEASUREMENTS

S.K. SADHYA and S.N. SEN

*Department of Physics, North Bengal University, Darjeeling, India*

Received 6 March 1980

Revised manuscript received 4 July 1980

The electron temperature of a helium plasma has been measured spectroscopically as a function of the magnetic field. For lower values of the magnetic field, the variation of  $T_e$  with the field can be represented by an expression deduced by Sen and Gupta.

It has been shown by several authors [1-4] that the electron temperature  $T_e$  and the axial electric field of a steady uniform positive column in a low pressure d.c. discharge change in the presence of a transverse magnetic field. When such a magnetic field is present, the electrons and ions drift across the magnetic lines of force in cycloidal motion between collisions. The flow of ions and electrons in the direction of the Lorentzian force causes a deflection of the current and cylindrical symmetry of the discharge towards the wall, causing a corresponding increase in the axial electric field and electron temperature. For relatively small values of the reduced field  $B/P$ , where  $B$  is the transverse magnetic field in Gauss and  $P$  the pressure in Torr, Sen et al. [2] have shown

$$T_{eB} = T_e [1 + C_1 B^2 / P^2]^{1/2}, \quad (1)$$

where  $C_1 = ((e/m)L/v_r)^2$ ,  $L$  being the mean free path of the electron at a pressure of 1 Torr and  $v_r$  the random velocity of the electron and  $e$  and  $m$  are the charge and mass of the electron, respectively.

We have investigated the variation of  $T_e$  with the applied transverse magnetic field for an a.c. (50 Hz) low pressure helium discharge and have checked the validity of eq. (1) for such plasmas.  $T_e$  was determined spectroscopically by measuring the intensity of the  $\lambda = 4471.5 \text{ \AA}$  ( $2^3P \rightarrow 4^3D$ ) and  $\lambda = 6678 \text{ \AA}$  ( $2^1P \rightarrow 3^1D$ ) lines. Since the electron density  $n_e$  for such low pressure, low power glow discharges is much less than the value of  $n_e$  required for the establishment of LTE or

partial LTE [5] we have assumed a semicoronal equilibrium to prevail inside the discharge tube [6]. In this model the atoms are excited by electron impact to the states concerned directly from the ground state. Since the levels chosen have no optically allowed transition to the ground level of He, the cross section of excitation by electron impact for optically forbidden transitions is to be considered. Limitations of binary or classical encounter theories for such cross sections have been discussed by Viens [7]. Allen [8] has described a semiempirical cross section for such transitions as

$$\sigma = \pi a_0^2 \Omega(E) / g_1 E, \quad (2)$$

where  $\Omega(E)$  is the dimensionless collision strength which varies from 0 at threshold to a constant value  $R$  of the order of unity at 1 Ry remaining constant above this energy.  $E$  is the electron energy in Ry,  $g_1$  is the statistical weight of the ground level and  $a_0$  the Bohr radius. Since for He glow discharges the electron energy distribution function may be approximated to be Maxwellian [9] taking  $R = E_H / E_0$  [10], where  $E_H = 13.6 \text{ eV}$  and  $E_0$  the transition energy of the level in eV, the rate of excitation from the ground level to a level ( $k$ ) is

$$n_e n_1 \langle \sigma v_e \rangle = n_e n_1 \frac{4E_H \pi a_0^2}{g_1 E_0} \left[ \frac{kT_e}{2\pi m} \right]^{1/2} \times \left[ \exp\left(-\frac{E_0}{kT_e}\right) \right] \left[ 1 - \exp\left(-\frac{E_H}{kT_e}\right) \right]. \quad (3)$$

Considering the plasma to be optically thin and uniform, the intensity of a line  $k \rightarrow i$  is given as

$$I_{ki} = \frac{h\nu_{ki}}{4\pi} n_e n_1 \langle \sigma v_e \rangle A_{ki} / \sum_{m < k} A_{km} \quad (4)$$

Taking the intensity ratio of two lines  $l \rightarrow j$  and  $k \rightarrow i$  we get

$$kT_e = (E_l - E_k) / \ln \left( \frac{I_{ki}}{I_{lj}} \frac{E_k}{E_l} \frac{\lambda_{ki}}{\lambda_{lj}} \right), \quad (5)$$

where the  $E$ 's and  $\lambda$ 's are the energy of the levels and the wavelength of the radiations. For the radiations chosen

$$A_{ki} / \sum_{m < k} A_{km} = 1.$$

When a magnetic field is present

$$\frac{1}{kT_e} - \frac{1}{kT_{eB}} = \ln \left[ \frac{(I_{ij})_B}{I_{ij}} \frac{I_{ki}}{(I_{ki})_B} \right] / (E_l - E_k). \quad (6)$$

Details of the experimental arrangement are given in a previous paper [3]. Experiments were performed on an a.c. glow discharge of helium at a pressure of 1 Torr. The discharge tube of radius 1 cm, and 15 cm in length, was placed vertically between the poles of an electromagnet and the magnetic field (0–1200 G) was uniform inside the poles. The electron temperature  $T_e$  and  $T_{eB}$  without and with the transverse magnetic field, respectively, were determined by taking the intensity ratios of the spectral lines 4471.5 Å and 6678 Å, see eqs. (5) and (6). An accurately calibrated constant deviation spectrograph was used to measure the wavelength of the spectral lines. Each line was focussed on the cathode of the photomultiplier tube M10FS29,  $V_\lambda$  and the intensities were obtained by measuring the output of the photomultiplier which was recorded by a difference amplifier. It is to be noted from eq. (5) that an error in the value of  $T_e$  can arise only in the measurement of the observed line intensity ratio  $[I_{ki}/I_{lj}]$  as all other quantities have standard values. To reduce the possible errors the recording system was calibrated [3]. The intensities of the lines were corrected for the spectral response of the photomultiplier tube. The recorded output of the difference amplifier was found

Table 1

Magnetic field (G)	$\frac{(I_{4471.5})_B}{I_{4471}}$	$\frac{I_{6678}}{(I_{6678})_B}$	$kT_e$ (eV)
0	1		1.78
240	1.0081		1.82
390	1.0232		1.90
550	1.0472		2.03
650	1.0593		2.11
750	1.0654		2.15
1000	1.0833		2.27

to be linearly proportional to the known spectral intensities (International Critical Table, Vol. 4) and the width of the entrance slit was adjusted to obtain a large deflection in the output microammeter of the difference amplifier, thereby increasing the sensitivity in the measurement of the line intensity ratio. The value of  $T_e$  obtained here is in close agreement with the experimentally determined value of  $T_e$  for helium (Franklin [11]). The accuracy in the measurement of  $T_{eB}$  depends upon the experimentally observed ratio of both line intensities when a magnetic field is present. The transverse magnetic field produces some asymmetry and inhomogeneity in the spectral column but since the inhomogeneity will be along the line of sight both lines will be affected by almost the same degree due to this inhomogeneity. The energy values of the levels are tabulated in ref. [12]. Axial spectral intensities were

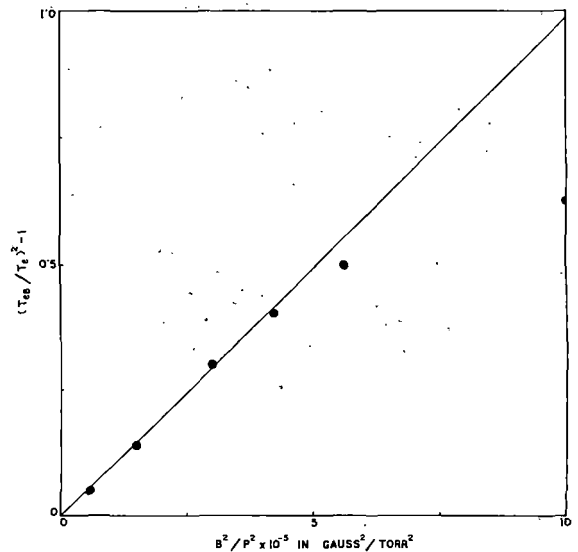


Fig. 1.

found to increase with magnetic field. Table 1 shows  $T_e$  values obtained spectroscopically up to 1000 G of magnetic field strength. Fig. 1 is a plot of  $[T_{eB}^2/T_e^2 - 1]$  against  $B^2/P^2$  and shows the validity of eq. (1) up to a magnetic field strength of 650 G. The slope of the curve gives a value of  $C_1 = 0.99 \times 10^{-6}$ .

It is observed that for  $B/P > 650$  G/Torr, the deduction is not valid which is due to the fact that in deducing eq. (1) from Beckman's equation it was assumed that  $B/P$  is small. The constant  $C_1 = ((e/m)/L/v_r)^2$  is the square of the mobility of the electrons in the gas at a pressure of 1 Torr and its numerical value as obtained here is consistent with the data found in the literature [11].

#### References

- [1] L. Beckman, Proc. Phys. Soc. 61 (1948) 515.
- [2] S.N. Sen and R.N. Gupta, J. Phys. D4 (1971) 510.
- [3] S.N. Sen, R.P. Das and R.N. Gupta, J. Phys. D5 (1972) 1260.
- [4] T. Kaneda, J. Phys. D12 (1979) 61.
- [5] J.D. Hey, Quant. Spectrosc. Radiat. Transfer 16 (1976) 69.
- [6] R. Mewe, Brit. J. Appl. Phys. 71 (1966) 1239.
- [7] L. Vriens, Case studies in atomic collision physics, Vol. 1, eds. E.W. McDaniel and M.R.C. McDowell (North-Holland, Amsterdam, 1969).
- [8] C.W. Allen, Astrophysical quantities, 2nd. Ed. (The Athlone Press, London, 1963).
- [9] A. Von Engel, Ionised gases, 2nd Ed. (Oxford U.P., London, 1965).
- [10] R.S. Benson and J.L. Kulander, Solar Phys. 27 (1972) 305.
- [11] R.N. Franklin, Plasma phenomena in gas discharge (Clarendon Press, Oxford, 1976).
- [12] C.E. Moore, Atomic energy levels, Vol. 1 (N.B.S. Circular 467, Washington, DC, 1971).

## Mercury arc plasma in an axial magnetic field

S. K. SADHYA† and S. N. SEN†

The electron temperature of a mercury arc plasma (arc current 2.25 A and 2.5 A) has been measured spectroscopically in an axial magnetic field varying from zero to 1050 gauss. It has been noted that the electron temperature decreases with the increase of the magnetic field. Considering the physical processes involved in a mercury arc discharge where the buffer gas is air and the pressure low, a model has been developed in which air plays the role of a quenching gas, and it has been found that in this type of discharge both atomic and molecular ions of mercury are present. Assuming the presence of both types of ions a radial distribution function for the electron density has been deduced and an expression for  $T_e/T_{eB}$  has been obtained. It has been found that within the range of  $(B/P)$  values used here the experimental results are in quantitative agreement with the theoretical deduction. The increase of radial electron density in an axial magnetic field as obtained by the probe method can also be explained by the theory developed.

### 1. Introduction

It is well known that plasma parameters such as electron density and electron temperature undergo a change when the plasma is subjected to a magnetic field, and in a detailed investigation (Sadhya *et al.* 1979) it has been shown that when the magnetic field is transverse to the direction of flow of the discharge current, the electron temperature increases and the azimuthal electron density decreases, whereas if the magnetic field is longitudinal the reverse effect takes place.

It is worthwhile investigating whether the physical processes undergo any significant change when we pass from the glow to the arc region, and in a previous investigation (Sen and Das 1973) it was established that in the case of a mercury arc plasma (current 1 A to 2.5 A) the electron temperature increases in a transverse magnetic field and that the results are in quantitative agreement with Beckman's theory (1948) as modified by Sen and Gupta (1971), especially for small values of the reduced magnetic field.

The effect of a longitudinal magnetic field on a low pressure mercury arc has been investigated by various workers (Cummings and Tonks 1941, Forest and Franklin 1966 and Vorobjeva *et al.* 1971); but there is shortage of data for high pressure, large current plasma with longitudinal magnetic field.

In the present investigation the variation of current and voltage across a mercury arc plasma as well as variation of the electron temperature are studied in a longitudinal magnetic field. Most of the results reported for mercury arc plasma are with argon as background gas; in the present investigation air is the background gas, which enables us to study how the excitation, ionization and de-ionization processes are influenced by the presence of air.

In the case of molecular gases the ionization is mainly due to electron impact of the ground state atom whereas in the case of a mercury arc, ionization is

---

Received 24 July 1980; accepted 28 July 1980.

† Department of Physics, North Bengal University, Darjeeling-734430, India.

mainly through inelastic electron impact with excited states like  $6^3P_2$  and with ground states, and the phenomena of associative ionization may also be present. Hence the physical processes occurring in a mercury arc plasma and how these processes are influenced by the magnetic field have to be taken into consideration in deducing the electron temperature and its variation in a magnetic field.

## 2. Experimental measurements and results

Experiments were performed on a d.c. mercury arc at low pressure, burning in air. The discharge currents were 2.25 A and 2.5 A, while the dry air pressure was varied from 0.05 torr to 2 torr. Electron temperature  $T_e$  and  $T_{eB}$  without and with magnetic fields were determined by measuring the intensities of  $\lambda 5770 \text{ \AA}$  ( $6^3D_2 \rightarrow 6^1P_1$ ) and  $\lambda 5790 \text{ \AA}$  ( $6^3D_1, 6^1D_1 \rightarrow 6^1P_1$ ) and taking their ratios. As the radiations differ by only 20  $\text{\AA}$  they would have equal response in the photomultiplier tube (MIOFS29V<sub>1</sub>) used.

A vertical mercury arc tube 10 cm in length and 1 cm in radius, burning in dry air and cooled externally was mounted in between the pole pieces (diameter 5 cm), and along the lines of force of the electromagnet. The discharge filled the tube totally. An accurately calibrated constant deviation spectrograph was used to measure the wavelength of the spectral lines. Each line was focused on the cathode of the photomultiplier tube operated at 1425 V. Detailed electronic arrangements for measuring the intensity of the spectral lines are given in an earlier paper (Sen, *et al.* 1972). The magnetic field (0–1100 gauss) was uniform inside the pole pieces.

The pressure of air which was introduced through a needle valve, was measured by a McLeod gauge and the pressure of mercury was determined after noting the temperature of the wall by a mercury-in-glass thermometer. In the present investigation we have taken measurements with two types of arc discharges, (a)  $i = 2.25 \text{ A}$   $P_{\text{air}} = 0.08 \text{ torr}$ ,  $P_{\text{Hg}} = 0.3032 \text{ torr}$ , (b)  $i = 2.5 \text{ A}$ .  $P_{\text{air}} = 0.08 \text{ torr}$  and  $P_{\text{Hg}} = 0.3731 \text{ torr}$ . The variation of current and voltage across the arc were noted for both types of discharge and for a wide range of magnetic field varying from 0 to 1100 gauss.

For the measurement of  $T_e$  from the intensity of spectral lines it has been shown by Griem (1963) that for LTE (Local Thermal Equilibrium) to be valid the electron density  $n_e$  should be greater than  $10^{16} \text{ cm}^{-3}$ . Since cross-sections increase rapidly with principal quantum numbers whereas radiative decay rates decrease, the highly excited states may be in equilibrium with the continuum, which leads to the idea of partial LTE and the condition for this to be valid has been obtained by Griem (1963) as  $n_e \geq 10^{12} \text{ cm}^{-3}$  which is valid in this case.

Hence under this condition

$$KT_e = \frac{(E_j - E_k)}{\ln \left[ \frac{I_{ki} A_{ji} \lambda_{ki} g_j}{I_{ji} A_{ki} \lambda_{ji} g_k} \right]} \quad (1)$$

where  $I_{ki}$  and  $I_{ji}$  are the intensities of spectral lines for the transitions  $k \rightarrow i$  and  $j \rightarrow i$  respectively and other symbols have their usual significance. The values of  $A_{ji}$  and  $A_{ki}$  have been taken from Mosberg and Wilkie (1978).

As the spectrograph used is unable to resolve the Zeeman splitting of the line in the magnetic field and the spectral intensity of the lines changes in the magnetic field (Sen *et al.* 1972) it can be deduced from eqn. (1) that

$$\frac{1}{KT_{eB}} - \frac{1}{KT_e} = \frac{\ln \left[ \frac{(I_{ki})_B}{I_{ki}} \frac{I_{ji}}{(I_{ji})_B} \right]}{(E_j - E_k)} \quad (2)$$

where  $(I_{ki})_B$  and  $(I_{ji})_B$  are the intensities of the lines in the presence of the magnetic field and  $T_{eB}$  is the electron temperature in the magnetic field. The results for the measurement of intensities of the lines with and without magnetic field and the corresponding electron temperature are shown in Tables 1 and 2.

Magnetic field in gauss.	$\frac{(I_{5790})_B}{I_{5790}} = A$	$\frac{(I_{5770})_B}{I_{5770}} = B$	$\ln \frac{A}{B}$	$T_e$ (eV)
0	1	1	0	0.412
255	1.02586	1.01852	$7.1806 \times 10^{-3}$	0.313
550	1.08621	1.07407	$1.1239 \times 10^{-2}$	0.282
835	1.14655	1.12963	$1.4867 \times 10^{-2}$	0.256
1050	1.17241	1.15278	$1.6887 \times 10^{-2}$	0.243

Table 1.  $i=2.5$  A,  $P_{\text{Hg}}=0.3731$  torr,  $P_{\text{air}}=0.08$  torr.

Magnetic field in gauss.	$\frac{(I_{5790})_B}{I_{5790}} = A$	$\frac{(I_{5770})_B}{I_{5770}} = B$	$\ln \frac{A}{B}$	$T_e$ (eV)
0	1	1	0	0.412
255	1.02913	1.02	$8.9072 \times 10^{-3}$	0.301
550	1.07282	1.06	$1.2017 \times 10^{-2}$	0.276
835	1.13592	1.12	$1.4116 \times 10^{-2}$	0.261
1050	1.19417	1.175	$1.6187 \times 10^{-2}$	0.247

Table 2.  $i=2.25$  A,  $P_{\text{Hg}}=0.3022$  torr,  $P_{\text{air}}=0.08$  torr.

### 3. Discussion of results

It is noted that when the magnetic field is applied the discharge current decreases, and since the supply voltage to the arc is constant the voltage across the discharge tube will increase.

To get the value of  $n_e$ , the electron density, we note that

$$i = \mu E e 2\pi \int_0^R n_r r dr$$

where  $n_r$  is the radial electron density and  $\mu E$  is the drift velocity of electrons for the mercury and air mixture. For this type of discharge no data for  $\mu E$  are available so values for electrons in mercury vapour are taken from the paper of Nakamura and Lucas (1978) where  $P_{\text{Hg}} \gg P_{\text{air}}$  as in this case.

Considering the distribution to be besseinain

$$i = \mu E e 2\pi n_{e0} \frac{R^2}{2.405} J_1(2.405)$$

From the above equation we get the value of  $\bar{n}_e$  the electron density averaged radially ( $\bar{n}_e = 0.432 n_{e0}$ ); when  $i = 2.5$  A,  $\bar{n}_e = 1.645 \times 10^{13}$  cm<sup>-3</sup> and for  $i = 2.25$  A  $\bar{n}_e = 5.687 \times 10^{12}$  cm<sup>-3</sup>. This result indicates that for the mercury arc discharge used here partial LTE is valid and eqns. (1) and (2) can be used for the measurement of  $T_e$  and  $T_{eB}$  respectively.

Further

$$i = e^2 E \frac{D_e}{KT_e} 2\pi \int_0^R n_r r dr \quad (3)$$

and

$$i_B = e^2 E_B \frac{D_{eB}}{KT_{eB}} 2\pi \int_0^R n_{rB} r dr \quad (4)$$

where  $D_e$  is the diffusion coefficient of electrons and the subscript B denotes quantities in the magnetic field. To get an expression for the electron density distribution we have to consider the model of a mercury arc burning in air at low pressure.

The discharge is axially homogeneous and cylindrically symmetric. The concentration of mercury ground-state atoms is taken to be constant across the cross-section of the tube and is determined by the temperature of the wall. Only the mercury atoms are excited and ionized by electron impact. No line emission from air (i.e. N<sub>2</sub> or O<sub>2</sub>) was observed. The concentration of the buffer gas which is dry air is also uniform across the tube cross-section and it plays a role in ambi-polar diffusion and mobilities of charged particles and in deactivating excited mercury atoms. We disregard the depletion of mercury ground-state atoms density at the axis of the discharge tube which is generally observed in low gas temperature experiments.

It is assumed that (i) the principal excited species are  $6^3P_2$ ,  $6^3P_1$  and  $6^3P_0$  with densities  $n_2$ ,  $n_1$  and  $n_0$  respectively and that cascading to these levels is not important in maintaining the densities, (ii) the diffusion losses can be accounted for by introducing a diffusion length, and (iii) the presence of a buffer gas like air will result in de-activation or quenching of excited species. It is assumed here that energy differences are given to molecular gases as vibrational energies.

Air constituents, chiefly nitrogen and oxygen are found to be good deactivating agents. The chief deactivating processes are

- I  $6^3P_0 + O_2 \rightarrow 6^1S + O_2^*$
- II  $6^3P_1 + N_2 \rightarrow 6^3P_0 + N_2^*$
- III  $6^3P_1 + N_2 \rightarrow 6^1S + N_2^*$
- IV  $6^3P_1 + O_2 \rightarrow 6^1S + O_2^*$
- V de-activation of  $6^3P_0$  atoms by Hg ground-state atoms should be considered.

The cross-sections of the processes are given in Messay *et al.*, (1971)

$$\begin{aligned} \sigma_I &= 0.31 \times 10^{-16} \text{ cm}^2, & \sigma_{II} &= 1.3 \times 10^{-16} \text{ cm}^2 \\ \sigma_{III} &= 3 \times 10^{-16} \text{ cm}^2, & \sigma_{IV} &= 4.4 \times 10^{-16} \text{ cm}^2 \\ \sigma_V &= 23.9 \times 10^{-16} \text{ cm}^2 \end{aligned}$$

Including these processes in the equation of Forrest and Franklin (1969) we get

$$-d_0 n_0 + E n_e n_g + W n_e n_1 + G n_1 n_g - (U + C + S) n_e n_0 - H n_e n_0 - B n_0 n_2 - Z n_g n_0 - Y n_0 n_{O_2} + X_1 n_1 n_{N_2} = 0 \quad (5)$$

$$-d_0 n_2 + F n_e n_g + J n_e n_1 - K n_2 n_g - (R + D + T) n_e n_2 - B n_0 n_2 = 0 \quad (6)$$

$$-d_0 n_1 + L n_e n_g - n_1/\tau + M n_g n_p - (N + J + W) n_1 n_e + G n_1 n_g + T n_e n_2 + U n_0 n_e - H n_0 n_1 + K n_2 n_g - X n_1 n_{N_2} - V n_1 n_{O_2} = 0 \quad (7)$$

$$-d_p n_1 - M n_g n_p + n_1/\tau = 0 \quad (7')$$

where

- $Y$  is related to process I
- $X_1$  is related to process II
- $X$  is related to process II + III
- $V$  is related to process IV
- $Z$  is related to process V

and other symbols have their significance as in Forrest and Franklin (1969) and  $n_{O_2}$  and  $n_{N_2}$  are the number densities of oxygen and nitrogen molecules.

To calculate the densities we note that for the  $6^1S_0$  state atom densities are as follows

$$\text{at } T_w = 96^\circ\text{C}, \quad P_{Hg} = 0.3032 \text{ torr}, \quad n_g = 7.83 \times 10^{15} \text{ cm}^{-3}$$

$$\text{at } T_w = 106^\circ\text{C}, \quad P_{Hg} = 0.3731 \text{ torr}, \quad n_g = 1.3282 \times 10^{16} \text{ cm}^{-3}$$

and evidently  $n_g > n_2, n_1, n_0$  or  $n_e$ .

To get the values of  $n_0, n_1$  and  $n_2$  as a first approximation we can neglect the terms  $J n_e n_1$  and  $B n_0 n_2$  in eqn. (6) as  $n_g \gg n_2, n_1, n_0, n_e$  which leaves us with an equation containing  $n_2$ , and values of  $n_g$  and  $n_e$  are known.

The values of different coefficients can be evaluated by assuming the electron energy distribution to be maxwellian and assuming the expression given by Sampson (1969) for the optically allowed transition for electron impact ionization as

$$\langle v_e \sigma \rangle = \pi a_0^2 \left( \frac{8KT_e}{m\pi} \right)^{1/2} \left[ 4f_{ig} \left( \frac{E_H}{E_0} \right)^2 \right] \frac{2\pi}{\sqrt{3}} \frac{E_0}{KT_e} \exp \left( -\frac{E_0}{KT_e} \right) P \left( \frac{E_0}{KT_e} \right)$$

where  $\pi a_0^2 = 8.797 \times 10^{-17} \text{ cm}^2$ ,  $E_0$  is the threshold energy of the transition, and  $f_{ig}$  the oscillator strength for the ( $6^1S_0 \rightarrow 6^3P_1$ ) transition, values of which have been given by Sampson (1969).

For optically forbidden transitions we have taken the expression of Benson and Kulandar (1972) which utilized Allen's cross section as

$$\langle v_e \sigma \rangle = \frac{4E_H \pi a_0^2}{g_e E_0} \left( \frac{KT_e}{2\pi m} \right)^{1/2} \exp \left( -\frac{E_0}{KT_e} \right) \left\{ 1 - \exp \left( -\frac{E_H}{KT_e} \right) \right\}$$

where  $g_e$  is the statistical weight of the state from which excitation is considered.

For the atom-atom/molecule reaction

$$\langle v \sigma \rangle = \sigma \left( \frac{8KT_g}{\mu\pi} \right)^{1/2}$$

where  $\sigma$  is the effective cross-section for the process considered and  $\mu$  is the reduced mass of the colliding atoms and molecules.

Having determined the value of  $n_2$ ,  $n_1$  can be found from eqn. (7) and putting this value of  $n_1$  in eqn. (5)  $n_0$  can be obtained. Taking these values of  $n_0$ ,  $n_1$ , and  $n_2$  the equations are evaluated afresh by considering all the terms of the three equations. This procedure is repeated and the change in the values of the  $n$ 's is found to be small. Results of calculation of species densities are entered in Table 3. To bring out the influence of buffer gas pressure, calculations are given for  $P_{\text{air}} = 0.05$  torr and  $P_{\text{air}} = 2$  torr.

Condition of plasma	$i$	2.5 A	2 A
	$P_{\text{air}}$	0.05 torr	2 torr
	$P_{\text{Hg}}$	0.3771 torr	0.222 torr
	$T_e$	0.5 eV	0.5 eV
Number of densities in $\text{cm}^{-3} \times 10^{-10}$	$n_{\text{N}_2}$	$1.424 \times 10^5$	$5.664 \times 10^6$
	$n_{\text{O}_2}$	$3.56 \times 10^4$	$1.424 \times 10^6$
	$n_{\text{g}}$	$1.328 \times 10^6$	$7.83 \times 10^5$
	$n_0$	68.6	7.788
	$n_1$	19.13	1.423
	$n_2$	86.2	42.7
	$n_e$	$1.64 \times 10^3$	$5.687 \times 10^2$

Table 3.

Now let us look into the ionization process in these types of discharges. The chief ionization processes in a mercury discharge are listed in Vriens *et al.* (1978).

1.  $\text{Hg}(6^1\text{S}_0) + e \rightarrow \text{Hg}^+ + 2e$
2.  $\text{Hg}(6^3\text{P}_0) + e \rightarrow \text{Hg}^+ + 2e$
3.  $\text{Hg}(6^3\text{P}_1) + e \rightarrow \text{Hg}^+ + 2e$
4.  $\text{Hg}(6^3\text{P}_2) + e \rightarrow \text{Hg}^+ + 2e$
5.  $\text{Hg}(6^3\text{P}_0) + \text{Hg}(6^3\text{P}_2) \rightarrow \text{Hg}_2^+(6^2\Sigma^+) + e$
- 6 (a).  $\text{Hg}(6^3\text{P}_1) + \text{Hg}(6^3\text{P}_2) \rightarrow \text{Hg}^* + \text{Hg}(6^1\text{S}_0)$
- 6 (b).  $\text{Hg}^* + e \rightarrow \text{Hg}^+ + 2e$

another process namely

7.  $\text{Hg}(6^3\text{P}_2) + \text{Hg}(6^3\text{P}_2) \rightarrow \text{Hg}^+(6^2\text{S}_{1/2}) + \text{Hg}(6^1\text{S}_0) + e$

is not considered by us as spin is not conserved. Electron impact ionization rates from different levels  $K_1 \rightarrow K_4$  for processes 1 to 4 are given by Sampson (1969)

$$n_e n_i \langle \sigma_e v \rangle = 5.465 \times 10^{-11} n_e n_i T_e^{1/2} \exp\left(-\frac{e\chi_i}{KT_e}\right) \Gamma_i(T_e) \quad (8)$$

$i = g, 0, 1, 2.$

here  $T_e$  is the electron temperature in K,  $e\chi_i$  is the ionization energy of the  $i$ th level and  $\Gamma_i = An/\chi_i^2$  where  $A = 200$  for neutral atoms, and  $n =$  number of electrons per atom in the outer orbit. For process 5, the rate is

$$\begin{aligned} K_5 &= n_0 n_1 \langle \sigma_5 v \rangle \\ &= n_0 n_1 \sigma_5 \langle v \rangle \end{aligned} \quad (9)$$

$\sigma_5$  is the effective cross-section for associative ionization. Tan and Von Engel (1968) have determined

$$\sigma_5 = 46 \times 10^{-15} \text{ cm}^2 \quad \text{and} \quad \langle v \rangle = \left( \frac{16KT_g}{\pi m} \right)^{1/2}$$

For process 6

$$K_6 = n_1 n_2 \sigma_6 \langle v \rangle B_i \quad (10)$$

$\sigma_6$  is estimated by Vriens *et al.* (1978) to have a value of  $10 \times 10^{-15} \text{ cm}^2$ ,  $B_i$  is the branching ratio and as calculated by the authors,  $B_i$  should be slightly less than unity.

All the atoms in the highly excited states populated by process 6(a), are ionized by electron impact, very few of them will make optically allowed transitions. We have neglected ionization from the  $6^1P_1$  level since the population density and natural life time of this level are small. With the help of eqn. (8), (9) and (10) and utilizing the values of  $n_e$ ,  $n_g$ ,  $n_0$ ,  $n_1$ , and  $n_2$  (Table 3) the rates of ionization for the two types of discharges considered here have been calculated and are entered in Table 4.

Discharge conditions	$i$	2.5 A	2 A
	$T_e$	0.5 eV	0.5 eV
	$P_{\text{air}}$	0.05 torr	2 torr
	$P_{\text{Hg}}$	0.3731 torr	0.222 torr
Rate of ionization in $\text{s}^{-1} \times 10^{-11}$	$K_1$	11.585	5.41
	$K_2$	21.94	1.98
	$K_3$	10.13	0.61
	$K_4$	181.37	71.2
	$K_5$	1700	8.72
	$K_6$	466.4	16.94

Table 4.

From Table 4 it is evident that for a plasma where air pressure is comparatively small, ionization is chiefly through the process of associative ionization and by electron impact ionization of highly excited Hg atoms whereas when  $P_{\text{air}}$  is comparatively large due to large quenching of  $6^3P_0$  levels ionization will be primarily through the process of electron impact of  $6^3P_2$  atoms. So in type I plasma where  $P_{\text{air}}$  is small two types of ions  $\text{Hg}_2^+$  and  $\text{Hg}^+$  prevail inside the discharge tube. To calculate the normal distribution in a mercury discharge with two types of ions, we can utilize the equations of Golubovskii and Lyaguschenko (1977)

$$\left. \begin{aligned} \text{div } \mathbf{J}_{i1} &= -D_{a1} \nabla \left( \frac{n_{i1}}{n_e} \nabla n_e \right) = F_1 \\ \text{div } \mathbf{J}_{i2} &= -D_{a2} \nabla \left( \frac{n_{i2}}{n_e} \nabla n_e \right) = F_2 \end{aligned} \right\} \quad (11)$$

and

$$F_1 + F_2 = F_e$$

where  $n_{i1}$  and  $n_{i2}$  are the number densities of  $\text{Hg}^+$  and  $\text{Hg}_2^+$  ions,  $J_{i1}$  and  $J_{i2}$  are the current densities,  $n_e$  is the electron density,  $D_{a12} = D_e(\mu_{i12}/\mu_e)$ .  $F_1$ ,  $F_2$  and  $F_e$  are the differences between the rates at which particles appear and disappear in the volume,  $\mu$  is the mobility.

Kovar (1964) has shown that actually  $\mu_{i2}/\mu_{i1} = 1.875$ . It may be interesting to note that heavier ions are faster. The reason behind this is that atomic ions moving in their parent gas will have large charge exchange cross-section and hence progress more slowly than the heavier molecular ions which do not suffer resonance charge exchange collisions. As the difference in  $\mu$  values is small and the presence of foreign gas will effectively reduce the charge exchange phenomena and obscure the vision of  $\text{Hg}^+$  ions for resonance to occur, the atomic and molecular ionic mobilities may be assumed equal.

Atomic ions will be produced mainly by (i) electron impact of highly excited states of Hg atoms at rate  $\nu_i n_e$  and these states are in thermal equilibrium with the electrons, (ii) by electron impact dissociation of molecular ions with a rate  $\omega n_{i2} n_e$  and they will be lost mainly by

- (i) ambi-polar diffusion to the wall,
- (ii) conversion to molecular ions in three-body collisions at rate  $\kappa n_{i1} n_e$

Hence

$$F_1 = \nu_i n_e + \omega n_{i2} n_e - \kappa n_{i1} n_e \quad (12)$$

Molecular ions will be produced mainly by

- (i) the process of associative ionization with rate  $g$ .
- (ii) conversion of atomic ions at a rate  $\kappa n_{i1} n_e$

and they will disappear by

- (i) ambi-polar diffusion
- (ii) electron impact dissociation to atomic ions at a rate  $\omega n_{i2} n_e$ .

We have neglected dissociative recombination of molecular ions. Hence

$$F_2 = g + \kappa n_{i1} n_e - \omega n_{i2} n_e \quad (13)$$

Hence from eqns. (11), (12) and (13) we get

$$\nu_i n_e + g = -D_a \nabla^2 n_e \quad \text{as } n_{i1} + n_{i2} = n_e \quad (14)$$

we have neglected any variation of excited state density across the tube cross section. In cylindrical co-ordinates system eqn. (14) reduces to

$$D_a \frac{1}{r} \frac{d}{dr} \left( r \frac{dn_r}{dr} \right) + g + \nu_i n_r = 0 \quad (15)$$

The solution of the equation is

$$n_r = \frac{n_{e0}}{1 - J_0 \left( R \sqrt{\frac{\nu_i}{D_a}} \right)} \left\{ J_0 \left( r \sqrt{\frac{\nu_i}{D_a}} \right) - J_0 \left( R \sqrt{\frac{\nu_i}{D_a}} \right) \right\} \quad (16)$$

where  $n_{eo}$ , the electron density at the axis is

$$\left. \begin{aligned} n_{eo} &= \frac{g}{\nu_i J_0 \sqrt{\alpha}} [1 - J_0 \sqrt{\alpha}] \\ \alpha &= R^2 \nu_i / D_a \end{aligned} \right\} \quad (17)$$

and

(A standard derivation of eqn. (15) can be found in the Appendix).

It is evident from eqn. (16) that the normal distribution in presence of the magnetic field will be given by

$$\left. \begin{aligned} n_{rB} &= \frac{n_{eoB}}{1 - J_0 \left( R \sqrt{\frac{\nu_{iB}}{D_{aB}}} \right)} \left\{ J_0 \left( r \sqrt{\frac{\nu_{iB}}{D_{aB}}} \right) - J_0 \left( R \sqrt{\frac{\nu_{iB}}{D_{aB}}} \right) \right\} \\ n_{eoB} &= \frac{g_B}{\nu_{iB} J_0 \sqrt{\alpha_B}} [1 - J_0 \sqrt{\alpha_B}] \end{aligned} \right\} \quad (17 a)$$

and

Cummings and Tonks (1941), from their experimental observations have predicted that the normal distribution for a mercury arc plasma is not affected by the presence of a longitudinal magnetic field. Hence since the distribution is a function of  $\nu/D_a$  we can assume that  $\nu_i/D_a = \nu_{iB}/D_{aB}$ . Consequently from eqns. (3) and (4)

$$\frac{i}{i_B} = \frac{E}{E_B} \frac{D_e}{D_{eB}} \frac{T_{eB}}{T_e} \frac{n_{eo}}{n_{eoB}} \quad (18)$$

Bickerton and Von Engel (1956) have shown that if  $T_{eB}$  is not much different from  $T_e$  the fractional change of energy of an electron to its total energy also remains constant with magnetic field. This leads us to  $E/E_B = T_e/T_{eB}$ . Hence

$$\frac{i}{i_B} = \frac{D_e}{D_{eB}} \frac{n_{eo}}{n_{eoB}} \quad (19)$$

Further if the change of electron temperature is small, then the rate of molecular ion formation due to associative ionization will almost remain the same so that  $g = g_B$ . The metastable population densities may be considered unaffected by the magnetic field. Hence since  $\nu_i/D_a = \nu_{iB}/D_{aB}$  we get from eqns. (17) and (17 a)  $n_{eo}/n_{eoB} = \nu_{iB}/\nu_i$ . Then from eqn. (19)

$$\frac{i}{i_B} = \frac{D_e}{D_{eB}} \frac{\nu_{iB}}{\nu_i} \quad (20)$$

As we are considering electron impact ionization of highly excited states only,  $\nu_i$  is as given by Elton (1970), from eqn. (8) and since  $eX_i \ll KT_e$  we have

$$\frac{i}{i_B} = \frac{D_e}{D_{eB}} \sqrt{\frac{T_{eB}}{T_e}} \quad (21)$$

When the frequency of ionization is much less than the frequency of momentum transfer

$$D_{eB} = \frac{D_e}{1 + \omega_B^2 \tau^2} = \frac{D_e}{1 + C_1(B^2/P^2)} \quad (20)$$

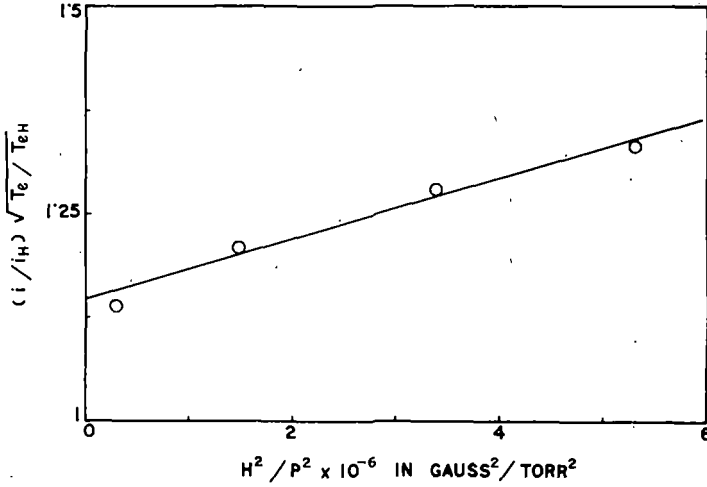


Figure 1. Variation of  $(i/i_B)\sqrt{(T_e/T_{eB})}$  with  $B^2/P^2$ ,  $i=2.5$  A.

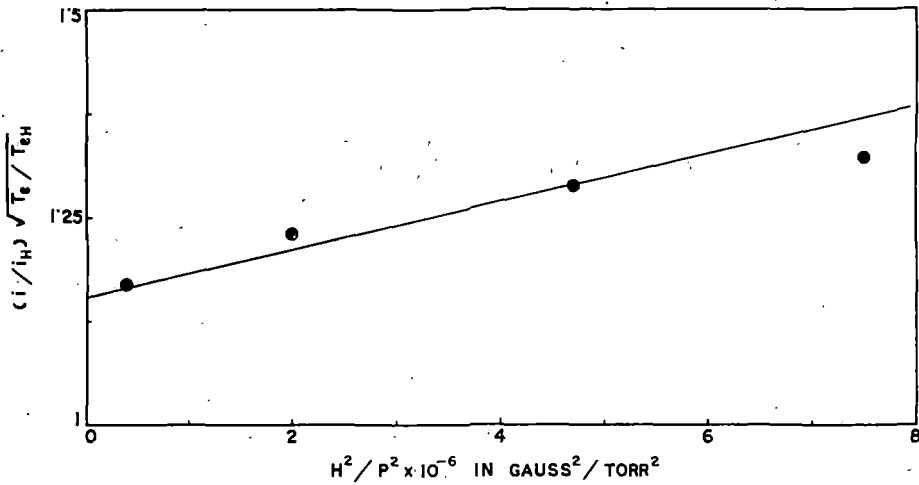


Figure 2. Variation of  $(i/i_B)\sqrt{(T_e/T_{eB})}$  with  $B^2/P^2$ ,  $i=2.25$  A.

where  $C_1 = [(e/m)(L/v_r)]^2$ .  $L$  is the mean free path of an electron at a pressure of 1 torr,  $P$  is the total pressure and  $v_r$  is the random velocity. Hence from (19) and (20)

$$1 + C_1 \frac{B^2}{P^2} = \frac{i}{i_B} \left( \frac{T_e}{T_{eB}} \right)^{1/2} \quad (21)$$

A plot of  $(i/i_B)(T_e/T_{eB})^{1/2}$  against  $B^2/P^2$  (figs. 1 and 2) will be a straight line and the gradient determines the value of  $C_1$  as entered in Table 5.

Magnetic field in gauss		$\frac{B^2}{P^2} \times 10^{-6}$	$\sqrt{\left(\frac{T_e}{T_{eB}}\right)_{\text{expt}}}$	$\left(\frac{i}{i_B}\right)_{\text{expt}}$	$\sqrt{\left(\frac{T_e}{T_{eB}}\right)\left(\frac{i}{i_B}\right)}$	$C_1$ from Figs 1 and 2
0	X	0	1	1	1	
	Y	0	1	1	1	
250	X	0.44	1.169	1.002	1.17	
	Y	0.3	1.138	1.0014	1.14	
550	X	2.0	1.2218	1.006	1.23	$0.3 \times 10^{-7} = X$
	Y	1.47	1.2087	1.005	1.21	$0.39 \times 10^{-7} = Y$
835	X	4.7	1.2564	1.0117	1.27	
	Y	3.4	1.2686	1.011	1.28	
1050	X	7.5	1.2915	1.0156	1.32	
	Y	5.3	1.302	1.017	1.33	

Table 5.

X corresponds to  $i=2.25$  A,  $P_{\text{air}}=0.08$  torr,  $P_{\text{Hg}}=0.3032$  torr  
 Y corresponds to  $i=2.5$  A,  $P_{\text{air}}=0.08$  torr,  $P_{\text{Hg}}=0.3731$  torr

#### 4. Conclusion

Considering the physical processes involved in a mercury arc discharge where the buffer gas is air and the pressure is low, we have evolved a model in which air plays the role of quenching gas and have found that in this type of discharge both atomic and molecular ions of mercury are present. Assuming the existence of both types of ion we have obtained the distribution function and deduced an expression for  $T_e/T_{eB}$  (eqn. (21)), and have found that within the range of  $(B/P)$  values used here the experimental results are in quantitative agreement with the theoretical deduction.

That the electron temperature decreases in presence of an axial magnetic field in the case of mercury discharge has also been shown by Franklin (1976).  $C_1 = [(e/m)(L/v_r)]^2$  is evidently the square of the mobility of the electron in the mercury air mixture at 1 torr. The value of mobility calculated from  $C_1$  agrees in order of magnitude with that obtained experimentally by Nakamura and Lucas (1978). Further the results show that frequency of ionization changes with the magnetic field as has been previously noted by Bickerton and Von Engel (1956).

It is also noted that  $(n_{e0B}/n_{e0}) = \sqrt{(T_e/T_{eB})}$ , and as experimentally we have found that  $T_e > T_{eB}$ , then we will have  $n_{e0B} > n_{e0}$  which was previously found to be true in the case of molecular gases, as determined by the probe method (Sadhya, *et al.* 1979, Cummings and Tonks 1941) in the case of mercury arc plasma.

#### ACKNOWLEDGMENTS

The authors are indebted to Professor K. G. Emeleus for offering useful comments and suggestions.

## Appendix

The solution of eqn. (15)

$$D_a \frac{1}{r} \frac{d}{dr} \left( r \frac{dn_r}{dr} \right) + g + \nu_i n_r = 0$$

can be obtained by putting  $r/R = y$  and  $n_r/n_{e0} = N_r$ , where  $n_{e0}$  is the electron density at the axis. We then attain

$$\frac{d^2 N_r}{dy^2} + \frac{1}{y} \frac{dN_r}{dy} + \frac{R^2}{D_a} N_r \nu_i + \frac{gR^2}{D_a n_{e0}} = 0 \quad (22)$$

Let us first consider the equation

$$\frac{d^2 N_r}{dy^2} + \frac{1}{y} \frac{dN_r}{dy} + \alpha N_r = 0 \quad \text{where } \alpha = R^2 \frac{\nu_i}{D_a}$$

Its solution is

$$y_1 = J_0(\sqrt{\alpha} \cdot y) \quad (23)$$

with the condition  $N_r = y_1 = 1$  at  $y = 0$  and we have,

$$\frac{d^2 y_1}{dy^2} + \frac{1}{y} \frac{dy_1}{dy} + \alpha y_1 = 0 \quad (24)$$

Multiplying (22) by  $y_1$  and (24) by  $N_r$  and subtracting we have

$$\frac{d}{dy} [y(y_1 \dot{N}_r - N_r \dot{y}_1)] = -\beta y y_1 \quad (25)$$

where

$$\beta = \frac{gR^2}{n_{e0} D_a}$$

On integrating equation (25) with conditions that at  $y = 0$  both  $\dot{N}_r$  and  $\dot{y}_1 = 0$  we have

$$y_1 \dot{N}_r - N_r \dot{y}_1 = -\frac{\beta}{\sqrt{\alpha}} J_1(\sqrt{\alpha} \cdot y) \quad (26)$$

Dividing (26) by  $y_1^2$  we get

$$d \left( \frac{N_r}{y_1} \right) = -\frac{\beta}{\alpha} \frac{d[J_0(\sqrt{\alpha} y)]}{[J_0(\sqrt{\alpha} y)]^2} \quad (27)$$

Integrating (27) with conditions  $y = 1$ ,  $N_r = 0$

$$N_r = \frac{g}{n_{e0} \nu_i} \left[ \frac{J_0(\sqrt{\alpha} y)}{J_0(\sqrt{\alpha})} - 1 \right] \quad (28)$$

Now at  $y = 0$ ,  $N_r = 1$  so eqns. (17) and (16), in the text, follow.

## REFERENCES

- BECKMAN, L., 1948, The influence of a transverse magnetic field on a cylindrical plasma. *Proc. Phys. Soc.*, **61**, 515.  
 BENSON, R. S., and KULANDER, J. L., 1972, Electron impact excitation rates for helium. *Solar Phys.*, **27**, 305.

- BICKERTON, R. J., and VON ENGEL, A., 1956, The positive column in a longitudinal magnetic field. *Proc. Phys. Soc.*, **76**, 468.
- CUMMINGS, C. S., and TONKS, L., 1941, Influence of a longitudinal magnetic field on an electric discharge in mercury vapour at low pressure. *Phys. Rev.*, **59**, 514.
- ELTON, R. C., 1970, *Methods of Experimental Physics*, Vol. 9 part A (New York : Academic Press).
- FORREST, J. R., and FRANKLIN, R. N., 1966, The positive column in a magnetic field at low pressures : The transition from free-fall to ambipolar conditions. *Brit. J. Appl. Phys.*, **17**, 1569 ; 1969, Two stage processes in mercury positive column. *J. Phys. B*, Ser. 2, **2**, 471.
- FRANKLIN, R. N., 1976, *Plasma phenomena in gas discharges* (Oxford : Clarendon Press).
- GOLUBOVSKU, Y. B., and LYAGUSCHENKO, R. I., 1977, Limiting current in a steady-state diffusion-recombination discharge. *Sov. Phys. Tech. Phys.*, **22**, 1073.
- GRIEM, H. R., 1963, *Plasma Spectroscopy* (New York : McGraw Hill).
- KOVAR, F. R., 1964, Mobility of mercury ions in mercury vapour. *Phys. Rev.*, **A133** 681.
- MASSEY, H. S. W., BURHOP, E. H. S., and GILBODY, H. B., 1971, *Electron and Ion Impact Phenomena*, Vol. III, 2nd, edn. (Oxford : Clarendon Press).
- MOSBERG, E. R., and WILKIE, M. D., 1978, Some new transition probabilities for mercury. *J. J. Quant. Spectros. Radiat. Transfer*, **19**, 69.
- NAKAMURA, Y., and LUCAS, J., 1978, Electron drift velocities in mercury, sodium and thallium vapours, I. Experimental. *J. Phys. D. Appl. Phys.*, **11**, 325.
- SADHYA, S. K., JANA, D. C., and SEN, S. N., 1979, Measurement of electron temperature and electron density in low density magnetised plasma by probe method. *Proc. Ind. Nat. Sci. Acad.*, **45A**, 309.
- SAMPSON, D. H., 1969, Comparison of some recently proposed excitation and ionization rates. *Astrophys. J.* **155**, 575.
- SEN, S. N., and DAS, R. P., 1973, Voltage-current characteristics and power relation in arc plasma in a transverse magnetic field. *Int. J. Electron.*, **34**, 527.
- SEN, S. N., and GUPTA, R. N., 1971, Variation of discharge current in a transverse magnetic field in glow discharge. *J. Phys. D. Appl. Phys.*, **4**, 510.
- SEN, S. N., DAS, R. P., and GUPTA, R. N., 1972, Spectral line intensity in a glow discharge in transverse magnetic field. *J. Phys. D. Appl. Phys.*, **5**, 1260.
- TAN, K. L., and VON ENGEL, A., 1968, Measurement of the associative ionization cross section of mercury vapour. *J. Phys. D. Ser.*, **2**, **1**, 258.
- VOROBEVA, N. A., ZAHAROVA, V. M., and KAGON, YU. M., 1969, Probe measurements in plasma in a magnetic field. *9th. Int. Conf. Pheno. Ionized Gases, Bucharest* p. 620.
- VRIENS, L., KEIJSER, R. A. J., and LIGTHART, F. A. S., 1978, Ionisation processes in the positive column of the low pressure Hg-Ar discharge. *J. Appl. Phys.*, **49**, 3807.

## CHAPTER VI

### MERCURY ARC PLASMA IN AN AXIAL MAGNETIC FIELD.

#### 6.1. Introduction

Plasma parameters such as electron density and electron temperature undergo a change when the plasma is subjected to a magnetic field and in chapters III through V, it has been shown that when the magnetic field is transverse to the direction of flow of the discharge current, electron temperature increases and radial electron density decreases whereas if the magnetic field is longitudinal, the reverse effect takes place. The investigations have been carried out in molecular gases such as hydrogen, oxygen, nitrogen and air and in inert gas like helium. The parameters have been measured by Langmuir probe method and spectroscopic method. It is worthwhile to investigate whether the physical processes occurring in a glow discharge undergo any significant change when we pass from glow to arc region and in one of our previous investigations (Sen and Das, 1973) it has been established that in case of a mercury arc plasma carrying a current from 1 amp. to 2.5 amps., electron temperature increases in a transverse magnetic field and the results are in quantitative agreement with Beckman's theory (1948, modified by Sen et al, 1971, 1972) specially

for small values of reduced magnetic field. The effect of a longitudinal magnetic field on a low pressure mercury arc has been investigated by various workers (Cummings and Tonks, 1941, Forrest and Franklin, 1966 and Vorobjeva, Zaharova and Kagan, 1971). The investigations were carried out in comparatively lower pressure region ( $p \leq 0.2$  torr) and there is shortage of data for comparatively high pressure large current plasma in longitudinal magnetic field.

In the present investigation the variation of current and voltage across a mercury arc plasma (admixed with air) as well as variation of electron temperature <sup>are</sup> and studied in a longitudinal magnetic field. Most of the results reported for mercury arc plasma are with argon as background gas; in the present investigation air is the background gas, which enables us to study how the excitation, ionization and deionization processes are influenced by the presence of air.

In the case of molecular gases, the ionisation is mainly due to electron impact of the ground state molecule whereas in the case of mercury arc, ionisation is predominantly through inelastic electron impact with excited states like  $6^3P_2$  and with ground states and the phenomena of associative ionisation may also be present. Hence the physical processes occurring in a mercury arc plasma and how these processes are influenced by magnetic field have been taken into consideration in deducing the electron temperature and its variation in a magnetic field.

## 6.2. Experimental measurements and results

Experiments were performed on a d.c. mercury arc at low pressure burning in air. The discharge currents were 2.25 and 2.5 amps, while the dry air pressure was varied from 0.05 torr to 2 torr. Electron temperature  $T_e$  and  $T_{eB}$  without and with magnetic fields were determined by measuring the intensities of  $5770 \text{ \AA}$  ( $6^3D_2 \rightarrow 6^1P_1$ ) and  $5790 \text{ \AA}$  ( $6^3D_1, 6^1D_1 \rightarrow 6^1P_1$ ) and taking their ratios. As the radiations differ by  $20 \text{ \AA}$  they would have equal response to the photomultiplier tube (MIOFS29V $\lambda$ ) used. A vertical mercury arc tube of 10 cm. in length and 1 cm in radius, burning in dry air, and cooled externally was mounted in between the pole-pieces of an electro-magnet. A diffuse discharge filled the tube totally. An accurately calibrated constant deviation spectrograph was used to measure the wavelength of the spectral lines. The slit of the spectrograph was illuminated by condensing the light from the arc on the slit by a collimating lens. Each line was focussed on the cathode of the photomultiplier tube operated at 1425 volt. Detailed electronic arrangement for measuring the intensity of the spectral lines is given in Chapter II. The magnetic field ( 0 - 1100 gauss ) was uniform inside the pole-pieces of the electromagnet. The pressure of air which was introduced through a needle valve, was measured by a McLeod gauge and the pressure of

mercury was determined from Handbook (1956) after noting the temperature of the inside wall by a mercury in glass thermometer (details in chapter II). Currents through the discharge was measured by an ammeter and the voltage across the tube was measured by a V.T.V.M. of internal resistance  $35 \text{ M}\Omega$ . In the present investigation we have taken measurements with two types of arc discharges, (a)  $i = 2.25 \text{ am.}$ ,  $p_{\text{air}} = 0.08 \text{ torr}$ ,  $P_{\text{Hg}} = 0.3032 \text{ torr}$ , (b)  $i = 2.5 \text{ amp.}$ ,  $p_{\text{air}} = 0.08 \text{ torr}$ , and  $P_{\text{Hg}} = 0.3731 \text{ torr}$ . The variation of current and voltage across the arc are noted for both type of discharges for a wide range of magnetic fields varying from 0 to 1100 gauss and a few representative data are shown in table 6.1. In fig. 6.1, discharge current, arc voltage and effective impedance of the arc have been plotted as a function of axial magnetic field  $B$ .

TABLE 6.1.

(Representative current/voltage variation with magnetic field).

Magnetic field in (Gauss)	$i = 2.5 \text{ amp.}$ , $P_{\text{Hg}} = 0.3731 \text{ torr}$ , $p_{\text{air}} = 0.08 \text{ torr.}$		$i = 2.25 \text{ amp.}$ , $P_{\text{Hg}} = 0.3032 \text{ torr}$ , $p_{\text{air}} = 0.08 \text{ torr.}$	
	Voltage across the arc (volts)	Current in amps.	Voltage across the arc (Volts)	Current in amps.
0	22	2.5	22	2.25
255	22.5	2.49	22.8	2.24
550	23.3	2.48	23.8	2.23
835	24.4	2.46	25.2	2.22
1050	25.5.	2.45	26.5	2.21

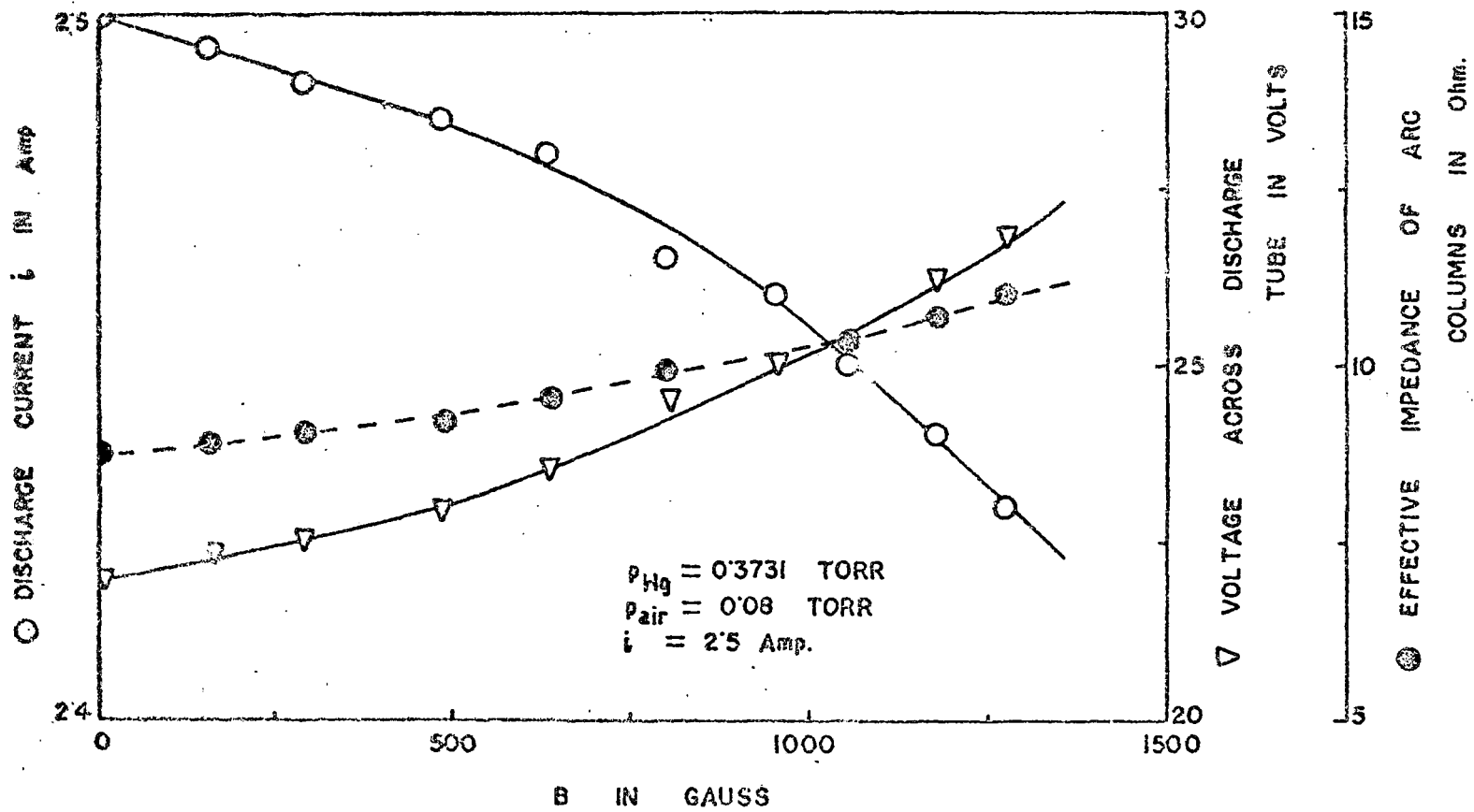


FIG. 6.1.

Fig. 6.1. Variations of arc current, voltage across the arc and effective impedance of arc column with a longitudinal magnetic field.

For measurement of electron temperature from the intensity of spectral lines, it has been shown by Griem (1964) that for LTE to be valid, the electron density  $n_e$  should be greater than  $10^{16} \text{ cm}^{-3}$ . Since cross section increases rapidly with principal quantum numbers whereas radiative decay rates decreases, the higher excited states may be in equilibrium with the continuum, which lead to idea of partial LTE, and the condition for partial LTE to be valid has been obtained by Griem (1964) as

$$n_e \geq 4.48 \times 10^8 \frac{1}{n^4} \left( \frac{kT_e}{E_H} \right)^{1/2} \sum_{i < k} A_{ki} \quad (6.1)$$

where  $\sum_{i < k} A_{ki}$  is the sum of all transition probabilities from the level  $k$  to all  $i$ 's,  $\sum A_{ki}$  values for levels  $6^3D_{1,2}$  and  $6^1D_2$  are given by Mosberg and Wilkie (1978).  $E_H = 13.6 \text{ eV}$ . and  $n$  is the effective quantum number of the state defined in chapter I. We thus find that  $n_e > 10^{12} \text{ cm}^{-3}$  for partial LTE to be valid for the levels and as our theoretical calculation shows that in the type of mercury arc discharge under investigation,  $n_e \approx 10^{13} \text{ cm}^{-3}$ , we can assume that partial LTE is valid in this case for the levels under consideration. Hence if we consider a transition  $k \rightarrow i$  then the intensity of the line

$$I_{ki} = \frac{h\nu_{ki}}{4\pi} A_{ki} \frac{g_k}{g_i} n_1 \exp\left(-\frac{E_k}{kT_e}\right) \quad (6.2)$$

and for a transition  $j \rightarrow i$

$$I_{ji} = \frac{h\nu_{ji}}{4\pi} A_{ji} \frac{g_j}{g_i} n_1 \exp\left(-\frac{E_j}{kT_e}\right) \quad (6.3)$$

where  $\nu$  and  $g$ 's are the frequency of the transitions and statistical weights of the levels,  $A_{\alpha i}$  is the transition probability for transition ( $\alpha \rightarrow i$ ),  $h$  is Planck constant and  $l$  is the length of plasma along the line of sight, From equations (6.2) and (6.3) it can be shown that

$$kT_e = \frac{E_j - E_k}{\ln\left[\frac{I_{ki}}{I_{ji}} \frac{A_{ji}}{A_{ki}} \frac{\lambda_{ki}}{\lambda_{ji}} \frac{g_j}{g_k}\right]} \quad (6.4)$$

As the spectrograph used is unable to resolve the Zeeman splitting of the line in the magnetic field and the spectral intensity of the lines changes in the magnetic field it can be deduced from equations (6.2) and (6.3) that

$$\frac{1}{kT_{eB}} - \frac{1}{kT_e} = \frac{\ln\left[\frac{(I_{ki})_B}{I_{ki}} / \frac{(I_{ji})_B}{I_{ji}}\right]}{E_j - E_k} \quad (6.5)$$

where  $(I_{ki})_B$  and  $(I_{ji})_B$  are the intensities of the lines in presence of magnetic field and  $T_{eB}$  is the electron temperature in magnetic field. The results for the measurement of intensities of the lines with and without

magnetic field and the corresponding electron temperature are shown in Tables 6.2 and 6.3. In fig. 6.2 variation of electron temperature with axial magnetic field for a mercury arc ( $i = 2.5$  amp.  $p_{\text{Hg}} = 0.3731$  torr and  $p_{\text{air}} = 0.08$  torr) has been shown. In calculating electron temperature,  $A_{\infty}$  and  $g_{\infty}$  values have been taken from Mosberg and Wilkie (1978).

TABLE 6.2.

Variation of electron temperature with axial magnetic field for mercury arc ( $i = 2.5$  amp.,  $p_{\text{Hg}} = 0.3731$  torr,  $p_{\text{air}} = 0.08$  torr).

Magnetic field in (gauss)	$\frac{(I_{5790})_B}{I_{5790}} = x$	$\frac{(I_{5770})_B}{I_{5770}} = y$	$\ln(x/y)$	$T_e$ in eV
0	1	1	0	0.422
255	1.02586	1.01852	$7.1806 \times 10^{-3}$	0.313
550	1.08621	1.07407	$1.1239 \times 10^{-2}$	0.282
835	1.14655	1.12963	$1.4867 \times 10^{-2}$	0.256
1050	1.17241	1.15278	$1.6887 \times 10^{-2}$	0.243

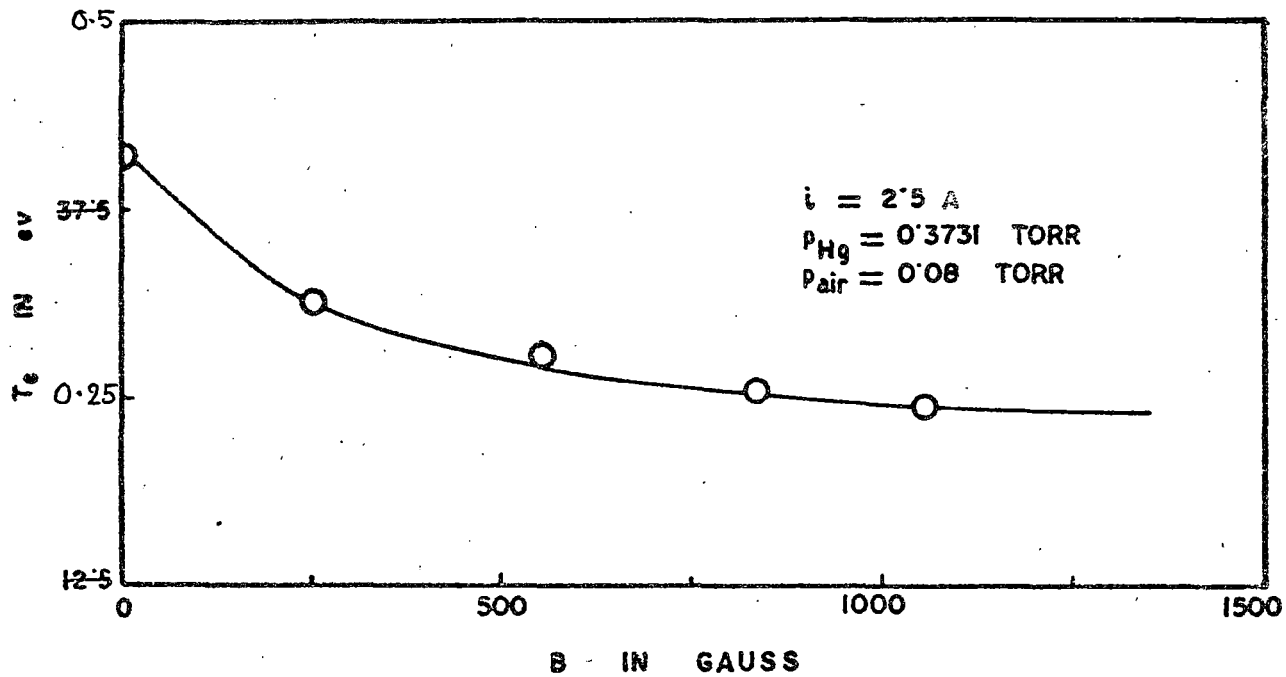


FIG. 6.2.

Fig. 6.2. Variation of electron temperature of a mercury arc discharge with longitudinal magnetic field.

TABLE 6.3

Variation of electron temperature with axial magnetic field for mercury arc ( $i = 2.25$  amp.,  $p_{\text{Hg}} = 0.3022$  torr,  $p_{\text{air}} = 0.08$  torr).

Magnetic field in (gauss)	$\frac{(I_{5790})_B}{I_{5790}} = x$	$\frac{(I_{5770})_B}{I_{5770}} = y$	$\ln(x/y)$	$T_e$ in eV
0	1	1	0	0.412
255	1.02913	1.02	$8.9072 \times 10^{-3}$	0.301
550	1.07282	1.06	$1.2017 \times 10^{-2}$	0.276
835	1.13592	1.12	$1.4116 \times 10^{-2}$	0.261
1050	1.19417	1.175	$1.6187 \times 10^{-2}$	0.247

### 6.3. Discussion of Results

It is thus apparent from table 6.1 that when magnetic field is applied, the discharge current decreases and since the supply voltage to the arc is constant, the voltage across the discharge tube will increase.

To get the value of  $n_e$  the electron density we note that

$$i = \mu E e 2\pi \int_0^R n_r r dr \quad (6.6)$$

where  $n_r$  is the radial electron density and  $\mu E$

is the drift velocity of electrons for mercury and air mixture. For this type of discharge no data for  $\mu E$  is available so  $\mu E$  values for electrons in Hg. vapour is taken from the paper of Nakamura and Lucas (1978) and for the type of discharge where  $P_{\text{Hg}} \gg P_{\text{air}}$  this result is likely to be more valid. Since the potential drop across the arc was observed to be nearly 22 - 24 volts with a cathode fall determined by Lamar and Compton (1931) as nearly 10 volts, the electric field  $E$  in the positive column of the discharge will be  $E \gtrsim 1$  volt/cm and hence  $\mu E$  was taken to be  $0.7 \times 10^6$  cm/sec. Now assuming Basseleén distribution for electrons and putting  $\frac{r}{R} = y$

$$\dot{i} = e \mu E 2\pi R^2 \int_0^1 n_{e0} J_0(2.405 y) dy$$

or

$$\dot{i} = e \mu E 2\pi n_{e0} \frac{R^2}{2.405} J_1(2.405) \quad (6.7)$$

where  $n_{e0}$  is the number density of electrons at the axis and  $R$  is the radius of the discharge tube. From the above equation we get the value of  $\bar{n}_e$  the electron density averaged radially ( $\bar{n}_e = 0.432 n_{e0}$ ), when  $\dot{i} = 2.5$  amp.,  $\bar{n}_e = 1.645 \times 10^{13}$  cm<sup>-3</sup> and for  $\dot{i} = 2$  amp,  $\bar{n}_e = 5.687 \times 10^{12}$  cm<sup>-3</sup>. This result

shows that for mercury arc discharge used here, partial LTE is valid and equation (6.4) and (6.5) can be used for the measurement of  $T_e$  and  $T_{eB}$  respectively.

Further

$$i = e^2 E \frac{D_e}{kT_e} 2\pi \int_0^R r n_r dr \quad (6.8)$$

and

$$i_B = e^2 E_B \frac{D_{eB}}{kT_{eB}} 2\pi \int_0^R r n_{rB} dr \quad (6.9)$$

where  $D_e$  is the diffusion coefficient of electrons and the subscript B denote quantities in magnetic field. To get an expression for the electron density distribution, we have to consider the model of a mercury arc burning in air at low pressure.

The variation of voltage across the arc with axial magnetic field may be analysed in the following manner:

Let  $V_s$  = voltage generated by the source  
(a d.c. generator).

$V_A$  = voltage across the arc

$R$  = external resistance (ballast resistor)  
in the discharge circuit

and  $R_i$  = internal resistance of the source  
+ control resistance in the source.

We can write,

$$V_s = \dot{\lambda} (R + R_i) V_A \quad (6.10)$$

and similarly in a magnetic field

$$V_s = \dot{\lambda}_B (R + R_i) + V_{AB} \quad (6.11)$$

From equations (6.10) and (6.11) it is evident that any increase in  $\dot{\lambda}$  would be associated with a decrease in  $V_A$ . From equations (6.10) and (6.11) we get

$$R + R_i = \frac{V_{AB} - V_A}{\dot{\lambda} - \dot{\lambda}_B} \quad (6.12)$$

In fig. (6.3)  $(V_{AB} - V_A)$  has been plotted against  $(\dot{\lambda} - \dot{\lambda}_B)$  and the plot is a straight line in accordance to equation (6.12)

### 6.3.1. A model of a mercury arc burning in dry air

The discharge is axially homogeneous and cylindrically symmetric. The concentration of mercury ground state atoms ( $6^1S_0$ ) is taken to be constant across the cross-section of the tube and is determined by the temperature of the wall. Only the mercury atoms are excited and ionised by electron impact. No line emission from air (i.e.  $N_2$  or  $O_2$ ) was observed. The concentration of the buffer gas which is dry air, is also uniform across the

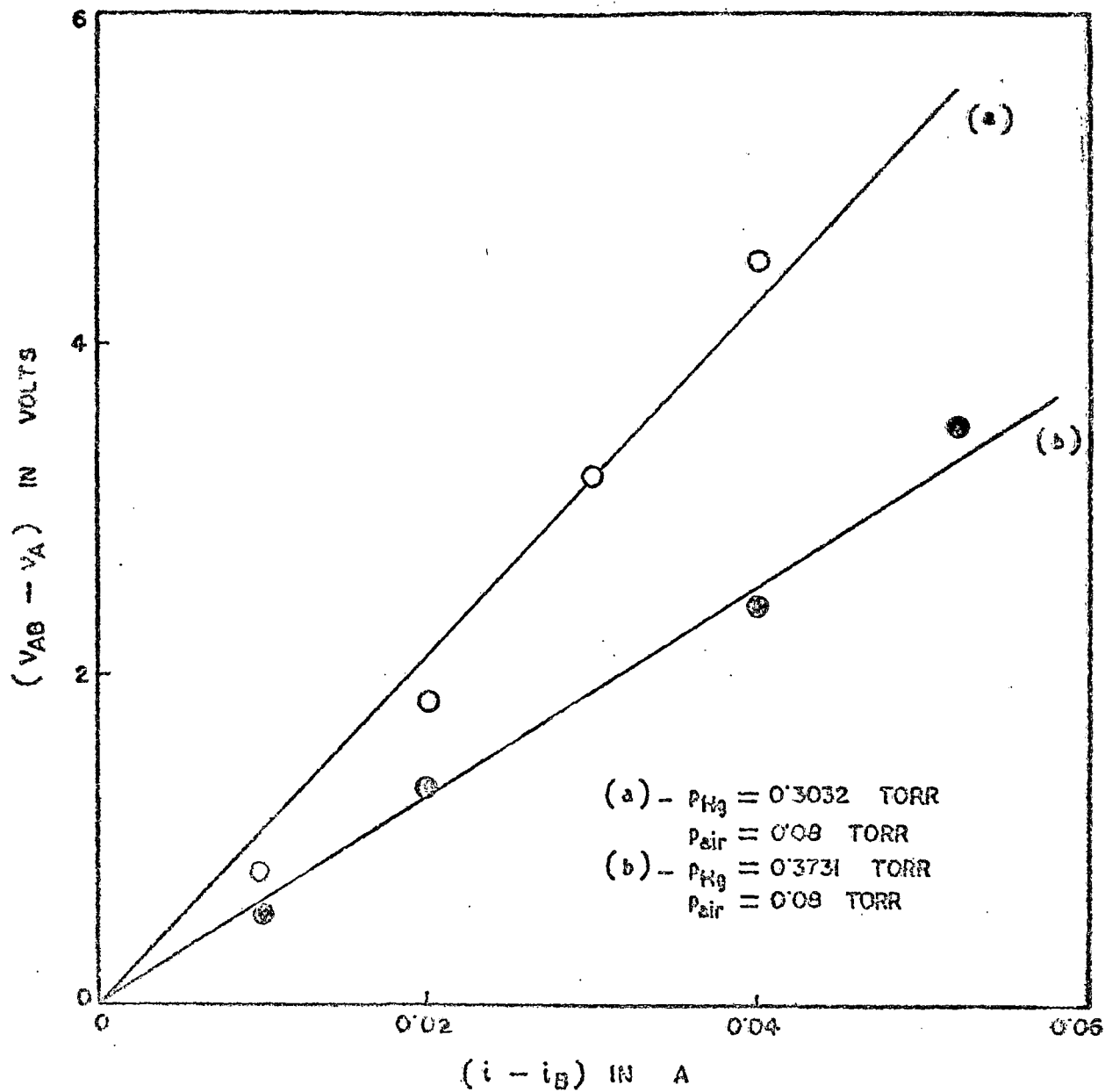


FIG. 6.3.

Fig. 6.3. Plot of  $(V_{AB} - V_A)$  against  $(i - i_B)$  for two types of mercury arc discharges.

tube cross section and it plays a role in the ambipolar diffusion and mobilities of charged particles and in deactivating the excited mercury atoms. We disregard the depletion of mercury ground state atom density at the axis of the discharge tube which is generally observed in low gas temperature experiments. Assuming that (i) the principle excited species are  $6^3P_2$ ,  $6^3P_1$  and  $6^3P_0$  with densities  $n_2$ ,  $n_1$  and  $n_0$  respectively and cascading to these levels is not important in maintaining the densities and (ii) the diffusion losses can be accounted for ~~at~~ by introducing a diffusion length; we can write the following equations for the excited species densities from the density balance equations of Forrest ~~x~~ and Franklin (1969). For  $6^3P_0$  atoms:

$$\begin{aligned} -d_0 n_0 + E n_e n_g + W n_e n_1 + G n_1 n_g \\ - (U + C + S) n_e n_0 - H n_1 n_0 - B n_0 n_2 = 0 \end{aligned} \quad (6.13)$$

For  $6^3P_2$  atoms:

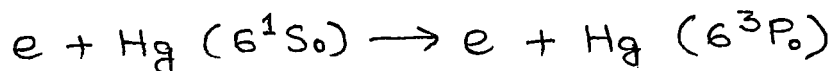
$$\begin{aligned} -d_0 n_2 + F n_e n_g + J n_e n_1 - K n_2 n_g \\ - (R + D + T) n_e n_2 - B n_0 n_2 = 0 \end{aligned} \quad (6.14)$$

For  $6^3P_1$  atoms:

$$\begin{aligned} -d_0 n_1 + L n_e n_g - \frac{n_1}{\tau} + M n_g n_p \\ - (N + J + W) n_e n_1 - G n_1 n_g + T n_e n_2 \\ + U n_0 n_e - H n_0 n_1 + K n_2 n_g = 0 \end{aligned} \quad (6.15)$$

$$-d_p n_1 - M n_g n_p + \frac{n_1}{\tau} = 0 \quad (6.16)$$

where  $d_0$  is the loss coefficient for excited atoms through diffusion and  $n_g$  is the number density of mercury ground state atoms.  $d_p$  is the loss coefficient of resonance photons (2537 Å) and  $n_p$  is the number of photon particles per unit volume. In this way a five tier system for mercury is considered, the chief populating levels being ground state ( $6^1S_0$ ), two metastable levels ( $6^3P_0$ ,  $6^3P_2$ ), one resonance level ( $6^3P_1$ ) and the mercury ions. The energy levels have been shown in fig. (6.4 a). The populations of ground state atoms are determined from inside wall temp.  $T_w$  of the discharge tube and populations of metastable and resonance levels can be determined from Forrest and Franklin's equations (6.13) to (6.16). The meaning of the terms in those equations has been entered into Table 4.4. As for example, the term  $E n_e n_g$  means, rate ( $\text{Sec.}^{-1}$ ) of the reaction



$E$  is the rate coefficient given by

$$E = \langle v_e \sigma \rangle = \int_{v_0}^{\infty} v \sigma(v) f(v) dv$$

where  $\sigma$  is the cross section of the reaction,  $v_0$  is the threshold value and  $f(v)$  is velocity distribution function for electrons which is assumed

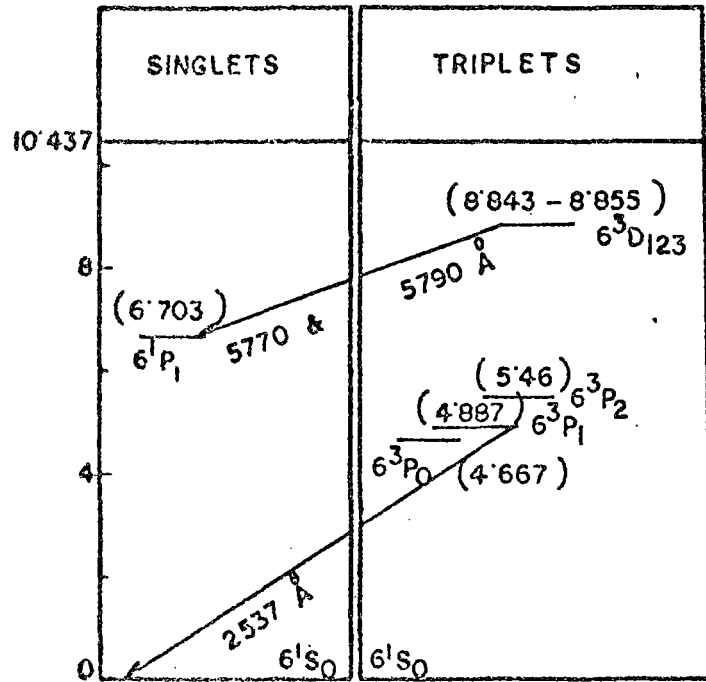


FIG. 6.4a. ENERGY LEVEL DIAGRAM OF MERCURY (ENERGIES OF THE LEVELS SHOWN IN BRACKETS).

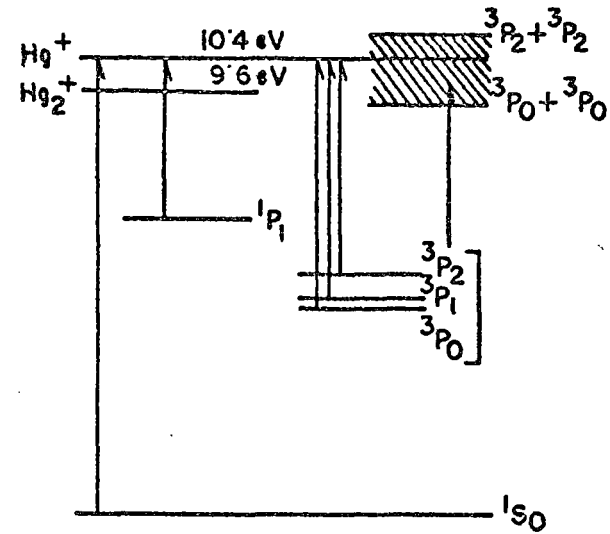


FIG. 6.4b. IONISATION REACTION OF MERCURY ATOMS.

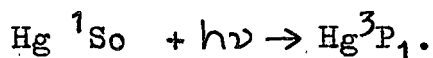
TABLE 6.4

Reactions considered in equation (6.13) to (6.16).

Term	Reaction	Calculated from equa- tion no.
E	$e + \text{Hg } ^1\text{S}_0 \longrightarrow e + \text{Hg } ^3\text{P}_0$	(6.23)
W	$e + \text{Hg } ^3\text{P}_1 \longrightarrow e + \text{Hg } ^3\text{P}_0$	(6.23)
G	$\text{Hg } ^3\text{P}_1 + \text{Hg } ^1\text{S}_0 \longrightarrow \text{Hg } ^3\text{P}_0 + \text{Hg } ^1\text{S}_0$	(6.24)
U	$e + \text{Hg } ^3\text{P}_0 \longrightarrow \text{Hg } ^3\text{P}_1 + e$	(6.23)
<del>M</del> C	$e + \text{Hg } ^3\text{P}_0 \longrightarrow \text{Hg}^+ + e + e$	(6.25)
S	$e + \text{Hg } ^3\text{P}_0 \longrightarrow \text{Hg } ^1\text{S}_0 + e$	(6.23)
H	$\text{Hg } ^3\text{P}_0 + \text{Hg } ^3\text{P}_1 \longrightarrow e + \text{Hg}_2^+ + e$	(6.24)
B	$\text{Hg } ^3\text{P}_0 + \text{Hg } ^3\text{P}_2 \longrightarrow \text{Hg}^+ + e + \text{Hg } ^1\text{S}_0$	(6.24)
F	$e + \text{Hg } ^1\text{S}_0 \longrightarrow \text{Hg } ^3\text{P}_2 + e$	(6.23)
J	$e + \text{Hg } ^3\text{P}_1 \longrightarrow \text{Hg } ^3\text{P}_2 + e$	(6.23)
K	$\text{Hg } ^3\text{P}_2 + \text{Hg } ^1\text{S}_0 \longrightarrow \text{Hg } ^3\text{P}_1 + \text{Hg } ^1\text{S}_0$	(6.24)
R	$e + \text{Hg } ^3\text{P}_2 \longrightarrow \text{Hg } ^1\text{S}_0 + e$	(6.23)
D	$e + \text{Hg } ^3\text{P}_2 \longrightarrow \text{Hg}^+ + e + e$	(6.25)
T	$e + \text{Hg } ^3\text{P}_2 \longrightarrow \text{Hg } ^3\text{P}_1 + e$	(6.23)
L	$e + \text{Hg } ^1\text{S}_0 \longrightarrow \text{Hg } ^3\text{P}_1 + e$	(6.22)
N	$e + \text{Hg } ^3\text{P}_1 \longrightarrow \text{Hg}^+ + e + e$	(6.25)

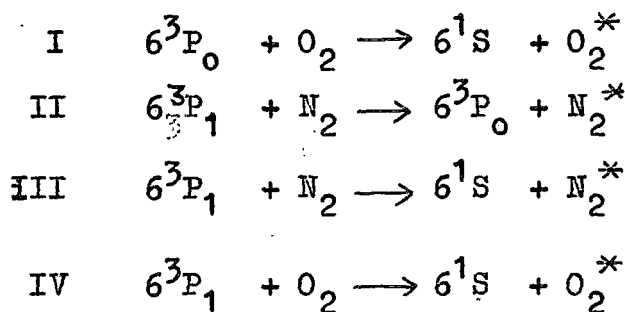
Apart from these reactions other reactions considered in

J.R. Forrest and R.N. Franklins' equations, are



to be Maxwellian.

The presence of buffer gas like air will result into deactivation or quenching of excited species. Deactivation of excited Hg. atoms by  $N_2$  and  $O_2$  molecules have been studied thoroughly. It is assumed that energy differences are given to molecular gases as vibrational energies. Air constituents chiefly nitrogen and oxygen are found to be good deactivating agents. The chief deactivating processes are:



V deactivation of  $6^3P_0$  atoms by Hg.

ground state atoms should be considered. The cross section of the processes are given in Massey, Burhop and Gilbody (1971),

$$\begin{array}{ll}
 \sigma_I = 0.31 \times 10^{-16} \text{ cm}^2 & \sigma_{II} = 1.3 \times 10^{-16} \text{ cm}^2 \\
 \sigma_{III} = 3 \times 10^{-16} \text{ cm}^2 & \sigma_{IV} = 4.4 \times 10^{-16} \text{ cm}^2 \\
 \sigma_V = 23.9 \times 10^{-16} \text{ cm}^2
 \end{array}$$

Including these processes in Forrest and Franklin's equations  $k$  in (6.13) and (6.15)

$$\begin{aligned}
 & -d_0 n_0 + E n_e n_g + W n_e n_1 + G n_1 n_g \\
 & - (U + C + S) n_e n_0 - H n_0 n_1 - B n_0 n_2 \\
 & - Z n_g n_0 - Y n_0 n_{O_2} + X_1 n_1 n_{N_2} = 0
 \end{aligned} \tag{6.17}$$

$$\begin{aligned}
 & -d_0 n_1 + L n_e n_g - \frac{n_1}{\tau} + M n_g n_p \\
 & - (N + J + W) n_1 n_e - G n_1 n_g + T n_e n_2 + U n_0 n_e \\
 & - H n_0 n_1 + K n_2 n_g - X n_1 n_{N_2} - V n_1 n_{O_2} = 0
 \end{aligned} \tag{6.18}$$

where  $Z$  is related to process No. V

$Y$  is related to process No. I

$X_1$  is related to process No. II

$X$  is related to process No. II + III

$V$  is related to process No. IV

and  $n_{O_2}$  and  $n_{N_2}$  are the number densities of oxygen and nitrogen molecules.

To calculate the densities, we note that for  $6^1S_0$  state atom densities are as follows:

$$p_{Hg} = 0.3032 \text{ torr}, \quad n_g = 7.83 \times 10^{15} \text{ cm}^{-3}$$

$$p_{Hg} = 0.3771 \text{ torr}, \quad n_g = 1.3282 \times 10^{16} \text{ cm}^{-3}$$

and evidently  $n_g > n_2, n_1, n_0,$  or  $n_e$

Equation (6.16) is the balance equation for resonance photons  $2537 \text{ \AA}$ . The effective diffusion coefficient of resonance radiation at the wall has been shown by

Cayless (1963) to be

$$d_{pw} = \frac{g_j R^2}{8\tau} \quad (6.19)$$

where  $\tau$  = natural life time of  $6^3P_1$  atoms

$$\approx 120 \text{ nsec (King and Adam (1974))}$$

R = radius of the discharge tube = 0.75 cm.

$g_j$  = Holstein's escape factor given, for cylindrical discharge tube, as

$$g_j = 1.60 \left[ k_0 R \left\{ \pi \ln(k_0 R) \right\}^{1/2} \right]^{-1} \quad (6.20)$$

$$k_0 = \frac{\lambda_1^3 n_g}{8\pi} \frac{g_k}{g_0} A_{k0} \left[ \frac{M}{2\pi k T_g} \right]^{1/2} \quad (6.21)$$

$\lambda = 2537 \text{ \AA}$ ,  $g_k = 3$ ,  $g_0 = 1$ ,  $A_{k0} = 1/\tau$ , M is the mass of mercury atom and  $k T_g$  is gas temperature (in eV), considered to be uniform across the cross section of the discharge tube and equal to the inner wall temperature  $k T_w$ . Putting these values in equation (6.16), value of  $(-M n_p n_g + n_1/\tau)$  may be calculated and this reduces the four particle balance equations to three.

To get the values of  $n_0$ ,  $n_1$  and  $n_2$ , as a first approximation we can neglect the terms  $Jn_en_1$  and  $Bn_0n_2$  in equation (6.14) as  $n_g \gg n_2, n_1, n_0, n_e$  which leaves us with an equation containing and values of  $n_g$  and  $n_e$  are known. The values of different coefficients can be evaluated by assuming electron energy distribution to be Maxwellian and assuming the expression given by Sampson (1969) for optically allowed transition for electron impact <sup>excitation</sup> ionization as

$$\langle \nu_{e\sigma} \rangle = \pi a_0^2 \left( \frac{8kT_e}{m\pi} \right)^{1/2} \left[ 4 f_{ij} \left( \frac{E_H}{E_0} \right)^2 \right] \frac{2\pi}{\sqrt{3}} \frac{E_0}{kT_e} P \left( \frac{E_0}{kT_e} \right) \exp \left( - \frac{E_0}{kT_e} \right) \quad (6.22)$$

where  $\pi a_0^2 = 8.797 \times 10^{-17} \text{ cm}^2$ ,  $E_0$  is the threshold energy of transition,  $f_{ij}$  the oscillator strength, For ( $6^1S_0 \rightarrow 6^3P_1$ ) transition  $f_{ij} = 0.0247$  (Skerbele and Lassttre, 1972).  $P(E_0/kT_e)$  is the Gaunt factor and values have been given by Sampson (1969). For optically forbidden transition we have taken the expression of Benson and Kulander (1972) utilising C.W.Allen's cross section,

$$\langle \nu_{e\sigma} \rangle = \frac{\pi a_0^2 4 E_H}{g_e E_0} \left[ \frac{kT_e}{2\pi m} \right]^{1/2} \exp(-E_0/kT_e) \left\{ 1 - \exp(-E_H/kT_e) \right\} \quad (6.23)$$

here  $g_\ell$  is the statistical weight of the state from which excitation is considered and  $E_H = 13.6$  eV. For atom-atom/molecule reaction,

$$\langle \psi, \sigma \rangle = \sigma \langle \psi \rangle = \sigma \left( \frac{8kT_g}{\pi\mu} \right)^{1/2} \quad (6.24)$$

where  $\sigma$  is the effective cross section for the process considered and  $\mu$  is the reduced mass of the colliding atoms and molecules.

Having determined the value of  $n_2$  the equation for  $n_1$  can be solved from equation (6.18) and putting this value of  $n_1$  in equation (6.17),  $n_0$  can be obtained. Taking these values of  $n_0$ ,  $n_1$  and  $n_2$  the equations are evaluated afresh by considering all the terms of the three equations. This procedure is repeated and the change in the values of  $n$ 's is found to be small. Results of calculation of species densities are entered in Table 6.5.

To bring out the influence of buffer gas pressure calculations are given for  $p_{\text{air}} = 0.05$  torr and  $p_{\text{air}} = 2$  torr. In the calculations, diffusion coefficients of excited mercury atoms have been considered to be equal to that of ground state atom given in International critical Tables (1929). McDaniel (1964) has discussed that diffusion coefficient of excited atoms is rather small. However, calculations show that diffusion losses of excited atoms are negligible in comparison to collisional losses. This is inconformity with observations of Cayless (1963) and Polman et al (1972).

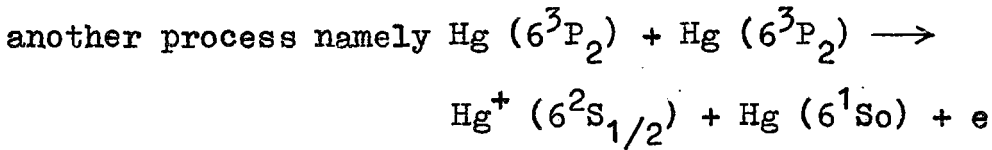
TABLE 6.5

Number densities of mercury atoms with varying conditions of discharge.

	$\lambda$	2.5 A	2A
Condition of plasma	$p_{air}$	0.05 torr	2 torr
	$p_{Hg}$	0.3771 torr	0.222 torr
	$T_e$	0.5 eV.	0.5 eV.
	$n_{N_2}$	$1.424 \times 10^5$	$5.667 \times 10^6$
	$n_{O_2}$	$3.56 \times 10^4$	$1.424 \times 10^6$
	$n_g$	$1.328 \times 10^6$	$7.83 \times 10^5$
Number densities	$n_0$	68.6	7.788
in $cm^{-3} \times 10^{-10}$	$n_1$	19.13	1.423
	$n_2$	86.2	42.7
	$n_e$	$1.64 \times 10^3$	$5.687 \times 10^2$

Now let us look into the processes in these types of discharges. The chief ionization processes in a Hg. discharge are listed by Vriens, Keijser and Ligthart (1978) as

1.  $Hg(6^1S_0) + e \longrightarrow Hg^+ + 2 e$
2.  $Hg(6^3P_0) + e \longrightarrow Hg^+ + 2 e$
3.  $Hg(6^3P_1) + e \longrightarrow Hg^+ + 2 e$
4.  $Hg(6^3P_2) + e \longrightarrow Hg^+ + 2 e$
5.  $Hg(6^3P_0) + Hg(6^3P_1) \longrightarrow Hg_2^+ (6^2 \Sigma^+) + e$
6. (a)  $Hg(6^3P_1) + Hg(6^3P_2) \longrightarrow Hg^* + Hg(6^1S_0)$   
 (b)  $Hg^* + e \longrightarrow Hg^+ + 2 e$



is not considered by us as spin is not conserved in this process. The ionisation processes are shown in fig. 6.4(b).

Electron impact ionisation rates from different levels

$K_1$  to  $K_4$  for processes 1 to 4 are given by Sampson (1969)

$$n_e n_i \langle v_e \sigma \rangle = 5.465 \times 10^{-11} n_e n_i T_e^{1/2} \\ \exp(-\chi_i/kT_e) \Gamma_i(T_e) \quad (6.25)$$

$$i = 0, 1, 2$$

here  $T_e$  is the electron temperature in °K,  $\chi_i$  is the ionisation energy of  $i$ th level and  $\Gamma_i = An/\chi_i^2$  where  $A = 200$  for neutral atoms,  $n$  = number of electron per atom in the outer orbit. For process 5, the rate is

$$K_5 = n_0 n_1 \langle v \sigma_5 \rangle = n_0 n_1 \sigma_5 \langle v \rangle \quad (6.26)$$

$\sigma_5$  is the effective cross section of associative ionisation. Tan and von-Engel (1968) have determined

$$\sigma_5 = 46 \times 10^{-15} \text{ cm}^2 \quad \text{and} \quad \langle v \rangle = \left( \frac{16 k T_g}{\pi M} \right)^{1/2}$$

For process 6,

$$K_6 = n_1 n_2 \sigma_6 \langle v \rangle B_i \quad (6.27)$$

$\sigma_6$  is estimated by Vriens et al (1978) to have a value of  $10 \times 10^{-15} \text{ cm}^2$ ,  $B_i$  is the Branching ratio and as calculated by the authors,  $B_i$  should be slightly less than unity i.e. all the atoms in the highly excited states populated by process 6 (a), are ionised by electron impact. Very few of them will make optically allowed transitions. We have neglected ionization from  $6^1P_1$  level, since the population density and natural life time of this level is small. With the help of equations (6.25), (6.26) and (6.27) and utilizing the values of  $n_e$ ,  $n_2$ ,  $n_0$ ,  $n_1$  and  $n_2$  (table 6.5) the rate of ionization for the two types of discharges considered here has been calculated and are entered in Table 6.6.

TABLE 6.6

Ionisation rates with varying discharge condition.

Discharge conditions	Rate of ionization in $\text{Sec.}^{-1} \times 10^{-11}$					
	$K_1$	$K_2$	$K_3$	$K_4$	$K_5$	$K_6$
$i = 2.5 \text{ amp.}$						
$T_e = 0.5 \text{ eV.}$						
$P_{\text{air}} = 0.05 \text{ torr}$	11.585	21.94	10.13	181.37	1700	466.4
$P_{\text{Hg}} = 0.3731 \text{ torr}$						
$i = 2 \text{ amp.}$						
$T_e = 0.5 \text{ eV.}$						
$P_{\text{air}} = 2 \text{ torr}$	5.41	1.98	0.61	71.2	8.72	16.94
$P_{\text{Hg}} = 0.222 \text{ torr}$						

From the Table 6.6 it is evident that for a plasma where air pressure is comparatively small, ionization is chiefly through the process of associative ionisation and by electron impact ionisation of highly excited Hg. atoms whereas when  $p_{\text{air}}$  is comparatively large due to large quenching of  $6^3P_0$  levels ionisation will be primarily through the process of electron impact of  $6^3P_2$  atoms. So in type I plasma where  $p_{\text{air}}$  is small two types of ions  $\text{Hg}_2^+$  and  $\text{Hg}^+$  prevail inside the discharge tube. To calculate the normal distribution in a Hg discharge with two types of ions, we can utilize the equations of Golubovskii and Lyaguschenko (1977)

$$\left. \begin{aligned} \vec{j}_{i_1} &= -D_{i_1} \vec{\nabla} n_{i_1} + n_{i_1} \mu_{i_1} \vec{E}_r \\ \vec{j}_{i_2} &= -D_{i_2} \vec{\nabla} n_{i_2} + n_{i_2} \mu_{i_2} \vec{E}_r \\ \vec{j}_e &= -D_e \vec{\nabla} n_e - n_e \mu_e \vec{E}_r \end{aligned} \right\} \quad (6.28)$$

$\vec{j}$ 's are the current densities towards wall,  $n$ 's are species densities,  $D$  and  $\mu$ 's are diffusion coefficients and mobilities and  $E_r$  is the radial electric field. Subscripts  $i_1$  and  $i_2$  denote atomic and molecular ions whereas subscript  $e$  denotes an electronic quantity.

Since  $n_{i_1} + n_{i_2} = n_e$  and  $\vec{j}_{i_1} + \vec{j}_{i_2} = \vec{j}_e$  eliminating  $E_r$  from equation (6,28) and considering  $\mu_{i_1} = \mu_{i_2}$  and hence  $D_{a_1} = D_{a_2} = D_e \mu_{i_1} / \mu_e$

we get,

$$\left. \begin{aligned} \text{div } \vec{J}_{i_1} &= -D a_1 \nabla \left( \frac{n_{i_1}}{n_e} \nabla n_e \right) = F_1 \\ \text{div } \vec{J}_{i_2} &= -D a_2 \nabla \left( \frac{n_{i_2}}{n_e} \nabla n_e \right) = F_2 \\ F_1 + F_2 &= F_e \end{aligned} \right\} \quad (6.29)$$

$F_1$ ,  $F_2$  and  $F_e$  are the differences between the rates at which particles appear and disappear in the volume.

Kovar (1964) has shown that actually  $\mu_{i_2}/\mu_{i_1} = 1.875$ . It may be interesting to note that heavier ions are faster. The reason behind this is that atomic ions moving in their parent gas will have large charge exchange cross section and hence progress more slowly than the heavier molecular ions which do not suffer resonance charge exchange collisions. As the difference in values is not much and the presence of foreign gas will effectively reduce the charge exchange phenomena and obscures the visions of  $\text{Hg}^+$  ions for resonance to occur, the atomic and molecular ionic mobilities may be assumed equal.

Atomic ions will be produced mainly by (i) electron impact of highly excited states of Hg. atoms at rate  $\nu_i n_e$  and these states are in thermal equilibrium with the electrons.

(ii) by electron impact dissociation of molecular ions with a rate  $\omega n_{i_2} n_e$  and they will be lost mainly by

- i) ambipolar diffusion to the wall,  
 ii) some of them will be converted to molecular ions  
 in three body collisions at rate  $k n_{i_1}$

$$\text{Hence } F_1 = \nu_i n_e + \omega n_{i_2} n_e - k n_{i_1} \quad (6.30)$$

Molecular ions will be produced mainly by (i) the process of associative ionisation with rate  $g$ .

- (ii) conversion of atomic ions at a rate  $k n_{i_1}$   
 and they will disappear by  
 (i) ambipolar diffusion,  
 (ii) electron impact dissociation to atomic ions  
 at a rate  $\omega n_{i_2} n_e$

We have neglected dissociative recombination of molecular ions which is a comparatively slow process than the diffusion in an active discharge.

$$\text{Hence, } F_2 = g + k n_{i_1} - \omega n_{i_2} n_e \quad (6.31)$$

In the above analysis it has been considered that the diffusion of charged particles towards the wall of the discharge tube is ambipolar in nature. For usual plasmas obtained by electric discharges, the diffusion can be considered ambipolar if  $\lambda_D / \pi \Lambda \ll 0.01$  i.e. if

$$n_e \gg 4.77 \times 10^4 (T_e / \Lambda^2) \text{ cm}^{-3} \quad (6.32)$$

where  $\lambda_D$  is the Debye shielding length  $\Lambda$  is the diffusion length,  $T_e$  is temperature in °K. In the cylindrical geometry the lowest or fundamental diffusion length is given by

$$\frac{1}{\Lambda^2} = \left(\frac{2.4}{R}\right)^2 + \left(\frac{\pi}{L}\right)^2 \quad (6.33)$$

Expression (6.32) has been confirmed experimentally by Gerber and Gerardo (1973). Calculations show that for  $R = 0.5\text{cm.}$ , when  $n_e \gg 5 \times 10^9$  the diffusion is ambipolar in nature.

Hence from equations (6.29), (6.30) and (6.31)

$$\begin{aligned} F_e &= F_1 + F_2 = v_i n_e + g \\ &= -Da_1 \nabla \left\{ \frac{n_{i_1}}{n_e} \nabla n_e \right\} - Da_2 \nabla \left\{ \frac{n_{i_2}}{n_e} \nabla n_e \right\} \end{aligned}$$

as we have assumed  $\mu_{i_1} = \mu_{i_2}$  and  $Da_1 = Da_2 = Da$

$$v_i n_e + g = -Da \left[ \nabla \left\{ \frac{n_{i_1}}{n_e} \nabla n_e \right\} + \nabla \left\{ \frac{n_{i_2}}{n_e} \nabla n_e \right\} \right]$$

or

$$v_i n_e + g = -Da \nabla^2 n_e \quad (6.33)$$

as  $n_{i_1} + n_{i_2} = n_e$

we have neglected any distribution of excited state density across the tube cross section. In cylindrical co-ordinate system equation (6.33) reduces to

$$D_a \frac{1}{r} \frac{d}{dr} \left( r \frac{dn_r}{dr} \right) + g + \nu_i n_r = 0 \quad (6.34)$$

Putting  $r/R = y$  and  $n_r/n_{e0} = N_r$  in equation (6.34) where  $n_{e0}$  is the number of density of electrons at the axis,

$$\frac{d^2 N_r}{dy^2} + \frac{1}{y} \frac{dN_r}{dy} + \frac{R^2}{D_a} N_r \nu_i + \frac{gR^2}{D_a n_{e0}} = 0 \quad (6.35)$$

Let us first consider the equation

$$\frac{d^2 N_r}{dy^2} + \frac{1}{y} \frac{dN_r}{dy} + \alpha N_r = 0 \quad \text{where } \alpha = \frac{R^2 \nu_i}{D_a}$$

Its solution is  $y_1 = J_0(y\sqrt{\alpha})$  (6.36)

with conditions  $N_r = y_1 = 1$  at  $y = 0$  and we have

$$\frac{d^2 y_1}{dy^2} + \frac{1}{y} \frac{dy_1}{dy} + \alpha y_1 = 0 \quad (6.37)$$

Now multiplying (6.35) by  $y_1$  and (6.37) by  $N_r$  and subtracting we have,

$$\frac{d}{dy} \left[ y (y_1 \dot{N}_r - N_r \dot{y}_1) \right] = -\beta y y_1 \quad (6.38)$$

where  $\beta = \frac{gR^2}{n_{eo} D_a}$

On integration of (6.38) with conditions that at  $\gamma = 0$  both  $\dot{\gamma}_1$  and  $\dot{N}_r = 0$ , we have

$$\gamma_1 \dot{N}_r - N_r \dot{\gamma}_1 = -\frac{\beta}{\sqrt{\alpha}} J_1(\gamma\sqrt{\alpha}) \quad (6.39)$$

Dividing (6.39) by  $\gamma_1^2$  we get,

$$d\left(\frac{N_r}{\gamma_1}\right) = -\frac{\beta}{\alpha} \frac{d[J_0(\gamma\sqrt{\alpha})]}{[J_0(\gamma\sqrt{\alpha})]^2} \quad (6.40)$$

Integrating (6.40) with condition at  $\gamma = 1$ ,  $N_r = 0$  we get,

$$N_r = \frac{g}{n_{eo} v_i} \left[ \frac{J_0(\gamma\sqrt{\alpha})}{J_0(\sqrt{\alpha})} - 1 \right] \quad (6.41)$$

Now at  $\gamma = 0$ ,  $N_r = 1$ , so

$$n_{eo} = \frac{g}{v_i J_0(\sqrt{\alpha})} [1 - J_0(\sqrt{\alpha})] \quad (6.42)$$

Hence,  $n_r = N_r n_{eo}$

$$= \frac{n_{eo}}{1 - J_0\left(R\sqrt{\frac{v_i}{D_a}}\right)} \left\{ J_0\left(r\sqrt{\frac{v_i}{D_a}}\right) - J_0\left(R\sqrt{\frac{v_i}{D_a}}\right) \right\} \quad (6.43)$$

It is evident from equation (6.43) that the normal distribution in presence of magnetic field will be given by

$$n_{rB} = \frac{n_{e0B}}{1 - J_0(R\sqrt{\nu_{iB}/D_{aB}})} \left\{ J_0(r\sqrt{\nu_{iB}/D_{aB}}) - J_0(R\sqrt{\nu_{iB}/D_{aB}}) \right\} \quad (6.44)$$

Cummings and Tonks (1941) from their experimental observation have predicted that the normal distribution for a mercury arc plasma is not affected by the presence of a longitudinal magnetic field, Hence, since the distribution is a function of  $\nu_i/D_a$ , we can assume that  $\nu_i/D_a = \nu_{iB}/D_{aB}$ . Consequently from equations (6.8) and (6.9)

$$\frac{\dot{z}}{z_B} = \frac{E}{E_B} \frac{D_e}{D_{eB}} \frac{T_{eB}}{T_e} \frac{n_{e0}}{n_{e0B}} \quad (6.45)$$

Bickerton and von-Engel (1956) have shown that if  $T_{eB}$  is not much different from  $T_e$  the fractional change of energy of an electron to its total energy also remains constant with magnetic field. This leads us to

$$E/E_B = T_e/T_{eB}$$

Hence

$$\frac{\dot{z}}{z_B} = \frac{D_e}{D_{eB}} \frac{n_{e0}}{n_{e0B}} \quad (6.46)$$

Further if the change of electron temperature is small, then the rate of molecular ion formation due to associative ionisation will almost remain the same so that the

metastable population densities may be considered unaffected by the magnetic field. Since

$$\nu_i / D_a = \nu_{iB} / D_{aB}$$

we get from eqn. (6.42)

$$n_{e0} / n_{e0B} = \nu_{iB} / \nu_i \quad (6.47)$$

Then from equation (6.46)

$$\frac{i}{i_B} = \frac{D_e}{D_{eB}} \frac{\nu_{iB}}{\nu_i} \quad (6.48)$$

As we are considering electron impact ionization of highly excited states only and  $\nu_i$  is given by Elton (1970) as,

$$\nu_i = n^* 9 \times 10^{-7} \left[ \frac{\delta}{\chi_i} (kT_e)^{1/2} \right] \exp(-\chi_i / kT_e) \quad (6.49)$$

where  $\chi_i$  and  $n^*$  is the ionisation energy and number density of highly excited states.  $\delta$  is a correction factor analogous to that used in the line broadening calculations for quadrupole interaction and other high order effects given by the larger of  $(1 + 2kT_e / \chi_i)$  or 3. Considering  $\delta$  and  $n^*$  to be invariant with magnetic field and since  $\chi_i \ll kT_e$

$$\nu_{iB} / \nu_i = \sqrt{T_{eB} / T_e} \quad (6.50)$$

Then,

$$\frac{i}{i_B} = \frac{D_e}{D_{eB}} \sqrt{\frac{T_{eB}}{T_e}} \quad (6.51)$$

It is well known that when the frequency of ionization is much less than the frequency of momentum transfer,

$$D_{eB} = \frac{D_e}{1 + c_1 B^2 / p^2} \quad (6.52)$$

where  $c_1 = (e \lambda_{e1} / m v_r)^2$ ,  $\lambda_{e1}$  is the mean free path of electron at a pressure of 1 torr,  $p$  is the total pressure and  $v_r$  is the random velocity.

Hence from (6.51) and (6.52)

$$1 + c_1 \frac{B^2}{p^2} = \frac{i}{i_B} \sqrt{\frac{T_e}{T_{eB}}} = \frac{i}{i_B} \frac{n_{e0B}}{n_{e0}} \quad (6.53)$$

A plot of  $(i/i_B) (n_{e0B}/n_{e0})$  vs.  $\frac{B^2}{p^2}$  (Figs. 6.5 and 6.6) will be straight line and the gradient determines the value of  $c_1$  as entered in Table 6.7.

TABLE 6.7

Magnetic field in Gauss	$\frac{B^2}{p^2} \times 10^{-6}$ Gauss <sup>2</sup> /torr <sup>2</sup>		$\sqrt{\frac{T_e}{T_{eB}}}$ (expt.)		$\frac{\dot{z}}{\dot{z}_B}$ (measured)		$\sqrt{\frac{T_e}{T_{eB}}} \times \frac{\dot{z}}{\dot{z}_B}$	
	X	Y	X	Y	X	Y	X	Y
0	0	0	1	1	1	1	1	1
250	0.44	0.3	1.169	1.138	1.002	1.0014	1.17	1.14
550	2.0	1.47	1.2218	1.2087	1.006	1.005	1.23	1.21
835	4.7	3.4	1.2564	1.2686	1.0117	1.011	1.27	1.28
1050	7.5	5.3	1.2915	1.302	1.0156	1.017	1.32	1.33

X Corresponds to  $\dot{z} = 2.25$  amp.,  $p_{\text{air}} = 0.08$  torr,  $\frac{p_{\text{Hg}}}{p_{\text{g}}} = 0.3032$  torr,  $C_1 = 0.3 \times 10^{-7}$

Y Corresponds to  $\dot{z} = 2.5$  amp.,  $p_{\text{air}} = 0.08$  torr,  $\frac{p_{\text{Hg}}}{p_{\text{g}}} = 0.3731$  torr,  $C_1 = 0.39 \times 10^{-7}$

Values of  $C_1$  have been calculated from figs. 6.5 and 6.6.

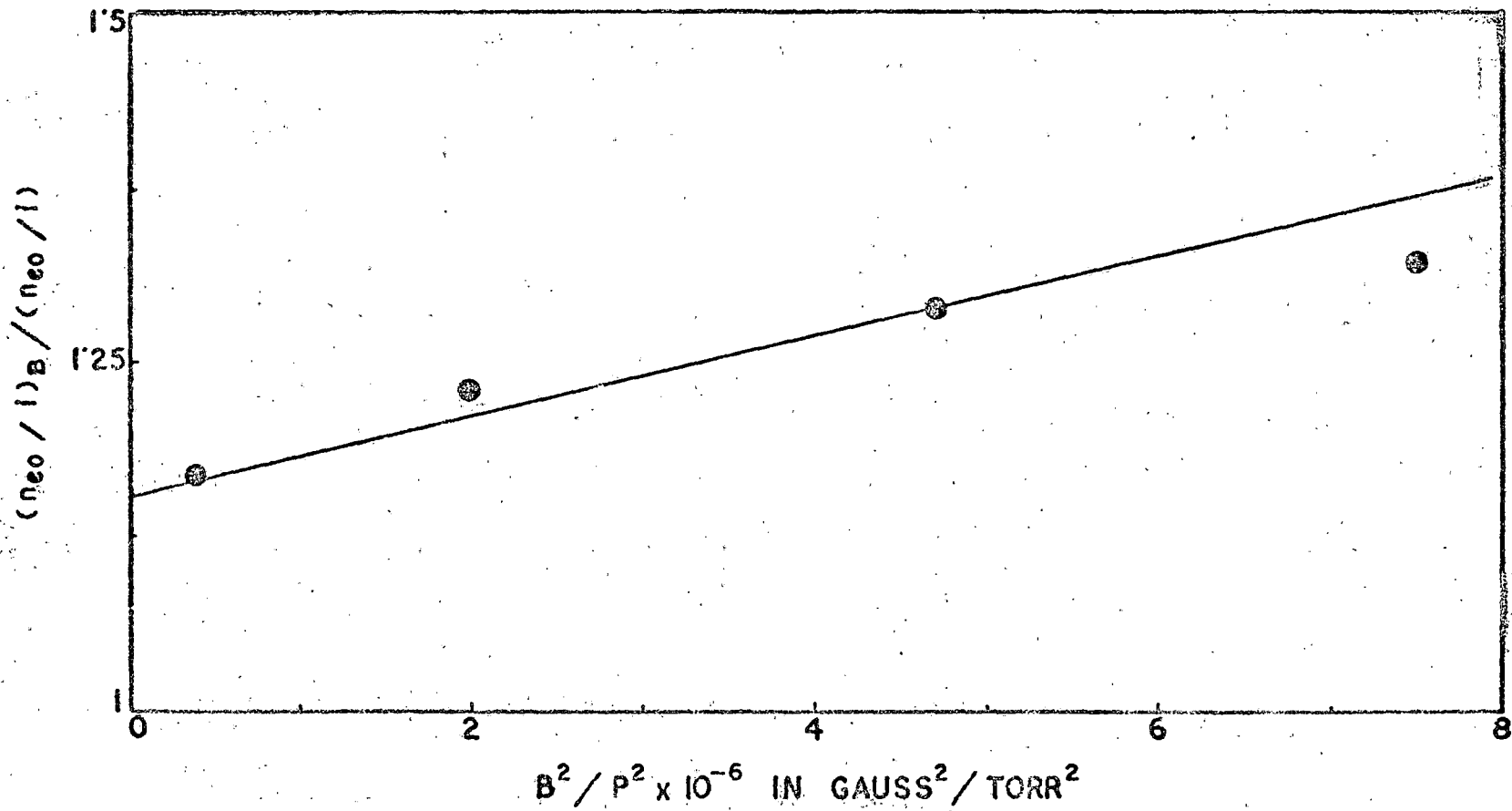
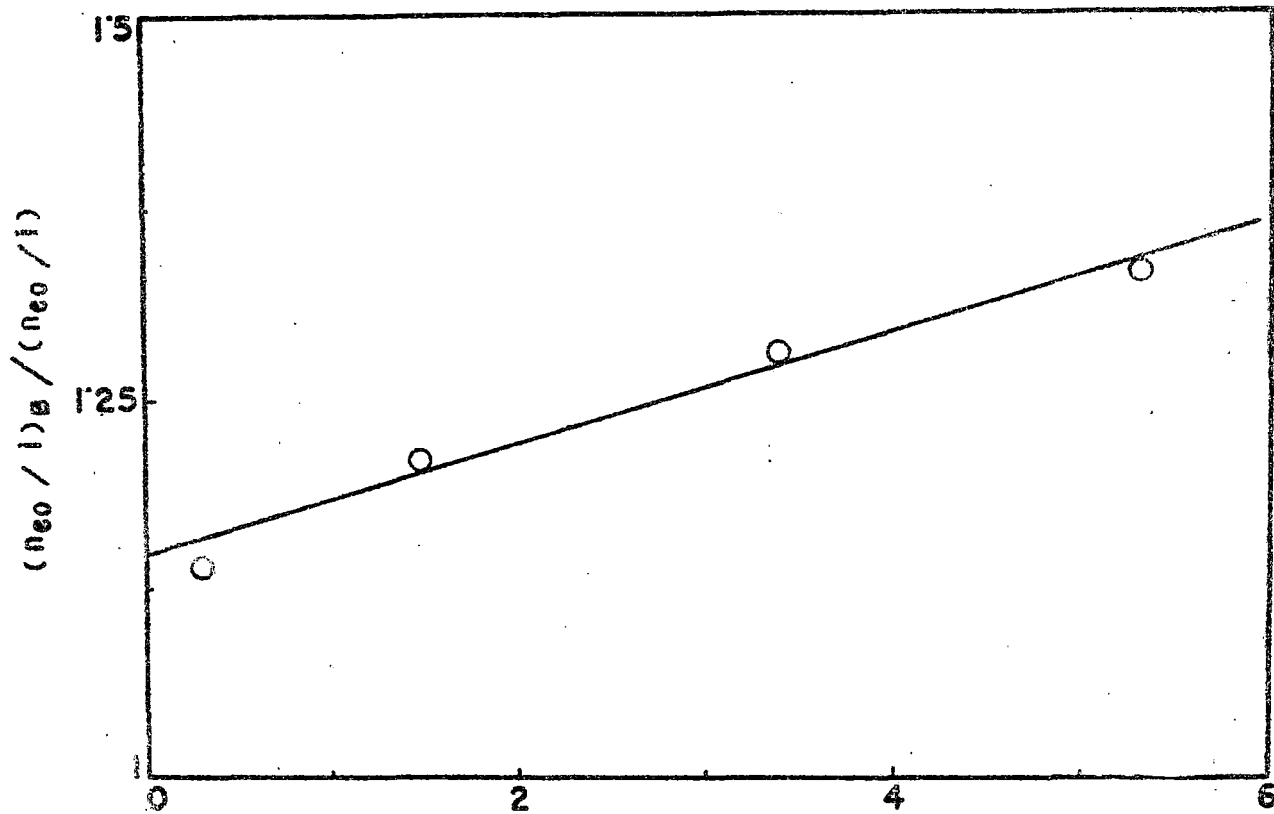


FIG. 6.5. Variation of  $(n_{e0}/i)_B / (n_{e0}/i)$  with  $B^2/p^2$ ,  $i = 2.25$  A.



$B^2/P^2 \times 10^{-6}$  IN GAUSS<sup>2</sup>/TORR<sup>2</sup>  
 FIG. 6.6. Variation of  $(n_{e0}/i)_B / (n_{e0}/i)$  with  $B^2/p^2$ ,  $i = 2.5A$ .

#### 6.4. Conclusions

Considering the physical processes involved in a mercury arc discharge where the buffer gas is air and the pressure is low, a model has been considered in which ~~the~~ air plays the role of quenching gas and it has been found that in this type of discharge both atomic and molecular ions of mercury are present. Assuming the existence of both types of ions, we have obtained the distribution function and deduced an expression for  $T_e/T_{eB}$  and have found that within the range of  $B/p$  values used in the experiment, the experimental results are in quantitative agreement with the theoretical deduction.

That the electron temperature decreases in presence of an axial magnetic field in the case of mercury discharge, has also been shown by Franklin (1976).  $C_1$  is evidently the square of the mobility of electrons in the mercury and air mixture at 1 torr. The value of mobility calculated from  $C_1$  differs by an order of magnitude with that obtained experimentally by Nakamura and Lucas (1978). Further the results show that frequency of ionization changes with magnetic field as has been previously noted by Bickerton and von-Engel (1956).

It is also noted that

$$\frac{n_{e0B}}{n_{e0}} = \sqrt{\frac{T_e}{T_{eB}}}$$

and as experimentally we have found that  $T_e > T_{eB}$ ,  
then  $n_{e0B} > n_{e0}$  which was previously found to be  
true for molecular gases, as determined by Langmuir probe  
method in chapter III.

## References:

1. Beckman, L. (1948) Proc. Phys. Soc. 61 515.
2. Benson, R.S. and Kulander, J.L. (1972) Solar Phys. 27 305.
3. Bickerton, R.J. and von-Engel, A. (1956), Proc. Phys. Soc. 76 468.
4. Cayless, M.A. (1963) Brit. J. Appl. Phys. 14 863.
5. Cummings, C.S. and Tonks, L. (1941) Phys. Rev. 59 514.
6. Elton, R.C. (1970) in Methods of experimental Physics 9 p. 149 (Academic Press, New York).
7. Forrest, J.R. and Franklin, R.N. (1966) Brit. J. Appl. Phys. 17 1569.
8. Forrest, J.R. and Franklin, R.N. (1969) J. Phys. B 2 Ser. 2 471.
9. Franklin, R.N. (1976) Plasma Phenomena in gas discharges (Oxford University Press).
10. Gerber, R.A. and Gerardo, J.B. (1973) Phys. Rev. A7 781.
11. Golubovskii, Y.B. and Lyaguschenko, R.I. (1977) Sov. Phys. Tech. Phys. 22 1073.
12. Griem, H.R. (1964) Plasma Spectroscopy (McGraw Hill, New York).
13. International Critical Tables for numerical data (1929) Vol.5, p. 62 (McGraw Hill, New York).
14. King, G.C. and Adam. A. (1974) J. Phys. B 7 1712.
15. Kovar, F.R. (1964) Phys. Rev. A133 681.
16. Lamar, E.S. & Compton, K.T. (1931) Phys. Rev. 37 1069.

17. McDaniel, E.W. (1964) Collision phenomena in ionised gases p. 51 (John Wiley, New York).
18. Massey, H.S.W., Burhop, E.H.S. and Gilbody, H.B. (1971) Electron and ion impact phenomena, 2nd. Edn. Vol.3, p. 1693 (Oxford University Press).
19. Mosberg (Jr.) E.R. and Wilkie, M.D. (1978) J.Q.S.R.T. 19, 69.
20. Nakamura, Y. and Lucas, J. (1978) J. Phys. D. 11 325.
21. Polman, J. and vander-Werf, J.E. and Drop, P.C. (1972) J. Phys. D. 5 266.
22. Sampson, D.H. (1969) Astrophys. J. 155 575.
23. Sen, S.N. and Das, R.P. (1973) Int.J. Electronics 34 527.
24. Sen, S.N., Das, R.P. and Gupta, R.N. (1972) J. Phys. D. 5 1260.
25. Sen, S.N. and Gupta, R.N. (1971) J. Phys. D. 4 510.
26. Skerbele, A. and Lassttre, E.N. (1972) J. Chem. Phys. 56 845.
27. Tan, K.L. and von-Engel, A. (1968) J. Phys. D. 1 258.
28. Vorobjeva, N.A., Zaharova, V.M. and Kagan, Yu, M. (1971) 9th.Int.Conf.on Phenomena in Ionised Gases p. 260.
29. Vriens, L., Keijser, R.A.J. and Ligthart, F.A.S. (1978) J. Appl.Phys. 49 3807.

## CHAPTER VII

### ENHANCEMENT OF SPECTRAL INTENSITIES OF MERCURY TRIPLET LINES IN LONGITUDINAL MAGNETIC FIELDS.

#### 7.1. Introduction

Enhancement of spectral intensities in a magnetic field has long been observed (Rokhlin, 1939 in inhomogeneous longitudinal magnetic field, Forrest and Franklin, 1966 and Hegde and Ghosh, 1979 in longitudinal magnetic field, Kulkarni, 1944 and Sen, Das and Gupta, 1972 in transverse magnetic field). In transverse magnetic field it has been observed that as the magnetic field increases, the spectral intensities of lines increases and attaining a maximum value <sup>at</sup> of a certain magnetic field, gradually decreases. Sen et al (1972) have shown that the enhancement phenomenon can be quantitatively interpreted by the increase of electron temperature and decrease of radial electron density caused by the presence of a transverse magnetic field. In case of longitudinal magnetic field Hegde and Ghosh (1979) applied a collisional radiative model to the positive column of helium plasma and interpreted the enhancement of radiation with field.

In this chapter, investigation has been reported for enhancement of sharp series triplet radiations of mercury in longitudinal magnetic field. The sharp series

triplet lines have a common upper level. For transitions originating from the same upper level, the relative intensities do not depend on its excitation cross section, but only on the line strength. The signal strength at the detector should be proportional to emission rate integrated both along the detector line of sight and over the spectral profile and might be modified by any self absorption. Variation of signal strength with longitudinal magnetic field has been obtained in terms of variation of these parameters.

## 7.2. Experimental arrangement

Measurements were carried on the radiation enhancement of spectral lines in the sharp series triplets of mercury atoms in a low pressure mercury arcs placed in a longitudinal magnetic field. A d.c. vertical mercury arc was placed between the pole-pieces of an electromagnet. The arc was constructed of pyrex tube of 0.75 cm. internal radius and 8 cm. in length and was forced cooled externally. The buffer gas was dry air whose concentration was regulated through a needle valve. Radiations from the axial region of positive column of the diffuse arc discharge were focussed by lens arrangements on the slit (of width 0.5 mm.) of an accurately calibrated constant deviation spectrograph.

The triplet radiations:  $5461 \text{ \AA}$  ( $7^3S_1 \rightarrow 6^3P_2$ ),  $4358 \text{ \AA}$  ( $7^3S_1 \rightarrow 6^3P_1$ ) and  $4047 \text{ \AA}$  ( $7^3S_1 \rightarrow 6^3P_0$ ) were focussed separately on the cathode of a photomultiplier (M10 FS29V  $\lambda$ ). Details of electronic arrangements for measuring the intensities of spectral lines are given in Chapter II.

In the present investigation, the arc current was varied between 2 to 3 amps., pressure of air was varied from 0.05 torr to 1 torr. and temperature of the inner wall of discharge tube  $T_W$  was observed to vary between  $98^\circ\text{C}$  to  $115^\circ\text{C}$ .

### 7.3. Results and discussions

The triplet radiations ( $7^3S_1 \rightarrow 6^3P_{0,1,2}$ ) escaping from the axial region of positive column of a low pressure mercury arc discharge are observed to be enhanced in presence of a longitudinal magnetic field (0-1560 gauss). The ratio  $I_B/I$ , where  $I_B$  and  $I$  are the intensities of radiation when a magnetic field is present and not, increases, thereafter passing through a broad maxima, very slowly decreases. Fig. 7.1, shows the variation of  $I_B/I$  with  $B$  when the discharge current is 2 amp. and pressure of air inside the discharge tube is 0.05 torr. It is observed that  $(I_B/I)_{\text{max}}$  values are different for three lines. The  $4047 \text{ \AA}$  line ratio increases rather rapidly and reaches the broad maxima in comparatively low magnetic field. For other two lines  $I_B/I$  reaches

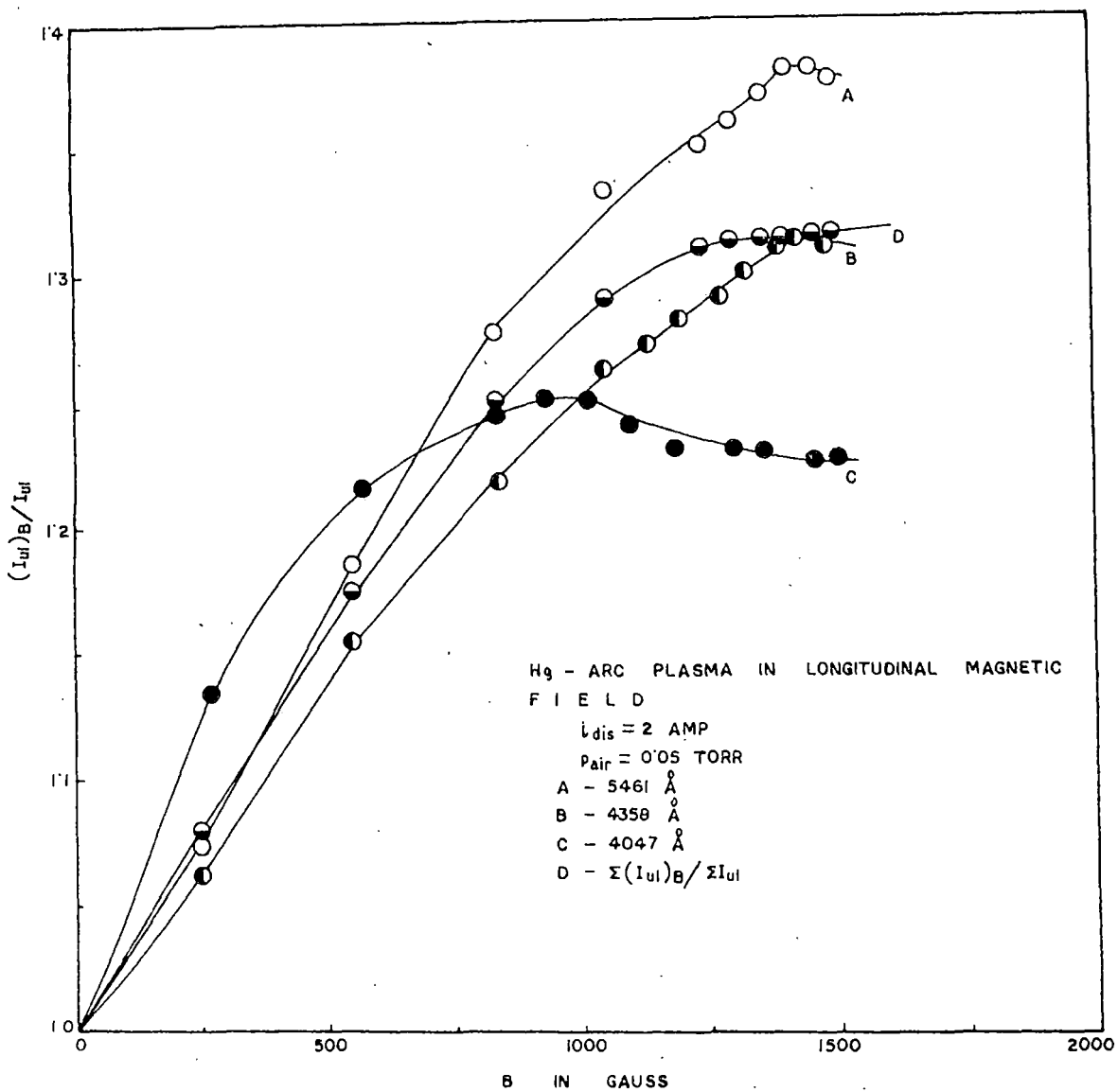


FIG. 7.1.

Fig. 7.1. Variation of spectral intensity enhancement factors ( $I_B/I$ ) with longitudinal magnetic field for lines originating from  $7^3S_1$  level of mercury,  $i = 2A$ .

its maximum value nearly in the same field. The nature of the curves remains same when the discharge current was varied from 2 to 3 amps. and pressure of air inside the discharge tube was changed from 0.05 torr to 1 torr. Fig. 7.2 shows a plot of  $I_B/I$  Vs.  $B$  when the discharge current is 2.25 amp. and  $p_{air}$  is 0.9 torr.

For a comparison of the effect of a longitudinal magnetic field to that of a transverse magnetic field the measured values of radiation enhancements ( $I_B/I$ ) for different values of transverse magnetic field has been plotted in Fig. 7.3.

Table 7.1 shows the values of  $B_{max}$  when the enhancement maxima occurs along with the values of  $(I_B/I)_{max}$  for the three lines considered for different discharge conditions.

In chapter III it was observed that when a discharge column was subjected to a magnetic field there occurred a coupled variation of axial electron density  $n_e(0)$  and electron temperature  $T_e$ . ( $T_e$  is assumed to be uniform along the cross section of discharge tube). In the case of a longitudinal magnetic field  $n_e(0)$  increases and  $T_e$  decreases, whereas when the magnetic field is transverse to the direction of current,  $n_e(0)$  decreases and  $T_e$  increases with the increase of magnetic field. In the latter case, the cylindrical symmetry of the plasma column is shifted towards the wall in the direction

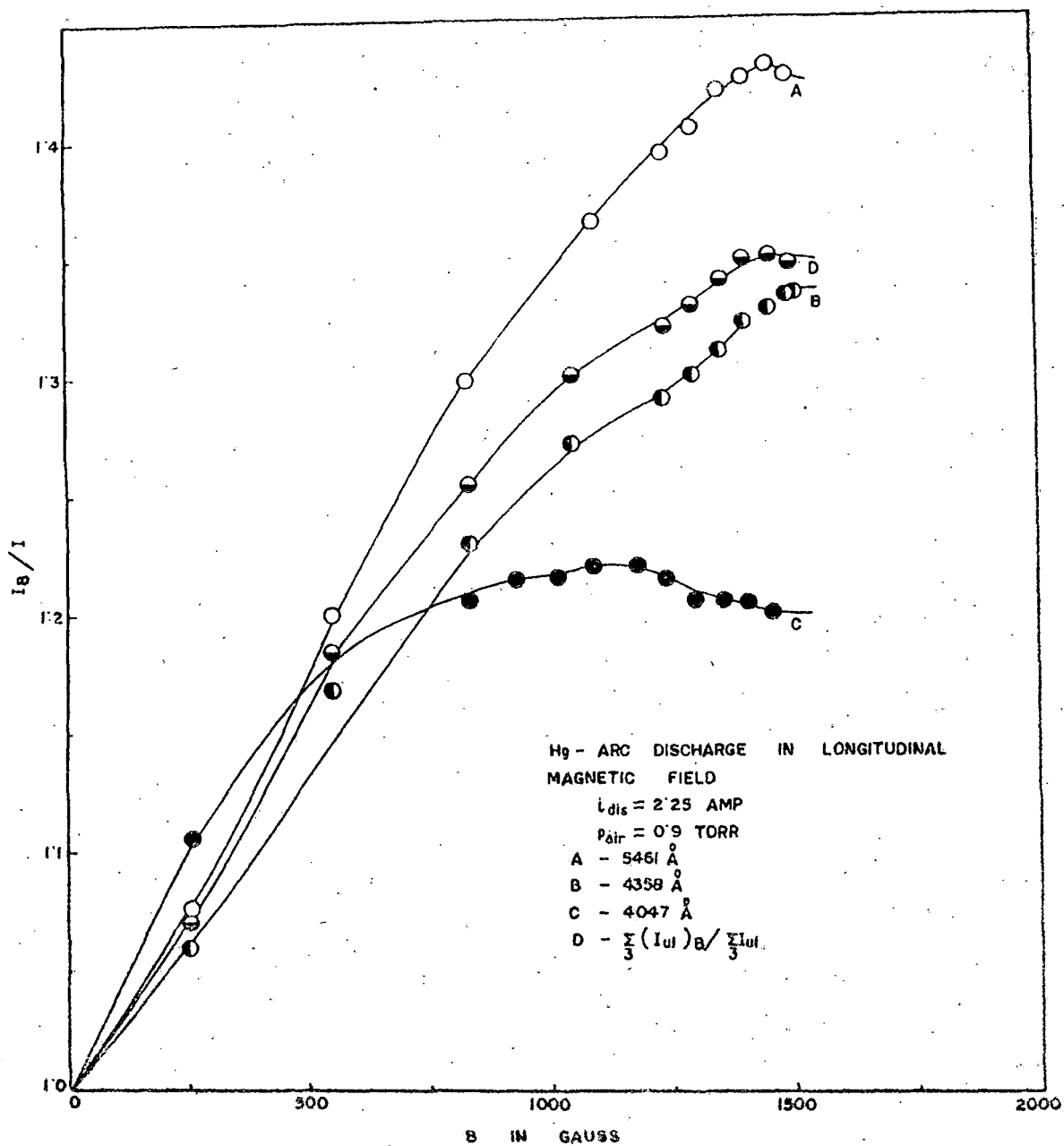


FIG. 7.2.

Fig. 7.2. Variation of spectral intensity enhancement factors ( $I_B/I$ ) with longitudinal magnetic field for lines originating from  $7^3S_1$  level of mercury,  $i = 2.5A$ .

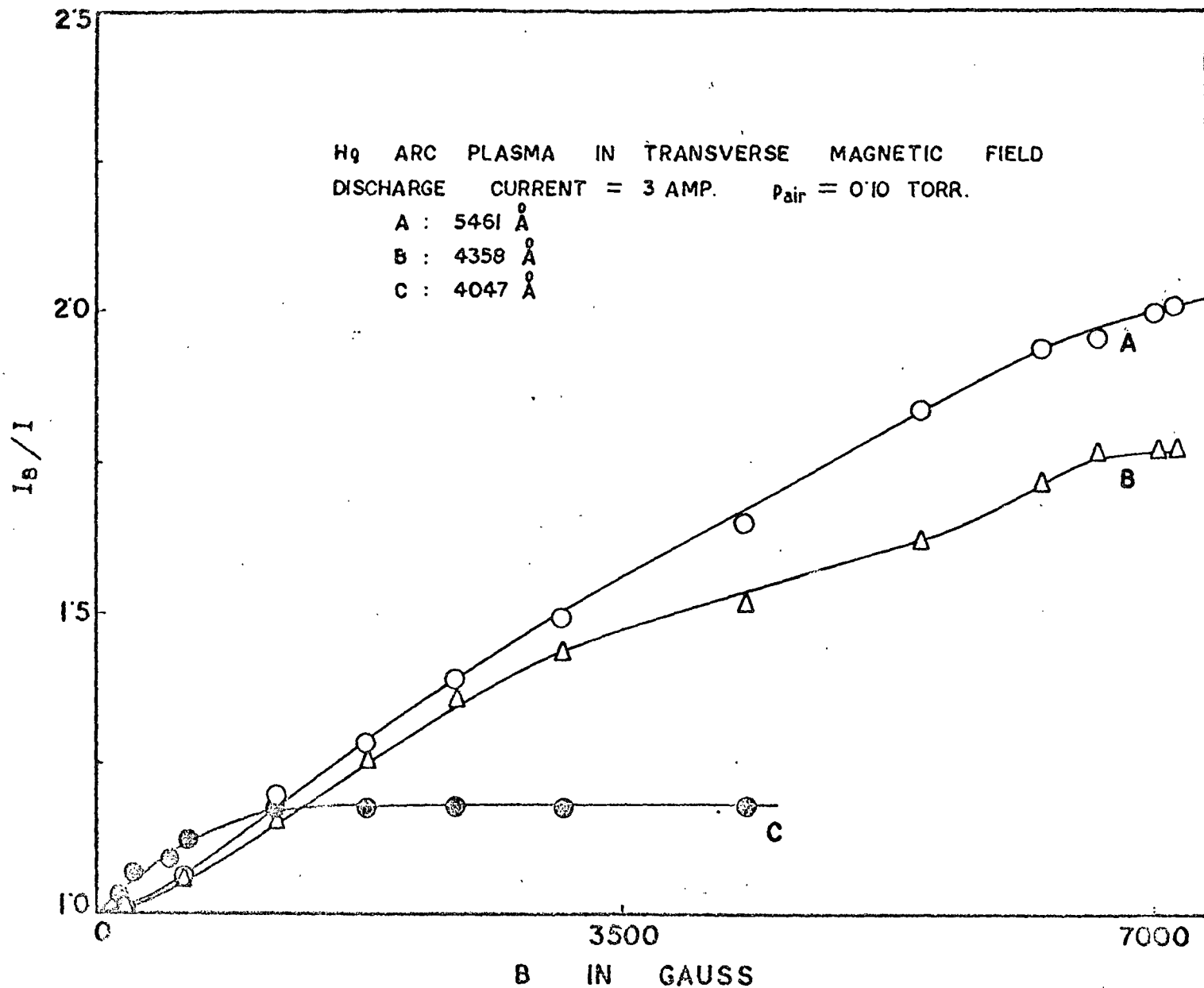


FIG. 7.3.

Fig. 7.3. Variation of spectral intensity enhancement factors with transverse magnetic field for mercury arc.

TABLE 7.1

Wavelength (Å)	Values of $B_{\max}$ and $(I_B/I)_{\max}$	$p_{\text{air}} = 0.5$ torr.		$p_{\text{air}} = 0.9$ torr.	
		$\lambda = 3\text{A}$	$\lambda = 2\text{A}$	$\lambda = 2.25\text{ A}$	$\lambda = 2.75\text{ A}$
5461	$B_{\max}$	1405 G	1405 G	1455 G	1455 G
	$(I_B/I)_{\max}$	1.312	1.38	1.43	1.46
4358	$B_{\max}$	1455 G	1425 G	1495 G	1455 G
	$(I_B/I)_{\max}$	1.275	1.316	1.332	1.33
4047	$B_{\max}$	1015 G	930 G	1055 G	1015 G
	$(I_B/I)_{\max}$	1.25	1.25	1.22	1.23

of Lorentz force. Spectral enhancement is dependent  $\lambda$  on  $n_e(0)$  and  $T_e$ . Since all the three lines originate from a single upper level ( $7^3S_1$ ), their dependence on  $n_e(0)$  and  $T_e$  will be same resulting in same rate of radiation enhancement for the three lines. Since this is not the case in reality, it may be concluded that a third factor which is different for three lines, is important in the process of radiation enhancement. Les' et al (1961) have observed that intensity ratios of the visible triplets of mercury atoms

differ widely depending upon the condition of source. All these divergences can be explained by the phenomena of re-absorption of lines. The lower levels of the lines are two metastables ( $6^3P_{0,2}$ ) and a resonance ( $6^3P_1$ ) level. In the steady state they are supposed to build up appreciable populations, thereby causing self absorption of the lines. As self absorption affects the intensity of emission lines and is strongly related to the population of lower levels, the enhancement factor will also depend on population densities of lower levels of the lines. In the next section a quantitative estimate of this effect has been discussed.

### 7.3.1. Self absorption and enhancement factors in magnetic field:

When there is appreciable self absorption, spectral intensity  $I_{ul}$  of a line with upper level  $u$  and lower level  $l$  is given as,

$$I_{ul} = \text{const. } A_{ul} \int_{-R}^R n_u(r) \left[ \int_{-\infty}^{\infty} \alpha(\nu) \exp(-\beta(\nu)\sigma) \int_r^R n_l(r) dr \right] d\nu dr \quad (7.1)$$

where  $n_{u,l}(r)$  are the local number densities of the upper radiating level and the lower level as a function

of position  $r$  along the line of sight.  $A_{ul}$  is the transition probability of the line and  $\alpha(\nu)$  is the normalised spectral emission profile  $\int \alpha(\nu) d\nu = 1$ . The fraction of emitted line which reaches the detector after traversing  $l_{ne}$  medium from position  $r$  is

$$\exp. \left( -\sigma \beta(\nu) \int_r^R n_e(r) dr \right)$$

$\sigma$  is the absorption cross section per atom at the line centre, independent of  $r$  and  $\beta(\nu)$  is the line profile of absorption normalised to unity at the line centre  $\beta(\nu_0) = 1$ , and  $r = 0$  at the centre of the discharge.

When there is no self absorption

$$\begin{aligned} I_{ul}^0 &= \text{const.} \cdot A_{ul} \int_{-R}^R n_u(r) \left[ \int_{-\infty}^{\infty} \alpha(\nu) d\nu \right] dr \\ &= \text{const.} \cdot A_{ul} \int_{-R}^R n_u(r) dr \end{aligned} \quad (7.2)$$

Vriens et al (1978) and Uvarov and Fabrikant (1965) have shown that excited mercury atoms distribution function across the cross section of discharge is nearly parabolic. Thus considering a parabolic distribution of  $n_u(r)$  we get

$$I_{ul}^0 = \text{const.} \cdot A_{ul} \frac{4}{3} n_u(0) R \quad (7.3)$$

Here  $n_u(0)$  is the <sup>number</sup> ~~no~~ density of radiating atoms at the axis of the discharge tube.

Now self absorption  $A_s$  of a spectral line is defined as

$$\begin{aligned} I_{ul} &= (1 - A_s) I_{ul}^{\circ} \\ &= \text{const.} (1 - A_s) n_u(0) A_{ul} \end{aligned} \quad (7.4)$$

when a longitudinal magnetic field  $B$  is present

$$(I_{ul})_B = \text{const.} (1 - A_s)_B n_u(0)_B A_{ul} \quad (7.5)$$

From (7.4) and (7.5) we get,

$$\frac{(I_{ul})_B}{I_{ul}} = \frac{(1 - A_s)_B}{1 - A_s} \frac{n_u(0)_B}{n_u(0)} \quad (7.6)$$

If both the upper and lower level population densities are parabolic

$$n_x(r) = n_x(0) \left( 1 - \frac{r^2}{R^2} \right)$$

we are assuming that source is of type 'uniform excitation' i.e. a source in which the radiating and absorbing atoms are distributed in the same manner.

Now,

$$\begin{aligned}
 1 - A_s &= \frac{I_{ul}}{I_{ul}^0} \\
 &= \left( \int_{-R}^R n_u(r) \left[ \int_{-\alpha}^{\alpha} \alpha(v) \exp(-\beta(v)\sigma \int_r^R n_e(r) dr) dv \right] dr \right) / \frac{4}{3} R n_u(0)
 \end{aligned} \tag{7.7}$$

We first decouple the integrals over  $n_u(r)$  and  $n_e(r)$

$$\begin{aligned}
 \sigma \int_r^R n_e(r) dr &= \sigma R \int_y^1 n_e(0) (1-y^2) dy \\
 &= \sigma R n_e(0) \left[ \frac{2}{3} - y \left( 1 - \frac{y^2}{3} \right) \right]
 \end{aligned}$$

where  $y = r/R$

putting this value in third bracket of R.H.S. of eqn.(7.7) and replacing the exponential by its power series,

$$\begin{aligned}
 &\int_{-\alpha}^{\alpha} \alpha(v) \exp(-\beta(v)\sigma R n_e(0) \left[ \frac{2}{3} - y \left( 1 - \frac{y^2}{3} \right) \right]) dv \\
 &= \int_{-\alpha}^{\alpha} \alpha(v) \sum_{n=0}^{\infty} \frac{(-1)^n R^n \sigma^n \beta^n(v)}{n!} n_e(0)^n \left[ \frac{2}{3} - \left( y - \frac{y^3}{3} \right) \right]^n dv \\
 &= \sum_{n=0}^{\infty} \frac{(-1)^n R^n \sigma^n n_e(0)^n}{n!} \left[ \frac{2}{3} - \left( y - \frac{y^3}{3} \right) \right]^n \int_{-\alpha}^{\alpha} \alpha(v) \beta^n(v) dv
 \end{aligned}$$

For a discharge type like ours we can safely assume that emission and absorption profiles are identical and Gaussian in nature which is the outcome for Doppler broadening of spectral lines. That is we assume all other broadenings of the spectral lines negligible compared to Doppler broadening. Validity of these criteria is discussed in text books (Corney, 1977) and for resonance line by Hearn (1963). For a Gaussian profile of absorption and emission, Mosberg and Wilke (1978) have shown

$$\int_{-\infty}^{\infty} \alpha(\nu) \beta^n(\nu) d\nu = \frac{1}{n+1}$$

Putting all these results in (7.7) we obtain

$$1 - A_s = 1 - \frac{3}{4} \sum_{n=1}^{\infty} \frac{(-1)^{n+1} \sigma^n n_e(0)^n R^n}{n!(n+1)} \int_{-1}^{+1} \left[ \frac{2}{3} - \left( y - \frac{y^3}{3} \right) \right]^n (1-y^2) dy$$

or,

$$1 - A_s = 1 - \frac{3}{4} \sum_{n=1}^{\infty} \frac{(-1)^{n+1} \sigma^n n_e(0)^n R^n}{(n+1)!} \left[ \int_{-2/3}^{+2/3} \left[ \frac{2}{3} - \left( y - \frac{y^3}{3} \right) \right]^n d \left( y - \frac{y^3}{3} \right) \right] \quad (7.8)$$

values of  $n_e(0)$ 's are calculated by employing Forrest and Franklin's (1969) equation in a fashion stated in chapter VI. To determine the value of  $n_0(0)$ ,  $n_1(0)$  and  $n_2(0)$  the population densities of  $6^3P_{0,1,2}$

levels at the axis of the discharge, we have utilised the values of collision integrals  $\langle Q_{ij} \rangle$  given by Johnson, Cooke and Allen (1978) (author's Fig. No. 7 and reproduced in fig. 7.4). A survey of literature revealed a large range of cross section ( $Q_{ij}$ ) values. From these large data the authors have chosen a set which appears self consistent and in which the forward and reverse rates are related by Klein-Rosseland formula. The density of electron at the axis  $n_e(0)$  without a magnetic field is determined from the expression of current considering a parabolic distribution of electron.

$$\begin{aligned} i &= \mu E e 2\pi \int_0^R n_e(r) r dr \\ &= \mu E e 2\pi n_e(0) R^2 \int_0^1 y(1-y^2) dy \end{aligned}$$

where  $\mu E$  is the drift velocity of electrons in mercury vapour at the corresponding  $E/p$  determined by Nakamura and Lucas (1978). This value of  $n_e(0)$  was utilised in the calculations of population densities in a manner stated in chapter VI.

For a discharge with a Maxwellian electron energy distribution function and for current  $i = 2.5$  amp.,  $p_{\text{air}} = 0.5$  torr and  $p_{\text{Hg}} = 0.2729$  torr determined by inner

Fig. 7.4. Collision integrals  $\langle Q_{ij} \nu \rangle$  for Hg. levels: (a) inelastic with ground state, (b) inelastic with  $6^3P$  levels; (c) super-elastic. A,  $6^1S_0 \rightleftharpoons 6^3P_0$ , B,  $6^1S_0 \rightleftharpoons 6^3P_1$ , C,  $6^1S_0 \rightleftharpoons 6^3P_2$ , D,  $6^3P_0 \rightleftharpoons 6^3P_1$ , E,  $6^3P_1 \rightleftharpoons 6^3P_2$ .

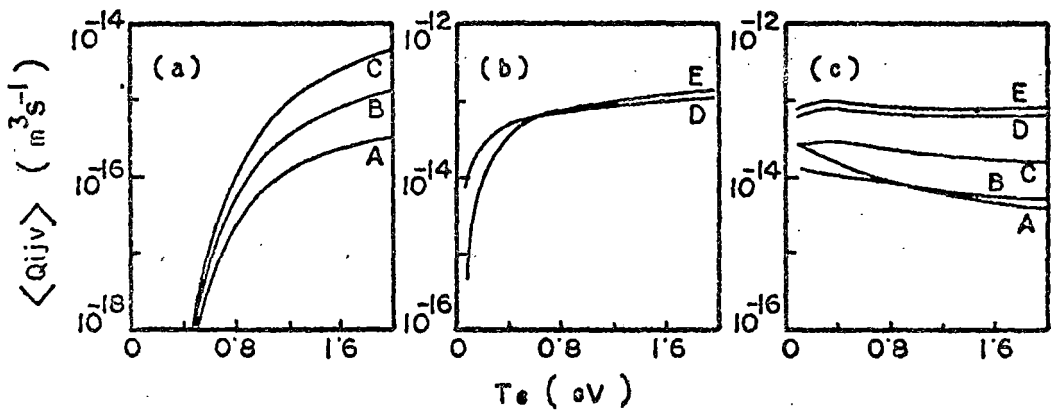


FIG. 7.4.

wall temperature  $T_g$ , and  $T_e = 0.412$  eV. as determined by spectral intensity ratio method in chapter VI, the result of calculations is:  $n_g$  (considered uniform across c.s.) =  $9.6 \times 10^{15} \text{ cm}^{-3}$ ,  $n_e(0)$

$$= 5.95 \times 10^{13} \text{ cm}^{-3}.$$

$$n_2(0) = 1.13 \times 10^{10} \text{ cm}^{-3}$$

$$n_1(0) = 2.38 \times 10^{10} \text{ cm}^{-3}$$

$$n_0(0) = 3.92 \times 10^{10} \text{ cm}^{-3}$$

Again  $\sigma$  the cross section of absorption at the line centre, when Doppler broadening is the sole broadening mechanism of spectral lines, is given as

$$\sigma = \pi r_0 c f_{lu} \lambda_{ul} \left( \frac{M}{2\pi k T_g} \right)^{1/2} \quad (7.9)$$

where  $r_0$  is the classical electron radius, ( $2.818 \times 10^{-13}$  cm).  $c$  is the velocity of light,  $f$  and  $\lambda$  are the absorption oscillator strength and wavelength of the transition,  $M$  is the mass of mercury atom and  $k$  is the Boltzmann constant. Taking  $f$  values of the transitions from Gruzdev (1967), the calculated value of  $\sigma$  by equation (7.9) and the values of  $k_0 = \sigma n_e(0)$  where  $k_0$  is the absorption coefficient of radiation at the line centre has been shown in Table 7.2.

TABLE 7.2

$\lambda$ (Å)	5461	4358	4047
$f$ (Ref. Gruzdev (1967))	0.14	0.11	0.10
$\sigma$ (cm <sup>2</sup> )	$6.5 \times 10^{-12}$	$4.077 \times 10^{-12}$	$3.44 \times 10^{-12}$
$k_0$ (cm <sup>-1</sup> )	0.0735	0.0938	0.1348

It is evident from Table 7.2 that  $k_0 R$ , ( $R = 0.75$  cm.) which may be called the optical depth is much smaller than unity. Since the series in eqn. (7.8) is a converging one we discard all the terms except the first term  $n = 1$ .

Thus

$$1 - A_s = 1 - \frac{3}{4} \sigma n_e(0) R \frac{1}{2} \left[ \frac{8}{9} \right]$$

$$\text{or, } 1 - A_s = 1 - \frac{1}{3} \sigma n_e(0) R$$

$$= 1 - f_{lu} \lambda_{ul} \rho n_e(0)$$

(7.9)

where

$$\rho = \frac{1}{3} \pi n_e c \left( \frac{M}{2\pi k T_g} \right)^{1/2} R$$

Putting the value of  $(1 - A_s)$  from eqn. (7.9) in eqn. (7.6)

we obtain,

$$\frac{(I_{ul})_B}{I_{ul}} = \frac{1 - f_{lu} \lambda_{ul} \rho n_e(0)_B}{1 - f_{lu} \lambda_{ul} \rho n_e(0)} \frac{n_u(0)_B}{n_u(0)}$$

We have assumed here that neutral atom temperature is constant with magnetic field though we were unable, to measure the change of  $T_g$  with  $B$  experimentally.

Hence

$$\begin{aligned} & (I_{ul})_B / I_{ul} \\ &= \left[ 1 - f_{lu} \lambda_{ul} \rho (n_e(0)_B - n_e(0)) \right] \frac{n_u(0)_B}{n_u(0)} \end{aligned} \quad (7.10)$$

Due to coupled change of  $n_e(0)$  and  $T_e$  with magnetic field,  $n_u(0)$  and  $n_l(0)$  will change. Equation (7.10) qualitatively predicts that due to these changes enhancement of spectral radiations will also change but will be lessened by self absorption as  $n_l(0)$  increases with  $B$ . The effects will be different for three lines as  $f$ ,  $\lambda$  and  $n_l(0)_B$  will be different for them. It may be noted here that  $\sigma$  is maximum for  $5461 \text{ \AA}$  radiation where as  $n_2(0)$  is relatively small. The case is reversed for  $4047 \text{ \AA}$  radiation, the case for  $4347 \text{ \AA}$  radiation is in between them.

Moreover, measurement of  $T_e$  with  $B$  in chapter VI (fig. 6.2) shows that as  $B$  increases,  $T_e$  decreases and reaches a saturated lower value. The case is

reversed for  $n_e(0)$ . Anyway it may be concluded that due to coupled change of  $n_e(0)$  and  $T_e$  with  $B$  both  $n_l(0)$  and  $n_u(0)$  will attain a saturated upper value. Moreover, it is established that for a source of uniform excitation, there will be no self-reversal (Cowan and Diecke (1948)), on the other hand effect due to self absorption will also reach a saturated maximum value. Thus we can expect that when  $B$  is sufficiently large there will be no change in enhancement factor with the increase of magnetic field. Fig. 7.1 and 7.2 however shows a slow fall of the factor at that stage.

Now we consider a discharge in sufficiently high magnetic field (as  $B = 1500$  gauss), so that all changes are saturated. In that case  $n_e(0)_B \gg n_e(0)$  Since relative populations of the excited levels always obey a Boltzmann distribution with  $T_e$  as temperature (Richter, 1968), eqn. (7.10) may be re-written as

$$\begin{aligned} & (I_{ul})_{\max} / I_{ul} \\ &= \left[ 1 - f_{lu} \lambda_{ul} \rho n_0(0)_B \exp\left(-\frac{E_l - E_0}{kT_{eB}}\right) \right] \frac{n_{ul}(0)_B}{n_{ul}(0)} \\ & \quad (l=0, 1, 2) \end{aligned} \quad (7.11)$$

here  $E$ 's are the energy of the corresponding levels. In the L.H.S. of eqn. (7.11) we have written the subscript

max indicating that the saturation maxima has been reached. For 4047 Å, for which the maxima is attained earlier, we consider ~~xxx~~ that this is also the value for  $I_B$  when B is much greater than  $B_{\max}$  where the intensity maximum was first attained.

$$\text{A plot of } (I_{ul})_{\max} / I_{ul} \quad \text{against} \\ f_{lu} \lambda_{ul} \exp(-(E_l - E_o) / kT_{eB})$$

has been shown in Fig. 7.5 for two discharge conditions, and the plots are straight lines as predicted by eqn. (7.11).

The slope of the lines are :

i) for  $i = 2$  amp.,  $p_{\text{air}} = 0.05$  torr, slope  $3.33 \times 10^4 \text{ cm}^{-1}$ .

ii) for  $i = 2.25$  amp.,  $p_{\text{air}} = 0.9$  torr, slope =  $5.19 \times 10^4 \text{ cm}^{-1}$ . The slope =  $\frac{1}{3} \pi r_0 e R \times (M / 2 \pi k T_g)^{1/2} n_o(0)_B n_u(0)_B / n_u(0)$

From the intercept of the graph  $n_u(0)_B / n_u(0) \approx 1.4$

if  $n_o(0)_B \approx 10 \times$  magnitude of  $n_o(0)$   
 $\approx 10^{11} \text{ cm}^{-3}$

the calculated value of slope is,

$$\text{(slope) calculated} = \frac{1}{3} \times 3.14 \times 2.82 \times 10^{-13} \times 3 \times 10^{10} \times 0.75 \\ \times 10^{11} \times 1.4 \times \left( \frac{200 \times 1.66 \times 10^{-24}}{2 \times 3.14 \times 1.38 \times 10^{-16} \times 373} \right)^{1/2}$$

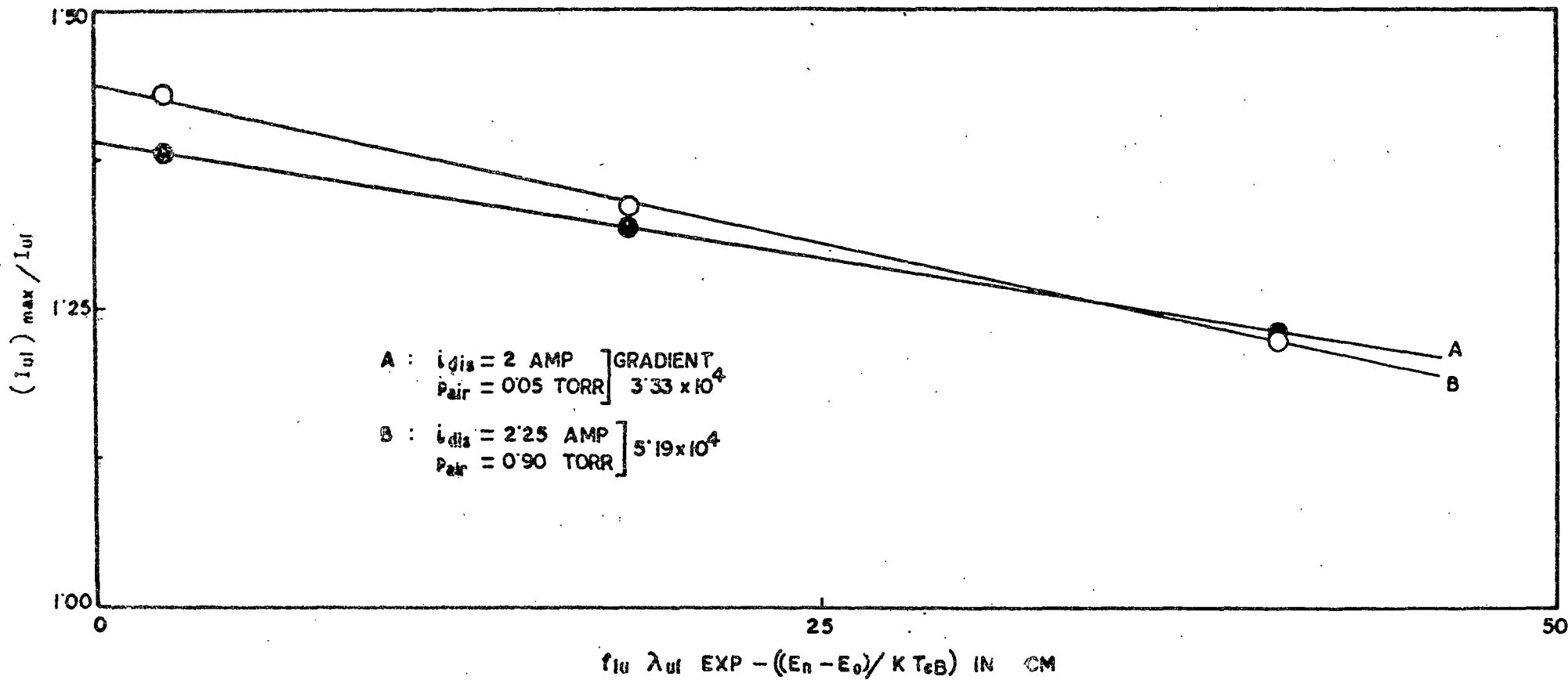


FIG. 7.5.

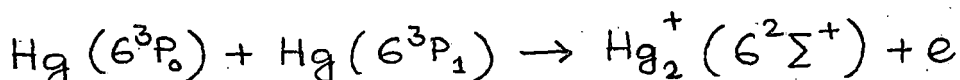
Fig. 7.5. Variation of enhancement maxima against  $f_{lu} \lambda_{ul} \exp[-(E_n - E_0) / k T_e B]$  for two types of mercury arc discharges in longitudinal magnetic field.

$\approx 3 \times 10^4 \text{ cm}^{-1}$  which is in agreement with the values determined from graph.

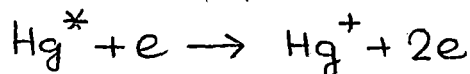
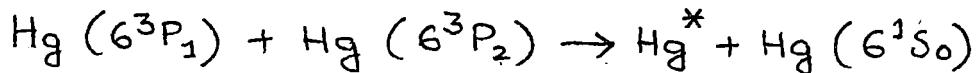
In the next sections we shall try to evaluate the value of  $n_L(0)_B / n_L(0)$  from the total intensity of the triplet lines. Before doing this we shall consider the positive column of mercury arc discharge in detail so that the coupled variation of  $T_e$  and  $n_e(0)$  may be predicted and this has been shown in the following section.

### 7.3.2. Coupled variation of $n_e(0)$ and $T_e$ with magnetic field :

We shall consider a wall confined diffuse mercury arc discharge the type of which was discussed in detail in chapter VI. It was observed there that chief ionised species are  $\text{Hg}_2^+$  molecular ions formed by the process of associative ionisation when  $p_{\text{air}}$  is relatively small and when  $p_{\text{air}}$  is relatively high ( $> 2 \text{ torr.}$ ) due to quenching of  $6^3P_0$  and  $6^3P_1$  levels by  $\text{N}_2$  and  $\text{O}_2$  molecules,  $\text{Hg}^+$  ions, created by electron collision of  $6^3P_2$  level atoms, are the chief ionised species. When  $p_{\text{air}}$  is relatively small,  $\text{Hg}_2^+$  molecular ions are formed by reactions like



this process has a large cross-section. If we consider that the axial neutral particle temperature of the arc is larger than the inner wall temperature, which is generally the case as an appreciable amount of energy which is supplied to the arc is carried away by the thermal conductivity of mercury vapour atoms and air molecules, the rate of production of  $\text{Hg}_2^+$  ions will further increase than as calculated in chapter VI. For a group of processes like



the ~~Hg~~  $\text{Hg}^*$  states are highly excited states and are very near to the ionisation level. These levels are definitely in thermal equilibrium with the free electrons. Principle of detailed balancing predicts an equal downward collision of  $\text{Hg}^*$  atoms with  $\text{Hg} (6^1S_0)$  atoms to form  $6^3P_1$  and  $6^3P_2$  atoms instead of reaction like  $\text{Hg}^* + e \rightarrow \text{Hg}^+ + 2e$ .

Hence one of the chief  $\text{Hg}^+$  ion production mechanism can not be considered as  $\text{Hg}^*$  atoms are in thermal equilibrium with continuum, rendering the ionic species of the discharge more molecular.

Thus we consider a positive column of discharge where  $\text{Hg}_2^+$  ions are produced by the process of associative ionisation and lost by ambipolar diffusion to the wall.

We neglect the effect of conversion of molecular ions to atomic ions and vice-versa and the process of dissociative recombination of molecular ions. Ignoring the radial variation of  $6^3P_0$  atoms, the equation of continuity for electron is

$$\frac{1}{r} \frac{d}{dr} \left( r \frac{dn_e(r)}{dr} \right) = - \frac{g}{D_a} \quad (7.12)$$

where  $g = n_0 n_1 \sigma_{ass} \langle v \rangle$  ,  $\sigma_{ass} = \text{c.s. for associative ionisation}$  and  $\langle v \rangle = (16 k T_g / \pi M)^{1/2}$  and  $D_a$  is ambipolar diffusion coefficient. The solution of (7.12) with  $n_e(R) = 0$  at the wall is

$$n_e(r) = \frac{g R^2}{4 D_a} \left[ 1 - \left( \frac{r}{R} \right)^2 \right] \quad (7.13)$$

Since  $D_a = \mu_i k T_e / e$  where  $\mu_i$  is the mobility of  $Hg_2^+$  ions, the plasma balance condition is obtained

$$\frac{g R^2}{n_e(0) \mu_i k T_e / e} = 4 \quad (7.14)$$

It may be noted here that for a parabolic profile of  $6^3P_{0,1}$  atoms the eqn. (7.13) changes to

$$n_e(r) = \frac{g R^2}{4 D_a} \left[ \frac{11}{72} - \frac{1}{4} \left( \frac{r}{R} \right)^2 + \frac{1}{8} \left( \frac{r}{R} \right)^4 - \frac{1}{36} \left( \frac{r}{R} \right)^6 \right]$$

but eqn. (7.14) virtually remains unchanged only 72/11 replacing 4 in the R.H.S.

Since the conditions for ions to be magnetised is  $B/p > 0.5 \text{ tesla torr}^{-1}$  (Franklin, 1976), we consider for our experimental conditions  $\mu_i = \mu_{iB}$ , more over it was observed by Cummings and Tonks (1941) that normal distribution of electrons is characteristic of an arc in its steady state even in presence of a longitudinal magnetic field, the plasma balance equation in the presence of a magnetic field will be

$$\frac{g_B R^2}{n_e(0)_B \mu_i k T_{eB} / e} = 4 \quad (7.15)$$

the subscript B signifies the corresponding quantities when a magnetic field is present. From (7.14) and (7.15) we get

$$\frac{n_e(0)_B}{n_e(0)} \cdot \frac{k T_{eB}}{k T_e} = \frac{g_B}{g} \quad (7.16)$$

The ratio  $g_B/g$  is again a function of  $n_e(0)$  and  $T_e$ . This functional relationship may be estimated very approximately in the following manner:

$6^3P_0$  and  $6^3P_1$  level populations which enter into  $g$  are a metastable and resonance level. In the steady state, they are supposed to build up appreciable

populations and collisional processes chiefly populate and depopulate the levels. Let us assume that they build up an equilibrium population distribution as determined by Saha equation

$$\begin{aligned}
 & [n_o(0)] \text{ equilibrium} \\
 & = \frac{g_o}{2g_i} \left( \frac{2\pi\hbar^2}{mkT_e} \right)^{3/2} n_e(0)^2 \exp(\chi_o/kT_e) \quad (7.17)
 \end{aligned}$$

here  $g_o$  and  $g_i$ 's are the statistical weights of  $6^3P_o$  state and atomic ions,  $\chi_o$  is the ionisation potential of  $6^3P_o$  state,  $m$  equals the mass of electron and  $\hbar$  is the rationalised Plank's constant,  $n_e(0)$  here is the density of  $Hg^+$  ions which may be roughly calculated knowing  $T_e$  and  $n_g$  by Saha equation and was calculated as  $1.78 \times 10^{13} \text{ cm}^{-3}$ . Now for a level to be in thermal equilibrium microreversibilities would have to exist for all processes. In this way, one of the processes say electron impact ionisation of  $6^3P_o$  atoms should be balanced by three body collisional recombination of atomic ions with electrons to that level. But unfortunately for discharges under consideration, this is not the case. Microreversibilities for ionisation process are totally absent. Instead, the ions produced in the volume are carried away to discharge tube wall by

irreversible ambipolar diffusion process, thereby they recombine at the wall and return to the plasma region as neutral ground state species. This is also equally ~~true~~ true for molecular ions. Molecular ions do not recombine totally in the volume, instead a large amount of excess of ions are carried away towards the wall by ambipolar diffusion. In short in these types of plasma, ionisation does not balance with recombination. This type of discharges are named as 'ionising plasma' by Fujimoto (1979). In this case, following Numano et al (1975) we can write,

$$n_0(0) = (1 + C_p) [n_0(0)]_{\text{equilibrium}} \quad (7.18)$$

Here  $C_p$  is a quantity which determines the excess of ionisation over volume recombination and  $C_p$  is given as (approximately)

$$C_p = 10^{31} \frac{D_a}{n_e(0)^2 \Lambda^2} \left( \frac{E_H}{kT_e} \right)^{1/2} \frac{1}{g_0 g_{elb}} \exp\left(-\frac{\chi_i'}{kT_e}\right) \quad (7.19)$$

here  $\Lambda$  is the effective diffusion length and  $1/\Lambda^2 = (2.4/R)^2$ ,  $E_H$  is the ionisation potential of hydrogen atoms,  $\chi_i'$  being the ionisation potential of the lowest excited state, in the case of mercury

atoms  $\chi_i' = \chi_0$  and  $g_{eff}$  is identified as effective quantum no. of the state defined as (Griem, 1964),

$$g_{eff} = z \left( \frac{R}{T_\alpha - T_p} \right)^{1/2}$$

where

$R =$  Rydberg constant,  $T_\alpha$  is the ionisation limit of the system under consideration,  $T_p$  is the term value of the  $x$  level  $p$  and for neutral atoms  $Z = 1$ .

Nishikawa et al (1971) have determined the value of  $D_a = 160/p \text{ cm}^2 \text{ sec}^{-1}$ , with this value of  $D_a$  and  $n_e(0) = 1.78 \times 10^{13} \text{ cm}^{-3}$  determined by Saha equation, the value of  $C_p$  is found to be 28.85. Since  $C_p \gg 1$ , we rewrite equation (7.18) as

$$n_o(0) = \delta \left( \frac{1}{kT_e} \right)^2 D_a \quad (7.20)$$

where 
$$\delta = 10^{31} \frac{1}{\Lambda^2} (E_H)^{1/2} \frac{1}{2g_i g_{eff}} \left( \frac{2\pi\hbar^2}{m} \right)^{3/2}$$

Again considering  $D_a = \mu_i kT_e / e$

we arrive at the conclusion

$$n_o(0) \propto \frac{1}{kT_e} \quad (7.21)$$

This result is also evident from the generalised expression for electron temperature (von-Engel, 1965) in which it has been shown that  $T_e \propto (E/p)$  where  $p$  is

the pressure which is a measure of  $n_0(0)$ .

Since relative populations of excited states obey Boltzman distribution we can write also,

$$n_1(0) \propto \frac{1}{kT_e} \quad (7.22)$$

Here we have neglected the exponential term since

$$kT_e > \Delta E$$

It may be noted here that the proportionality constants in (7.21) and (7.22) would be independent of magnetic field, so long  $B/p$  is less than  $\frac{kT_e}{\mu_B}$  limit for which ions remain un-magnetised.

So eqn. (7.16) may be ~~rewritten~~ rewritten as

$$\frac{n_e(0)_B}{n_e(0)} = \left( \frac{kT_e}{kT_{eB}} \right)^3 \quad (7.23)$$

Here we have assumed once again that

$$T_g = T_{gB}$$

As measured values of  $T_e$  in chapter VI, show a decrease with the increase of  $B$ , equation (7.23) predicts a coupled increase of  $n_e(0)$  with  $B$  though very approximately. However, we have plotted  $T_{eB}/T_e$  and  $n_e(0)_B/n_e(0)$  with  $B$  in Fig. 7.6. This relationship (7.23) will be utilised in next section while determining the population density of  $6^3P_2$  level from total intensity of triplet lines.

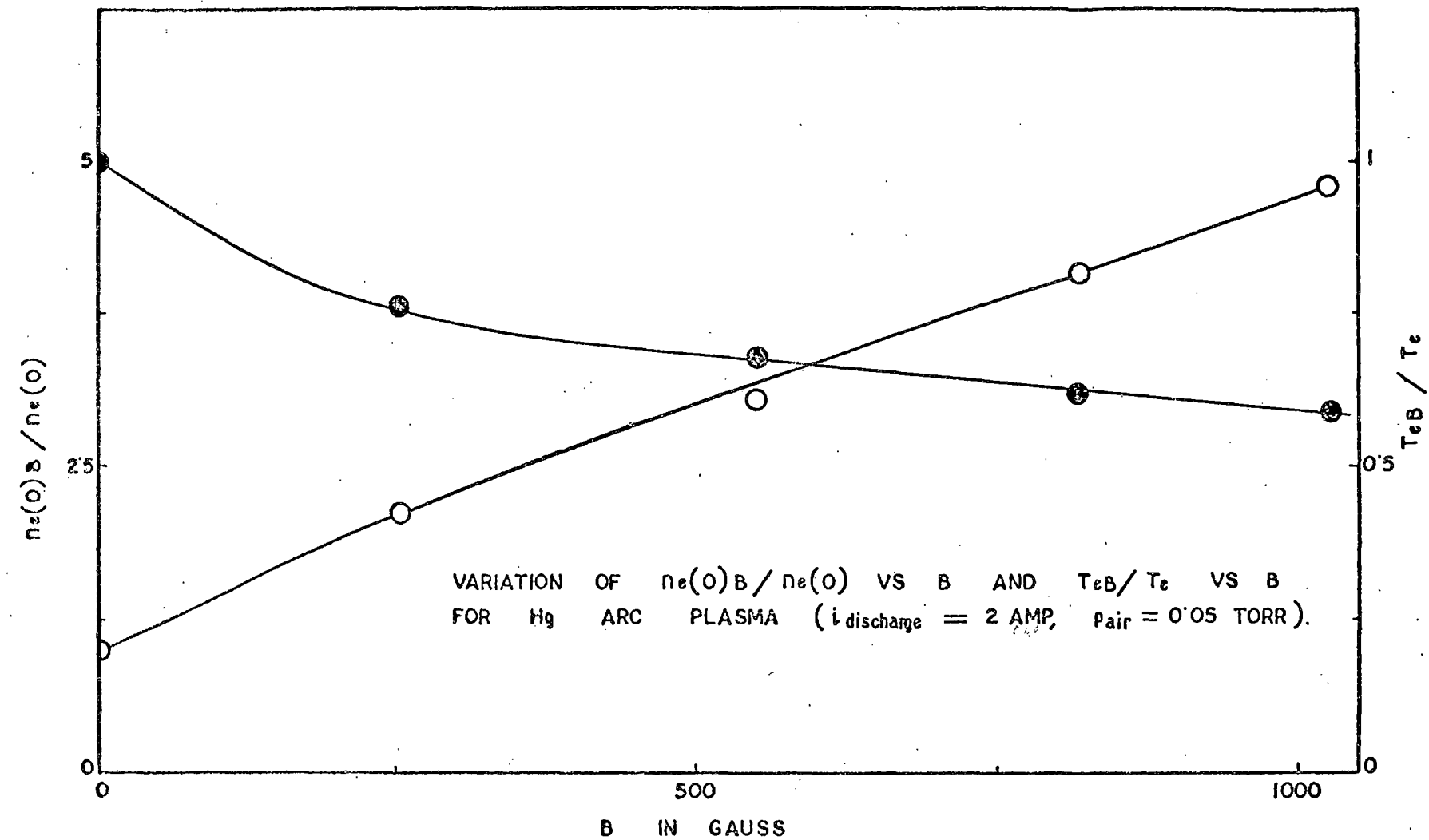


FIG. 7.6.

7.3.3. Total intensity of triplet lines with and without magnetic field.

For a homogeneous and isotropic source, the intensity of a spectral line is given as,

$$I_{ul} = \frac{h\nu_{ul}}{4\pi} A_{ul} \theta_{ul} \int n_u(r) dr \quad (7.24)$$

where  $\theta_{ul}$  is the optical escape factor which accounts for the self absorption of the line.

Thus for the three lines considered together,

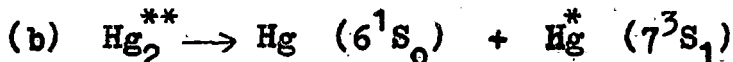
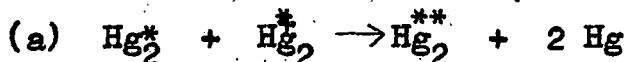
$$\frac{\sum_3 (I_{ul})_B}{\sum_3 (I_{ul})} = \left( \sum A_{ul} \theta_{ul} \right)_B \frac{n_u(0)_B}{n_u(0)} \cdot \frac{1}{\sum A_{ul} \theta_{ul}} \quad (7.25)$$

Here  $n_u(0)$  represents the axial density of  $7^3S_1$  atoms. To determine  $n_u(0)$ , we shall consider the production and loss mechanism of  $7^3S_1$  atoms.

The level  $7^3S_1$  may be populated by one or more of the following ways:

- i) direct excitation of the ground level atoms.
- ii) stepwise excitation of  $6^3P_{0,1,2}$  levels.
- iii) cascade radiations chiefly from  $7^3P_2$  level.
- iv) transfer of excitation by electron collision, from other higher levels.

v) bi-molecular excited dimer collision followed by a decomposition to  $7^3S_1$  level.



vi) recombination of  $\text{Hg}^+$  ions to the  $x$  level.

The level may be depopulated by one or more of the following processes:

i) spontaneous emission.

ii) collisional de-excitation to a lower level.

iii) collisional excitation to a higher level.

iv) ionisation from the level.

v) quenching by  $\text{N}_2$  and  $\text{O}_2$  molecules.

Now let us consider the relative importance of production and loss terms. In the production side contribution due to processes (iv), (v) and (vi) may be neglected in our conditions of discharge. We also disregard cascade contribution to  $7^3S_1$  level as the electron temperature is small enough rendering population in  $7^3P$  levels small. So the important terms will be direct and stepwise excitations. Again it is evident that contribution of stepwise excitations from  $6^3P_2$  level will dominate over that for other levels  $6^3P_{0,1}$ . We have calculated the rate of this excitation corresponding to a optically allowed transition by M.J. Seaton's

cross section (Sampson, 1969) and rate of ( $6^1S_0 \rightarrow 7^3S_1$ ) from the ground state which is a optically forbidden transition by C.W.Allen's cross section (Benson and Kulander, 1972). The calculated values of the rates are

$$\text{rate for } (6^1S_0 \rightarrow 7^3S_1) \text{ transition} = 2.69 \times 10^{13} \text{ sec}^{-1}$$

$$\text{rate for } (6^3P_2 \rightarrow 7^3S_1) \text{ transition} = 1.4 \times 10^{14} \text{ sec}^{-1}$$

i.e. stepwise excitation is nearly a magnitude greater than the direct excitation.

In the loss side collisional excitation to the nearest higher level  $7^1S_0$  (7.926 eV.) will be dominating to that for all other higher levels and collisional excitation to a higher level will be greater than collisional de-excitation to a lower level. Hence comparable terms will be spontaneous emission lessened by self absorption and collisional excitation to  $7^1S_0$  level. Self absorption of a transition is accounted for by introducing escape factor parameter  $\Theta_{ul}$  which is given by a relation deduced by Phelps et al (1960, 1958),

$$\Theta_{ul} = \frac{1.92 - \frac{1.3}{1 + (k_0 R)^{6/5}}}{(k_0 R + 0.62) \{ \pi \ln (1.375 + k_0 R) \}^{1/2}} \quad (7.26)$$

The transition probabilities  $A_{ul}$  for three lines for  $7^3S_1$  level are given by Mosberg & Wilkie (1978).

With these values of  $A_{ul}$  and  $\Theta_{ul}$  calculated by

equation (7.26) with values of  $k_0$  given in table 7.2, we calculate contribution for spontaneous emission

$$n_u(0) \sum A_{ul} \theta_{ul} = 6.77 \times 10^8 n_u(0) \text{ sec}^{-1}$$

The contribution of optically forbidden transition ( $7^3S_1 \rightarrow 7^1S_0$ ) is  $3.23 \times 10^6 n_u(0) \text{ sec}^{-1}$ , whereas the rate of quenching of  $7^3S_1$  atoms by  $N_2$  and  $O_2$  molecules will be in the order  $10^4 n_u(0) \text{ sec}^{-1}$ , the cross sections for quenching collisions are given by Massey (1971). Thus we arrive at the balance equation for  $7^3S_1$  atoms

$$n_u(0) \sum A_{ul} \theta_{ul} = n_e(0) n_2(0) \langle Q_{2u} v_e \rangle \quad (7.27)$$

where  $Q_{2u}$  is the cross section for ( $6^3P_2 \rightarrow 7^3S_1$ ) transition and  $v_e$  is electron random velocity.

Equation (7.27) has been verified experimentally in Fig. 7.7. Where we have plotted intensities of the lines with  $i^2$ . The  $n_2$  atoms are mainly produced by electron impact of ground level atoms, as this is the leading term in rate of production of  $n_2$  atoms calculated in section 7.3.2, the intensity of lines will be proportional to  $n_e^2 i.e.$  to  $i^2$ . The plots  $I_{ul}$  vs.  $i^2$  are straight lines as evident from fig. 7.7, where a plot of  $I_{ul}$  vs.  $i$  does not yield a straight line.

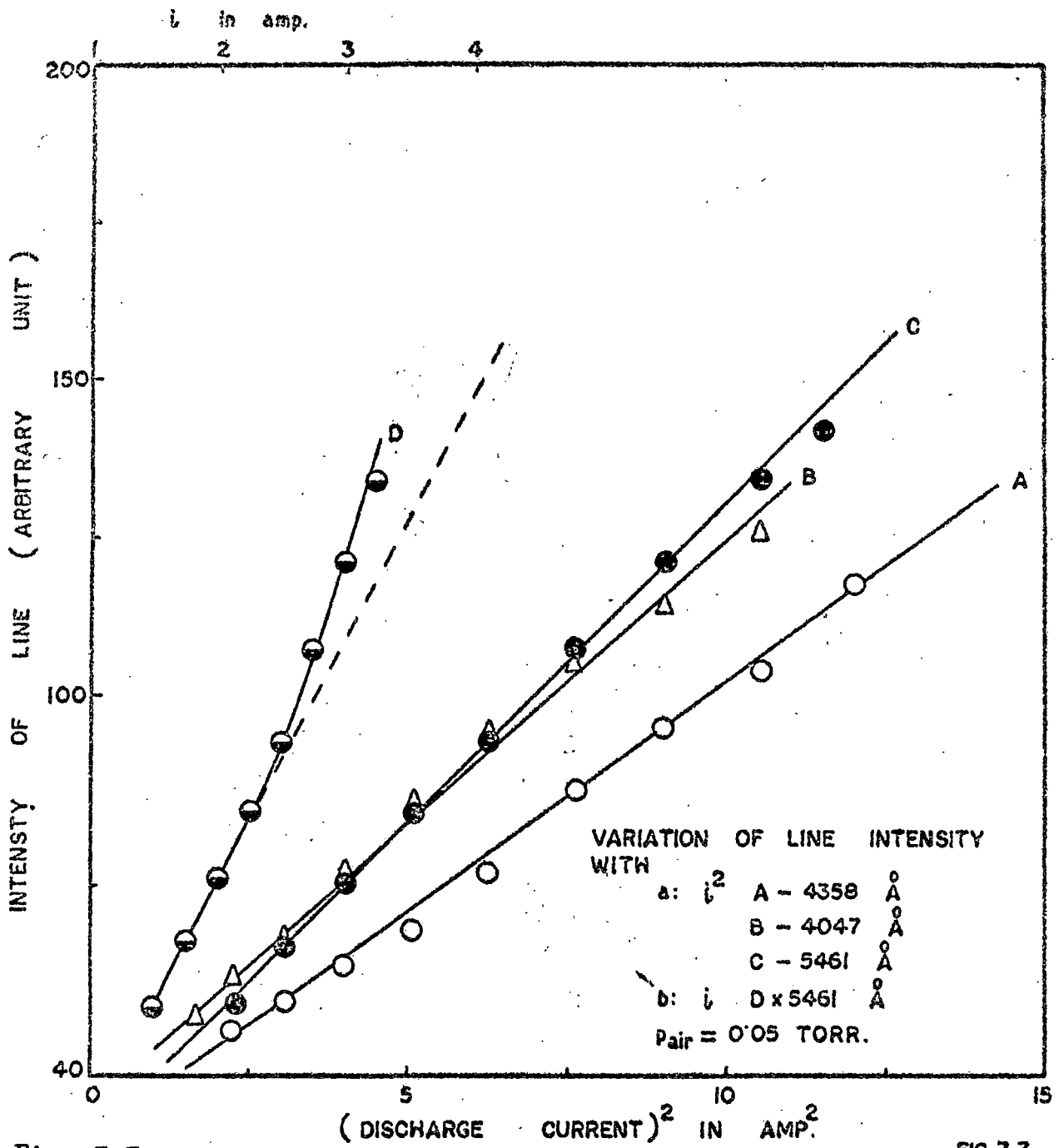


Fig. 7.7.

FIG.7.7.

Variation of spectral intensities of mercury arc with  $i^2$  and  $i$ .

Hence equation (7.27) may be considered to be valid in the discharges concerned, if the value of  $n_u$  thus determined is put into eqn. (7.25) we get

$$\frac{\sum_3 (I_u)_B}{\sum_3 I_u} = \frac{n_2(0)_B}{n_2(0)} \frac{n_e(0)_B}{n_e(0)} \frac{\langle Q_{2u} v_e \rangle_B}{\langle Q_{2u} v_e \rangle} \quad (7.28)$$

Johnson and Hinnoy (1969) have given a semi-empirical cross section for optically allowed transitions in helium,

$$Q_{ij}(i \rightarrow j) = 4 \left( \frac{E_H}{E_{ij}} \right)^2 f_{ij} \pi a_0^2 \left( \frac{E}{E_{ij}} \right)^{-1} \left[ 1 - \exp \left\{ -\beta \left( f_{ij} \frac{E_H}{E_{ij}} \right)^\gamma \left( \frac{E}{E_{ij}} + 1 \right) \right\} \right] \ln \left( \frac{E}{E_{ij}} + \delta \right) \quad (7.29)$$

where  $E$  is energy,  $E_{ij}$  is the threshold energy for transition and,  $\beta$ ,  $\gamma$  and  $\delta$  are non-negative, dimensionless, adjustable parameters. Grizinski's classical cross sections for  $n \rightarrow n+1$  transition in hydrogen are adequately represented by the choice

$$\beta = 1, \quad \gamma = 0.4 \text{ and } \delta = 0. \text{ A choice } \beta = 1.2, \\ \gamma = 0.7, \text{ and } \delta = 0, \text{ reproduces satisfactorily,}$$

M.J. Seaton's impact parameter cross section.

Considering a Maxwellian velocity distribution for electrons and utilising the cross section in eqn. (7.29)

we obtain

$$\langle Q_{ij} v_e \rangle = \left( \frac{8kT_e}{m\pi} \right)^{1/2} 4 \left( \frac{E_H}{E_{ij}} \right)^2 \pi a_0^2 f_{ij} \left( \frac{E_{ij}}{kT_e} \right)^2 \left[ -\frac{1}{\frac{E_{ij}}{kT_e}} \text{Ei} \left( -\frac{E_{ij}}{kT_e} \right) + \frac{\exp \left[ -\beta \left( f_{ij} \frac{E_H}{E_{ij}} \right)^{-\gamma} \right]}{\frac{E_{ij}}{kT_e} + \beta \left( f_{ij} \frac{E_H}{E_{ij}} \right)^{-\gamma}} \right] \times \left[ \text{Ei} \left( -\left[ \frac{E_{ij}}{kT_e} + \beta \left( f_{ij} \frac{E_H}{E_{ij}} \right)^{-\gamma} \right] \right) \right]$$

Since  $E_{ij} = 2.269 \text{ eV.}$  and  $kT_e = 0.4 \text{ eV,}$

$$\frac{E_{ij}}{kT_e} \gg \beta \left( f_{ij} \frac{E_H}{E_{ij}} \right)^{-\gamma}$$

and asymptotic value of exponential integrals is given by Griem (1964) as

$$\text{Ei}(-x) \xrightarrow{x > 5} \frac{e^{-x}}{x}$$

the above expression becomes

$$\langle Q_{ij} v_e \rangle = \left( \frac{8kT_e}{m\pi} \right)^{1/2} 4 \left( \frac{E_H}{E_{ij}} \right)^2 \pi a_0^2 f_{ij} \exp \left( -\frac{E_{ij}}{kT_e} \right) \left[ 1 - \exp \beta \left( f_{ij} \frac{E_H}{E_{ij}} \right)^{-\gamma} \right] \quad (7.30)$$

Thus

$$\frac{\langle Q_{2u} v_e \rangle_B}{\langle Q_{2u} v_e \rangle} = \sqrt{\frac{kT_{eB}}{kT_e}} \exp E_{2u} \left( \frac{1}{kT_e} - \frac{1}{kT_{eB}} \right) \quad (7.31)$$

From equation (7.28), (7.31) and (7.23), we get,

$$\frac{n_2(0)_B}{n_2(0)} = \frac{\sum (I_{ul})_B}{\sum I_{ul}} \left( \frac{kT_{eB}}{kT_e} \right)^{5/2} \exp E_{2u} \left( \frac{1}{kT_{eB}} - \frac{1}{kT_e} \right) \quad (7.32)$$

From equation (7.32), we can determine the values of

$$n_2(0)_B / n_2(0)$$

and the values have been shown in Table 7.3. It is observed that as B increases, due to the coupled variation of

$n_e(0)$  and  $T_e$  the value of  $n_2(0)$

also increases at least upto a magnetic field of 1000 gauss.

TABLE 7.3.

Magnetic field B (Gauss)	$T_e$ (eV)	$\frac{\sum (I_{ul})_B}{\sum I_{ul}}$	$\frac{n_2(0)_B}{n_2(0)}$
0	0.412	1.0	1.0
255	0.313	1.068	3.0
550	0.282	1.170	5.7
836	0.256	1.249	10.7
1050	0.243	1.293	15.6

## 7.4. Conclusions

The triplet radiation lines of mercury namely  $(7^3S_1 \rightarrow 6^3P_{0,1,2})$  ( $\lambda$  5461 Å,  $\lambda$  4358 Å and  $\lambda$  4047 Å) have the same upper level and consequently the intensity pattern of these lines should behave in a similar manner when a magnetic field is applied, but as it has been observed that the effect of magnetic field is different as regards the variation of intensity and the occurrence of maxima in case of three lines it has been assumed after Le's et al (1961) that these variations can be explained by considering the reabsorption of the spectral lines. Considering this effect, an expression for  $(I_{ul})_B / I_{ul}$  has been deduced. The slope of the line when  $(I_{ul})_B / I_{ul}$  is plotted against  $f_{lu} \lambda_{ul} \exp[-(E_n - E_0) / kT_{eB}]$  gives a value which is in close agreement with the theoretical calculated slope

$$\frac{1}{3} \pi n_0 c R \left( \frac{M}{2\pi k T_g} \right)^{1/2} n_0(0)_B n_u(0)_B / n_u(0)$$

for two different discharge currents, justify the assumption that self absorption factor plays a dominant role in the intensity profile of these lines.

In the next section a detailed mathematical formulation has been presented showing a coupled variation of  $n_e(0)$  with electron temperature. Utilising this relation an expression for the excited atom density

has been obtained in terms of the total integrated intensity of the three lines and the electron temperature with and without magnetic field. The results indicate that due to coupled variation of electron density with electron temperature, the excited atom density increases with the magnetic field at least up to a field of 1000 gauss.

Increase of electron density has been observed in case of a glow discharge in a longitudinal magnetic field. The rate of increase is however, much higher than in case of glow discharge which shows that an arc plasma is much more affected by an external magnetic field.

## References

1. Benson, R.S. and Kulander, J. L. (1972), Solar Physics, 27, 305.
2. Corney, A. (1977) Atomic and Laser Spectroscopy, Oxford University Press.
3. Cowan, R.D. and Diecke, G.H. (1948), Rev. Mod. Phys. 20 418.
4. Cummings, C.S. and Tonks, L. (1941) Phys. Rev. 59 514.
5. Forrest, J.R. and Franklin, R.N. (1966), Brit. J. Appl. Phys. 17 1569.
6. Forrest, J.R. and Franklin, R.N. (1969) J. Phys. B. Ser. 2, 2, 471.
7. Franklin, R. N. (1976) Plasma Phenomena in gas discharges (Oxford University Press).
8. Fujimoto, T. (1970) J. Phys. Soc. Japan 47 273, 265.
9. Griem, H.R. (1964), Plasma Spectroscopy (McGraw Hill, New York).
10. Gruzdev, P.F. (1967) Opt. Spectrosc. 22, 89.
11. Hearn, A.G. (1963) Proc. Phys. Soc. 81 648.
12. Hegde, M. S. and Ghosh, P.K. (1979) Physica 97C, 275.
13. Johnson, P.C., Cooke, M.J. and Allen, J.E. (1978) J. Phys. D. 11 1877.
14. Johnson, L.C. and Hinnov, E. (1969) Phys. Rev. 187 143.
15. Kulkarni, S.B. (1944) Curr.Sci. 13 254.
16. Les', Z. and Niewodniczan'ski, H. (1961) Acta. Phys. Polon 20 701.

17. Massey, H.S.W. (1971) *Electronic and Ionic impact phenomena*, Vol. 3 (Oxford University Press).
18. Mosberg (Jr.), E.R. & Wilkie, M.D. (1978) *J.Q.S.R.T.* 19 69.
19. Nakamura, Y. and Lucas, J. (1978) *J. Phys. D.* 11 325.
20. Nishikawa, M., Fujii-e, Y. and Suita, T. (1971) *J. Phys. Soc. Japan* 31 910.
21. Numano, M., Cussenot, J.R., Fabry, M. and Felden, M. (1975), *J.Q.S.R.T.* 15 1007.
22. Phelp, A.V. (1958) *Phys. Rev.* 110 1362.
23. Phelp, A.V. and McCoubrey, A.O. (1960) *Phys. Rev.* 118 1561.
24. Richter, J. (1968) in *Plasma diagnostics* (Ed. Lochte-Holtgreven, W., North Holland Publishing Co., Amsterdam).
25. Rokhlin, G.N. (1939) *Fiz. Zh.* 1 347.
26. Sampson, D.H. (1969) *Astrophys. J.* 155 575.
27. Sen, S.N., Das, R.P. and Gupta, R.N. (1972) *J. Phys. D.* 5 1260.
28. Uvarov, F.A. and Fabrikant, V.A. (1965) *Opt. Spectros.* 18 323.
29. von-Engel, A. (1965) *Ionised gases* 2nd. Edn. (Oxford University Press).
30. Vriens, L., Keijser, R.A.J. and Ligthrt, F.A.S. (1978), *J. Appl. Phys.* 49 3807.

## CHAPTER VIII

### PERSISTENCE TIMES IN AFTERGLOWS IN MERCURY ARC MAINTAINED BY r.f. FIELD IN PRESENCE OF MAGNETIC FIELD.

#### 8.1. Introduction

Study of the afterglow process in decaying plasma and the measurements of the coefficient of recombination have been carried out by a large number of investigators. The study has provided us with information regarding the various processes of electron ion dissociative and radiative recombination and their relative importance in a decaying plasma. The afterglow we are considering here is of a different type than that investigated hitherto in the sense that whereas in a normal afterglow the decaying time is of the order of a microsecond or less, in our experiments the glow was allowed to exist for a few tens of seconds by applying a radiofrequency field which provided additional ionization and allowed the plasma to decay at a much slower rate. The object is to study the ionization and loss mechanism in a decaying plasma.

Since the ionization and loss mechanism processes are functions of an externally applied magnetic field, it was thought worthwhile to study the persistence time of an afterglow in presence of a magnetic field. The perturbation

in the deionization processes that will occur due to the presence of magnetic field is expected to help us in identifying the main operating factors. Hence in the present investigation, the variation of persistence time of a decaying afterglow plasma in mercury vapour has been investigated in presence of a radio frequency field both in the presence and in absence of external magnetic field.

## 8.2. Experimental arrangements

Investigation has been carried out in a mercury afterglow (admixed with dry air) in a cylindrical discharge vessel. As we are more interested to study the behaviour of a recombining plasma with and without a magnetic field, the effect due to diffusion transport of charge carriers is to be lessened. Since the characteristic time of disappearance of charges by diffusion, varies with the square of the diffusion length, a better study of particle recombination can be achieved by taking a discharge vessel of large diameter. Hence a discharge vessel of diameter 3.6 cm. and 9 cm. long was placed in between the pole-pieces of an  $k$  electromagnet.

An outline of the discharge vessel fitted with a simple mercury trap through a standard joint is shown in Fig. (2.1). A d.c. mercury arc was generated inside the discharge tube. To increase the pressure inside the

discharge tube so that diffusion of charged particles which is definitely ambipolar in nature, can further be diminished, dry air which acts as a buffer gas influencing only the diffusion and mobilities of the charges, was introduced by a variable microleak of a needle valve. Two aluminium couplers, clamped in the middle of the discharge tube from outside, was connected to a Hartley oscillator to supply the radio frequency voltage. The couplers were separated, by 2.35 cm. The level of the r.f. power supplied by the oscillator was low enough so as not to cause a breakdown of the gas.

The arc discharge was run for a few minutes so that a steady condition was reached and the outside wall temperature was noted. Then the primary arc discharge was switched off. A glow which developed in wake of switching off persisted for a few seconds and then disappeared. Time of persistence of the glow was recorded by two stop watches. When there was no r.f. power to the coupler, no glow was visible after the switching off of the parent discharge. The glow time was measured under different conditions of the discharge e.g. pressure, current of the parent arc discharge, outer wall temperature and with and without an axial magnetic field.

### 8.3. A description of the decay of visual intensity during the afterglow

The time variation of the total visual intensity has been shown in Fig. 8.1. When the d.c. arc was switched off, a greenish white glow existed throughout whole of the discharge vessel as shown in Fig. 8.1 A. Thereafter, the glow in the furthest regions from the coupler vanished first and this process of gradual disappearance of glow continued for a few seconds. Ultimately the glow survived only in between the couplers where the r.f. field existed as shown in Fig. 8.1D. In between the couplers, the glow shape was first an ellipsoid, then a sphere and lastly a spheroid. The colour of this glow, in between the couplers, was ~~an~~ bluish white and after an interval of a few seconds it also vanished.

It was observed that the persistence times of the glows in the field free region (outside the couplers) and in the region with an applied r.f. field (in between the couplers) vary in different ways with other parameters of the discharge. This led us to divide the total period of persistence of the glow in two parts. The first part is the persistence time type 1 which is the measure of period starting from switching off of parent arc discharge to the moment when the glow was confined only in between the couplers. Thus in this period the glow in the field free

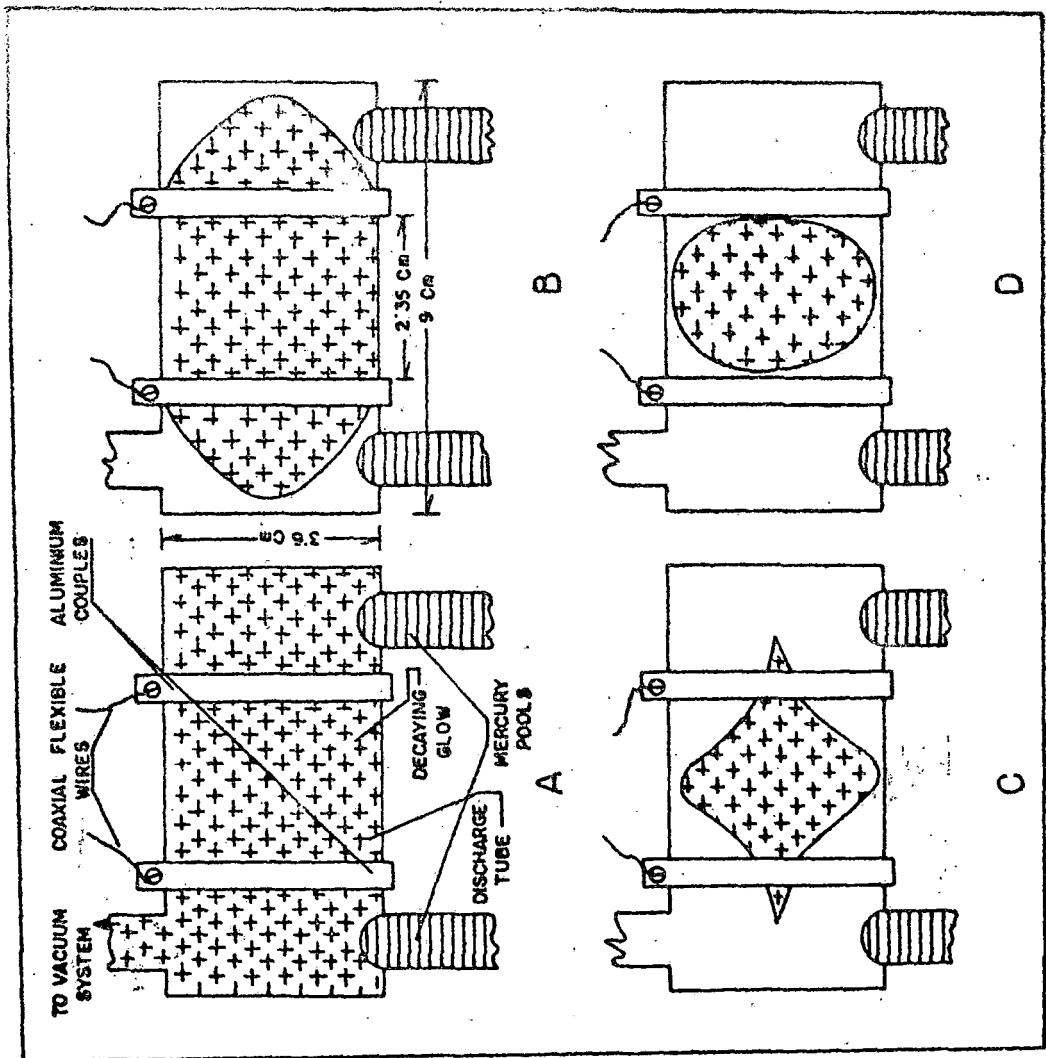


Fig. 8.1. Decay of mercury afterglow maintained by r.f. field: At the beginning the afterglow filled the total discharge tube (A) then the glow at the furthest points from the couplers disappeared gradually (B and C) and lastly the glow survived only in between the couplers (d) for a while and then disappeared completely.

region, outside the couplers, slowly diminishes in size and ultimately gives away to the glow surviving  $k$  in between the aluminium couplers. The next part, persistence time type 2 is the record for persistence of glow in between the couplers only. As soon as persistence time 1 was over, recording of persistence time 2 begins until the glow disappears totally.

As these two types of persistence times vary differently with discharge conditions, it may be concluded that different mechanisms are responsible for their survival and extinction.

It may be noted that persistence of the glows was observed visually and times were recorded by two stop-watches. The demarkation between the two types is not a sharp one, rather the transformation is gradual. As such, an error of  $\pm 1$  to 2 seconds in recording times could not be avoided. Nevertheless, the persistence times for glow are in the order of tens of seconds, so this possible error in the recordings of times is expected to cause not much appreciable error. In this investigation, we have, however, recorded the persistence times only. Generally for fuller information of an afterglow, densities of different particles are measured as a function of time. A plot of them is analysed with rate or continuity equations of particles and with a knowledge of electron temperature relaxation, different macroscopic co-efficients for

the particles are measured. Simply a knowledge of persistence time, can not give a clear picture of the decay rates of particles. Lastly, the disappearance or occurrence of a discharge was inferred by visually observing the glow. So when the glow vanished, we considered that the afterglow ceased to exist. But the decay rate of charged particles may be different from the decay rate of excited atoms which are responsible for creating the visual picture of the glow. Generally it is believed that, during the decay, production of new charged particles ceases, and concentrations of charged particles then decreases by different loss mechanisms like recombination, ambipolar diffusion etc., approaching a finite but small value. However, for an analysis of experimental data we have correlated the visual glow with the plasma since the radiation is definitely an electron - atom process (either it is a recombination radiation or a electron excitation radiation). Hence, due to this limitation no attempt has been made to put forward a quantitative analysis of the experimental results.

#### 8.4. Results and Discussions

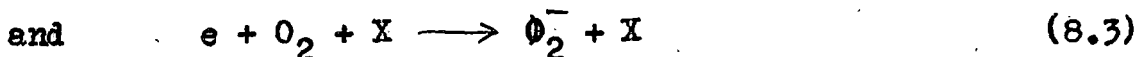
##### 8.4.1. Without a magnetic field

###### (a) Variation of persistence time $\tau$ with pressure

Two types of glow persistence times e.g. persistence time 1 and persistence time 2 are found to

vary with conditions of the discharge differently. Fig. 8.2 shows a plot of persistence time  $\tau$  Vs  $1/p_{tot}$ . Here  $p_{tot}$  is the total pressure inside the discharge tube i.e.  $p_{tot} = p_{air} + p_{Hg}$ . It can be seen that when  $p_{tot}$  is comparatively large ( $p_{tot} > 0.5$  torr), persistence time  $\tau$  is directly proportional to  $1/p_{tot}$ . In the field free region, when the arc current is off, the electrons of the parent discharge will be lost by ambipolar diffusion, attachment and by dissociative recombination. It is, however, assumed that the r.f. field produces ionization in between the couplers and due to the diffusion of charged and other particles from the source region (region with an r.f. field in between the aluminium couplers), the loss processes in the field free region will be delayed, thus making the glow in field free region to continue for a longer time. After being created in the source region, the charged particles will diffuse away through the couplers, hence the diffusive gain term will be proportional to  $1/p_{tot}$ .

For attachment loss, three processes may be considered,



For first of the processes (8.1) the reaction rate will be proportional to  $n_{Hg}^2$  i.e.  $p_{Hg}^2$ . But as

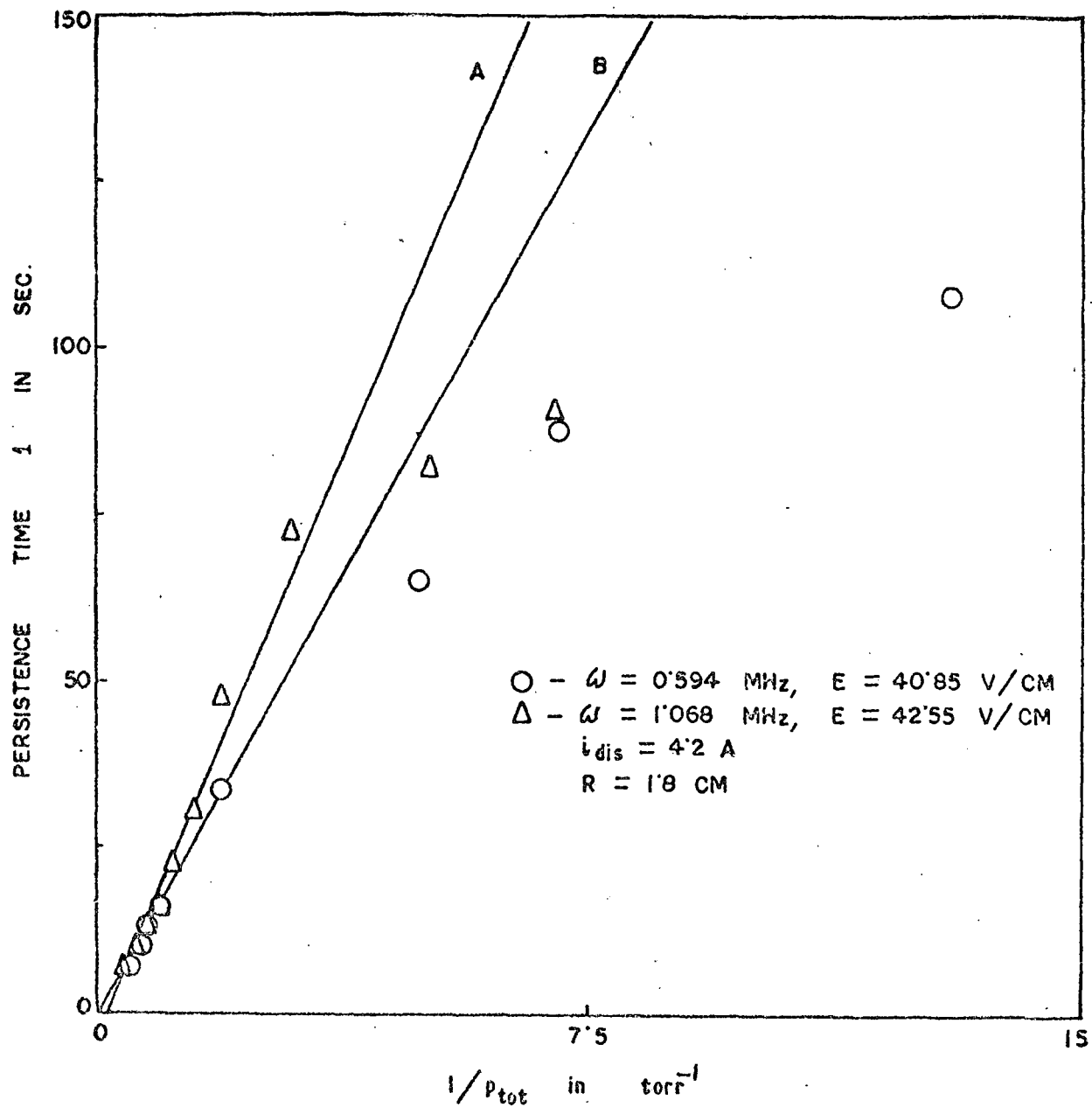


Fig. 8.2.

Fig. 8.2. Variation of persistence time  $t$  with inverse of total pressure.

oxygen, an electromagnetive gas, is present in abundance when  $P_{\text{air}} > P_{\text{Hg}}$  (when  $P_{\text{tot}} > 0.5$  torr), we can disregard the process. The dissociative attachment process (8.2) is generally believed to be of importance when  $T_e$  is comparatively high. Hence where  $T_e$  (as is the case in a decaying discharge) is comparatively small, this process will be of lesser importance. The threebody attachment process (8.3) is proportional to  $P_{\text{air}}^2$ . X is a stabilising molecule, both  $O_2$  and  $N_2$  molecules can take part in the process of stabilisation. Where attachment of electron is a dominating loss mechanism, it is observed that negative ions generally accumulate in the volume. They tend to remain in the body of the afterglow owing to the disposition of electric field which builds up. This accumulation of  $-ve$  ions which should be proportional to time, influences the electron ambipolar diffusion coefficient  $D_{ae}$ . Truby (1968) has shown that

$$D_{ae} = D_{a+} \left( 1 + \frac{n_-}{n_e} \right) \quad (8.4)$$

here  $D_{a+}$  is the ambipolar diffusion coefficient for positive ions and  $n_-$  is the number density of negative ions. Thus,  $D_{ae}$  increases as  $n_-$  increases for a constant value of  $D_{a+}$  throughout the electron decay process. In this way attachment loss can be interpreted as an enhanced diffusion process.

The last of the loss processes is the recombination process. For mercury it is a dissociative recombination and the dissociative recombination being a two body process is independent of  $p_{\text{air}}$ .

In the comparatively high pressure region, the straight line (passing through the origin) plot of persistence time  $\tau$  with  $1/p_{\text{tot}}$  suggests that the gain of particles by a diffusive flow from the source is balanced by recombination which is pressure independent. The breakdown from linearity in the low pressure region, may be interpreted in terms of other pressure dependent loss mechanisms like ambipolar diffusion. It is evident from Fig. 8.1 that at the further point from the source the glow in field free region begins to disappear first, then this process is conducted away towards the source. The way, glow in field free region diminishes, suggests that loss processes <sup>is</sup> a volume phenomenon.

(b) Variation of persistence time  $\tau$  with r.f. field strength.

In Fig. (8.2) the dependence of persistence time on r.f. field strength may be observed. The persistence time  $\tau$  increases with the r.f. field which was applied to the source. This dependence is also evident in Fig. (8.3) where corresponding to  $p_{\text{air}} = 1$  torr, persistence time  $\tau$  is plotted against r.f. ~~the~~ field applied to the source. Thus it may be

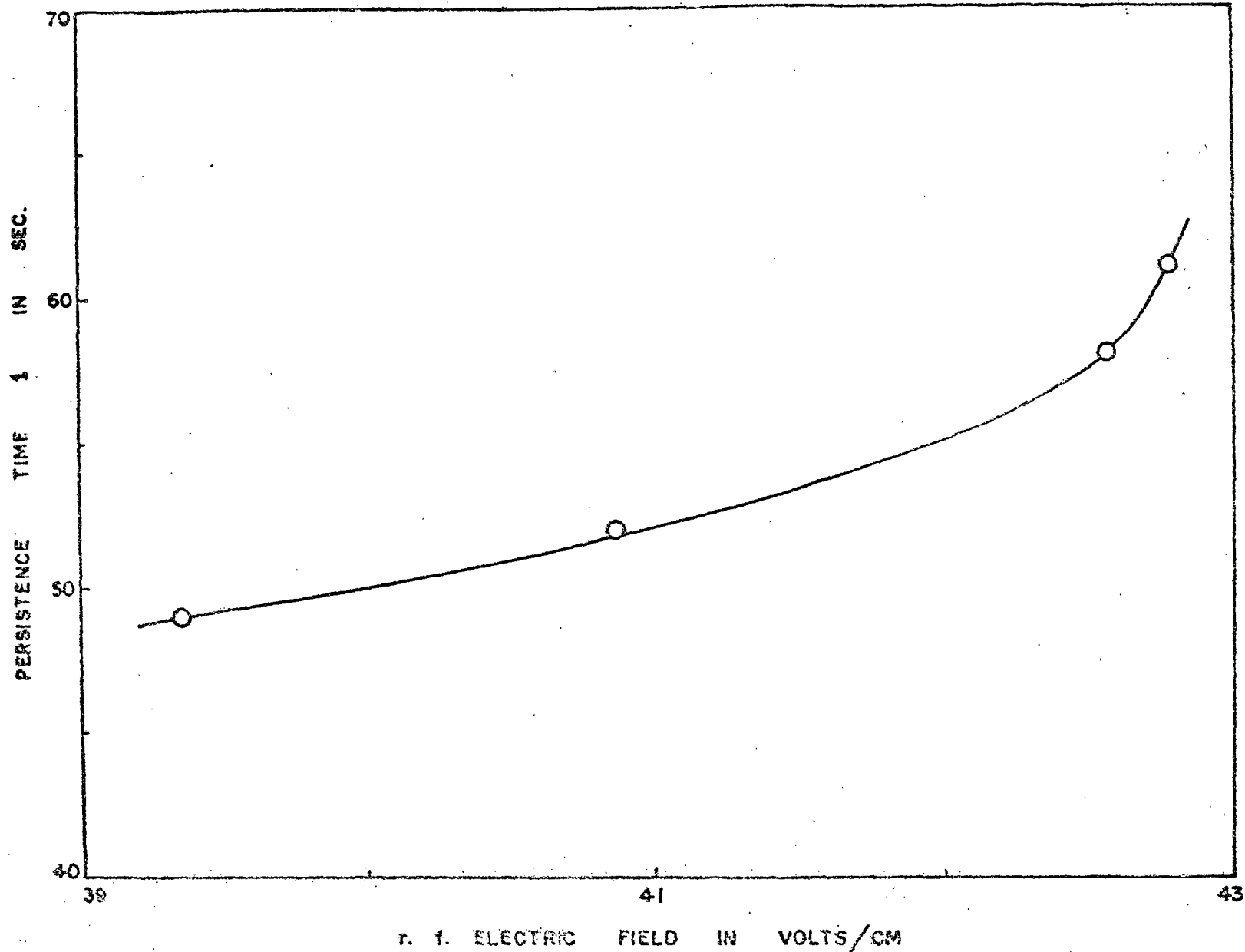


Fig. 8.3. Variation of persistence time  $\tau$  with r.f. electric field supplied to the couplers ( $p_{\text{air}} = 1$  torr,  $i = 2.4$  A).

FIG. 8.3.

assumed that electrons and ions that diffuse out axially from the source also carry their energies which should be proportional to  $E/p_{\text{tot}}$ , where  $E$  is the r.f. field in the source. As these electrons further diffuse axially in the field free region, they lose much of their energies in elastic collision with air molecules. Some of them, the high energetic ones, lose energies in inelastic collision like collisional excitation of mercury atoms and vibrational excitation of nitrogen and oxygen molecules. They may also gain some energy in collisions of second kind. The relaxation time of  $T_e$  should be directly proportional to  $1/p_{\text{tot}}$ . Thus at the furthest point of the source electrons may be considered to be nearly thermalised, making recombination high and the glow disappears. It may also be noted that as time elapses, gas temperature also decreases as heat is radiated to the surroundings by the discharge vessel. This reduction of gas temperature will be effective in an enhanced recombination of charged particles. For the reduction of gas temperature, the number density of mercury atoms  $n_{\text{Hg}}$  will also be effectively reduced. So there exists a gradient of  $T_e$  in the field free region along the axis of discharge tube.

## (c) Variation of persistence time 2 with pressure

The persistence time 2 varies with pressure in a different way. This variation has been shown in Fig. (8.4). It is observed that persistence time 2 first increases with pressure. In a certain interval of pressure, the glow in between the couplers, giving rise to persistence time 2, never diminishes so long r.f. power is supplied. Thereafter, persistence time 2 decreases as pressure increases.

When the primary arc is switched off,  $n_e$  is in the range of  $10^{13} \text{ cm}^{-3}$  corresponding to the arc. As time passes on,  $n_e$  decays. When  $n_e$  equals a critical value  $n_{cr}$  a glow is sustained in between the couplers. In this region electrons are heated by the r.f. field. During this period, visible mercury lines (only mercury lines were observable) was observed through a constant deviation spectrograph. The line intensities increased markedly with the increase of r.f. electric field. It appeared that the glow intensity (type 2) did not diminish with time slowly, on the otherhand it remained fairly constant and at a certain moment very rapidly became zero and the glow disappeared. The only factor that changes during this period is the neutral particle temperature  $T_g$  or outerwall temperature  $T_w$ , owing to the radiative cooling of the discharge vessel. So a cooling down of discharge vessel effectively influences the production and loss processes of this sustained glow. Owing to the decrease of  $T_w$  when

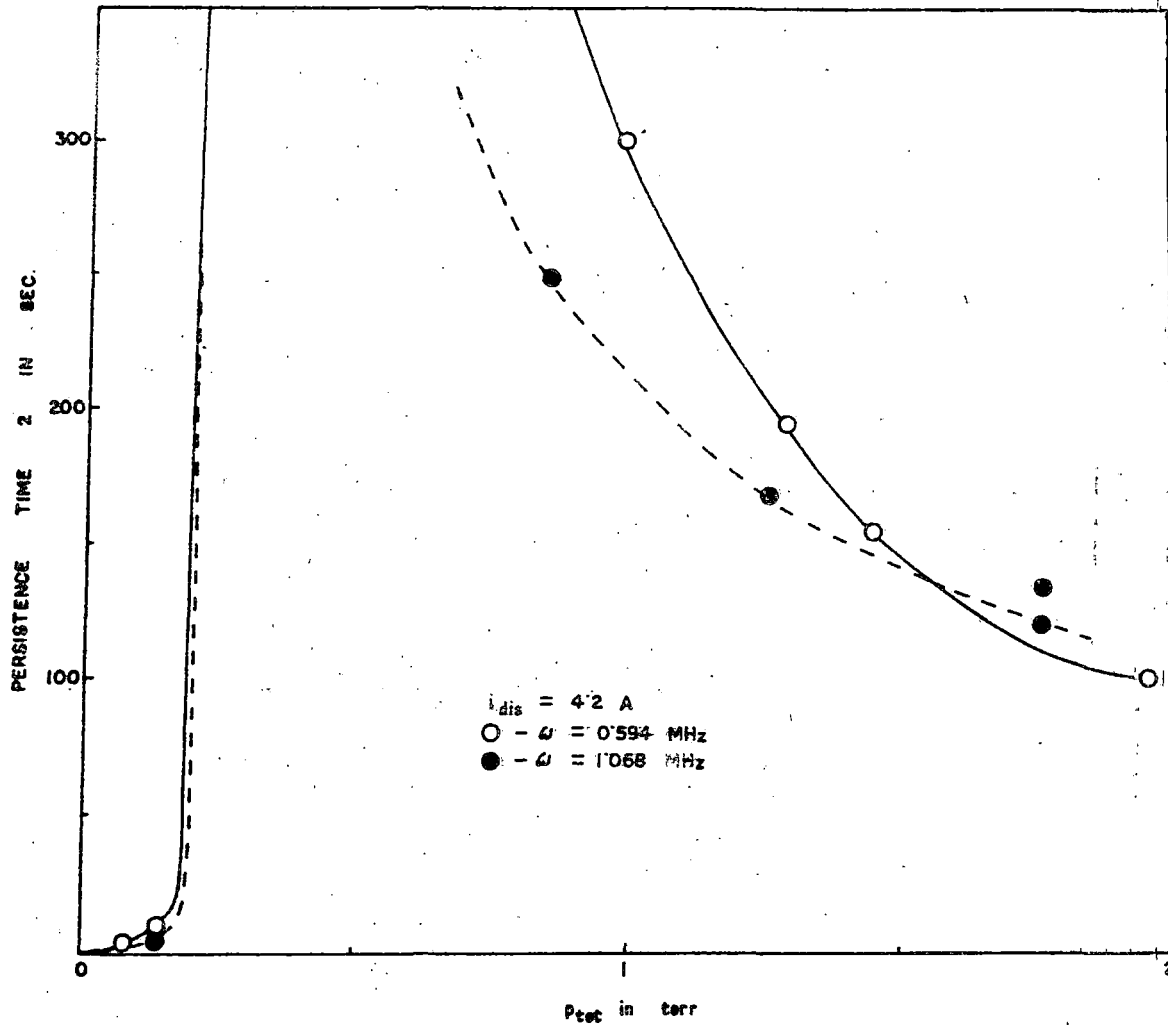


Fig. 8.4. Variation of persistence time 2 with pressure inside the discharge tube.

Fig. 8.4.

the gain and loss processes can not balance each other, the glow vanishes. The processes in this glow are very complex. As  $T_w$  drops,  $p_{Hg}$  hence  $p_{tot}$  also is reduced. This will make  $\nu_m$  the collision frequency of electrons for momentum transfer to change with time. Since  $E_e$ , the effective field that will produce the same energy transfer as a steady field, is given by

$$E_e^2 = E^2 / \left( 1 + \frac{\omega^2}{\nu_m^2} \right) \quad (8.5)$$

where  $E$  and  $\omega$  are the r.m.s. r.f. field and angular frequency of r.f. source.  $E_e$  decreases with time and so the power absorbed from the r.f. field will decrease. It is well known that for an r.f. discharge ionisation rate is a very strong function of electric field, a substantial change in  $\nu_i$  can be caused by a tiny change in  $E_e$ . Thus at a time when production terms can not supplement for the losses, the r.f. glow in between the coupler vanishes.

It was observed that as  $p_{air}$  (hence  $p_{tot}$ ) increases, the outerwall temperature corresponding to ceasing of persistence time  $2 \tau$  first decrease and then increases. The cases of subsistence of glow so long r.f. power is supplied in some pressure interval may be interpreted by considering that the temperature at which

these glows will disappear are definitely below room temperature. As  $p_{\text{tot}}$  increases,  $E_e/p$  increases which will make  $D_i/p$  to increase. For this glow where  $T_e$  is comparatively high, radial ambipolar diffusion loss will be most dominating loss mechanism.  $D_a = kT_e / M \nu_{in}$  where  $M$  is the mass of heavy particles and  $\nu_{in}$  is ion-neutral collision frequency, also decreases with pressure. But at comparatively high pressure, owing to increased energy loss of electron in elastic (also rotational and vibrational excitation) collisions, ionisation rate will be decreased. The pressure dependence of  $T_W$  (hence, the particle generation and loss processes) may best be interpreted by considering the a.c. ionisation coefficient defined by Brown ~~and~~ (1959). When loss is by diffusion, a.c. ionisation coefficient  $\xi = D_i / D_a E^2$  first increases rapidly, then after passing through a maxima decreases as  $E/p$  increases.

Since rate of cooling, determining  $T_W$ , has significant effect on the discharge, care was taken in the recordings of persistence time 1 and 2 that the discharge tube may cool down in the same surrounding.

(d) Dependence of persistence times with varying arc currents

Dependence of persistence times with current of the primary arc discharge was observed in two different ways.

First the primary arc was allowed to burn for different currents for different time interval so that  $T_w$  at the moment of switching off of primary arc, remained same. In this way the heating effect of the current may be disregarded and only the dependence of persistence times with  $n_e$  of primary arc may be observed. Results have been shown in Table 8.1. Secondly, the primary arc was burned for a fixed time interval of 4 minutes with different current. In this way  $T_w$  during switching off varied as well as  $n_e$ . In Table 8.1, it is seen that persistence time 1, probably depends on  $n_e$  but persistence time 2 does not. But considering the range of accuracy of measurement nothing specific may be concluded upon.

When primary arc was burned for fixed interval of 4 minutes so that  $T_w$  at switching off varied persistence time 1 is seen to vary linearly with current (Fig. 8.5). In this fig. variation of  $T_w$  with current has also been shown. It appears that proportionality constants for variation of persistence time 1 and  $T_w$  at switching off with current are the same.

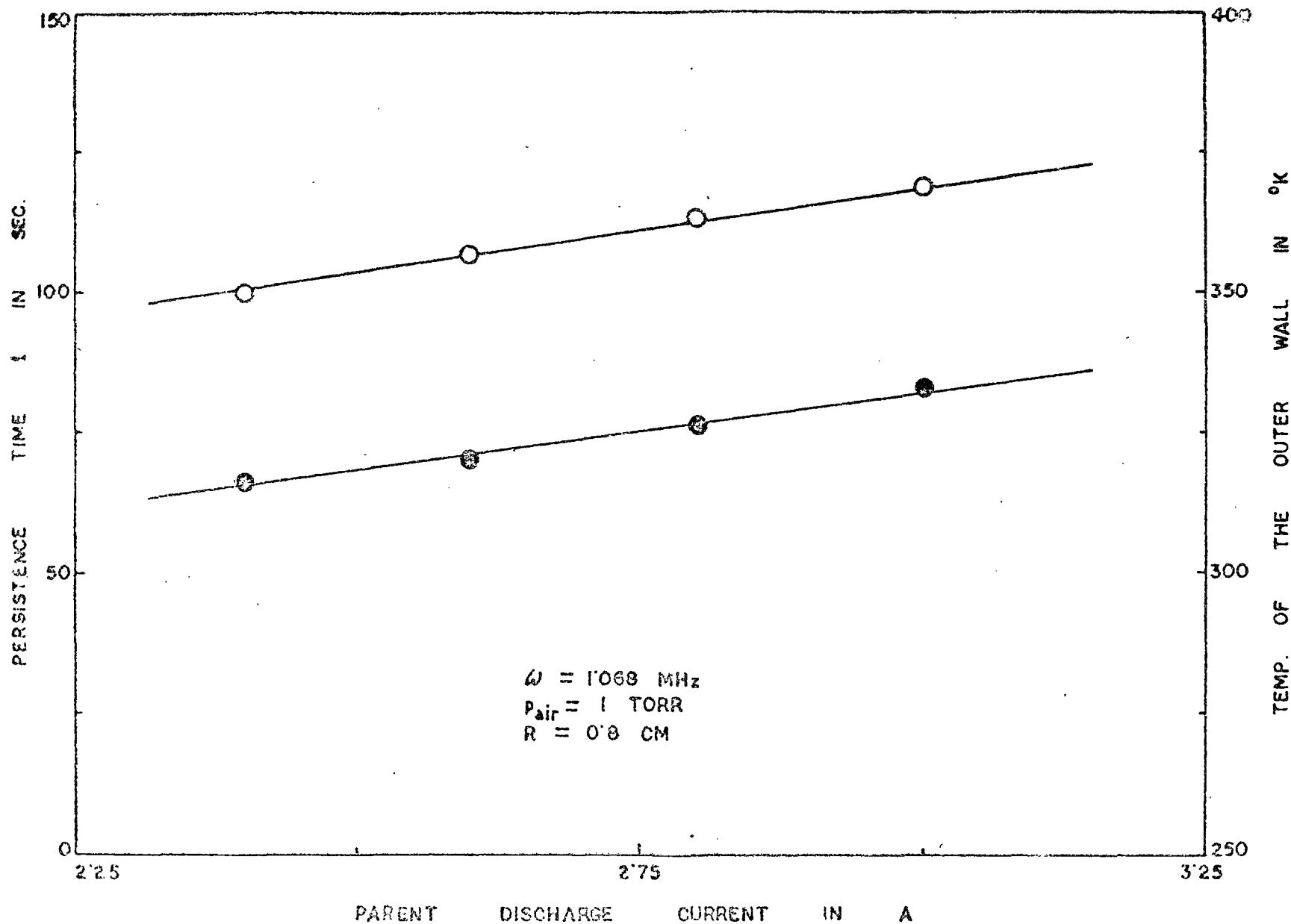


Fig. 8.5. Variation of persistence time  $\tau$  (black circles) and temperature of the outer wall (white circles) with current of the parent arc discharge. FIG. 8.5.

TABLE 8.1Variation of persistence time with  $n_e$ .

Pair (torr)	r.m.s. field of r.f. source (volts/ cm)	Current in prima- ry arc (ampere)	Persis- tence time 1 (Sec)	Persis- tence time 2 (Sec)	$T_{wat}$ the mo- ment of switch- ing off of primary arc ( $^{\circ}C$ )	$T_w$ when the glow in- side r.f. field disa- ppear ( $^{\circ}C$ )
0.975	40.86	2	74	106	85.5	69
		2.4	77	109	85.75	68.5
		2.8	77	103	85	69
		3	79	107	85.5	68
1.2	42.56	3.8	19	277	69.5	52.75
		4	19	277	69.5	53.5
		4.2	18	281	69.5	52.5
		4.4	20	275	69.5	53
		4.6	21	276	69.75	54

So it may be concluded that rise in  $T_w$  is the chief cause for the increase of persistence time 1. This is further evident in Fig. (8.6) where persistence time 1 is plotted against  $T_w$  at the switching off of primary arc discharge of 2.4 amp., run for different time intervals.

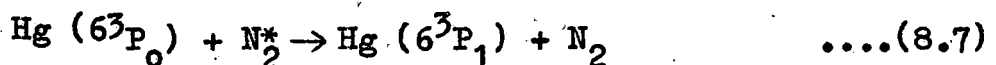
Considering the case of persistence time 1 we may consider the ways how  $T_w$  (also  $T_g$ ) enters into the rate processes.

i) In the process of associative ionisation in the formation of  $Hg_2^+$ ,  $T_g$  enters explicitly in the reaction rate. In chapters VI~~X~~ and VII it has been shown that  $Hg_2^+$  ions are the chiefly ionised species.

ii) Quenching rate for heavy particle metastable levels will increase with  $T_g$ . An effective quenching process of mercury  $6^3P_1$  atoms by  $N_2$  is  $Hg(6^3P_1) + N_2 \rightarrow Hg(6^3P_0) + N_2 + 0.218 \text{ eV}$ .

....(8.6)

It has been discussed by Mitchel and Zemansky (1961) that the energy discrepancy of 0.218 eV. in this reaction is taken up by  $N_2$  molecules as vibrational energy. But when the neutral particles are hot enough, much of  $N_2$  molecules will be in vibrational state, so that reverse reaction e.g.



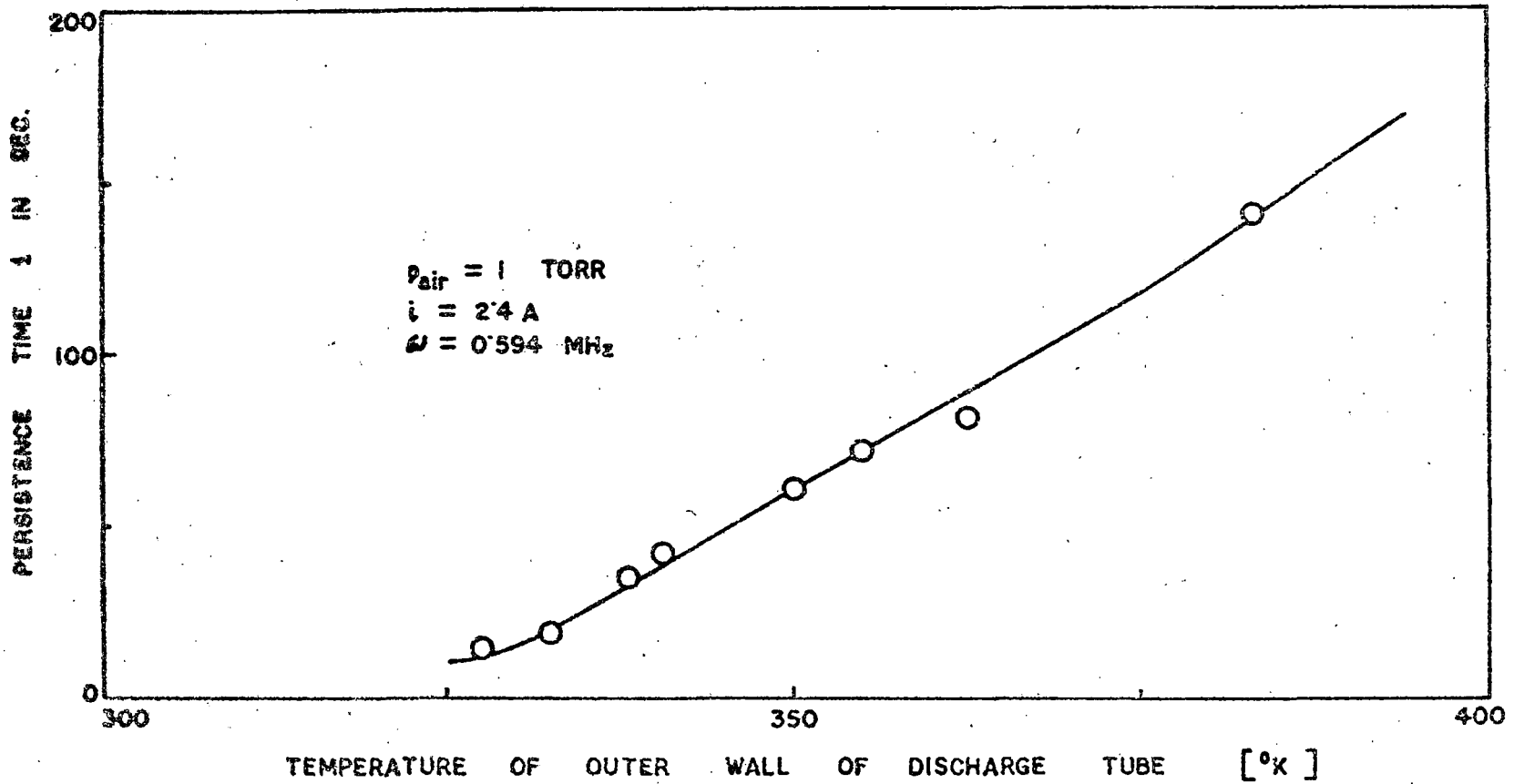


FIG. 8.6.

Fig. 8.6. Variation of persistence time 1 with temperature of the outer wall.

may be one of the important processes that populate  $6^3P_1$  level.

- iii) As  $T_g$  increase,  $T_e$  also increases.
- iv) The diffusion coefficient of metastable atoms decreases with gas temperature. It has been shown by Chapman and Cowling (1970) that coefficient of mutual diffusion of a gas is given by

$$D_{12} = \frac{3}{8(n_1 + n_2)\sigma_{12}^2} \left\{ \frac{kT_g (m_1 + m_2)}{2\pi m_1 m_2} \right\}^{1/2} \quad (8.8)$$

where  $\sigma_{12} = \frac{1}{2}(\sigma_1 + \sigma_2)$  the diameters of atoms with densities  $n_1$ ,  $n_2$  and masses  $m_1$  and  $m_2$ . Equation (8.8) predicts a decrease of diffusion coefficient of metastable atoms with decrease of gas temperature.

For a better understanding of individual reaction processes in persistence time 1, we write down the continuity equation of the particles. For molecular ions  $Hg_2^+$  with density  $n_{2+}$

$$\frac{dn_{2+}(r, z, t)}{dt} = \nabla \cdot \Gamma_{2+}(r, z, t) - \alpha n_{2+} n_e + \frac{1}{2} n_0 n_1 \langle v\sigma \rangle_{ass} + \nu_c P_{tot}^2 n_{1+} + f\left(\frac{1}{P_{tot}}, t\right) \quad (8.9)$$

here  $\Gamma$  is a particle flux,  $n_0$ ,  $n_1$  and  $n_{1+}$  are the number densities of  $6^3P_0$ ,  $6^3P_1$  and  $Hg^+$  ions

respectively.  $\alpha$  is the two body dissociative recombination coefficient,  $\mathcal{D}_c$  is the collision integral for three body conversion of atomic ions to molecular ions.  $\langle v\sigma \rangle_{ass}$  is the collision integral for associative ionisation and

$f(1/p_{tot}, t)$  is the diffusive ~~diffusive~~ source term. The source term may be considered as

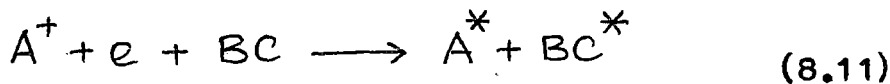
$$f = \nabla \cdot D_a \nabla_z n_c(t)$$

$n_c(t)$  is the average particle density at the position of coupler and  $z$  is the direction of discharge tube axis. The flux due to r.f. field mobility may be disregarded.

For atomic ions,

$$\frac{dn_{1+}(r, z, t)}{dt} = \nabla \cdot \Gamma_{n_{1+}}(r, z, t) - \mathcal{D}_c p_{tot}^2 n_{1+} + f(1/p_{tot}, t) \quad (8.10)$$

We have disregarded recombination of  $Hg^+$  ions which may of the type



where  $BC$  is an <sup>vibr</sup>molecule which is excited rotationally and vibrationally to  $BC^*$ .

In the above rate equations it has been assumed that apart from associative ionisation no further ionisation takes place in the field free region. Of course field builds up for the space charges that produce ambipolar diffusion. The plasma is field free in the sense that space charge field is so small that it can not contribute to ionization.

Since charged particle neutrality is not appreciably disturbed, for electrons,

$$\frac{dn_e}{dt} = \frac{dn_{2+}}{dt} + \frac{dn_{1+}}{dt} \quad (8.12)$$

For  $6^3P_0$  atoms,

$$\frac{dn_0}{dt} = -\nu n_0 + \delta(p, t) \quad (8.13)$$

where  $\nu n_0$  is the loss term given by

$$\begin{aligned} \nu n_0 = & \frac{n_0}{\tau_0} + n_0 n_1 \langle \nu \sigma \rangle_{ass} + n_0 n_{Hg} \langle \nu \sigma \rangle_{que} \\ & + n_0 n_{N_2} \langle \nu \sigma \rangle_{que} \end{aligned} \quad (8.14)$$

the first term being diffusive loss, the second loss for associative ionisation and the other terms are quenching by heavy particles.  $\delta(p, t)$  is the gain term given by  $\delta$  = gain by recombination

$$+ f(1/p_{tot}, t) \quad (8.15)$$

Here also electron collisional excitation transfers are neglected and  $f$  may be considered to be equal to  $\nabla \cdot D_m \nabla_z n_0$ .

For  $6^3P_1$  atoms, mechanisms will be different depending on  $Z$  co-ordinate.  $6^3P_1$  being a resonance level ~~its~~ its effective life time ~~is~~ is of the order of  $10^{-5}$  sec. which is very much smaller than the persistence time. So at a point nearer the source, loss for  $6^3P_1$  atoms will be mainly supplemented by diffusive flow from the source whereas at the furthest points, generation will be mainly by reactions of type (8.7).

These continuity equations along with an equation for time variation of  $T_e$ , giving proper weightage for the nature of electron energy distribution function and its space variation, if solved simultaneously the phenomena of afterglow can be described. In simplified conditions like, particles diffuse in their fundamental diffusion mode,  $\alpha$  does not depend on space and time, electron energy distribution is Maxwellian and space and time independent, the continuity equations can be solved for appropriate boundary conditions and equations may be obtained for time variation or decay for particle densities. However, persistence time can not be calculated from the solutions.

#### 8.4.2. When an axial magnetic field is present

Results, when an axial magnetic field was present, have been shown in Table (8.2). For all sets, the primary arc was run for 3 minutes at a current of 4.2 ampere. The discharge tube cooled in the same environment during time recording. Magnetic field was switched on just before the switching off of primary discharge. For readings marked by a star (\*) in Table (8.2), an instability developed during late times of persistence time 2, the glow flickered and ultimately disappeared. It is observed that persistence time 1 does not change with magnetic field, whereas persistence time 2 definitely increases with magnetic field. The outerwall temperature when glow in the r.f. field ceases to exist, decrease with the magnetic field. Visually it was observed that as magnetic field increases, the r.f. glow, generating persistence time 2, becomes more bright. When an axial magnetic field is present, effective, r.f. field is given by

$$E_{\text{eff}}^2 = E^2 \left[ \frac{\nu_m^2}{\nu_m^2 + (\omega - \omega_b)^2} + \frac{\nu_m^2}{\nu_m^2 + (\omega + \omega_b)^2} \right] \quad (8.16)$$

where  $\omega_b = |eB/m| = 1.77 \times 10^7 B$ ,  $B$  is the value of magnetic field in gauss. As  $B$  increases,  $E_{\text{eff}}$  decreases and so the power absorbed. A magnetic field will

affect the glow in another way. The path of electrons lost by ambipolar diffusion will be changed and diffusion will be reduced as fundamental diffusion length is changed to

$$\frac{1}{\Lambda^2} = \frac{\nu_{en}^2}{\nu_{en}^2 + \omega_b^2} \left( \frac{2.405}{R} \right)^2 + \left( \frac{\pi}{L} \right)^2 \quad (8.17)$$

As diffusion of charged particle towards the wall decreases, the energy carried by a pair of charge particles towards the wall where they are neutralized by recombination, also decreases. For discharges we are considering, energy is carried mainly by diffusing charged particles and deposited to wall as neutralisation energy. So the magnetic field affects the energy balance terms of the wall. As the glow exists for longer time in a magnetic field due to a reduction of diffusion loss,  $T_w$  cools down.

It is interesting to note the invariance of persistence time  $\tau$  with axial magnetic field. We have already discussed the continuity equations for the particles. The chief production process is the axial diffusion of particles from the source. Since axial diffusion does not depend on an axial magnetic field, the production process will not depend on magnetic field. Hence the constancy of the persistence time  $\tau$  in magnetic field makes the particle loss terms also independent of magnetic field. The ambipolar

diffusion, one of the loss process will be mainly axially (as  $L$  is shorter than  $R$  in the field free region) which will be invariant in magnetic field (equation 8.17). The pressure inside the discharge tube and its size was so chosen that recombination may dominate over diffusion. So it may be concluded that sum total of recombination and diffusion losses does not depend on magnetic field. Conversely, since losses do not depend on magnetic field, dissociative recombination is the only dominating loss mechanism in the field free region. This is the same argument that was forwarded by Kuckes et al (1961) while investigating the decay of helium plasma in B-1 stellarator. As they observed that loss rate is independent of magnetic field between 2.9 and 3.5 kilo gauss, it was concluded that plasma was recombination dominated (for helium it is collisional radiative recombination, and diffusion is negligible).

However, in our experiment magnetic fields used were comparatively low so that no definite conclusion can be drawn for the behaviour of recombination reaction in a strong magnetic field as desired by Fowler (1978).

TABLE 8.2

Behaviour of persistence times in an axial magnetic field.

$P_{\text{air}}$ (torr)	r.f. field (volts/cm)	Magnetic field (gauss)	'Persis- 'tence 'time 1 (sec)	'Persis- 'tence 'time 2 (sec)	$T_w$ at 'switching 'off of 'primary 'discharge (°C)	$T_w$ when 'r.f. 'glow dis- 'appears (°C)
		0	16	233	68	56.5
		180	16	261	68	55
1.05	42.56	350	16	306	67.75	52.25
	<del>520</del>	520	15	374	67.75	49.5
		675	15	351 (*)	68.5	50.5 (*)
		0	12	179	68.75	60.5
1.2	42.56	180	13	241	69.75	57.25
		350	13	247 (*)	69	57.00 (*)
		520	13	294	69.5	54.5
		675	13	358	69.5	51.5
		0	10	159	71	63
1.4	42.56	180	11	167	70.5	62.5
		350	9	187	69.5	61
		675	11	206	70.5	60.5
		1090	12	234	71.5	59
		0	13	167	69.25	62.5
1.2	40.86	180	14	177	69	61.75
		350	13	196	69.25	60.5
		520	14	223	69.25	58
		675	13	298	69.25	54.75

## References

1. Brown, S. C. (1959) Basic data of plasma physics, p. 137 (M.I.T. Press).
2. Chapman, S. and Cowling, T.G. (1970) The mathematical theory of non-uniform gases, 3rd. Edn. p. 258 (Cambridge University Press).
3. Fowler, A.G. (1978) Phys. Lett. 65A, 239.
4. Kuckes, A.F., Motley, R.W., Hinnov, E. and Hirschberg, J.G. (1961) Phys. Rev. Lett. 6 337.
5. Mitchel, A.C.G. and Zemansky, M.W. (1961) Resonance radiation and excited atoms. (Cambridge University Press).
6. Truby, F.K. (1968) Phys. Rev. 172 24.

## SUMMARY AND CONCLUSIONS.

### Summary

In the present work measurements and calculations of some plasma parameters are described relating to the positive column of glow and arc discharges with and without magnetic field. The investigation was particularly directed to evaluate the properties of magnetoplasma which are determined by different methods in the following experiments. In the interpretation of the results the basic physical processes operating in the discharge have been sought to be evaluated.

- A. Measurement of electron temperature and electron density in low density magnetised plasma by probe method.

A Langmuir probe was utilised to measure the electron temperature and electron density near the axis in ionised molecular gases like air, hydrogen, oxygen and nitrogen. The limitations of the probe theory and precise method in measuring electron temperature and electron density both in the absence and in presence of the magnetic field have been discussed and experiments have been performed under the conditions in which the assumption of probe theory are strictly valid. It has been observed that in case of transverse magnetic field, the electron temperature increases whereas the radial electron density

decreases and in case of longitudinal magnetic field, the electron temperature decreases and the axial electron density increases. The results are in quantitative agreement with theoretical deductions which take into account the influences of magnetic field on the plasma balance equation. Further, it is noted that in case of molecular gases the electron energy distribution is Maxwellian in presence of or in the absence of magnetic field, but in the former case it becomes a function of the reduced magnetic field  $B/p$ .

B. Measurement of electron temperature in glow discharge in transverse magnetic field by spectroscopic method.

The electron temperature in the positive column of d.c. glow discharge in hydrogen and helium and a.c. (50 Hz) glow discharge in helium as a function of transverse magnetic field in the range of 0 to 1000 G has been obtained by measuring the intensities of two spectral lines. Since the electron number density in the column is of the order of  $10^{10} \text{ cm}^{-3}$ , the semicorona model suitably modified has been used to calculate the plasma electron temperature in a magnetic field. After detailed analysis an appropriate cross-section for electron collisional excitation has been utilised, which enables a fair determination of electron temperature.

It has been observed that for low values of reduced magnetic field, the results are in quantitative agreement with existing theoretical deductions.

C. Mercury arc plasma in an axial magnetic field.

The electron temperature of a mercury arc plasma (arc current 2.25 A and 2.5 A) has been measured spectroscopically in an axial magnetic field varying from zero to 1050 G. It has been noted that electron temperature decreases with the increase of magnetic field. Considering the physical processes involved in a mercury arc discharge where the buffer gas is air and the pressure is low, a model has been developed in which ~~an~~ air plays the role of quenching gas, and it has been found that in this type of discharge both atomic and molecular ions of mercury are present. Assuming the presence of both types of ions, a radial distribution function for the electron density has been deduced and an expression for  $T_e / T_{e0}$  has been obtained. Variation of arc current and voltage across the arc with axial magnetic field has also been noted and the variations have been interpreted in terms of the effect of magnetic field on the diffusion of plasma electrons. It has been found that within the range of  $B/p$  values used,

the experimental results are in quantitative agreement with theoretical deduction. The increase of axial electron density in axial magnetic field determined by probe method can also be explained by the theory developed.

- D. Enhancement of spectral intensities of mercury triplet lines in longitudinal magnetic field.

Enhancement of spectral lines of mercury sharp series triplets with longitudinal magnetic varying between zero to 1500 G field has been studied. A theoretical model has been developed which includes the effect of self absorption of the lines to explain the enhancement of intensities. It has been observed that the experimental results agree fairly well with the theoretical model. Moreover, the plasma balance equation of the mercury arc plasma with and without magnetic field has been reconsidered and variation of mercury metastable level population with longitudinal magnetic field has been determined.

- E. Persistence times in afterglows in mercury arc maintained by r.f. field in presence of magnetic field.

In presence of an external radio frequency field, when the main arc current is switched off, it has been observed that the glow persists and this glow can be distinctly identified as two individual processes

depending upon their time of persistence. The persistence time  $T_1$  which extends throughout the tube is directly proportional to inverse of total pressure, and increases with the increase of intensity of r.f. field whereas persistence time  $T_2$ , within the r.f. couplers, first increases with pressure, never diminishes as long as r.f. power is present and then decreases as pressure is increased. Regarding the variation with arc current it can be stated that  $T_1$  depends on electron density and hence on current but  $T_2$  is independent of it. The effect of magnetic field is to change the persistent time  $T_2$ , but  $T_1$  is not affected by the field. These general observations have been sought to be explained qualitatively by considering the effect of pressure, temperature of the arc and the magnetic field on the process of generation of charged particles, loss by diffusion and the process of recombination.

In general in all the experiments, the discharges chosen ~~were~~ were of low pressure and low input power so that influence of magnetic field on the plasma parameters is fairly measurable.

## Conclusions

The investigation shows that the results obtained by different diagnostic methods agree fairly with theoretical deductions. In this way the diagnostics can be very useful in the investigation of positive column of the low pressure discharges within the range of measurements. The magnetic field influences the plasma loss processes. As the particle losses are changed in magnetic field, the plasma in positive column adjusts by changing the particle generation processes and the plasma parameters change in presence of magnetic field. These investigations thus provide useful information regarding the actual physical processes occurring in glow and arc discharges and how the nature of these physical processes change when the plasma is confined by an external magnetic field.